IDENTIFICATION AND CHARACTERISATION OF MYOFIBROBLAST MARKERS IN HUMAN COLON AND COLORECTAL CANCER MICROENVIRONMENT

LIN-TING HSIA

Brasenose College

A thesis submitted to the Division of Medical Sciences, University of Oxford, in partial fulfillment of the requirements for the degree of Doctor of Philosophy in Oncology

Michaelmas Term, 2015

Weatherall Institute of Molecular Medicine

University of Oxford

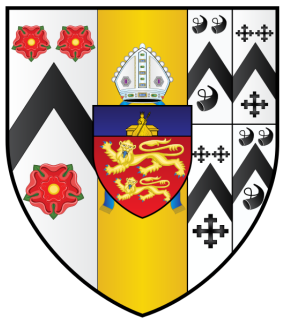

This thesis is dedicated to my family and friends for their support and encouragement.

Thank you for always being there for me.

ABSTRACT

Myofibroblasts (MFs) are one of the most significant stromal cell types in epithelia such as in the gut. They play an important role in regulating the normal colorectal stem cell niche and facilitating tumour initiation, growth and progression through inter-cell signalling. Abundant presence of MFs is often associated with poor prognosis in cancers. The aim of this project is to identify new myofibroblast markers to distinguish them from others cells in the stroma, and also to establish patterns of myofibroblast gene regulation.

First, we identify the membrane protein that home-raised IgG1 antibody PR2D3 recognises on myofibroblasts, by using immunoprecipitation and mass spectrometry based amino acid sequencing, as the AOC3 membrane primary amine oxidase, with additional reactivity to myosin heavy chain 11 (**Chapter 3**). The AOC3 expression in myofibroblasts *in vivo* and *in vitro* is validated by extensive expression profiling analyses. Our results demonstrate that AOC3 is expressed by myofibroblasts and that it functions as an SSAO enzyme (**Chapter 4**). Furthermore, we successfully separated primary myofibroblasts from fresh tissues by FACS sorting using AOC3 as a myofibroblast-specific surface marker (**Chapter 5**). Analysis of whole genome microarray mRNA expression profiles between myofibroblasts and fibroblasts revealed 4 candidate genes that were the most significantly differentially expressed in the two cell types; *NKX2.3* and *LRRC17* are highly expressed in myofibroblasts, while *SHOX2* and *TBX5* are highly expressed in fibroblasts (**Chapter 6**). NKX2.3 is essential for TGFβ-induced myofibroblast contraction and migration ability. Knockdown of *NKX2.3* using siRNA caused a decrease of myofibroblast-related gene (*ACTA2, MYH11* and *AOC3*) expression and an increased expression of fibroblast gene, *SHOX2* in myofibroblasts. This suggests that NKX2.3 is a key mediator for maintaining myofibroblast characteristics and functions. Our work presented here shows that myofibroblasts and fibroblasts have significantly different expression profiles for a few key genes and that they differ in their response to TGFβ.

In conclusion, the results clearly show that TGFβ activated fibroblasts and myofibroblasts, as defined by the expression of AOC3 and NKX2.3, are distinctly different cell types. (331 words)

ACKNOWLEDGEMENTS

I would like to express my gratitude to all those who have made this thesis possible. I am extremely grateful to Professor Sir Walter Bodmer for giving me the opportunity to work with, as well as his guidance and support throughout my DPhil study.

Furthermore, I would like to thank to the members of the Cancer and Immunogenetics Laboratory at Oxford, including Jenny Wilding, Neil Ashley, Djamila Ouaret, Ruchi Patel, Matt Jones, Mustak Ibn Ayub, Trevor Yeung and Kamila Koprowska for all you support and advice. It has been a privilege to work with you all. I would like to especially thank Neil for the daily supervision from the first day I joined the lab. Your always encourage me and push me forward. I also thank to Jenny and Djamila for your constant support and enlightening instruction.

I am grateful to Kevin Clark for the expertise in cell sorting, Peter Thomas and Dr Matteo Morotti for their expertise with the confocal and inverted microscope, Dr Lai Mun Wang for the tissue collection and Dr Katalin Di Gleria in Mass Spectrometry Laboratory. I also appreciate had the opportunity to discuss my work with Dr Lai Mun Wang and Professor Valentine Macaulay during for my transfer of status and confirmation as well as being my thesis committee. Finally, thanks to the Clarendon fund and Brasenose College for proving the funding for my research.

I thank all my friends, Guido, Allison, Ruchi and Djamila who have been my biggest support throughout these years.

DECLARATION

I, Lin-Ting Hsia, hereby declare that work on which this thesis is based on my original work and that neither the whole work nor any part of it has been, is being or will be submitted for another degree in this or any other university. The work is original expect where listed by reference in the text.

SIGNED:…….....DATE:…….....

TABLE OF CONTENTS

CHAPTER 1

GENERAL INTRODUCTION

CHAPTER 2

MATERIALS AND METHODS

CHPATER 3

IDENTIFICATION OF THE TARGET PROTEIN OF PR2D3 ON MYOFIBROBLASTS

CHAPTER 4

AOC3, A NOVEL MARKER OF MYOFIBROBLASTS

CHAPTER 5

ISOLATION OF MYOFIBROBLASTS FROM FRESH TISSUES BY FACS USING AOC3 AS CELL SURFACE MARKER

CHAPTER 6

GENE REGULATION OF *NKX2.3* & *SHOX2* IN MYOFIBROBLASTS AND FIBROBLASTS

CHAPTER 7

GENERAL DISCUSSION AND FUTURE DIRECTIONS

LIST OF FIGURES

LIST OF TABLES

LIST OF ABREVIATIONS

APC	Allophycocyanin
bp	Base Pairs
BSA	Bovine Serum Albumin
cDNA	Complementary DNA
CSC	Cancer Stem Cell
CRC	Colorectal cancer
CON	Control
DNA	Deoxyribonucleic Acid
DMEM	Dulbecco's Modified Eagle Medium
DMSO	Dimethylsulfoxdie
dNTP	Deoxyribonucleotide Triphosphate
ECL	Enhanced Chemiluminescence
ECM	Extracellular matrix
EDTA	Ethylenediaminetetraacetic acid
EMT	Epithelial to Mesenchymal Transition
FBS	Fetal Bovine Serum
FACS	Fluorescence-Activated Cell Sorting
FITC	Fluorescein isothiocyanate
IP	Immunoprecipitation
kb	Kilobase
kDa	Kilodalton
mAb	Monoclonal Antibody
MET	Mesenchymal to Epithelial Transition

mL	Milliliter
µL	Microliter
µM	Micromolar
ng	Nanogram
nM	Nanomolar
PAGE	Polyacrylamide Gel Electrophoresis
PBS	Phosphate Buffered Saline
PCR	Polymerase Chain Reaction
PE	Phycoerythrin
PVDF	Polyvinylidene Difluoride
qRT-PCR	Quantitative Reverse-Transcription Polymerase Chain Reaction
RNA	Ribonucleic Acid
RNAse	Ribonuclease
RPM	Reads Per Million
RPM	Revolutions Per Minute
RT	Reverse Transcription
SDS	Sodium Dodecyl Sulfate
SF	Serum free medium
s.e.m.	Standard Error of the Mean
TBS	Tris-Buffered Saline
TBST	Tris-Buffered Saline plus Tween-20
TEMED	N,N,N,N-Tetramethylethylene-diamine
UTR	Untranslated Region
UV	Ultraviolet

CHAPTER ONE

GENERAL INTRODUCTION

CHPATER 1: GENERAL INTRODUCTION

1.1 Human intestinal microstructure and mesenchymal cells

Intestinal epithelium turnover is a rapid process in which cells in the intestinal lining are replaced at least on a weekly basis. This makes the intestine a good model for the study of cell regulation in health and diseases (Heath, 1996). Intestinal homeostasis is closely controlled and depends on the signals from supportive mesenchymal cells and differentiated epithelium (Medema and Vermeulen, 2011). In the large intestinal mucosa, the innermost layer surrounding the lumen of the gut consists of invaginations lined by a columnar epithelium that forms the basic functional subunits called crypts, as well as the lamina propria and muscularis mucosae (**Figure 1.1**). Intestinal mesenchymal cells reside in lamina propria, and consist of pericryptal cells, fibroblasts, pericytes, bone marrow-derived stromal cells and smooth muscle of the muscularis mucosae (Powell et al., 2005).

Pericryptal cells are adjacent to the crypt, separated from epithelial cells by basement membrane. They were originally described as fibroblasts by morphological appearance (Donnellan, 1965, Kaye et al., 1968), but later found to be actively involved in the shrinkage process during wound healing. The first identification of the pericryptal cells as myofibroblasts was based on the staining with the monoclonal antibody, PR2D3 (Richman et al., 1987) and then confirmed by αSMA staining (Sappino et al., 1989). Myofibroblasts are believed to secrete hormones and growth factors that participate in control of epithelial cell proliferation and differentiation and (Humphries and Wright, 2008) and maintenance of the stem cell niche in colonic crypts, in addition to

regulating mesenchymal-epithelial interactions, wound healing, fibrosis and aspects of immune responses (Adegboyega et al., 2002, Owens and Simmons, 2013)

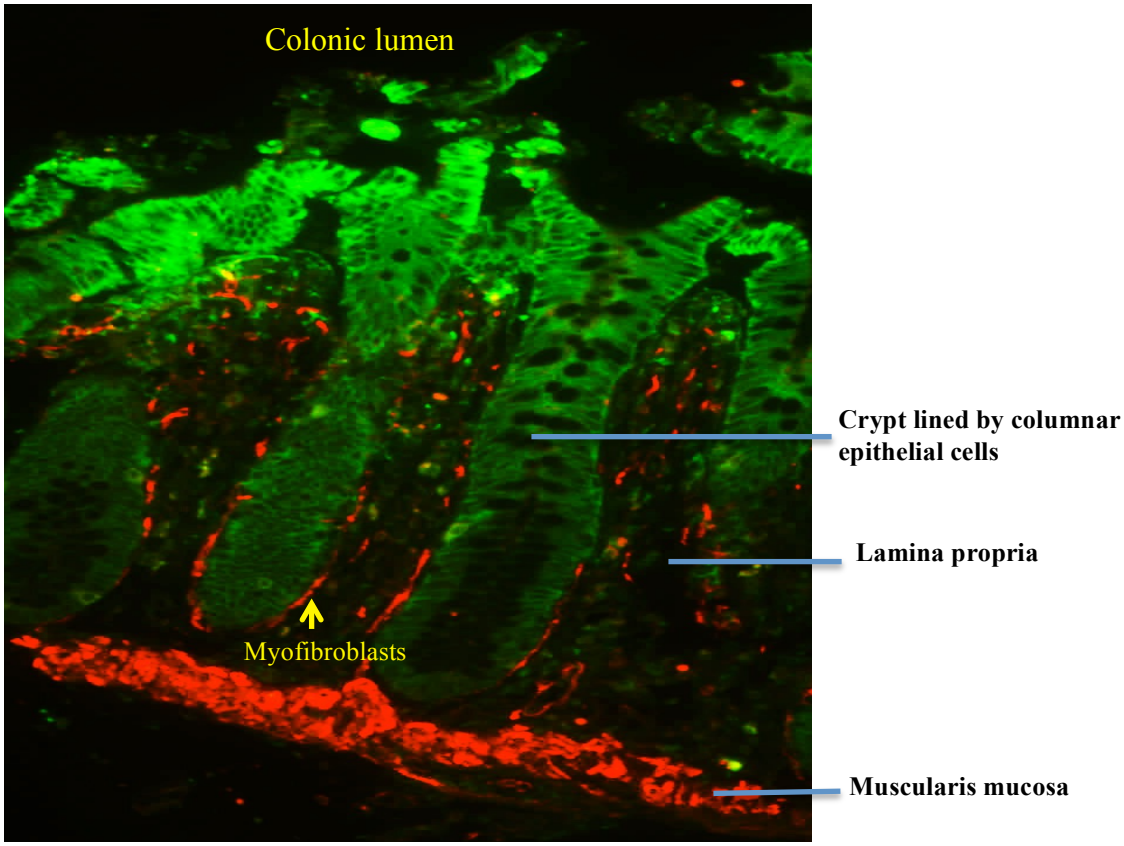

Figure 1.1
Microstructure of large intestinal mucosa
Colonic mucosa indicating polarised columnar intestinal epithelial cells lining crypts, lamina propria and muscularis mucosa. Myofibroblasts are the pericryptal stromal cells that form a sheath surrounding the crypts. Co-staining of paraffin section of human colon with αSMA for myofibroblasts and smooth muscle cells (red). EpCAM staining was used for epithelial cells (green). 40x magnification

1.2 Myofibroblasts

1.2.1 Fibroblasts and myofibroblasts

Fibroblasts are the most common mesenchymal cells in connective tissues that provide maintenance and support by synthesising extracellular matrix components and collagens. Fibroblasts function not only as a scaffold in tissues, but also contribute to the function and migration of other cells (Nolte et al., 2008). After tissue injury, fibroblasts become activated into modified fibroblasts that contract the stroma, bringing the wound margins closer together, and thereby facilitate the healing process (Gabbiani et al., 1971). These modified fibroblasts exhibit many similar properties to smooth muscle cells and were consequently named "myofibroblasts" (Majno et al., 1971). Myofibroblasts may be defined morphologically and immunologically through the expression of cytoskeletal proteins (Sappino et al., 1990, Schmitt-Graff et al., 1994). Currently, the simplest and most widely used definition of myofibroblasts relies on the expression of α-smooth muscle actin (αSMA)(Gabbiani et al., 1973). Following the demonstration by Desmouliere et al that after transforming growth factor β (TGFβ) stimulation, connective tissue fibroblasts were activated to express αSMA (Desmouliere et al., 1993), thereby seemingly acquiring the properties of myofibroblasts, it became widely accepted that TGFβ activated fibroblasts could be defined as myofibroblasts. Subsequently, myofibroblasts defined in this way have been shown to be widely distributed in many different tissues. In addition to TGFβ, mechanical tension has also been shown to induce αSMA expression within fibroblasts maintained on a stiff surface (Arora et al., 1999), through increased expression of αvβ3 integrin (Jones and Ehrlich, 2011).

In tumour stroma, the term myofibroblast comprises a rather heterogeneous cell population with different phenotypes, based on immunohistological observations (Sugimoto et al., 2006). The lack of a clear definition of cell types has lead to publications with confusing and sometimes contradicting terminology. For example, many studies refer to the stromal cells associated with a colon cancer as either cancer-associated fibroblasts (CAFs), stromal fibroblasts, peritumoral fibroblasts, myofibroblasts or αSMA-positive myofibroblasts (Orimo and Weinberg, 2007, De Wever et al., 2008, Semba et al., 2009). Mostly the only criterion used for identification relies on expression of αSMA. However, this generalized term causes confusion in not distinguishing between the various mesenchymal cell types that have different origins, location and function. A finer classification of fibroblasts in the skin (Driskell and Watt, 2015) and lung (Rock and Hogan, 2011) has helped clarify the issue, but clearly there is a need for more specific markers for a proper definition of mesenchymal cell types in tumour stroma.

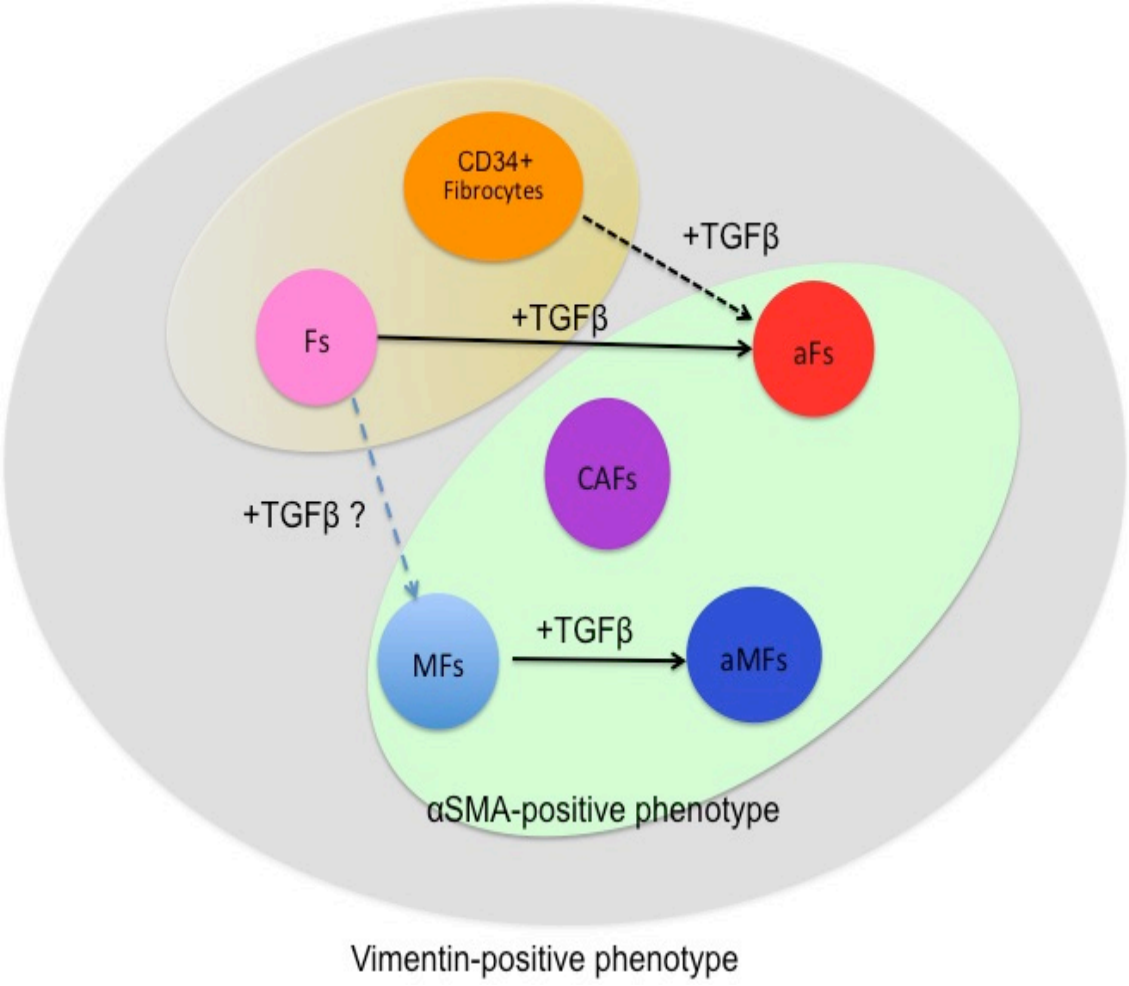

Figure 1.2
Schematic diagram showing the current definition of mesenchymal cells in tumour stroma
Mature fibrocytes are derived from monocyte precursors, express CD34 and exhibit features of both fibroblasts and macrophages. CAFs are extracted from tumour stroma and include a mixture of myofibroblasts, activated myofibroblasts and activated fibroblasts. Orange oval presents αSMA-positive phenotype cells. All stromal cells present here are vimentin positive. Fs: fibroblasts; aFs: activated fibroblasts; CAFs: cancer-associated fibroblasts; MFs: myofibroblasts; aMFs: activated myofibroblasts.

1.2.2 Characterization of myofibroblasts and origins

Myofibroblasts are cells with biochemical and morphological features of both fibroblasts and smooth muscle cells (Phan, 2008). Myofibroblasts are large spindle shape cells with expanded endoplasmic reticula, focal adhesion proteins and fibronexus containing intracellular myofilaments, which can be observed under electron microscopy (Singer et al., 1984, Dugina et al., 2001, Eyden, 2001). Numerous studies have attempted to describe the characteristics of myofibroblasts based on the expression of immunocytochemical markers. A clear definition of the myofibroblast has yet to be established, therefore studies currently use distinct but overlapping definitions. Unfortunately, there is not a single marker that can distinguish myofibroblasts specifically from other cells. The characterization of myofibroblasts has therefore relied variously on combinations of positive markers such as αSMA (ACTA2; alpha 2 smooth muscle actin; actin isoforms specialized in cellular contraction) (Gabbiani et al., 1973), the stress fibre controlling protein palladin 4Ig (PALLD)(Ronty et al., 2006), THY-1 (CD90; cell surface antigen) (Koumas et al., 2003), PDPN (podoplanin; mucin-type transmembrane glycoprotein) (Yamanashi et al., 2009), the intermediate filament vimentin (VIM)(Leader et al., 1987), TEM1 (CD248; sialylated transmembrane endosialin)(Christian et al., 2008), S100A4 (S100 calcium binding protein, formerly named fibroblast-specific protein-1)(Strutz et al., 1995) and platelet derived growth factor receptor β (PDGFRB)(Humphreys et al., 2010); along with negative markers such as the epithelial specific markers EPCAM (epithelial cell adhesion molecule) and specific cytokeratins, monocyte marker CD14, vascular endothelium markers CD31 and CD34, the smooth muscle marker smoothelin (van der Loop et al., 1996) and desmin (might be positive in some tissues). Despite the use of these markers, there still remains

confusion of terminology in the literature and difficulty in being able to distinguish myofibroblasts from fibroblasts.

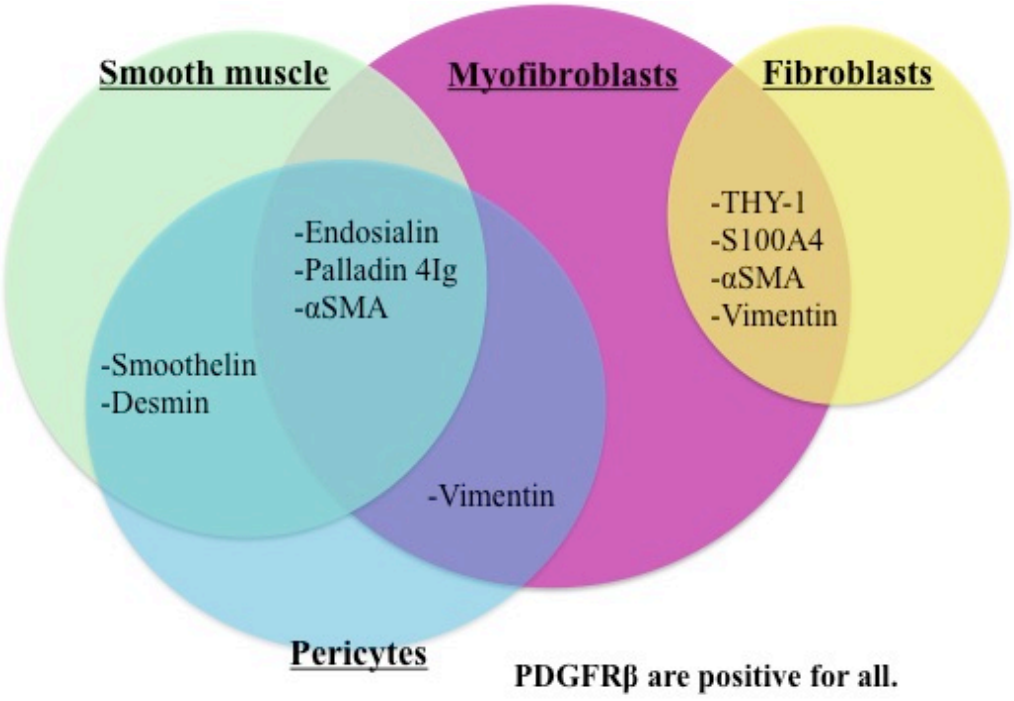

Figure 1.3
Venn diagram showing the current immunohistological markers of myofibroblasts, fibroblasts, smooth muscle cells and pericytes in stroma
No specific marker for either myofibroblasts or fibroblasts in literature so far. Identification of myofibroblasts relies on a combination of multiple markers.
However, αSMA has been reported to show heterogeneous staining in myofibroblasts and also to be positive in some fibroblasts. Note: Vimentin and PDGFRβ are positive for myofibroblasts, fibroblasts, pericytes and smooth muscle cells.

The origins of myofibroblasts in renal and hepatic fibrosis have been extensively described. Originally, myofibroblasts were thought to be the result of local recruitment of fibroblasts, pericytes, perivascular cells, smooth muscles or adipocytes (McAnulty, 2007, Wada et al., 2007, Humphreys et al., 2010). Recent studies showed the evidence that bone marrow cells have striking plasticity to differentiate into stromal myofibroblasts (Direkze et al., 2006) as well as into pericryptal myofibroblasts in the mouse and human small intestine and colon (Brittan et al., 2002). Myofibroblasts have also been suggested to arise from either mesenchymal stem cells (MSCs) or CD34+ fibrocytes (which have CD14+ monocytes as precursor) (Broekema et al., 2007). Another possible cellular source of myofibroblasts is thought to involve either epithelial to mesenchymal transition (EMT)(Kalluri and Neilson, 2003, Zeisberg and Kalluri, 2008) or endothelial to mesenchymal transition (EdoMT)(Zeisberg et al., 2008, Li et al., 2009). Numerous studies have suggested that EMT may be the dominant source of kidney and liver fibrosis (Strutz and Neilson, 2003, Zeisberg et al., 2008, Iwaisako et al., 2012). During the process of EMT, epithelial cells lose some epithelial characteristics, such as expression of E-cadherin (CDH1), ZO-1 (tight junction protein 1) and cytokeratins, and gain expression of more mesenchymal markers, such as vimentin (VIM1), fibronectin (FN1) and snail (SNAI1)(Kalluri and Weinberg, 2009). This transition allows the transformed cells to synthesize matrix proteinases that digest the basement membrane and thereby enable migration into other tissues.

1.2.3 Roles of myofibroblasts including in inflammation and fibrosis

Myofibroblasts can modulate the stroma through direct cell-cell contact or by secretion of extracellular matrix (ECM) proteins, matrix metalloproteinases (MMPs), tissue

inhibitors of metalloproteinase (TIMPs), growth factors, cytokines, and lipid products, or through the expression of specific receptors (De Wever et al., 2008). Myofibroblasts are present in many normal tissues, such as the gastro intestinal tract, prostate, lungs (interstitial contractile cells), liver (hepatic stellate cells), pancreas (pancreatic stellate cells) and uterus where their specific functions may differ (Powell et al., 1999). In normal tissues, myofibroblasts are essential for tissue morphology (Powell et al., 2005) and their contractile capability allows them to participate in the contraction of glands, such as the gastric gland (Adegboyega et al., 2002), and breast lobule (Gudjonsson et al., 2005).

In inflammatory response, myofibroblasts play a crucial role by producing chemokines (IL-8, macrophage proteins)(Andoh et al., 2000), cytokines (IL-1, IL-6, TNF-α)(Shimada et al., 2002, Theiss et al., 2005), and growth factors, such as hepatocyte growth factors (HGF) and fibroblast growth factors (FGF)(Tokunou et al., 2001). Myofibroblasts are also capable of enhancing or downregulating the inflammatory response by secretion of soluble mediators of inflammation, synthesis of prostaglandins and expression of cyclooxygenase-2 (COX-2)(Shattuck-Brandt et al., 2000, Mifflin et al., 2002). When activated, myofibroblasts express adhesion molecules such as intracellular adhesion molecule-1 (ICAM-1)(Doucet et al., 1998) and super-mature focal adhesion (cell–matrix adhesion, FAs)(Dugina et al., 2001), both of which facilitate adhesion to matrix proteins and participate in inflammatory and immune reactions.

Myofibroblasts also contribute in tissue or organ fibrosis. Similar to the healing process, fibrosis is the formation of excessive amount of connective tissues, which resulted from repeated cycles of tissue damages and repair. In many organs such as kidney (LeBleu et

al., 2013), lung, heart, liver (hepatic stellate cells)(Reeves and Friedman, 2002) and pancreas (pancreatic stellate cells)(Masamune et al., 2009), myofibroblasts are primarily involved in fibrosis that suggested being responsible for the increased extracellular matrix synthesis and synthesis of collagens and fibronectin (Benyon and Arthur, 2001, Kinnman et al., 2003).

1.2.4 Mesenchymal epithelial interactions

In the intestine, mesenchymal epithelial interaction is important not only for proper morphogenesis but also for appropriate maintenance of the intestinal homeostasis (Medema and Vermeulen, 2011). Stromal myofibroblasts and muscularis mucosa cells work together with epithelial cells to construct the intestinal stem cell niche in normal tissue and during cancer development through complex signalling mechanisms involving WNT, bone morphogenetic proteins (BMPs) and Hedgehog (Hh) pathways.

In the gut, the Hh pathway generally signals from differentiated epithelial cells to mesenchymal cells, where it is thought to induce secretion of BMPs (van Dop et al., 2009). Hh pathway signalling is essential for the development of mesenchymal cells as constitutive activation of Hh signalling in the colon leads to an accumulation of myofibroblasts and crypt abnormalities in mice (van Dop et al., 2009). In addition, the Gumucio laboratory showed that mislocated myofibroblasts can be found throughout the intestinal lamina propria when Hh paracrine action was disturbed (Madison et al., 2005).

In the intestinal stem cell niche, the Wnt pathway has a crucial role in driving intestinal epithelium proliferation and maintenance of intestinal stem cells. Recent studies have highlighted the importance of stromal myofibroblast secreted Wnt ligands in stem cell homeostasis (Farin et al., 2012). Bone morphogenetic protein (BMP) signalling, however, is a negative regulator of cell proliferation that antagonises Wnt signalling along the crypt axis (Zhang and Li, 2005). BMPs are members of the transforming growth factor- β (TGFβ) superfamily, which share intracellular signalling through the SMAD proteins. BMP2 and BMP4 are expressed by mesenchymal cells and are active at the top of crypt, where differentiation occurs (He et al., 2004). BMPs are also produced at the bottom of crypt but their action there is counteracted by BMP antagonists, such noggin (NOG), expressed by stromal myofibroblasts (Kosinski et al., 2007).

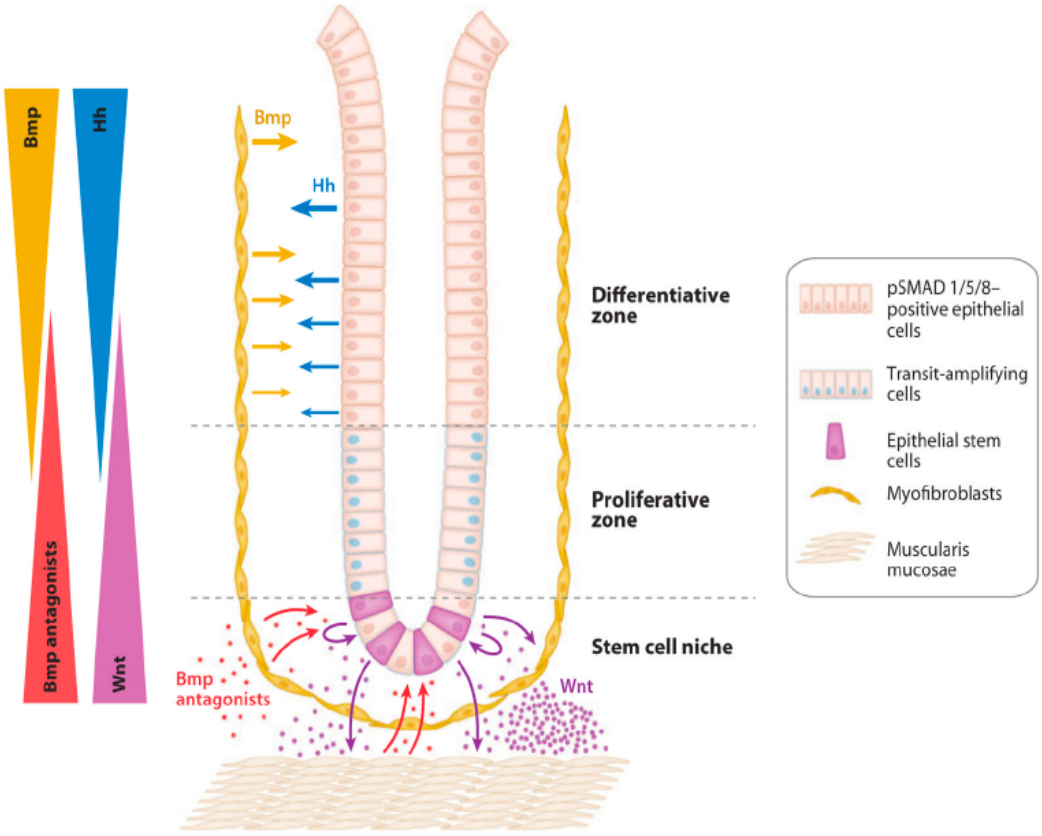

Figure 1.4
Mesenchymal-epithelial interactions in stroma
Epithelial-mesenchymal interactions result in modulation of hedgehog (Hh), bone morphogenetic protein (BMPs) and Wnt signalling pathways in the intestinal crypt. Wnt ligands are secreted around the base of crypt, whereas BMPs are active at the top of the crypt. Hh proteins produced by differentiated epithelial cells triggers stromal BMP synthesis. Figure taken from (Powell et al., 2011).

1.2.5 Contribution of stromal myofibroblasts to invasive cancers

Abundant clinical and experimental data highlight the contribution of tumour stroma to invasion and metastasis. An increase in the number of myofibroblasts associated with primary tumour tissues has been described in many cancers, including breast, colorectal, prostate, pancreatic and gastric carcinomas (Tuxhorn et al., 2002, Orimo et al., 2005, Tsujino et al., 2007, Farrow et al., 2008, Fuyuhiro et al., 2011), as well as in lymph node metastases (Yeung et al., 2013). In addition, increased αSMA expression by myofibroblasts is a predictor of disease recurrence in colorectal cancer (Tsujino et al., 2007) and an indicator of poor prognosis in patients with recurrent pancreatic cancer (Infante et al., 2007).

Dimanch-Boitrel et al showed early evidence in favour of a role for myofibroblasts in invasion *in vitro*. Epithelial cells isolated from a chemically induced colon cancer in rats failed to invade extracellular matric gels by alone, while successful invasion was observed after addition of tumour-associated mesenchymal cells to cancer cells (Dimanche-Boitrel et al., 1994). Similarly, De Wever et al demonstrated the invasive activity of human myofibroblasts *in vitro* by using cancer cells and myofibroblasts isolated from human colon tissues. Primary cancer cells invaded the collagen gels only when myofibroblasts were also added (De Wever et al., 2004). Furthermore, co-culture of cancer cells with myofibroblasts increases the clonogenicity of colorectal cancer cell and expands the cancer stem cell population (Richman and Bodmer, 1988) (S. Ghandi thesis, 2011). Likewise, myofibroblasts express increased levels of markers of activation such as smooth muscle actin when exposed to cancer cells (Webber et al., 2010). These studies suggest a mutual feedback loop resulting from the interaction

between myofibroblasts and cancer stem cells. Several tumour xenograft mouse models and transgenic mouse models have shown that myofibroblasts facilitate invasive tumour growth and explain the complex signaling between the epithelium and the stroma (De Wever et al., 2004, Orimo et al., 2005, Calon et al., 2015).

1.3 AOC3 (Amine oxidase copper containing 3)

The findings in this thesis identify AOC3 as a marker of myofibroblasts. Although its expression has not previously been linked to myofibroblasts, much of the work presented in this thesis involves characterization of AOC3 expression and function, and a summary of what is currently known about the function of AOC3 is therefore provided below.

AOC3 (amine oxidase copper containing 3; copper amine oxidase; semicarbazide sensitive amine oxidase, SSAO) is also called VAP-1 (vascular adhesion protein-1) because of its role in lymphocyte endothelial interaction. Although VAP-1 is the more commonly used gene symbol in many publications, the HGNC (human genome nomenclature committee) approved gene symbol is AOC3, and therefore, that is the symbol that will be used from this point forward.

AOC3 was originally identified as the target protein of mAb 1B2, a murine antibody that blocked lymphocyte binding to endothelial venules (Salmi and Jalkanen, 1992). AOC3 is abundantly present in normal tissues in the endothelial cells of veins, in adipocytes and in smooth muscle cells, but not in other types of muscles (Salmi and Jalkanen, 1992). The tissue distribution of AOC3 on endothelial cells highlights its

function as an adhesion molecule able to recognise and recruit lymphocytes during inflammation (Jalkanen and Salmi, 1993).

1.3.1 Protein structure of AOC3

AOC3 is a type II transmembrane protein of 90 kilo Dalton (kDa) attached to the cell surface by an N-terminal helix. It has a heavily glycosylated extracellular domain, while the intracellular domain is much shorter with only 4 amino acids (Smith et al., 1998, Bono et al., 1998). The X-ray crystal structure of this protein shows that AOC3 appears to be a heart-shape homodimer of 170-180 kDa, depending on the degree of glycosylation. The active sites are located on each extracellular domain, containing a copper and a topaquinon cofactor binding site (Airenne et al., 2005). There are multiple N-and O-linked oligosaccharides located on the top of the molecule, which may be important for its function in adhesion (Maula et al., 2005).

1.3.2 Semicarbazide-sensitive amine oxidase (SSAO)

AOC3 is an amine oxidase. Amine oxidases (AO) are enzymes that catalyse the oxidation of primary amines. Based on the attached cofactor, amine oxidases are classified into two groups: flavin-containing and copper-containing amine oxidases. Monoamine oxidases (MAO)-A and –B are flavin-containing amine oxidases, which are bound to the outer of membrane of mitochondria and have an important role in the metabolism of neurotransmitters and other biogenic amines. Cloning of human AOC3 revealed it belongs to the copper-containing amine oxidases based on its significant sequence homology with other enzymes with similar activity (Bono et al., 1998, Smith

et al., 1998). These copper-containing oxidases are known to be sensitive to inhibition by semicarbazide and are therefore referred to as SSAO (Jalkanen and Salmi, 2001). In humans, there are four copper-containing amine oxidase (AOC) genes encoding: diamine oxidase (*AOC1*), retina-specific amine oxidase (*AOC2*), vascular adhesion protein-1 (*AOC3*) and a pseudogene (*AOC4*) that has no known function in man (Schwelberger, 2010).

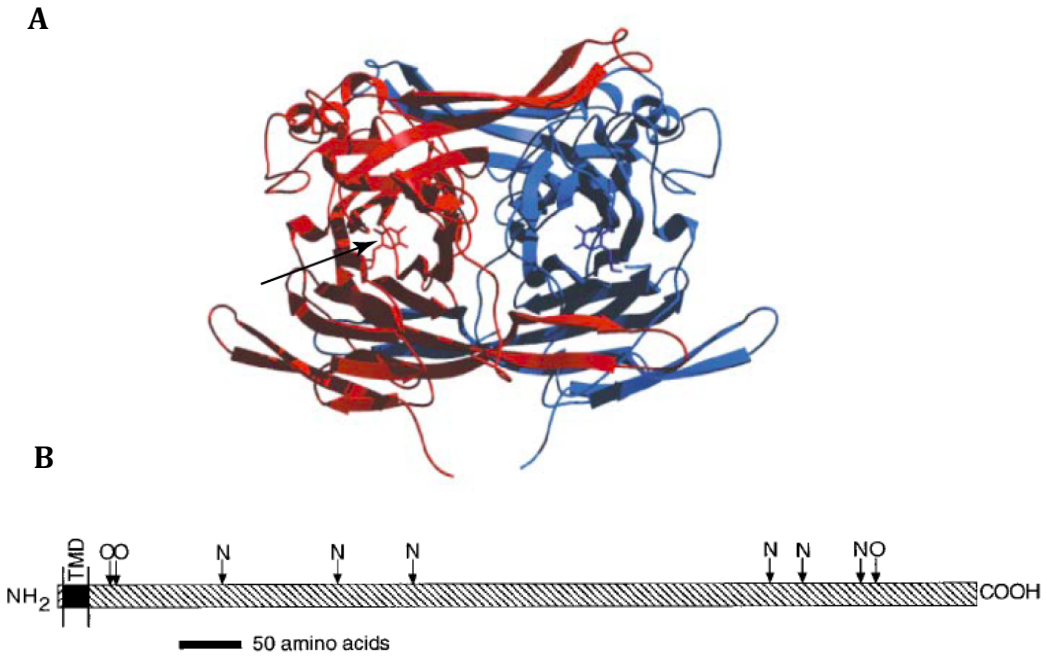

Figure 1.5
Structure of AOC3
AOC3 is a homodimeric transmembrane protein and (A) shows an overall fold of the active domain of AOC3. Monomers are indicated in blue and red, that contain the active site, which is indicated by the black arrow in the red colored monomer on the left. Figure taken from Salmi and Jalkanen, 2001. (B) Molecular cloning of AOC3 revealed a type 2 glycoprotein with potential N-glycosylation sites and putative O-glycosylation sites (indicated by N or O and arrows). The transmembrane domain is between residues 5 and 27 (TMD: transmembrane domain). Figure taken from (Smith et al, 1998)

1.3.3 AOC3 is a multifunctional protein

In addition to the membrane-bound form, a soluble form of AOC3 is also found in serum circulating in blood (Gokturk et al., 2003, Stolen et al., 2004b). The soluble form is cleaved and shed from the extracellular domains of membrane bound AOC3, the shedding which is controlled by TNF-α and insulin in some cell types (Abella et al., 2004). As a SSAO enzyme, AOC3 catalyzes the deamination of both endogenous (methylamine in endothelial cells)(Bonaiuto et al., 2010) and exogenous (benzylamine in smooth muscle cells) (Jaakkola et al., 1999) substrates, resulting in the generation of aldehydes, hydrogen peroxide and ammonia.

$$RCH_2NH_2+O_2+H_2O \rightarrow RCHO+NH_3+H_2O_2$$

(Reviewed in (Jalkanen and Salmi, 2008))

These products of the enzymatic activity of SSAOs have been shown to have biologically active effects on the local microenvironment and promote unwanted protein cross-linking (Mathys et al., 2002, Seiler, 2002). *In vitro* studies have shown that the product of methylamine oxidation (formaldehyde) is cytotoxic to human endothelial cells (Yu et al., 1997, Sole et al., 2008) and could initiate and sustain hepatic injury (Yu, 1998). Hydrogen peroxide can also act as a signalling molecule to regulate various biological processes or can initiate oxidative stress following conversion to hydroxyl free radicals (Muzykantov, 2001, Veal and Day, 2011).

Anti-AOC3 monoclonal antibodies (mAbs) are functional as blocking antibodies that block lymphocyte binding in several *in vitro* assays, while small molecule SSAO

enzyme inhibitors also block the interaction between leukocyte and endothelial cells (Martelius et al., 2008, Marttila-Ichihara et al., 2010). However, the SSAO enzyme activity is not inhibited by any anti-AOC3 mAbs, even when lymphocyte binding is inhibited (Koskinen et al., 2004, Maula et al., 2005). This suggests that enzyme activity is required and essential for cell adhesion, as well its inflammatory function (Noonan et al., 2013). As an adhesion molecule, it binds to leukocyte ligands through the surface epitopes defined by anti-AOC3 mAbs, and enzymatic activity of AOC3 contributes to leukocyte binding, rolling and adhesion (**Figure 1.6**).

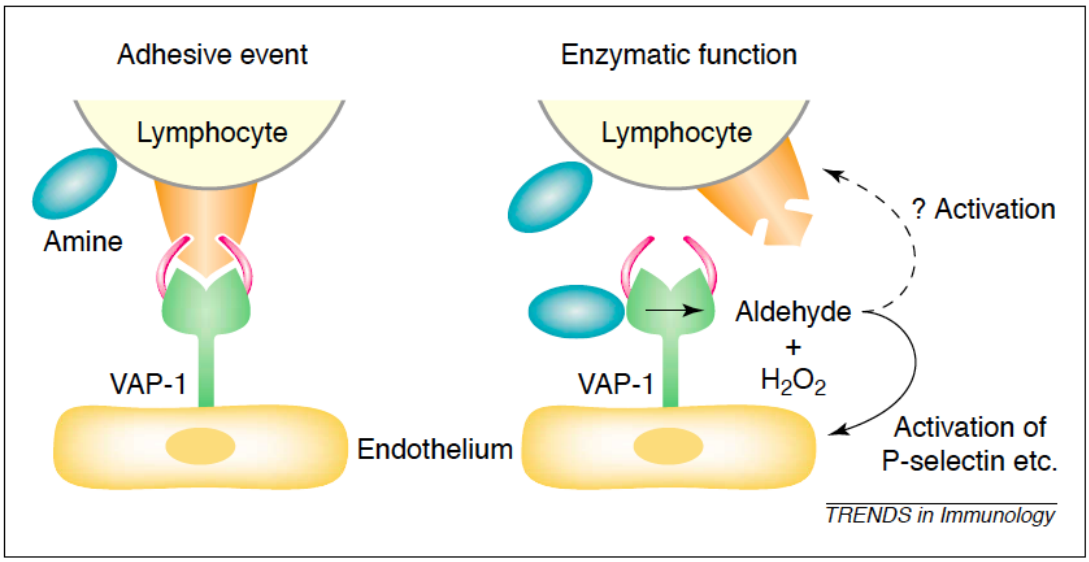

Figure 1. 6
Dual functions of AOC3/VAP1 in endothelial cells
AOC3 in endothelial cells is an adhesion molecule and semicarbazide-sensitive mono-amine oxidase (SSAO). The adhesion function involves binding to a counter receptor of lymphocytes with the modified oligosaccharides chains of AOC3. As an enzyme, AOC3 converts soluble primary amines into corresponding aldehyde with the reaction products. In addition, AOC3 can bind to the primary amine presented on lymphocytes and form a transient but covalent crosslink between endothelial cells and lymphocytes while rolling. Figure from (Salmi and Jalkanen, 2001)

1.3.4 AOC3 is inflammation-inducible in endothelial cells

In endothelial cells, AOC3 is abundantly expressed in high endothelial venules and flat endothelial cells. Under normal conditions, AOC3 is mainly stored in intracellular vesicles. In most inflamed tissues, it is translocated onto the luminal surface of endothelial cells where it mediates the adhesion and transmigration of circulating leukocytes into peripheral tissues (Jaakkola et al., 2000). Studies show that the soluble form of AOC3 is increased at many sites of inflammation, including inflammatory bowel disease and liver inflammation (Kurkijarvi et al., 1998, Koutroubakis et al., 2002).

1.3.5 AOC3 is an oxidase in smooth muscle cells

AOC3 in smooth muscle cells has several overlapping features with AOC3 in endothelial cells, but smooth muscle AOC3 is also functionally and structurally distinct. Smooth muscle AOC3 only functions as an SSAO and is not involved in lymphocyte binding. Structurally, smooth muscle AOC3 can be detected as diametric (160 kDa) and trimetric (250 kDa) forms and with abundant sialic acid decorations but no major O-linked glycosylation on the side chains, which results in the size difference from endothelial AOC3 (Jaakkola et al., 1999). Moreover, smooth muscle AOC3 is only present on the cell surface and cannot be induced *in vitro* by cytokine and other inflammatory mediators, while elevated levels of endothelial AOC3 can be seen in inflammatory sites (Arvilommi et al., 1997).

1.3.6 AOC3 in disease pathogenesis

In addition to the response to inflammation, AOC3 also has well-established roles in transporting glucose in adipocytes via the glucose transporter, GLUT4 (Enrique-Tarancon et al., 2000, Abella et al., 2003) and in lipid homeostasis (Morin et al., 2001). In mouse models, overexpression of human SSAO enzyme leads to an abnormal structure of arteries and diabetes-like complications in smooth muscle cells (Gokturk et al., 2003) and endothelial cells (Stolen et al., 2004a), respectively, while impaired leukocyte trafficking into lymph node and spleen during inflammation was observed in AOC3-deficicient mice (Stolen et al., 2005). Increased levels of serum AOC3 and SSAO enzyme activities have been reported in a number of inflammatory diseases, including rheumatoid arthritis, inflammatory bowel disease, diabetes and atherosclerosis

(Kurkijarvi et al., 1998, Meszaros et al., 1999, Garpenstrand et al., 1999, Koutroubakis et al., 2002). Such increased activity has also been used to suggest cancer-related mortality in hepatocellular carcinoma (Kemik et al., 2010) and colorectal cancer. The *AOC3* gene is amplified in gastric cancer (Varis et al., 2002) and it is overexpressed in the tumour endothelium of liver, head and neck cancers (Irjala et al., 2001). Recent studies showed that small molecule inhibitors of AOC3 enzyme activity could reduce melanoma and lymphoma tumour growth by reducing the myeloid cells or lymphocytes infiltration (Marttila-Ichihara et al., 2010, Li et al., 2013); AOC3 inhibitors have also been used in anti-inflammatory therapy, such as in vascular diseases and chronic inflammation caused hepatic fibrosis (Koskinen et al., 2004, Kurkijarvi et al., 2000).

1.4 Other transcription factors

In this section, two transcription factors NKX2.3 and SHOX2, identified from microarray expression profiles to be gene signatures of myofibroblasts and fibroblasts respectively will be discussed.

1.4.1 *NKX* genes

NK genes in vertebrates are a gene family encoding for homeodomain-containing transcription factors that have been shown to participate in cell specification and morphogenetic events (Guazzi et al., 1990, Lyons et al., 1995).

Nkx 2.1 was first identified in vertebrates, and five other family members were first identified in mice (Price et al., 1992, Price, 1993). Expression of *Nkx 2.1* overlaps with *Nkx 2.2*, expressed specifically in the central nervous system (Price et al., 1992); *Nkx 2.3*, *Nkx 2.5* and *Nkx 2.6* are expressed in mesendoderm and mesoderm derived cells (2000 Pabst). The *Nkx 2.4* expression pattern has not yet been characterised. During development, Mouse *Nkx 2.3* is expressed in mesoderm of the gut and spleen and involved in gut structures (Pabst et al., 1997). *Nkx 2.5* is an important paralog gene of *Nkx 2.3*, known to regulate genes involved in cardiogenesis (Kasahara et al., 1998, Stanley et al., 2002). Two additional *NKX2* genes, *nkx 2.7* and *nkx 2.8* have been cloned in zebrafish (Brand et al., 1997, Lee et al., 1996), and also *Nkx 2.9* from mouse (Pabst et al., 1998).

1.4.1.1 Expression and function of NKX2.3

The human *NKX2.3* gene (NK2 transcription factor related, locus 3) is located at chromosome 10q24.2. The gene encompasses 3592 base pairs (bp) and encodes for a 364 amino acid protein. NKX2.3 protein contains a transcriptional repressor tinman domain (TN), a homeodomain, a NK2 specific domain and a transcriptional activation domain (**Figure 1.7**). NKX2.3 is mesenchymally expressed in the small intestine and spleen, and also in lymph node B cells and microvascular endothelial cells (Pabst et al., 1997, Pabst et al., 1999, Wang et al., 2000, Yu et al., 2010a).

NKX2.3 acts as a transcription factor in the nucleus, where it plays an important role in regulating gene transcription. Studies from *NKX2.3* knock down followed by mRNA microarray analysis show there are several genes and pathways regulated by NKX2.3, including *EDN1* (endothelin 1) gene and nitric oxide (NO) synthase, vascular endothelial growth factor (VEGF) and AKT pathways, which are involved in immune and inflammatory responses, and cell adhesion and angiogenesis in endothelial cells and B cells (Yu et al., 2010a, Yu et al., 2011). NKX2.3 also regulates cell growth and proliferation by negative regulation of downstream targets, Bmp2 and Bmp-4 (Pabst et al., 1999).

Results from NKX2.3 deficient mice demonstrate impaired structure of the spleen and abnormal crypt development in the small intestine (Pabst et al., 1999), and show that it is required for heart formation (Fu et al., 1998) as well as salivary gland and tooth morphogenesis (Biben et al., 2002). Further studies have shown that NKX2.3 is essential for the correct localization of lymphocytes in spleen for B cell maturation and

T cell-dependent immune response in mice (Tarlinton et al., 2003), as well as being essential for the regulation of lymphocyte homing via the adhesion molecule, MAdCAM-1 in mice (Pabst et al., 2000, Wang et al., 2000, Czompoly et al., 2011).

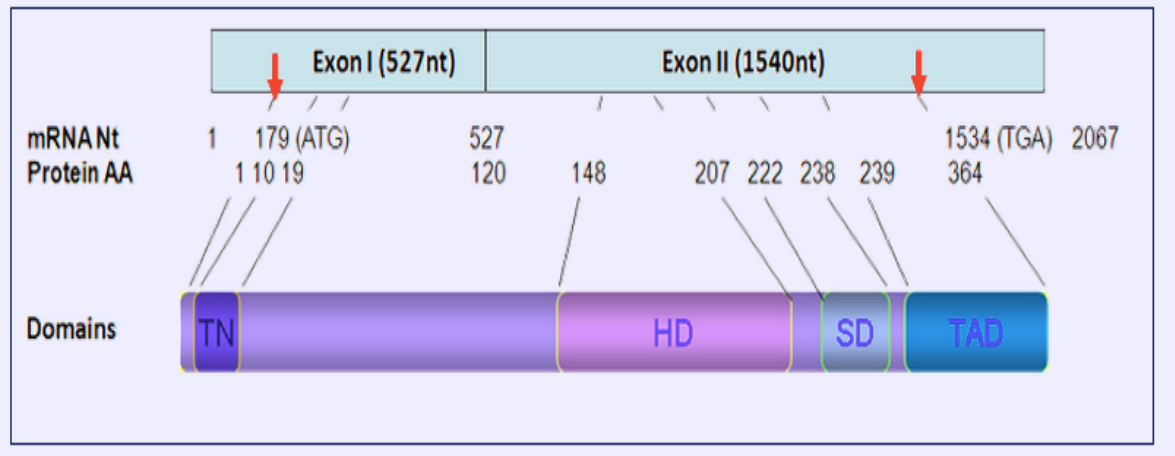

Figure 1. 7
Human NKX2.3 mRNA and protein domains
The gene for *NKX2.3* consists of two exons of 527 and 1540 bp, respectively and one intron of 1496 bp. The NKX2.3 protein is a 364 amino acid protein including a TN (tinman domain), HD (homeodomain), SD (NK2 specific domain) and TAD (transcriptional activation domain). Figure and data from ENSEMBL transcript (http://www.ensembl.org/index.html)

1.4.1.2 *NKX2.3* gene is associated with inflammatory bowel diseases (IBD)

Crohn's disease (CD) and ulcerative colitis (UC) are the two main severe subtypes of inflammatory bowel diseases (IBDs), both of which have a genetic component contributing to the development of IBD (Cho, 2008). *NKX2.3* was identified as an IBD associated gene from a genome wide association study (GWAS) (Welcome Trust Case Control Consortium)(2007) and several groups have confirmed this in different cohorts from the Netherlands, Eastern Europe, Japan and Italy (Weersma et al., 2009, Meggyesi et al., 2010, Latiano et al., 2011, Arimura et al., 2014). The later studies confirm that the *NKX2.3* mRNA level is upregulated in intestinal tissues from CD patients (Yu et al., 2009).

1.4.1.3 NKX2.3 is a negative regulator in colorectal cancer

NKX2.3 is located at chromosome 10, in a region suggested to be high frequency loss of heterozygosity (LOH) in sporadic colorectal cancer. RT-PCR results indicate that *NKX2.3* is down-regulated in sporadic CRC patients, and suggests an inhibitory role of epithelial proliferation (Gregorieff and Clevers, 2005, Wang et al., 2008). High expression of NKX2.3 was found in CRC patients who have response to FOLFOX4 chemotherapy compared to the drug-resistant group with 85% accuracy, suggesting it can be used as a biomarker to predict the efficacy of chemotherapy (Li et al., 2012). Furthermore, lower levels of NKX2.3 expression in liver metastasis compared to primary tumours also support a negative regulator role for NKX2.3 (Leja et al., 2009). Together, it indicated that NKX2.3 is associated with prognosis in a variety of cancers.

1.4.2 Short stature homeobox 2 (SHOX2)

SHOX2 is identified from the expression signature of fibroblasts from our microarray data analysis. Opposite to NKX2.3, SHOX2 is highly expressed in fibroblasts but absent in myofibroblasts. Given the specificity of SHOX2 expression in fibroblasts, which has not yet been described in the literature, further characterization of this gene in terms of its role in fibroblast activation is essential.

1.4.2.1 Function and expression of SHOX2

SHOX2, a second member of the short stature homeobox gene family, is found only in vertebrates. This suggests a role in internal skeletal development and related structures (Clement-Jones et al., 2000). Human *SHOX* and *SHOX2*, have overall 83% homology at the amino acid level and contain an identical homeodomain (Blaschke et al., 1998). In humans, *SHOX* mutations have been associated with inappropriate bone development and body growth conditions, including Turner syndrome, Leri-Weill dyschondrosteosis and Langer dysplasia (Bobick and Cobb, 2012, Hirschfeldova et al., 2012). *SHOX2* expression has been observed in developing limbs and heart in human embryos (Clement-Jones et al., 2000). *SHOX2* has not so far been linked to any known human syndromes. The mouse *Shox2* ortholog shares 99% identity at the amino acid level with its human counterpart (Cobb et al., 2006) and *Shox2* knock-out and knock-down mice have revealed its crucial role in the development of heart, limbs, palate and other organs (Cobb et al., 2006, Yu et al., 2005, Yu et al., 2007, Espinoza-Lewis et al., 2009). SHOX2 acts as a transcriptional factor, directly regulating the transcription of its target genes. It has been shown to be essential for control of differentiation of murine cardiac

pacemaker cells through direct transcriptional repression of Nkx2.5 (Espinoza-Lewis et al., 2009). It has also been shown to regulate Tbx5 by regulating Bmp4 transcription in cardiomyocytes (Puskaric et al., 2010).

1.4.2.2 SHOX2 in carcinogenesis

There is emerging evidence indicating that DNA hypermethylation of the *SHOX2* locus is associated with *SHOX2* gene amplification, (with no resultant observable effect on protein expression) in lung cancer patients (Schneider et al., 2011). DNA methylation of SHOX2 detected in plasma, bronchial aspirates and tumour tissues has been suggested to be a useful biomarker to predict outcome in lung cancer patients (Kneip et al., 2011, Dietrich et al., 2012). A potential role for SHOX2 in carcinogenesis is supported by observations that upregulated levels of SHOX2 mRNA and protein are significantly associated with tumour recurrence in hepatocellular carcinoma (Yang et al., 2013). Results from breast tumour profiling revealed that high expression of SHOX2 is correlated with poor survival in breast cancer patients (Luo et al., 2013). Further studies show that SHOX2 involved in epithelial-to-mesenchymal transition (EMT) via the TGFβ signalling pathway and is also a direct target of miR-375, which is an important suppressor of EMT in breast cancer cells (Hong et al., 2014).

1.5 Aims of this thesis

As discussed, a growing body of evidence has suggested the importance of myofibroblasts in both normal tissues and tumours. However, there still exists significant confusion in terms of the definition and identification of these cells, which strongly supports the need for further investigation. The main goal of this thesis is to characterize candidate myofibroblast markers through the identification of the target protein/s bound by PR2D3 mAb, along with the identification and characterization of novel candidate markers through whole genome microarray analysis of genes differentially expressed between colonic-derived myofibroblasts and normal human skin fibroblasts.

In summary, the primary aims of this thesis are as follows:

1. Identify the target protein/s of the in house mAb PR2D3.
2. Characterize the expression of AOC3 in myofibroblasts in a range of normal and cancerous tissues and explore mechanisms that control regulation of AOC3 expression and enzyme activity.
3. Evaluate the application of AOC3 in FACS sorting of myofibroblasts from fresh tissues.
4. Identify new gene expression signatures of myofibroblast and fibroblasts via whole genome microarray analysis.
5. Evaluate potential candidate genes in myofibroblasts or fibroblasts and characterize the gene regulatory effects of NKX2.3, the key transcriptional factor identified in myofibroblasts.

CHAPTER TWO

MATERIALS
&
METHODS

CHAPTER 2: MATERIALS & METHODS

2.1 Reagents and Suppliers

Reagents and chemicals were supplied from Sigma-Aldrich (UK) unless otherwise stated. Cell tissue culture flasks and plates were supplied from Corning (USA). All the cell lines were cultured in Gibco® cell culture media by Life Technologies.

2.2 Cell culture Methods

2.2.1 Cell lines

The human colorectal cancer cell lines HCT116, LS174T, RKO and SW1222 and human foreskin fibroblasts and normal skin fibroblasts were, for the purposes of this thesis, obtained from cryogenic storage of the Cancer and Immunogenetics laboratory (CIL) at the Weatherall Institute of Molecular Medicine (WIMM), Oxford, UK. The SW1222 cell line was originally a gift from Dr Meenhard Herlyn of the Wistar Institute, Philadelphia, USA. CCD-18CO cell line was purchased from American Type Culture Collection (ATCC, no. CRL1459) and was originally derived from neonatal colonic mucosa. Fore skin fibroblasts were purchased from ATCC, and skin fibroblasts were derived from two different adult individuals many years ago in the Bodmer laboratory using conventional approaches.

2.2.2 Establishment of primary colon myofibroblasts

Fresh surgical specimens from 12 patients undergoing surgery for colorectal tumours (Oxford University Hospitals, UK) were used for the establishment of primary colon myofibroblasts with consent from patients. The study was approved by the local research ethics committee. Myofibroblasts were isolated from cancer and normal colonic regions of whole colon tissues as determined by gross examination by Dr LaiMun Wang, a consultant histopathologist. Tissues were dissected and then digested with collagenase type IV (1 mg/ml; Worthington, Biochemical corporation) at 37°C for 3 hours in Dulbecco's Modified Eagle's Medium (DMEM) without serum. Cell-enriched suspension was filtered by a 250μM nylon mesh (Pierce Biotechnology Inc, Rockford, IL, USA) to remove tissue clumps, and was then centrifuged at a 250x*g* for 5 minutes. Supernatant was discarded and tissue pellet was resuspended in DMEM with 10% FBS and the cells were cultured on tissue culture plates. The successful primary myofibroblast cultures are myo1998, myo2020, myo2156, myo6024, myo6544, myo6769, myo6769C, myo6539, myo6550, myo6550C, myo6426 and myo7659. **Table 2.1** summarizes some information about the primary myofibroblasts cultures including the localization site of the tissue. We used myofibroblasts passaged for up to 10 passages for subsequent experiments, in order to minimize the culture stress and avoid studies with primary myofibroblast cultures undergoing replicative senescence.

Cell Lines	Cancer/Normal	Origin	Note
Myo 6024	Normal	Rectum	
Myo 6539	Normal	Sigmoid colon	
Myo 6550	Normal	Sigmoid colon	* from same patient
Myo 6550C	Cancer	Sigmoid colon	* from same patient
Myo 6769	Normal	Ascending colon	** from same patient
Myo 6769C	Cancer	Ascending colon	** from same patient
Myo 6544	Normal	Descending colon	
Myo 6526	Normal	Sigmoid colon	
Myo 7659	Normal	Sigmoid colon	
Myo 7395	Normal	Sigmoid colon	
Myo 1998	Normal	Normal	From Dr Neil Ashley
Myo 2020	Cancer	CRC	From Dr Neil Ashley
Myo 2156	Cancer	CRC	From Dr Neil Ashley

Table 2.1 List of the primary myofibroblasts established in the Bodmer lab. Cell lines derived from the same patient are highlighted with the same colour in column 1.

2.2.3 Cell culture condition

All cell lines were grown in 75cm^2 vented tissue culture flasks, (Corning) filled with 10 mL of culture medium. All cell lines were cultured in Dulbecco's modified Eagle medium (DMEM), supplemented with 10% fetal calf serum, 1% L-glutamine, and 1% Penicillin/Streptomycin, and incubated at 37°C in an atmosphere containing 95% humidity and 10% CO_2

2.2.4 Cell culture maintenance

Cells were cultured in flasks in DMEM and passaged when they were approximately 70-80% confluence. Cells were passaged into new flasks by washing with 10 mL absolute phosphate buffered saline (PBSA) and detached by incubating cells with 2 mL trypsin/EDTA solution for 5 minutes in 37 °C. 10 ml of complete medium were added to neutralize the trypsin and the cell suspension was gently pipetted up and down multiple times to break cellular clumps. Subsequently, cells were centrifuged at 1,500 rpm for 5 min and resuspended in 10 mL medium for continue culture. Based on cell line growth characteristics, cell suspensions were divided into new flasks at a 1:5 to 1:10 dilution.

2.2.5 Cell counting

The cell count was determined using a Cellometer Auto T4 (Nexcelom Biosciences, USA) allowing ~~an~~ automated cell counting. Briefly, 20 µL of the cell suspension were loaded onto a disposable cell counting chamber and inserted into the Cellometer. The software allows the capture of eight areas of the cell counting chamber and directly calculates the concentration of cells per mL

2.2.6 Cell storage and retrieval

To prepare cells for vapor phase of liquid nitrogen storage, myofibroblast cells, from 80% confluent tissue culture flasks were detached using trypsin and centrifuged at 1500 rpm for 5 minutes. Cell pellets were then resuspended in 1ml of fetal bovine serum (FBS) containing 10% dimethyl sulfoxide (DMSO) and transferred into sterile cryogenic vials (Corning, USA), placed on dry ice for 90 minutes before transferring them into cryogenic tanks with liquid nitrogen at -150ºC for long-term storage. To thaw

the cells, frozen cryogenic vials were incubated in a 37ºC water bath for about 1 min, resuspended in 10 mL of serum free media and then transferred into a 75 cm^2 cell culture flask for incubation at 37°C.

2.2.7 Mycoplasma contamination testing

Cell cultures were regularly tested for Mycoplasma contamination using MycoAlert Assay kit. (Lonza, Maine, USA). Briefly, cell lines to be tested were kept in culture for at least 48 hours before collecting 1mL of medium. This aliquot was then centrifuged (1000rpm, 5 minutes) to remove the cell debris. 100µL of cleared supernatant was transferred to one well of a white-walled microplates (96 wells) and 100 µL of MycoAlert reagent were added for 5 minutes incubation at room temperature. The background fluorescence (Reading A) was measured using FLUOstar OPTIMA Luminometer (Offenburg, Germany). Next, 100µL of substrate were added to each sample and incubated for 10 minutes, and then fluorescence was measured (Reading B). The cells were considered to be negative for mycoplasma if the ratio of reading B to reading A was less than 1. Cultures yielding a ratio between 1 and 2 were kept in culture for one more week before running another mycoplasma test. A ratio greater than 2 indicated a mycoplasma contamination and cells were immediately discarded.

2.2.8 Transient siRNA transfection

siRNAs were introduced into myofibroblast cells *in vitro* by direct transfection using Oligofectamine transfection reagent (Life Technologies, USA). siRNAs were ordered with pre-designed sequences from Eurofins (Eurofins MWG Operon, Luxembourg) or Qiagen (Qiagen, USA). A final concentration of 20nM siRNA was used in a total

volume of 3mL per well in a 6-well plate. siRNA complexes were prepared from a 10 μM siRNA stock solution. Briefly, a volume of 1.5 μL siRNA stock solution was diluted into 150 μL serum-free Opti-MEM® (Life Technologies, USA). Then that RNA-Opti-MEM solution was mixed 1:1 with the Oligofectamine transfection reagent solution. Cells were seeded one day before transfection in DMEM 10% FCS without antibiotics. Mixed siRNA complexes were then added into cells. After 4 hours incubation, 3X of the normal serum concentration DMEM was added to the end to adjust to 3 mL with DMEM + 10% FBS per well.

2.2.9 SSAO enzyme activity assay

The Amplex® Red Monoamine Oxidase assay (Life Technologies, USA) was used to measure SSAO activity from the cells. Briefly, cells were lysed in 0.2% NP-40 (Sigma-Aldrich) in PBS, and 100μg clarified supernatant by centrifugation was used in the assays. Samples were incubated with or without semicarbazide (SSAO inhibitor) and then benzylamine (SSAO substrate) was added. Formation of hydrogen peroxide was followed kinetically after addition of the Amplex red detection mixture by measuring the fluorescence using a SpectraMax M2 multimode microplate reader (Molecular devices, USA). Specific SSAO activity was counted by subtracting the values derived from the no-amine oxidase control.

2.2.10 Transwell® migration assay

Myofibroblast cells were transfected with siNKX2.3 for 24 h and subsequently trypsinized. 1 x 10^4 transfected cells were resuspended in serum-free media and placed in Transwell®-24 well inserts (Corning, USA) containing an 8.0 μm pore polycarbonate membrane. These inserts were placed in wells with colorectal cancer epithelial cells

seeded 48 hours previously as a chemoattractant on the lower compartment. Serum containing media were discarded and replaced by serum free medium in both upper and lower chambers. After 48 hours, cells that had migrated through the membrane of Transwell® inserts were fixed, stained by Diff-Quik Stain (Thermo Fisher Scientific, UK) and the number of migrating cells counted using EVOS® XL core microscope (Life technologies, USA).

2.2.11 Gel contraction assay

Collagen gels were prepared with Collagen 1, bovine (Life technologies, USA), 10X MEM, 0.005N NaOH and diH_2O. Myofibroblast cells were collected using trypsin-EDTA for 5 minutes, washed and resuspended into the collagen gel mixture (60 µl) with 10,000 cells in each well of a 96- well plate. The formation of collagen gel was induced by incubation at 37 °C under 10% CO_2 for 1 hour. After the gels formed, 100 µl of serum free DMEM was added to each well. The gels were freed from the walls of the culture wells with a microspatula 24 hours after gelling and used for the experiment. The diameter of the collagen gel was measured with Image J software at indicated time points after stimulation.

2.3 RNA Methods

2.3.1 RNA extraction

Total RNA was isolated from cells using the RNeasy (Qiagen, USA) kit according to the manufacturer's instructions. Cultured cells were washed by PBS and collected from culture dishes (6-well plate) by scraping into a microcentrifuge tube using a cell lifter. After gentle centrifugation, the supernatant was removed and 00 µL RNase-free water

and 350 µL Lysis buffer RLT were added. The cell lysates were homogenized by vortexing for 1 minute and diluted with 250 µL of 100% ethanol. Diluted sample was transferred into an RNeasy Mini spin column and spun for 15 seconds. The Column was then washed with 500µL of wash buffer RPE twice. Finally total RNA was eluted in 35 µL of nuclease-free H_2O, and stored at -80° for future use. Concentration and quality were assessed by Nano-Drop spectrophotometry after each thaw.

2.3.2 Reverse transcription

2µg of extracted total RNA was reversed transcribed to complementary DNA (cDNA) by using High Capacity cDNA Reverse Transcription Kit (Applied Biosystems Inc. CA) according to the manufacturer's instructions. In brief, diluted RNA (10 ng/µl) mixed with 10X RT buffer, 25x dNTP mix, 10x RT random primers and reverse transcriptase. The mixture was incubated in a thermal cycler using the protocol: 25°C for 10 minutes, 37°C for 120 minutes, and 85°C for 5 minutes.

2.3.3 mRNA quantitative real time PCR (qRT-PCR)

Quantitative real-time PCR was performed in triplicate using TaqMan® Gene Expression Assay, 20X FAM dye-labeled Kit (Applied Biosystems Inc. CA). cDNA sample was used as input for TaqMan quantitative PCR using pre-designed, manufacturer-validated primers and probes for genes of interest (Life Technologies). In brief, TaqMan® Gene Expression Assay (20X), cDNA, TaqMan® Universal PCR Master Mix II (2X), probes and nuclease-free water were mixed to a final volume of 20µL per reaction. The qRT-PCR was performed in 7500 Fast Real Time PCR Systems machine, Applied Biosystems. The samples were measured in a 96-well qPCR plate (Life Technologies, USA) sealed with optical adhesive film (Life Technologies, USA).

mRNA Ct values were normalized to a house keeping gene (*Ubiquitin C, UBC*) by using the comparative Ct method. Where appropriate, the fold change was calculated relative to a reference sample using the ΔΔCt method.

The calculation formula is:

Threshold cycles (Ct)

$\Delta C_{\mathrm{T}} = C_{\mathrm{T\ target}} - C_{\mathrm{T\ reference}}$

The $\Delta\Delta C_T$ values were calculated using the following formula:

$$\Delta\Delta C_T = \Delta C_{T\ test\ sample} - \Delta C_{T\ \ reference\ sample}$$

Finally, the fold change relative to the reference sample was calculated using the following formula:

$$fold\ change = 2^{-\Delta\Delta C_T}$$

For demonstrating the mRNA expression level across all cell lines, we chose not to represent the data using the typical ΔΔCt graphs. This is because choosing a reference sample in order to display the data as fold change involves expression of the data as ratios, making the statistical assessment of error less valid. Raw Ct values (mean of three triplicate wells) were first normalized to *UBC* to generate the ΔCt. Instead of the standard ΔΔCt method, which compares to an arbitrarily identified reference sample, the actual ΔCt mean linear value was used. However, as the ΔCt is actually inversely proportional to the starting amount of mRNA, we converted the ΔCt values by subtracting them from the highest ΔCt value obtained within any one experiment, and converted the resulting values from a logarithmic to a linear scale. Statistical analysis was based on using t-tests to assess the significance of differences between these values.

2.3.4 Microarray gene expression analysis

Details of RNA submission to the microarray facilities used, and their analysis, are described in Wong et al 2006. 10 μg of RNA of each cell line were sent to the Molecular Biology Core Facility at the Paterson Institute for Cancer Research for gene expression microarray analysis using Human Genome U133 plus 2.0 chips following the manufacturer's instructions (Affymetrix, USA). In brief, 500 ng of total RNA was converted to double-stranded cDNA from which produce biotin-labeled cRNA was produced. After fragmentation, 10 μg of cRNA were hybridized to Affymetrix U133 Plus 2.0 oligonucleotide arrays containing probes to more than 54,612 transcripts. Gene expression data was normalized using the Robust Multichip Analysis algorithm. A fold change of 1.5 with 95% significance level was selected as the threshold for comparison between the paired cell lines.

2.4 Protein Methods

2.4.1 Preparation of protein lysates from cell lines

Cells were grown in 6-well or 24-well plates in complete medium until 70-80% confluence. After brief rinsing with ice-cold PBS, the cells were scraped on ice in 1-2 ml ice-cold PBS and transferred to an Eppendorf tube. Then the cells were pelleted by centrifugation at maximum speed at 4°C. Supernatant was removed and the cell pellet was then lysed in 100-400μl RIPA buffer or Lysis buffer (1% Nonidet P-40, 0.5% nordeoxycholate, 150 mM sodium chloride, 50 mM Tris base, pH 8.3) with protease inhibitor cocktail (Complete Protease Inhibitor Cocktail tablets, Roche, Switzerland) and left on ice for 30 minutes followed by centrifugation at maximum speed for 30 minutes at 4°C. Cell debris were pelleted by centrifugation and total cell lysates in the

supernatant were transferred to a fresh tube and stored at -80°C for future use and the pellet discarded.

2.4.2 Antigen preparation from fresh human tissues

Fresh samples of normal colon were obtained from the Biobank, John Radcliffe hospital, Oxford. Smooth muscle samples were dissected from the muscularis layer of the colon tissue and were finely diced with scalpels and stirred by ultrasonic mixer for 10 minutes on ice in Lysis buffer with protease inhibitor cocktail (Complete Protease Inhibitor Cocktail tablets, Roche, Switzerland). The supernatant was clarified by centrifugation at maximum speed (15,000 xg for 30 minutes) and separate aliquots were kept at -80 °C for future use.

2.4.3 BCA assay

The bicinchoninic acid colorimetric assay, BCA™ Protein Assay (Pierce, USA) was used for quantitation of total protein. The assay is based on the principle that proteins in the sample reduce Cu^{2+} to Cu^{1+} ion in an alkaline medium. Cu^{1+} then combines with bicinchoninic acid (BCA) to form a purple colour. Protein standard was prepared by diluting one Albumin Standard (Pierce, USA) ampoule in Lysis buffer. The working range of BSA standards are 0-2000µg/ml. The BCA™ working reagent was then prepared by combining 50 parts of BCA™ solution A with 1 part of BCA™ solution B. 25 µL of diluted unknown samples and standards duplicates were added in a 96-well microplate. To each standard or sample well, 200 µL of working reagent was added. The microplate was incubated at 37°C for 30 minutes followed by measuring the absorbance at 562 nm on a plate reader (µQuant, Bio-Tek Instrument, USA). The

absorbance values were plotted against the concentration of the BSA standards to calibrate a standard curve. Concentrations of the unknown samples were calculated based on the standard curve.

2.4.4 Antibodies

Dilutions and sources of antibodies are listed in **Table 2.2**. Secondary antibodies were purchased from Dako (USA) or Cell Signaling (USA). Antibody dilutions and blocking media were optimized as needed.

Primary antibody	Source	Dilution	Secondary pAb	Secondary dilution
PR2D3 mAb	In house	WB: 1:10 IHC: 1:1	RAM	WB: 1:20,000
AOC3 mAb TK8-14	Santa Cruz	WB: 1:750 IHC: 1:50	RAM	WB: 1:20,000
AOC3 mAb 174-5	Abcam	IHC: 1:100	RAM	WB: 1:20,000
AOC3 mAb 393112	R&D	IHC: 1:250	RAM	WB: 1:20,000
AOC3 pAb H43	Abcam	IHC: 1:100	GAR	WB: 1:10,000
EpCam (AUA1)	In house	IHC: 1:600	RAM	WB: 1:20,000
SMA mAb 1A4	Sigma	WB: 1:2000 IHC: 1:800	RAM	WB: 1:20,000
SMA mAb E184	Abcam	WB: 1:2000 IHC: 1:500	GAR	WB: 1:10,000
Vimentin 3B4	Dako	IHC: 1:100	RAM	WB: 1:20,000
Anti-fibroblasts mAb, 1B10	Sigma	IHC: 1:200	RAM	WB: 1:20,000

MYH11 mAb ID8	Santa Cruz	WB: 1:1000	RAM	WB: 1:20,000
MYH11 mAb EPR5336	Abcam	WB: 1:2500 IHC: 1:150	GAR	WB: 1:10,000
α-Tubulin mAb DM1A	Abcam	WB: 1:5000	RAM	WB: 1:20,000
NKX2.3 mAb 4F4	Sigma		RAM	
NKX2.3 pAb	LSBio	WB:1:1000	GAR	WB: 1:10,000

Table 2.2
Dilutions of antibodies used in this study
RAM= Rabbit-anti-mouse, GAR= Goat-anti-rabbit; mAb= monoclonal antibody; pAb=polyclonal antibodies; WB=Western immunoblot; IHC=immunohistochemistry

2.4.5 Western immunoblot

2.4.5.1 SDS poly-acrylamide gel electrophoresis

Protein samples were analyzed in a Mini-PROTEAN® vertical electrophoresis unit (Bio-Rad, USA). 30 μg of protein were mixed with 5x SDS sample buffer and boiled for 10 minutes to denature the protein. For native protein, 30 μg of protein were mixed with sample buffer (without 2-mercaptoethanol) for loading. The samples were then centrifuged before loading into a 10% polyacrylamide gel. The protein samples along with the pre-stained full-range rainbow molecular weight marker (GE Healthcare, UK) were first concentrated in a 4% SDS stacking gel and then resolved in a 10% SDS separating gel at 100 V for 2-3 hours in 1x SDS running buffer. After electrophoresis, the SDS gel was removed from the glass plate and immersed into transfer buffer for 15 minutes before transferring to a PVDF membrane for immunoblot analysis.

2.4.5.2 Immunoblotting

Hybond-P PVDF membrane (Amersham Biosciences, USA) was used for immunoblotting (or Western blot). The membrane was first soaked in 100% methanol and then rinsed briefly in distilled water before immersing in transfer buffer for 15 minutes. Proteins were transferred to the membrane by semi-dry electrophoresis in SDS transfer buffer at 20 V at room temperature for one hour or 12 V for two hours. After transfer, the membrane was briefly rinsed in distilled water followed by blocking with 1% w/v BSA blocking solution for 1 hour at room temperature on a rocking platform. The membrane was then incubated with appropriate primary antibodies for 1 hour at room temperature or at 4°C overnight. After three 10 minutes washes with PBS-T (PBS with 0.5% Tween-20), the membrane was incubated in respective secondary antibodies in blocking solution for a further 1 hour at room temperature. The membrane was again washed by PBST three times for 10 minutes. Finally, the membrane was incubated with ECL Prime Western Blotting Detection System solution (GE Healthcare, UK) and the blot was exposed to a light-sensitive film and developed in a dark room using a film processor.

2.4.6 Immunoprecipitation

Immunoprecipitation was performed using Dynabeads® protein G (Invitrogen, UK). Protein lysate was prepared as previously described. First, 50 µL (1.5 mg) Dynabeads® were prepared with antibody (1-10 µg) diluted in 200 µL PBST in a tube. This mixture was then incubated with rotation for at least 30 minutes at 4°C. The supernatant was then removed from the magnet and the Ab-beads complex washed by PBST 3 times. Next, a 500µL sample containing the antigen (smooth muscle lysate or cell lysate) was incubated with the Ab-beads complex for 1hr at 4°C and the supernatant then removed.

The Dynabeads®-Ab-Ag complex was then washed three times using 200 µL washing buffer each time. The bead-antibody complex was separated on the magnet between each washing step, the supernatant removed and he complex re-suspended by gentle pipetting. Given the fact that mAb PR2D3 only recognizes native, non-denatured protein, mild acid elution was used to maintain antigen integrity. 40µl Elution buffer (Glycine 100 nM, pH 2.7) were added to each tube and gently pipetted to re-suspend the Dynabeads®-Ab-Ag complex and then incubated with rotation for 2 minutes at room temperature. The tube was then placed on the magnet and the supernatant (containing Ab and Ag) transferred to a clean tube, and the pH adjusted by adding 1M Tris pH 7.5. For denaturing the sample, the Dynabeads®-Ab-Ag complex was incubated with 2x SDS loading buffer for 5 minutes at 90°C and supernatant then loaded and subsequently analysed in SDS-PAGE.

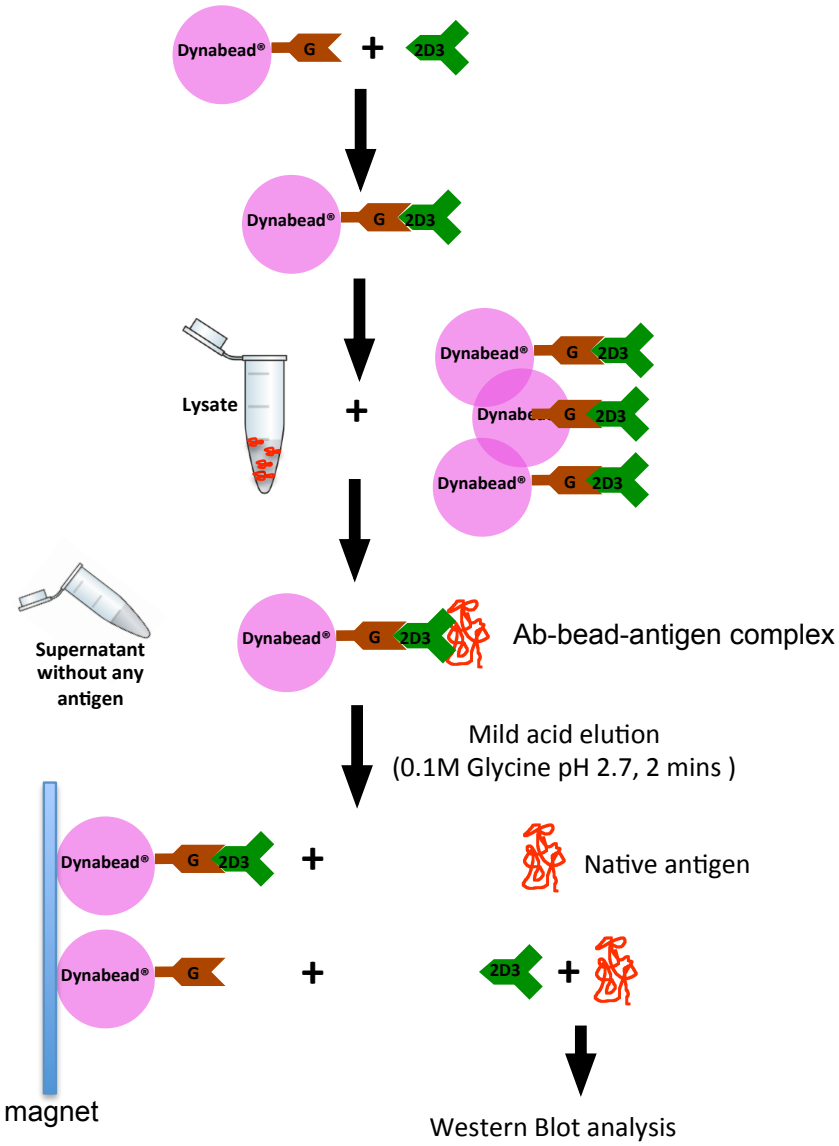

Figure 2.1
Workflow of immunoprecipitation using protein G magnet beads

2.5 Mass Spectrometry

2.5.1 Antigen preparation

Human colonic smooth muscle lysates were prepared in Lysis buffer with protease inhibitor. Briefly, tissue samples were minced and homogenized in 10 ml of the Lysis buffer. These lysates were then filtered using cell strainers (Millipore, USA) and centrifuged at 14,000 rpm for 30 min, 4°C after which the supernatant was collected and the protein concentration was determined using the BCA^{TM} Protein Assay protein assay.

2.5.2 Electrophoresis and gel digestion of the protein band

Lysates, containing 1 mg of the protein, were immunoprecipitated by Dynabeads® protein G (Invitrogen, UK) using anti-PR2D3 mAb (in house) and isotype anti-IgG mAb. After washing up to five times with PBST, the IP proteins were eluted either with elution buffer (Glycine 100 nM, pH 2.7) or incubated with 2x SDS loading buffer containing 2-mercaptoethanol for 5 minutes at 90°C. The immunoprecipitated samples were then analyzed using NuPAGE Bis-Tris precast gel (Life technologies, USA). After electrophoresis, the gel was stained with Coomassie blue stain (Bio-Rad, USA). Protein bands of interest were carefully manually excised and placed in microtubes (0.6 ml, Axygen). In-gel digestion with trypsin was performed according to standard procedures routinely used in the Central Proteomics Facilities, WIMM, Oxford.

2.5.3 Mass spectrometry and database analysis

The tryptic-digested samples were analyzed by MALDI-TOF mass spectrometry, which was performed on an Ultraflex time-of-flight (TOF) mass spectrometer (Bruker Daltonics, Bremen, Germany) in the Central Proteomics Facilities, WIMM, Oxford.

In brief, the spectra generated with a unique set of masses are called peptide-mass fingerprints (PMF). These can be matched with entries in protein databases using search engines (Mann *et al*., 2001). In this study, SWISS-PORT database was used and the Mascot search engine (Matrix Science, London, UK) for matching sample data with this database. Mascot is a fully automated search engine with probability-based algorithms. It also indicates whether a score is significant, which is determined according to individual cases. The resulting mass spectra of trypsin peptide digests from all the gel spots were matched against theoretical trypsin peptide digests in the SWISS-PORT 50.8 protein database using the Mascot search engine. The Mascot default significance threshold of $p<0.05$ for assignments was used in the searches and a minimum of two unique peptides was used as criterion for a match.

2.6 Microscopy

2.6.1 Antibodies used for immunofluorescence

Dilutions and sources of antibodies are listed in **Table 2.2**. Visualization was achieved using tyramide AlexaFluor® 488 or 555 dye (Invitrogen) together with UV excitation.

2.6.2 Cryostat sections and Paraffin-embedded archived materials

Archived paraffin-embedded and cryostat sections obtained from normal and cancer patients were studied. Material was obtained from Oxford University Hospitals, UK, approved by local research ethics committee. Commercial tissue array was purchased from SuperBioChips Laboratories (Seoul, Korea).

2.6.3 Antigen retrieval

2.6.3.1 Paraffin embedded sections

For immunohistochemistry analysis, paraffin-embedded human tissue sections were deparaffinised in Histo-clear twice for 5 minutes, and rehydrated in 100% ethanol, 100% Industrial Methylated Spirit (IMS) and 95% IMS for 5 minutes each and 70% IMS and 35% IMS for 2 minutes each. Slides were then rinsed in PBS. Some slides were stained with Hematoxylin to assess cellular morphology, and others stained for immunofluorescence. For the latter, antigen retrieval was done using the Dako Target Retrieval solution (Dako, pH 6.1) at 100°C for 20 minutes, followed by cooling to room temperature for 1 hour. Slides were then washed twice in PBST for 5 minutes each. Tissue specimens were then encircled using the hydrophobic ImmEdge pen (Vector Labs) and blocked for 30 minutes using Invitrogen blocking reagent (0.1g/10mL PBS-

Tween). Slides were then ready for incubation with the primary antibody.

2.6.3.2 Cryostat sections

Cryostat tissue sections were immersed in pre-cooled acetone (-20°C) for 10 minutes for fixation, and then 15 minutes at room temperature to allow the evaporation of acetone from tissue sections. This was followed by 2x5 minutes washes with PBS. Tissue specimens were then encircled using the hydrophobic ImmEdge pen (Vector Labs) and blocked for 30 minutes using Invitrogen blocking reagent (0.1g/10mL PBS-Tween). Slides were then ready for incubation with the primary antibody

2.6.4 Immunohistochemistry of tissue sections or cultured cells

Slides were incubated with a primary antibody at room temperature for 1 hour with the appropriate primary antibody in blocking solution and washed 2x5 minutes with PBS-Tween. Slides were next incubated with a secondary antibody (either goat anti-mouse or goat anti-rabbit) conjugated to HRP at a dilution of 1:100 at room temperature for 1 hour, followed by 2x5 minutes washes with PBS-Tween. Coverslips were mounted onto the tissue specimens using Vectashield containing DAPI. Immunofluorescent slides were examined using a Zeiss Axioscope 2 Plus microscope and representative images were captured with Axioscope software. Some slides were examined with a Zeiss LSM 510 inverted confocal microscope.

2.7 Flow Cytometry

2.7.1 Fluorescently labelled antibodies and antibody staining for analysis

Mouse anti-AOC3-PE (Clone: TK 8-14, isotype IgG2a), Mouse anti-EpCam-FITC (Clone: 9C4), were obtained from Santa Cruz biotechnology, USA and Abcam, UK. Mouse anti-PR2D3 was in house. Mouse isotype controls PE, isotype-FITC, and goat anti-mouse APC antibody were obtained from BD Biosciences.

Cells were filtered through a CellTrics® 20-μm filter to obtain single-cell suspensions, divided into aliquots of 10^6 cells, washed with wash buffer (0.1% BSA in PBSA) and incubated in 100 μL wash buffer containing an appropriate dilution of primary antibody or isotype control for 45 min on ice. Cells were washed with wash buffer, re-probed with secondary antibody for 45 min on ice if appropriate and washed again with wash buffer. Cells were resuspended in 400μL wash buffer with DAPI for 10 min and were then ready for analysis.

2.7.2 Flow cytometric analysis

Protein expression profiles were assessed by flow cytometry on a CyAn ADP analyzer using the integrated Summit data collection software. At a forward scatter gain of 2.0 and a side scatter gain of 1.0 and voltage 450 V, doublets and debris were excluded from the analysis using pulse width. At a 488-nm blue laser gain of 1.0 and voltage 450 V, FITC and PE fluorescence was detected; at a 633-nm red laser gain of 1.0 and voltage 750 V, APC was detected. Fluorescence logarithms were plotted to identify negatively- and positively-staining populations.

2.7.3 Fluorescent activated cell analysis and sorting using a FACS

Analysis was performed on $1x10^6$ cells and followed by standard staining procedures and kept sterile in a hood. For a live cell sort, $1x10^6$ cells were incubated with 1µg of AOC3 antibody on ice for 45 minutes and another 30 min incubation with goat anti-mouse APC in the dark. After washing, the cells were then resuspended in 1000µL of serum free DMEM medium. DAPI was added to the cellular suspension. Cells were sorted using a MoFlo™ cell sorter (Dako) using the integrated Summit data collection software. Single cells were obtained by gating out cellular aggregates and dead cells were excluded on the basis of DAPI staining. Cells expressing AOC3 are then gated on APC fluorescence signals as based on unstained samples.

2.8 Statistical Methods

2.8.1 General data analysis

All the data in the graphs are presented as the mean values ± SEM. P values are computed using a two-tailed student's t-test using the values from the biological replicates. For all statistical comparisons, $p<0.001$ was denoted by **, $p<0.01$ by * and $p< 0.05$ was by #, GraphPad Prism Software (La Jolla, California, USA) was used to perform all the data analysis.

2.8.2 Microarray expression analyses

Total RNA from primary myofibroblasts cultures, fibroblast cell cultures and cells from the CCD 18CO cell line were extracted, reverse-transcribed to cDNA and hybridized to the Human Genome Affymetrix GeneChip U133 plus 2.0 arrays. Partek genomic suite software (Partek, St. Louis, Missouri, USA) was used to compare expression profiles

between the fibroblast and myofibroblast cultures. For significant differential expression genes, correction for multiple testing was applied to mean comparisons to reduce the number of false significant results. (0.05 cutoff using false discovery rate FDR step up). A fold-change of 1.5 or greater a corrected *p*-value of less than or equal to 0.02 was considered statistically significant.

CHAPTER THREE

IDENTIFICATION OF THE TARGET PROTEIN OF PR2D3 mAb ON MYOFIBROBLASTS

CHPATER 3: IDENTIFICATION OF THE TARGET PROTEIN OF PR2D3 ON MYOFIBROBLASTS

3.1 Introduction

The crypts of the colon are surrounded by a continuous sheath of pericryptal cells called myofibroblasts, which have been shown to play an important role in regulating the normal intestinal stem cell niche through secretion of growth factors, cytokines and extra cellular matrix components (Richman et al., 1987, Yen and Wright, 2006, Yeung et al., 2011). Several studies have shown that an increased number of myofibroblasts associated with a primary colorectal cancer is associated with a higher grade of malignancy and poorer prognosis in patients (Ootani et al., 2009, Vermeulen et al., 2010). Myofibroblasts might have a supportive or facilitating role during the development and progression of colorectal cancer. Thus, understanding the biological role of myofibroblasts in normal as well as cancerous tissue, especially with respect to their influence on, and interaction with, epithelial cells may lead to improvements in the diagnosis and treatment of colorectal cancer (Tsujino et al., 2007).

Expression of α-smooth muscle actin (αSMA) in stromal fibroblasts is a widely used cytoplasmic marker to distinguish myofibroblasts from normal fibroblasts, but this does not adequately categorize the heterogeneity of myofibroblasts in stroma. Unfortunately there is no myofibroblast-specific marker available to date, the current way to identify myofibroblasts in tissue is based on combinations of positive markers and combined with negative markers, which we have discussed in introduction chapter (**Figure 1.3**).

However none of these markers can distinguish myofibroblasts from activated fibroblasts.

Home-raised mAb PR2D3

In 1987, Paul Richman raised a series of monoclonal antibodies against a fresh sample of human colorectal mucosa in the Bodmer laboratory. One of these, PR2D3, was found to bind human smooth muscle cells and pericryptal cells in tissue sections of gut mucosa but not connective tissue fibroblasts (Richman et al., 1987). This provided the first clear definition of the pericryptal cells as myofibroblasts rather than simply fibroblasts. This made it clear that PR2D3 mAb was a candidate myofibroblast-specific surface marker. PR2D3 is an IgG1 antibody and that binds to an approximately 140 kDa surface glycoprotein on myofibroblasts (and smooth muscle cells) in colorectal mucosa. Richman et al showed that PR2D3 mAb can only recognize native protein since the antigen activity was lost after denaturing treatment or paraffin fixation. Although PR2D3 mAb has been used in several publications (Wolfort et al., 1996, Strong et al., 1997), and is also commercially available (Santa Cruz Biotech, USA), the target protein to which it binds has not yet been identified. Thus, the first aim of this study has been to identify the protein, which PR2D3 mAb binds to.

The results presented in this chapter first identify the home-raised PR2D3 mAb target proteins on colonic smooth muscle lysates as AOC3, a membrane primary amine oxidase and Myosin Heavy Chain 11, by using mass spectrometry based amino acid sequencing in an immune pull-down assay. Subsequently, immunofluorescence and immunoblotting were used to assess the AOC3 expression on myofibroblasts, as well as the expression of MYH11. By comparing the mRNA expression levels from microarray,

our data suggest that AOC3 is expressed specifically in myofibroblasts, while MYH11 and αSMA showed their heterogeneous expression in myofibroblasts and fibroblasts.

3.2 Results:

3.2.1 Expression of PR2D3 in human colon smooth muscle lysates (Western Blot) and colon pericryptal myofibroblasts (Cryosection, IF)

PR2D3 mAb was purified from supernatant of the in-house PR2D3 hybridoma. As anticipated, a 150 kDa band was identified in human colonic smooth muscle lysate samples under native but not reduced conditions by immunoblot (**Figure 3.1A**). Pericryptal myofibroblasts were strongly labelled by fluorescent tagged PR2D3 mAb both in normal and cancer human colon cryostat sections (**Figure 3.1B,C**), consistent with previously published data. It confirmed that PR2D3 mAb only recognizes native (non-reduced) protein since the antigen activity was lost after denaturing treatment or paraffin fixation.

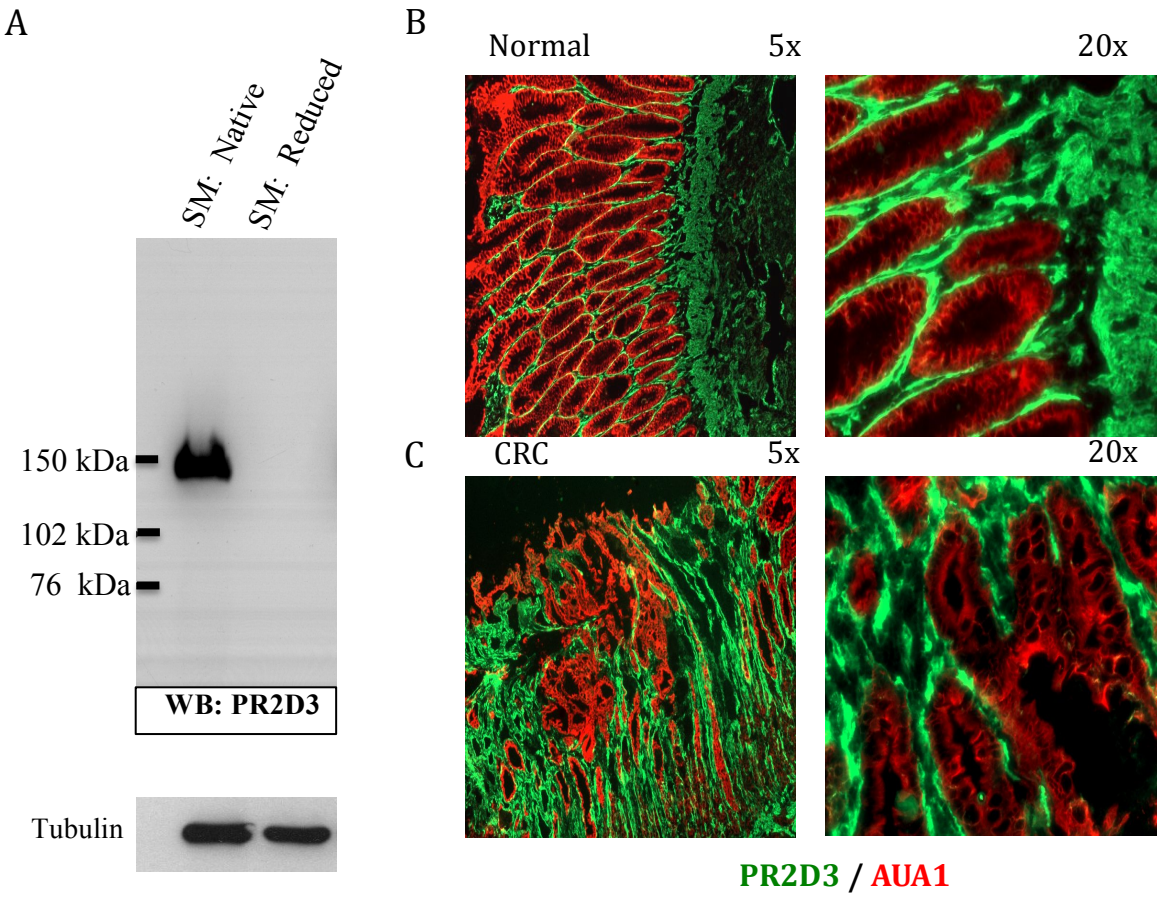

Figure 3.1
PR2D3 is expressed in human smooth muscle lysates and colon pericryptal myofibroblasts.
(A) Protein immunoblot of human colonic smooth muscle lysate with PR2D3 showing a band of about 150 kDa in native (non-reduced) sample. Tubulin is shown as a loading control. Molecular weight standards in kDa are shown on the left. Immunofluorescence staining of cryostat sections of normal colon tissues (B) and colorectal cancer tissues (C) with PR2D3 (green) for myofibroblasts and AUA-1 (red) to identify epithelial cells

3.2.2 Identification of PR2D3 targeted proteins by mass spectrometry based peptide sequencing: Membrane primary amine oxidase, AOC3 and Myosin Heavy Chain 11, MYH11

The target protein of PR2D3 was enriched from human smooth muscle lysates using an immunoprecipitation (IP) pull-down assay for proteome analysis. Smooth muscle lysates were immunoprecipitated using Dynabeads® with the anti-PR2D3 mAb as described in material and methods. Following immunoprecipitation, target proteins were Western blotted and probed with the same PR2D3 mAb. In **Figure 3.2A**, PR2D3 antigen enrichment can be observed after IP and immunoblot. The other band present in isoform control lane is most likely due to the contamination of the co-eluted IgG molecules used in the IP, which happened to be the same molecular weight as the PR2D3 bound protein (about 150 kDa).

For proteome analysis, the enriched PR2D3 bound proteins from smooth muscle lysates were analyzed by precast SDS- poly-acrylamide gel electrophoresis (**Figure 3.2B**). The gel was stained with coomassie dye to visualized protein bands. Again, the presence of the co-eluted IgG molecules in the samples obscured the results in the native sample lanes. However, two distinct bands were observed in the PR2D3 IP lane when samples were eluted under denaturing conditions, at about 250kDa and 100 kDa, compared to the control lane. Four bands, detected from the gels, including two from the native sample (both IP from PR2D3 and IgG isoform) and two specific bands from IP with PR2D3 in the reduced sample were excised and digested with trypsin. Proteins identified by MALDI-TOF MS/MS analysis (The Central Proteomics Facilities, WIMM, Oxford) are shown in **Figure 3.3.**

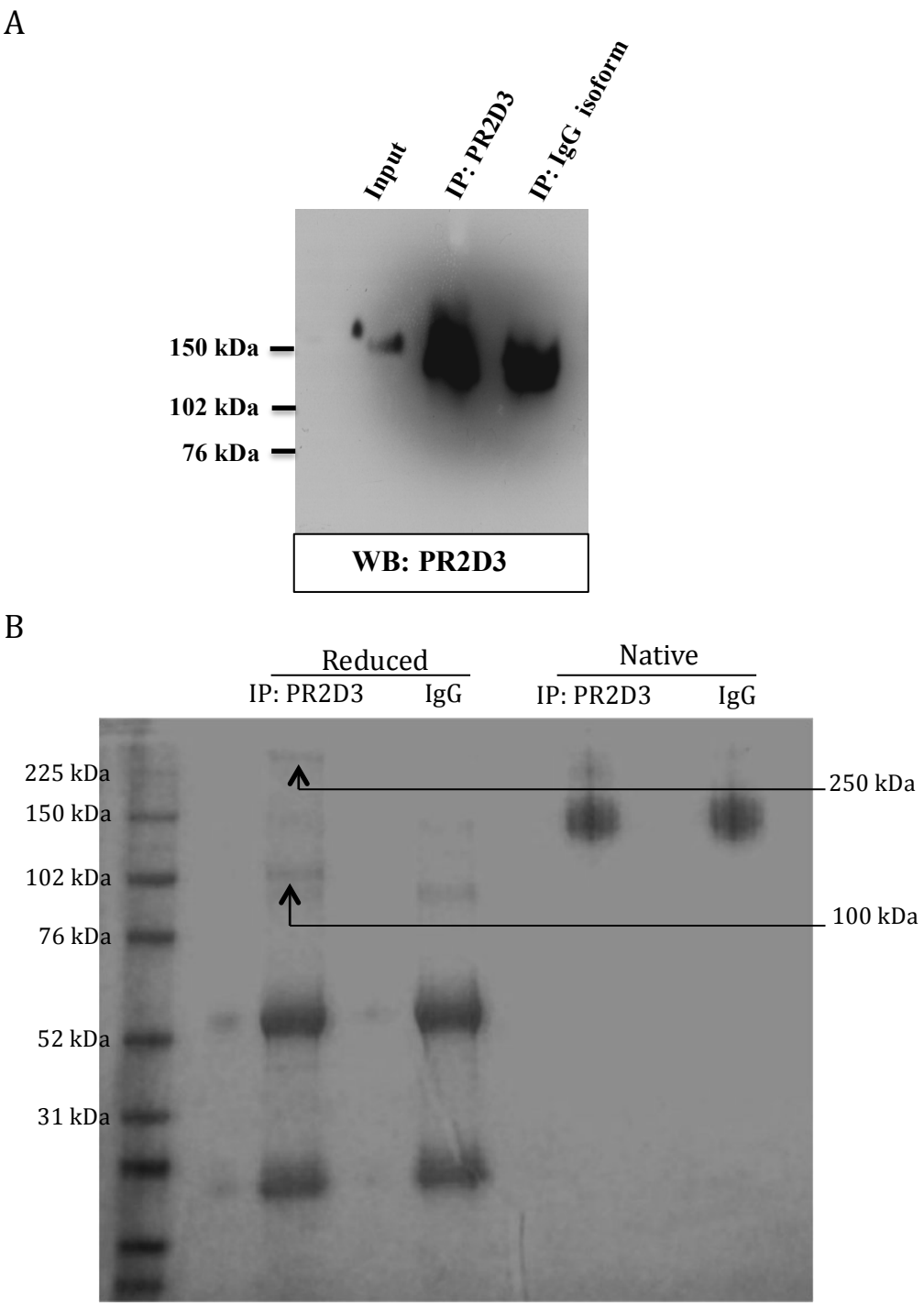

Figure 3.2
Identification of PR2D3 target protein
(A) Immunoprecipitation of smooth muscle lysates with PR2D3 and IgG isoform and immunoblotted with PR2D3. Band of IgG isoform lane resulted from co-eluted antibody from IgG-beads complex. (B) Coomassie stained gel of total human smooth muscle lysate immunoprecipitated with PR2D3 and IgG isoform in both reduced and native conditions. Two specific bands were observed using PR2D3, approximately 250 kDa and 100 kDa, but only under reducing conditions. Both bands were excised and submitted for mass spectrometry analysis.

MADLDI-TOF MS/MS (matrix-assisted laser-desorption-ionization-time-of–flight tandem MS) was performed using an Ultraflex III TOF/TOF mass spectrometer (Bruker Daltonics). For protein identification, raw MS/MS data were searched using the Mascot algorithm (Matrix Science, version 2.2.0) against database. The Mascot score was used to determine the probability that the observed matches between the experimental data and the database sequences were not random.

Analysis of mass spectrometry data of the two bands from the native sample, identified amino acid sequences that match only to IgG in the database, confirming the prediction that this band represented residual antibody contamination from the pull down assay. The two specific bands from IP with PR2D3 matched unique proteins or protein domains in the database respectively. The highest Mascot scores were for the 250 kDa protein detected with database sequences of myosin heavy chain 11 (MYH11) (**Figure 3.3A**) and the 100 kDa protein matched to membrane primary amine oxidase, AOC3 (**Figure 3.3B**).

A

250 kDa:
Myosin heavy chain 11,
Smooth muscle isoform

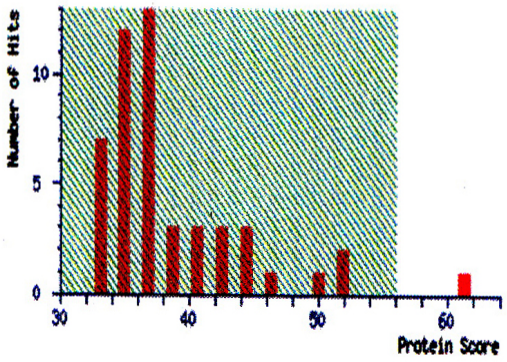

Number of mass values searched: 57
Number of mass values matched: 33
Sequence Coverage: 19%

Matched peptides shown in Bold Red

```
   1 MAQKGQLSDD EKFLFVDKNF INSPVAQADW AAKRLVWVPS EKQGFEAASI
  51 KEEKGDEVVV ELVENGKKVT VGKDDIQKMN PPKFSKVEDM AELTCLNEAS
 101 VLHNLRERYF SGLIYTYSGL FCVVVNPYKH LPIYSEKIVD MYKGKKRHEM
 151 PPHIYAIADT AYRSMLQDRE DQSILCTGES GAGKTENTKK VIQYLAVVAS
 201 SHKGKKDTSI TGELEKQLLQ ANPILEAFGN AKTVKNDNSS RFGKFIRINF
 251 DVTGYIVGAN IETYLLEKSR AIRQARDERT FHIFYYMIAG AKEKMRSDLL
 301 LEGFNNYTFL SNGFVPIPAA QDDEMFQETV EAMAIMGFSE EEQLSILKVV
 351 SSVLQLGNIV FKKERNTDQA SMPDNTAAQK VCHLMGINVT DFTRSILTPR
 401 IKVGRDVVQK AQTKEQADFA VEALAKATYE RLFRWILTRV NKALDKTHRQ
 451 GASFLGILDI AGFEIFEVNS FEQLCINYTN EKLQQLFNHT MFILEQEEYQ
 501 REGIEWNFID FGLDLQPCIE LIERPNNPPG VLALLDEECW FPKATDKSFV
 551 EKLCTEQGSH PKFQKPKQLK DKTEFSIIHY AGKVDYNASA WLTKNMDPLN
 601 DNVTSLLNAS SDKFVADLWK DVDRIVGLDQ MAKMTESSLP SASKTKKGMF
 651 RTVGQLYKEQ LGKLMTTLRN TTPNFVRCII PNHEKRSGKL DAFLVLEQLR
 701 CNGVLEGIRI CRQGFPNRIV FQEFRQRYEI LAANAIPKGF MDGKQACILM
 751 IKALELDPNL YRIGQSKIFF RTGVLAHLEE ERDLKITDVI MAFQAMCRGY
 801 LARKAFAKRQ QQLTAMKVIQ RNCAAYLKLR NWQWWRLFTK VKPLLQVTRQ
 851 EEEMQAKEDE LQKTKERQQK AENELKELEQ KHSQLTEEKN LLQEQLQAET
 901 ELYAEAEEMR VRLAAKKQEL EEILHEMEAR LEEEEDRGQQ LQAERKKMAQ
 951 QMLDLEEQLE EEEAARQKLQ LEKVTAEAKI KKLEDEILVM DDQNNKLSKE
1001 RKLLEERISD LTTNLAEEEE KAKNLTKLKN KHESMISELE VRLKKEEKSR
1051 QELEKLKRKL EGDASDFHFQ IADLQAQIAE LKMQLAKKEE ELQAALARLD
1101 DEIAQKNNAL KKIRELEGHI SDLQEDLDSE RAARNKAEKQ KRDLGEELEA
1151 LKTELEDTLD STATQQELRA KREQEVTVLK KALDEETRSH EAQVQEMRQK
1201 HAQAVEELTE QLEQFKRAKA NLDKNKQTLE KENADLAGEL RVLGQAKQEV
1251 EHKKKKLEAQ VQELQSKCSD GERARAELND KVHKLQNEVE SVTGMLNEAE
1301 GKAIKLAKDV ASLSSQLQDT QELLQEETRQ KLNVSTKLRQ LEEERNSLQD
1351 QLDEEMEAKQ NLERHISTLN IQLSDSKKKL QDFASTVEAL EEGKKRFQKE
1401 IENLTQQYEE KAAAYDKLEK TKNRLQQELD DLVVDLDNQR QLVSNLEKKQ
1451 RKFDQLLAEE KNISSKYADE RDRAEAEARE KETKALSLAR ALEEALEAKE
1501 ELERTNKMLK AEMEDLVSSK DDVGKNVHEL EKSKRALETQ MEEMKTQLEE
1551 LEDELQATED AKLRLEVNMQ ALKGQFERDL QARDEQNEEK RRQLQRQLHE
1601 YETELEDERK QRALAAAAKK KLEGDLKDLE LQADSAIKGR EEAIKQLRKL
1651 QAQMKDFQRE LEDARASRDE IFATAKENEK KAKSLEADLM QLQEDLAAAE
1701 RARKQADLEK EELAEELASS LSGRNALQDE KRRLEARIAQ LEEELEEEQG
1751 NMEAMSDRVR KATQQAEQLS NELATERSTA QKNESARQQL ERQNKELRSK
1801 LHEMEGAVKS KFKSTIAALE AKIAQLEEQV EQEAREKQAA TKSLKQKDKK
1851 LKEILLQVED ERKMAEQYKE QAEKGNARVK QLKRQLEEAE EESQRINANR
1901 RKLQRELDEA TESNEAMGRE VNALKSKLRR GNETSFVPSR RSGGRRVIEN
1951 ADGSEEETDT RDADFNGTKA SE
```

B

100 kDa:
Membrane primary amine oxidase, AOC3

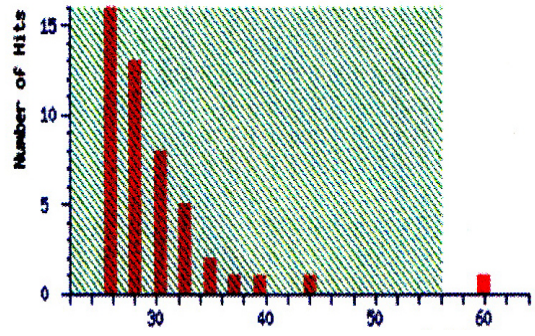

Number of mass values searched: 32
Number of mass values matched: 10
Sequence Coverage: 14%

Matched peptides shown in Bold Red

```
   1 GGDGGEPSQL PHCPSVSPSA QPWTHPGQSQ LFADLSREEL TAVMRFLTQR
  51 LGPGLVDAAQ ARPSDNCVFS VELQLPPKAA ALAHLDRGSP PPARÉALAIV
 101 FFGRQPQPNV SELVVGPLPH PSYMRDVTVE RHGGPLPYHR RPVLFQEYLD
 151 IDQMIFNREL PQASGLLHHC CFYKHRGRNL VTMTTAPRGL QSGDRATWFG
 201 LYYNISGAGF FLHHVGLELL VNHKALDPAR WTIQKVFYQG RYYDSLAQLE
 251 AQFEAGLVNV VLIPDNGTGG SWSLKSPVPP GPAPPLQFYP QGPRFSVQGS
 301 RVASSLWTFS FGLGAFSGPR IFDVRFQGER LVYEISLQEA LAIYGGNSPA
 351 AMTTRYVDGG FGMGKYTTPL TRGVDCPYLA TYVDWHFLLE SQAPKTIRDA
 401 FCVFEQNQGL PLRRHHSDLY SHYFGGLAET VLVVRSMSTL LNXDYVWDTV
 451 FHPSGAIEIR FYATGYISSA FLFGATGKYG NQVSEHTLGT VHTHSAHFKV
 501 DLDVAGLENW VWAEDMVFVP MAVPWSPEHQ LQRLQVTRKL LEMEEQAAFL
 551 VGSATPRYLY LASNHSNKWG HPRGYRIQML SFAGEPLPQN SSMARGFSWE
 601 RYQLAVTQRK EEEPSSSSVF NQNDPWAPTV DFSDFINNET IAGKDLVAWV
 651 TAGFLHIPHA EDIPNTVTVG NGVGFFLRPY NFFDEDPSFY SADSIYFRGD
 701 QDAGACEVNP LACLPQAAAC APDLPAFSHG GFSHN
```

Figure 3.3
Mass spectrometry results: Mascot score histogram and peptide sequence
The highest Mascot scores was observed from the 250 kDa band and identified the (A) Myosin heavy chain 11 (MYH11). The 100 kDa band corresponds to (B) Membrane primary amine oxidase (AOC3). Protein score is -10*Log(P), where P is the probability that the observed match is a random event. Protein scores greater than 56 are significant.

3.2.3 AOC3 expression in human colon smooth muscle lysates and colon pericryptal myofibroblasts (Cryosection & FFPE, IF)

We firstly validated that PR2D3 mAb was indeed recognizing AOC3 by using commercially available anti-AOC3 monoclonal antibodies (TK8-14, Santa Cruz Biotec). According to the product information, mAb TK8-14 was raised against affinity purified VAP-1/AOC3 from human tonsil stroma. Results from western blots showed that both PR2D3 and AOC3 recognized a protein of approximately 150kD (**Figure 3.4A**). Confirmation that AOC3 was the target of PR2D3 was obtained by showing that TK8-14 anti AOC3 reacted with the PR2D3 immunoprecipitated fraction of human smooth muscle lysates in a western blot (**Fig. 3.4B**). Moreover, confocal immunofluorescence staining indicated that pericryptal myofibroblast cells were strongly labelled by anti-AOC3 mAb (TK8-14) on normal colon crypts (**Figure 3.4C**).

In addition to mAb TK8-14, we also purchased other sources of anti-AOC3 mAb, which can be used in paraffin-embedded sections. Clone 393112 (R&D systems) anti-AOC3 mAb is against recombinant human VAP-1/AOC3 and it is used for the following immunohistochemistry analyses. To confirm that these AOC3 positive cells are myofibroblasts, co-staining was performed with the commonly used myofibroblast marker αSMA, and human mesenchymal marker vimentin (VIM), as well as endothelial marker CD31. As shown in **Figure 3.5**, AOC3 was strongly expressed on stromal cells in both normal colon and tumour tissue. It co-localized with αSMA -positive and VIM-positive cells but not with CD31 positive cells, confirming that anti AOC3 labels myofibroblasts and is a novel marker for myofibroblasts.

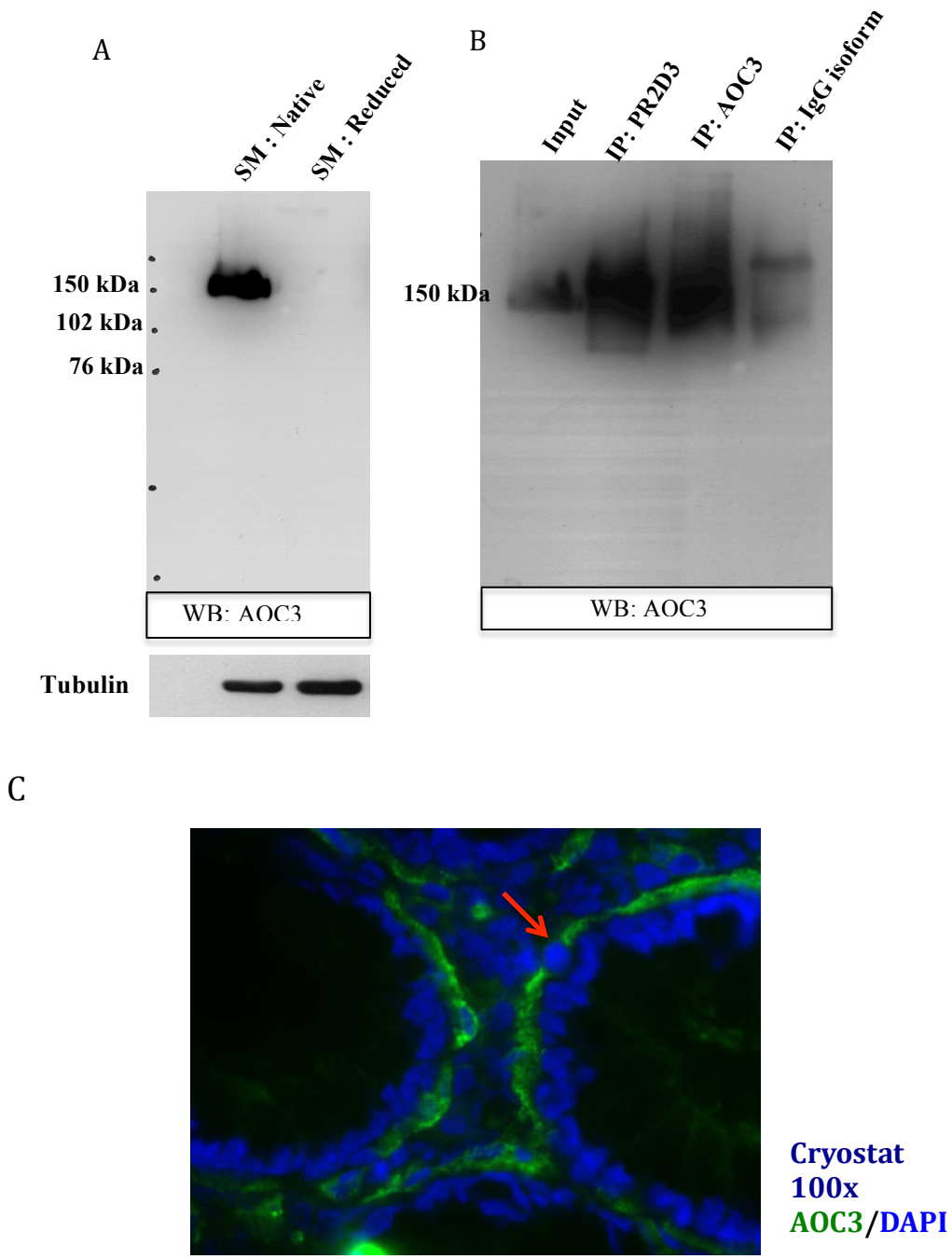

Figure 3.4
AOC3 expression in human smooth muscles lysates and colon pericryptal cells matches PR2D3 staining (A)Protein immunoblot of human smooth muscle lysate with AOC3 showing a band of about 150 kDa in the native (non-reduced) sample (B)Co-immunoprecipitation (CO-IP) with PR2D3 and blotting with AOC3 in smooth muscle lysates. (C) Confocal immunofluorescence of myofibroblasts. AOC3 (green), DAPI (blue), X100 magnification.

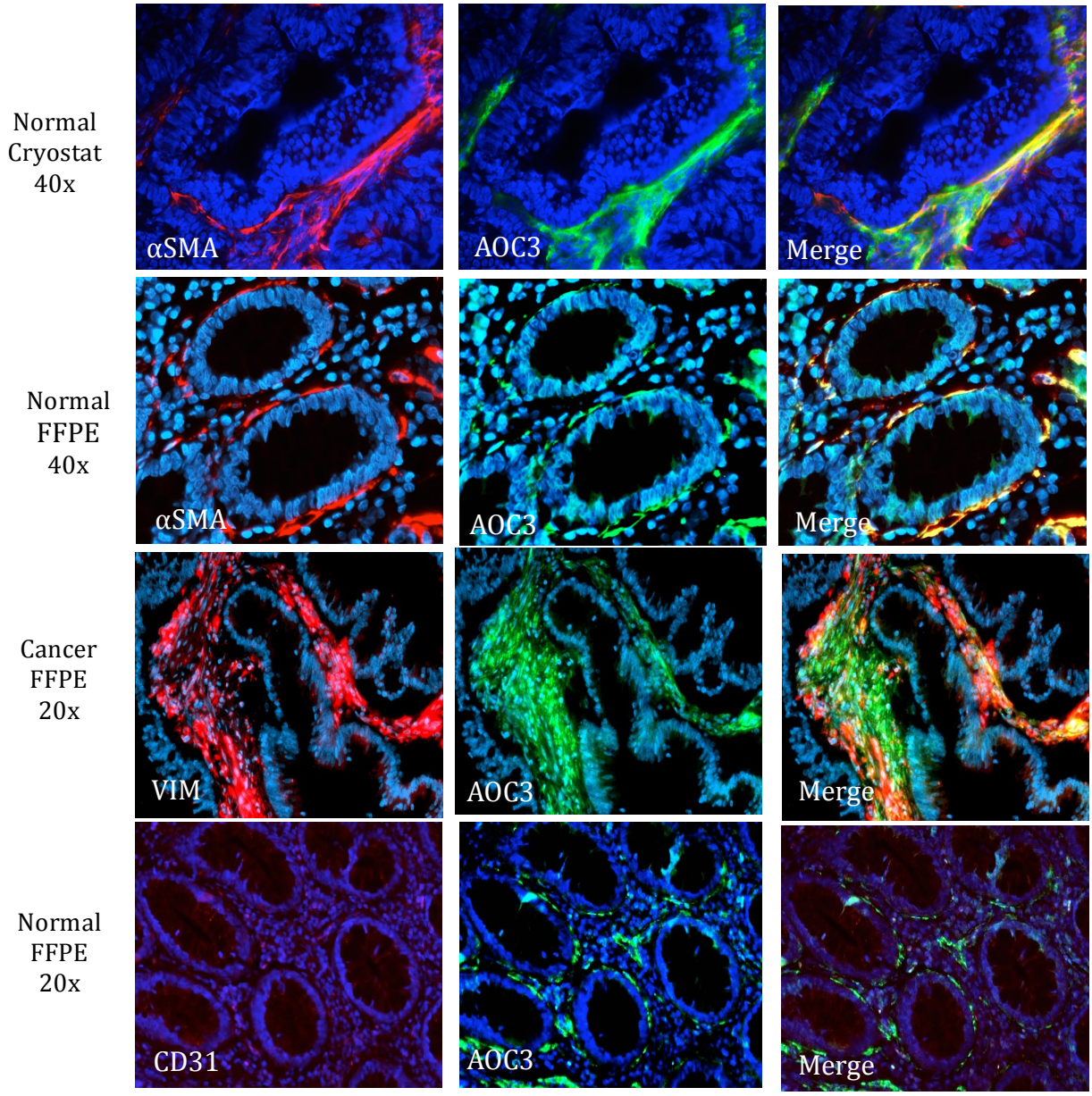

Figure 3.5
AOC3 expression in human colon stromal myofibroblasts. Cryosections (a) of human normal colon were co-stained with AOC3 (Green)(Santa Cruz, TK8-14) and antibody against αSMA (red)(Sigma, 1A4). Paraffin-embedded sections (b,c,d) of human normal and cancerous colon were double stained with AOC3 antibody (green)(R&D, 393112) and antibody against αSMA (red), Vimentin (VIM, red) or CD31(red). AOC3 staining co-localized with αSMA-positive and VIM-positive myofibroblasts but not with CD31 positive cells (endothelial marker).

3.2.4 MYH11 expression in human colon smooth muscle lysates (Western blot) and colon pericryptal myofibroblasts (FFPE, IF)

The 250 kDa band identified through mass spectrometry of proteins pulled down by PR2D3 mAb corresponded to myosin heavy chain 11 (MYH11) (**Figure 3.3A**). MYH11 is a protein that in humans is encoded by the *MYH11* gene (Deng et al., 1993). It is a major contractile protein, converting chemical energy into mechanical energy through the hydrolysis of ATP. We assessed the expression of MYH11 by immunoblotting human smooth muscle lysates and myofibroblast cell lysates using a commercial anti-MYH11 mAb (EPR5336(B), Abcam, UK). Unlike AOC3, MYH11 staining is located intracellular. Anti MYH11 was able to detect a clear band at 250 kDa in both reduced smooth muscle lysate and CCD 18CO cell lysates (**Figure 3.6A**). Immunofluorescence staining was performed on PFA-fixed myofibroblast cell line, CCD 18CO, showing myofibroblast stress fibers are strongly labelled by MYH11 (**Figure 3.6B**). The staining pattern is similar to anti αSMA. Anti MYH11 was also used to stain sections of paraffin-embedded human normal colon and tumour tissues (**Figure 3.6C**). The merged images of double staining with αSMA confirm the co-localization with MYH11 on human pericryptal myofibroblasts.

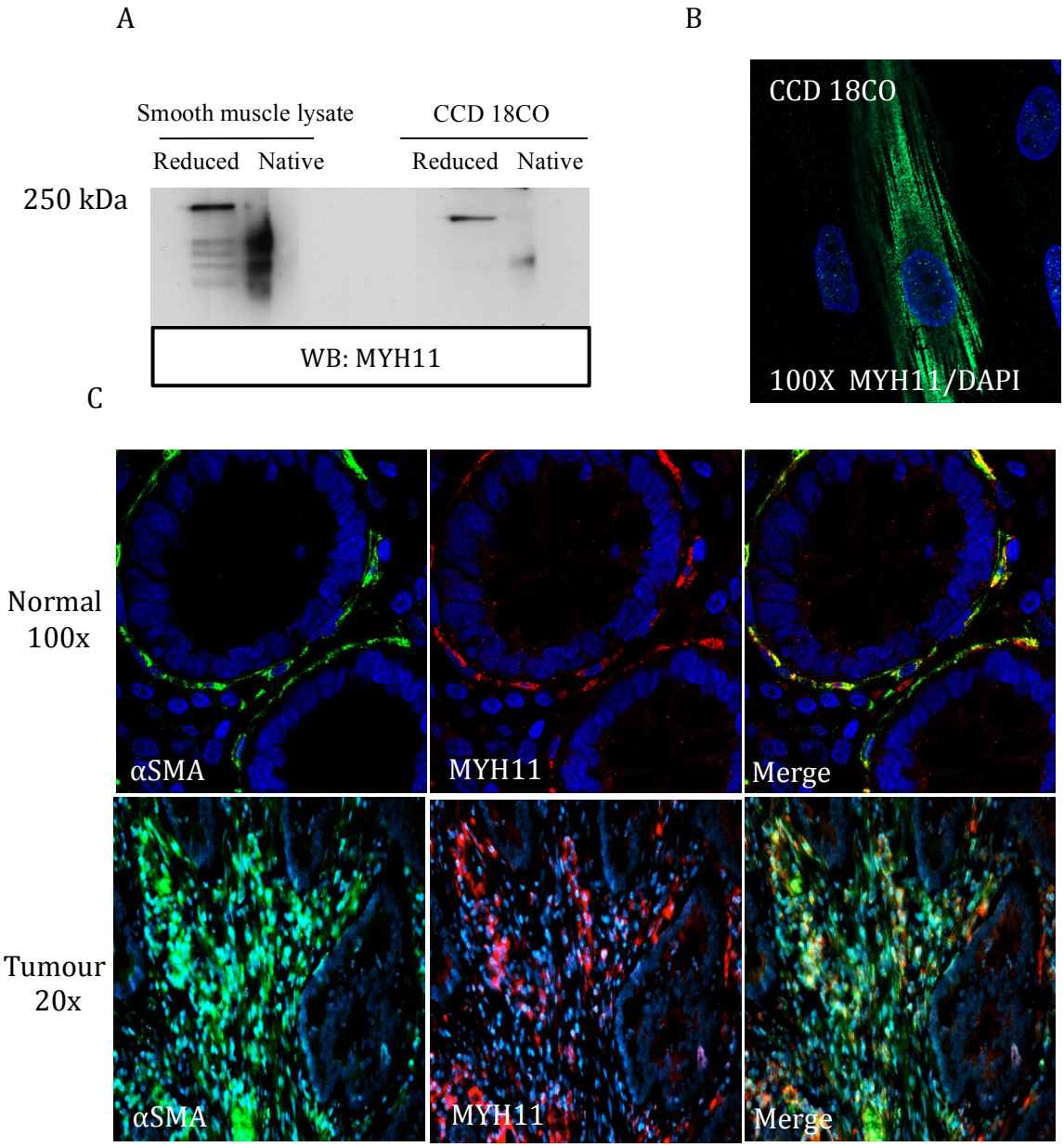

Figure 3.6
MYH11 expression in human smooth muscle lysates and colon stromal myofibroblasts (A) Protein immunoblot of human smooth muscle lysate and CCD-18CO cell lysates with MYH11 showing a band of about 250 kDa in reduced sample. (B) MYH11 is expressed in fixed CCD-18CO myofibroblast cells. (C) Double staining of paraffin-embedded sections of human normal and cancerous colon with MYH11 antibody (red) and antibody against αSMA (green).

3.2.5 mRNA expression levels of *AOC3*, *MYH11* and *ACTA2* from microarray analysis

AOC3 and MYH11 protein expression level were assessed in human tissue and cell lysates and results confirm that both stain colonic myofibroblasts in both normal and cancer tissue. In order to determine whether these two markers might be able to distinguish between myofibroblasts and fibroblasts, we used Affymetrix microarray gene expression data to compare the level of αSMA (human gene: *ACTA2*), *AOC3* and *MYH11* mRNA expression levels between a panel of myofibroblast primary cultures (derived from colonic tissues) and skin derived fibroblast cultures (as described in materials and methods **Chapter 2.2.2**). Partek genomic suite software was used to compare the levels of expression in the four primary myofibroblast cultures against the levels of expression in the four fibroblast cultures. In **Figure 3.7,** *ACTA2* and *MYH11* showed similar expression profiles in the two groups while *AOC3* was significantly differentially expressed in myofibroblasts ($p<0.05$). These results suggest that AOC3 is not only a new marker for myofibroblasts but that its expression is specific to myofibroblasts in contrast to αSMA which is expressed at similar levels in both colon derived myofibroblasts and skin derived fibroblasts.

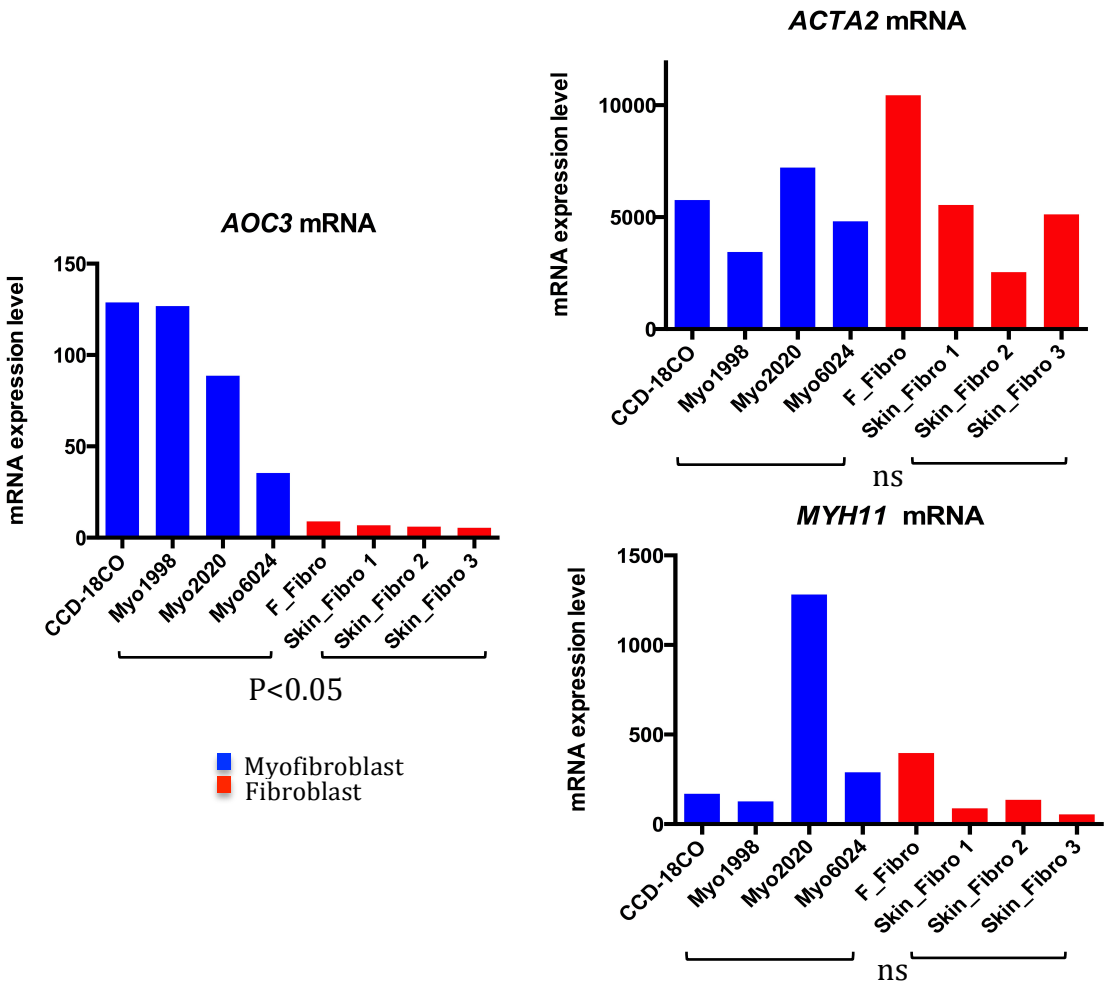

Figure 3.7
Comparison of mRNA expression levels of AOC3, MYH11 and ACTA2 between myofibroblast and fibroblast cells
AOC3, αSMA (human gene: *ACTA2*) and *MYH11* mRNA expression in 8 cell lines (4 of myofibroblast cultures and 4 of fibroblast cultures) measured by Affymetrix Human Genome U133 Plus 2.0 microarray. mRNA expression levels, along the Y axis, are linear fluorescent intensities. Among these three genes, *AOC3* is the only one significantly differentially expressed between myofibroblast and fibroblast cells ($p<0.05$) using a paired t test on the difference between the mean levels of expression in myofibroblast vs. fibroblast cells.

3.2.6 Heterogeneous expression of smooth muscle actin and myosin heavy chain 11 in myofibroblasts and fibroblasts

One of the most studied features of myofibroblasts relates to their contractile ability, which has been described as similar to that smooth muscle (Gabbiani et al., 1971). Alpha- smooth muscle actin (αSMA) has been widely used as a marker for identifying myofibroblasts because of this property. However, heterogeneous expression of αSMA in myofibroblasts has been reported in many studies and our own results confirm this observation. As shown in the top panel of **Figure 3.8A,** the immunofluorescent staining in 5 primary myofibroblast cultures showed αSMA staining of discreet subpopulations of myofibroblasts, rather than uniform staining, confirming the heterogeneous pattern of expression of αSMA in myofibroblasts. Similarly, some normal fibroblasts and foreskin fibroblasts also showed high levels of αSMA (foreskin and skin fibro 2) in normal culture conditions, as is demonstrated in the lower panel of **Figure 3.8A**. In addition, some positive staining of MYH11 could be found in foreskin fibroblasts (**Figure 3.8B**). Collectively, these results demonstrate that among these markers, αSMA and MYH11 are inadequate to distinguish myofibroblast cells from fibroblast cells.

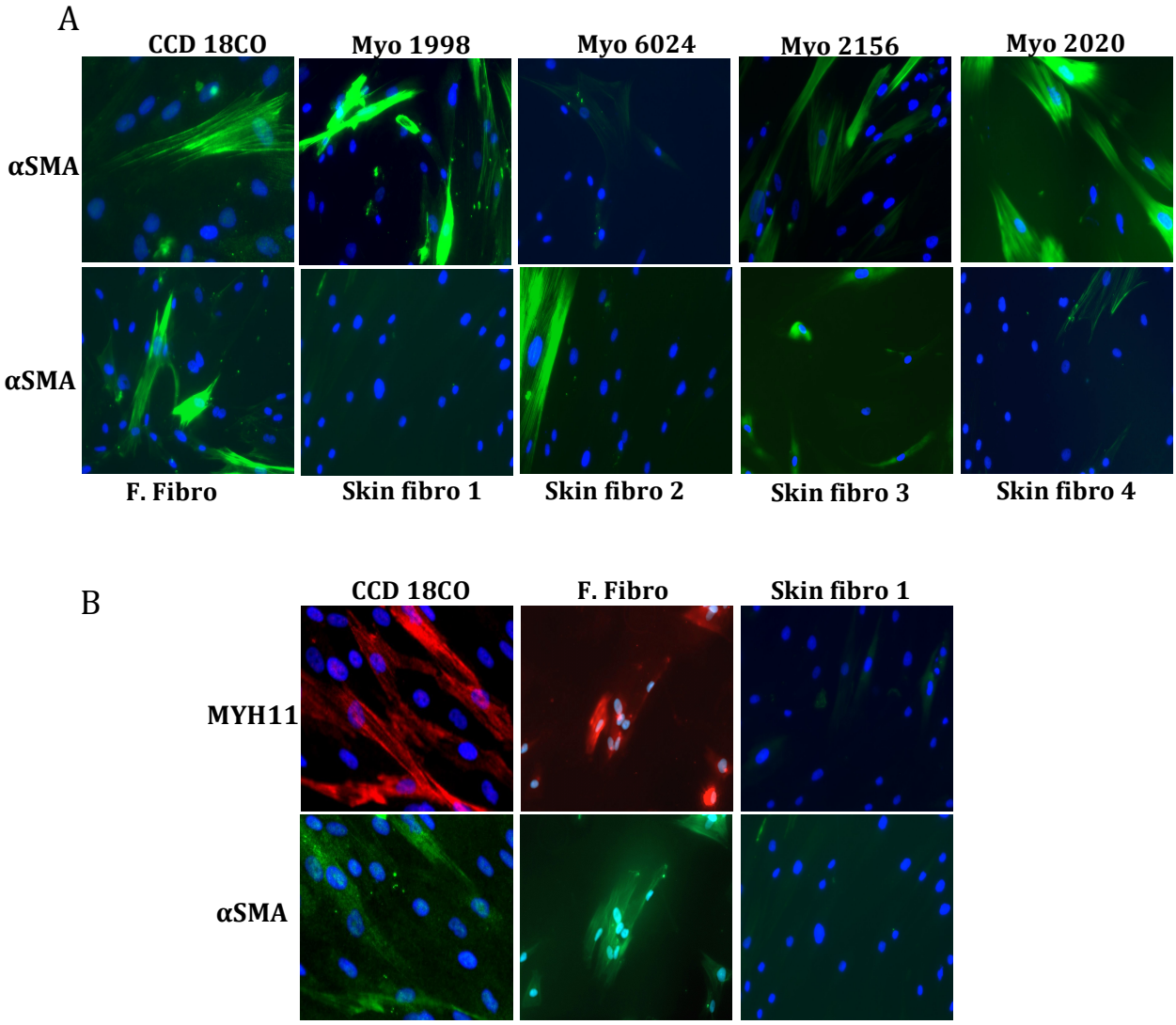

Figure 3.8
Analysis of α-smooth muscle actin (αSMA) and myosin heavy chain 11 (MYH11) expression in myofibroblast and fibroblast cultures.
(A) Immunofluorescent staining of 5 myofibroblast and 5 normal fibroblast cell cultures with αSMA. (B) Co-staining MYH11(red) and αSMA (green) on CCD18CO, foreskin fibroblasts and normal skin fibroblast cells. X20 magnification

3.3 Discussion

It is now widely accepted that myofibroblasts present within a tumour play a significant role in contributing to carcinoma growth. However, it is difficult to target them within stroma due to the lack of myofibroblast-specific immunocytochemical markers. To help understand the difference between myofibroblasts and conventional fibroblasts and further evaluate the role of myofibroblasts, we have identified myofibroblasts using a cell surface marker defined by the monoclonal antibody PR2D3. As an integral membrane protein, this marker is likely to have an important function that could so be identified and then help to characterize myofibroblasts both for *in vitro* studies and in clinical material.

In this study, PR2D3 antibody was made freshly from PR2D3 hybridoma that was raised by Richman, et al., 1987. Through the enrichment of the bound target proteins by immuno pull-down assay from human colonic smooth muscle lysates by PR2D3 mAb, two target proteins were identified using mass spectrometry based amino acid sequencing as AOC3 and MYH11.

AOC3 is a transmembrane glycoprotein also known as semicarbazide-sensitive amine oxidases (SSAOs), and vascular adhesion protein-1 (VAP-1), which plays a dual function as an adhesion molecule that also has enzymatic properties (Salmi and Jalkanen, 1992, Salmi and Jalkanen, 1996). AOC3 has been reported to be expressed in normal tissues in the endothelial cells of veins, in the pericytes and smooth muscle cells, as well as in adipocytes (Salmi and Jalkanen, 1992, Salmi et al., 1993), but there are no publications to date that describe its expression in colorectal pericryptal myofibroblast

cells. Our results show, for the first time, that AOC3 is present on myofibroblasts and that antibodies to AOC3 can be used as surface markers for detecting myofibroblasts in human tissue sections, primary cultures and cell lines. In subsequent chapters, we explore the extensive expression profiling analyses of AOC3 *in vivo* and *in vitro*, as well as the functional significance of its expression in myofibroblasts.

Given the evidence that myofibroblasts have been shown to express a number of contractile proteins in addition to α-smooth muscle actin, such as myosin heavy chain (MYH11) and SM22 (TAGLN) (Chambers et al., 2003, Popova et al., 2010). Myosin Heavy Chain 11 (MYH11) is a smooth muscle cell-specific protein. Smooth muscle myosin, the major contractile protein in these cells, is composed of a MYH11 dimer along with two pairs of non-identical light chains. Deletion and missense mutation located in the C-terminal domain of MYH11 are predicted to affect the structure and assembly of myosin thick filaments (Zhu et al., 2006). Several studies have shown that MYH11 was induced by TGFβ treatment in mesenchymal stem cells (Popova et al., 2010), where it was involved in many intracellular functions including cell migration, adhesion, intracellular transport and signal transduction. Moreover, there is a growing body of evidence suggesting that MYH11 may be involved in the progression of several cancer types including colorectal, breast and gastric cancers and is associated with poor prognosis (Loikkanen et al., 2009, Cui et al., 2010, Pessina et al., 2010, Wang et al., 2014). Our data showed strong expression of MYH11 in myofibroblast cells *in vivo* and *in vitro*, however, the mRNA expression level and immunostaining results indicated that MYH11 is not adequate to be the only marker for distinguishing myofibroblasts and normal fibroblast cells. The same is true for the commonly used myofibroblast marker αSMA.

The result of immunoprecipitation with PR2D3 mAb showed that two proteins were pulled down together by PR2D3, which suggested a potential interaction between these two proteins. However, there has so far been no indication that there is any direct interaction between AOC3 and MYH11. While we were able to demonstrate that pull-down using PR2D3 enriched for both AOC3 and MYH11, neither the AOC3 nor the MYH11 antibodies available were suitable for use in pull-down assays (despite several attempts), so we were not able to further explore the possibility that AOC3 physically interacts with MYH11. There remains the possibility of physical interaction via the intra cellular cytoplasmic tail of AOC3 to MYH11. It is also possible that this association is non-specific. Further investigation is needed to explore the possible functional significance of this interaction.

Collectively, the results of this chapter indicated that AOC3 is a novel marker of myofibroblasts, which was identified though home-raised PR2D3 antibody. The preliminary results presented in this chapter suggest that it may be able to distinguish between normal fibroblasts and myofibroblasts isolated from human colon more efficiently than the most commonly used marker for this purpose, αSMA.

CHAPTER FOUR

AOC3,
A NOVEL MARKER Of
MYOFIBROBLASTS

CHAPTER 4: AOC3, A NOVEL MARKER OF MYOFIBROBLASTS

4.1 Introduction

In the previous chapter, we identified AOC3 as a new marker of myofibroblasts in human colon through identification of the PR2D3 mAb binding protein. AOC3 is an endothelial, cell surface-expressed oxidase (amine oxidase, copper containing-3, also known as vascular adhesion protein-1, **VAP-1**). It was first described as a 180-kD dimeric type II transmembrane glycoprotein, which plays a dual function as an adhesion molecule and also has enzymatic properties in endothelial cells (Salmi and Jalkanen, 1992, Salmi and Jalkanen, 1996). In addition to synthesis in endothelial cells, where it mediates lymphocyte binding, AOC3 is also been found expressed in pericytes, adipocytes and also in smooth muscle cells. Smooth muscle AOC3 is functionally and structurally different from endothelial AOC3 with lower molecular mass, abundant N-linked oligosaccharide and only functions as monoamine oxidases (Jaakkola et al., 1999). Our data suggested that AOC3 in myofibroblasts might be more similar to the AOC3 in smooth muscle, as after cleavage of N-linked glycan by 2-mercaptoemthanol under the denaturing conditions of western blots, we observed the lower molecular weight of AOC3 in myofibroblasts.

Transforming growth factor-β (TGFβ) is a multifunctional regulatory cytokine, which is a potent growth inhibitor in most of normal epithelial cells and in the early phase of epithelial carcinogenesis but is produced in excessive quantities by many advanced tumour types (Barcellos-Hoff and Akhurst, 2009). The excess TGFβ is thought to drive malignant progression through its effect both on the tumour cell and on the tumour

microenvironment. TGFβ has been long recognized as an important factor in myofibroblast activation, which can induce the expression of αSMA via Samd3, and also induce a contractile phenotype (Hu et al., 2003, Lijnen et al., 2003). Moreover, TGFβ-mediated signalling is central to fibrotic responses in lung, liver and kidney (Desmouliere et al., 1993, Sheppard, 2006, Liu et al., 2006). However, it is not known whether AOC3 expression is regulated by TGFβ-mediated response in myofibroblasts.

The work presented in this chapter first shows the extensive protein expression profiling analysis of AOC3 in a variety of human normal tissues and cancer tissues based on immunofluorescence. Assessment of AOC3 expression by flow cytometric analysis of a panel of primary myofibroblast cultures confirmed the specificity of the marker and identified AOC3 as a candidate specific marker of myofibroblasts with application in flow cytometric analyses. The regulation of AOC3 expression by TGFβ in myofibroblasts and its potential functional significance were then investigated

4.2 Results

4.2.1 Characterization of AOC3 expression in human tissue

Immunofluorescent staining was performed on human paraffin-embedded sections, obtained from Oxford University Hospitals (UK) and a commercial tissue array, purchased from SuperBioChips Laboratories (Seoul, Korea).

4.2.1.1 AOC3 in normal tissues

In the previous chapter, we have shown the staining of AOC3 expression of human colon pericryptal myofibroblasts in normal and tumour derived tissue sections, and confirmed its specificity by double staining with other molecular markers (**Figure 3.5**). To extend the expression profiling to different human tissues, immunofluorescent staining was performed on a range of different normal human tissues. In **Figure 4.1**, we first assessed tissues of the gastrointestinal tract, including stomach, small bowel, colon and rectum. Strong AOC3 expression (shown in red) was seen in pericryptal myofibroblasts in colorectal tissues and periglandular myofibroblasts in stomach. The lamina muscularis mucosae, below crypts were also labelled by AOC3 and αSMA. Vascular smooth muscle cells were stained, but AOC3 expression was completely absent in epithelial cell layers.

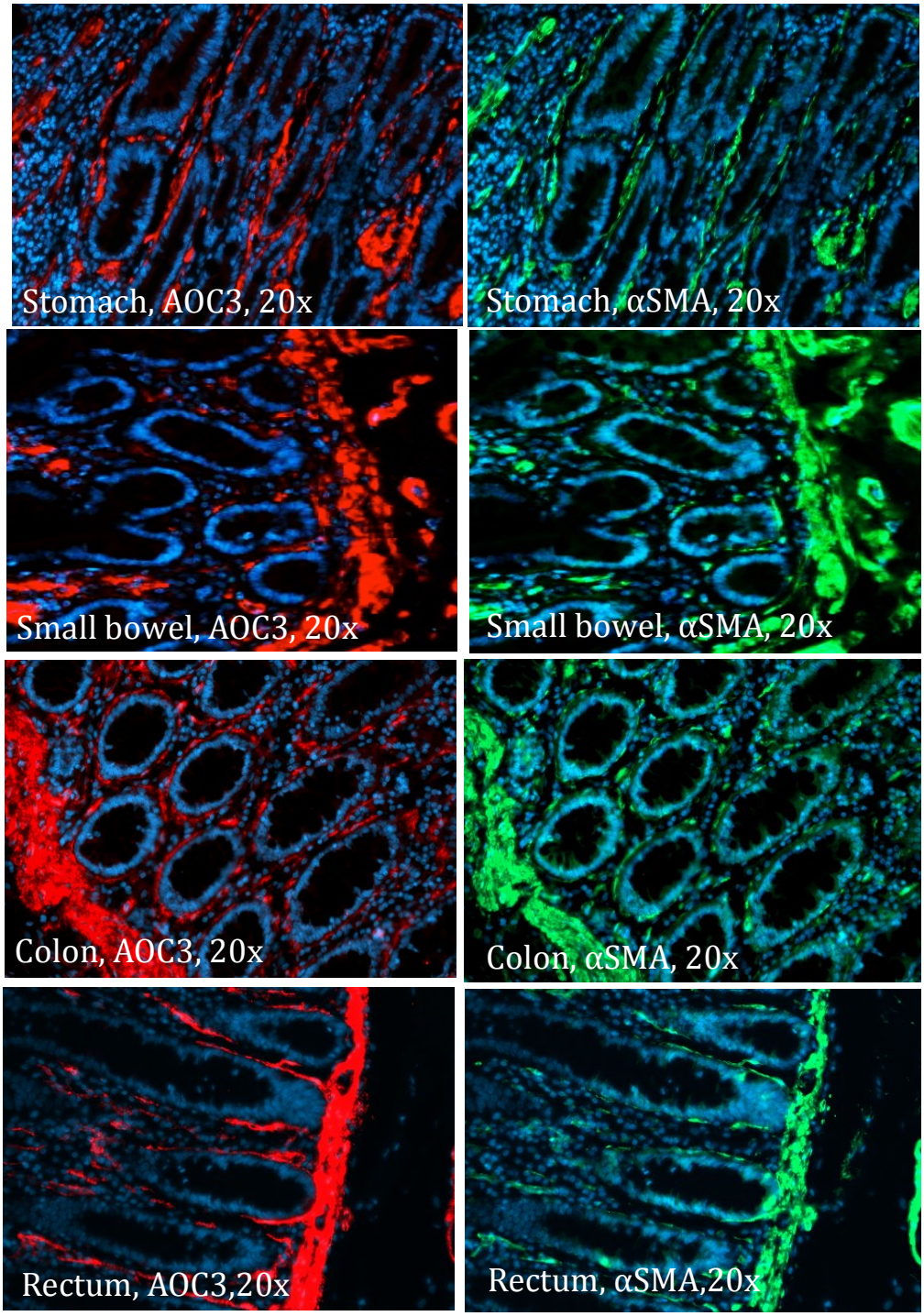

Figure 4.1
AOC3 expression in myofibroblasts in normal human gastrointestinal tract (GI tract)
Double staining of paraffin-embedded sections of human GI tract tissues (from top to bottom: stomach, small bowel, colon and rectum) with αSMA (green) and AOC3 (red). X20 magnification

In prostate tissues, there was strong AOC3 staining of stromal myofibroblasts but not of glandular or epithelial cells. Periacinar myofibroblasts in pancreatic tissues were also labelled by AOC3 (**Figure 4.2**).

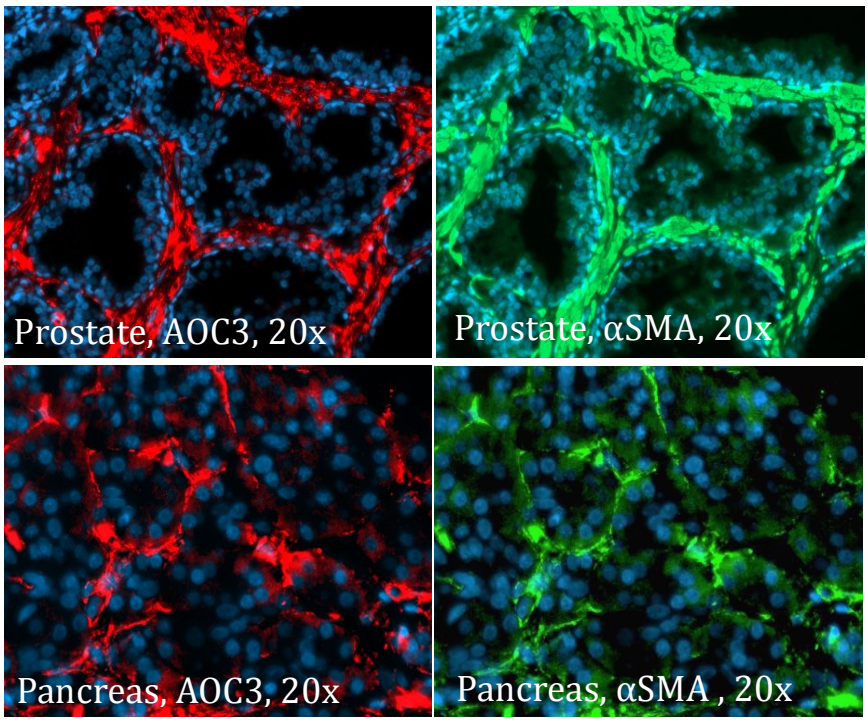

Figure 4.2
AOC3 expression in myofibroblasts of other normal human tissues
Double staining of normal prostate and pancreas tissues with αSMA (green) and AOC3 (red) confirms presumptive staining of myofibroblasts. X20 magnification

In addition to staining of myofibroblasts, AOC3 has been previously been reported to be expressed in smooth muscle cells and endothelial cells in heart, gut, endothelial vessels and tonsil (Salmi and Jalkanen, 1992, Salmi et al., 1993). In **Figure 4.3**, our results showed that AOC3 is present in smooth muscle cells surrounding testis seminiferous

tubules, as well as some contractile cells or to be myofibroblasts around the alveolar wall in lung, based on the AOC3 and αSMA positivity.

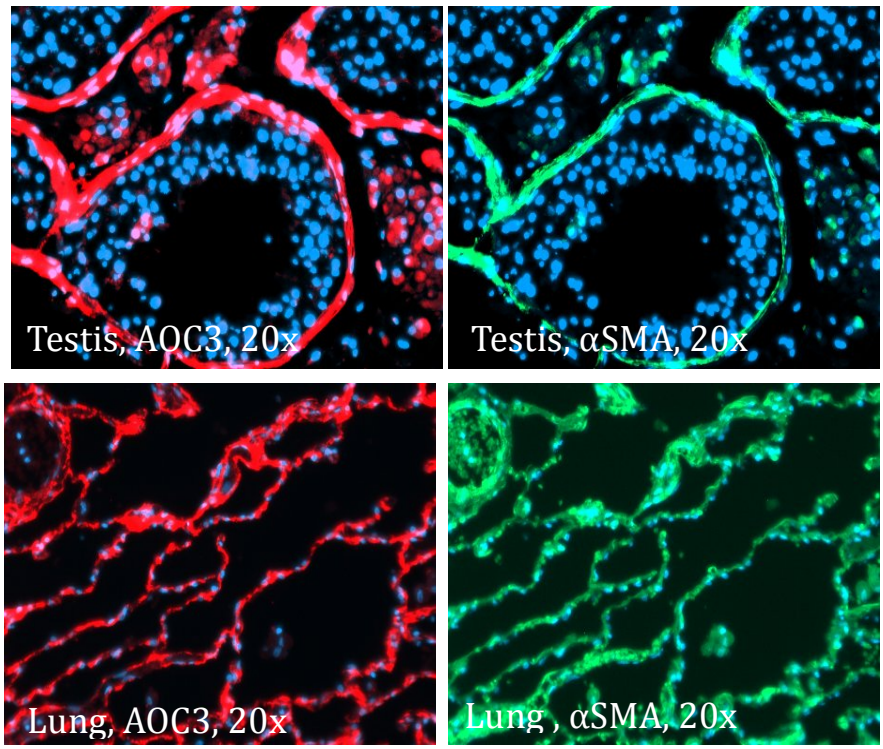

Figure 4.3
AOC3 expression in other normal human tissues
Double staining of normal tissues of testis, lung and kidney with αSMA (green) and AOC3 (red). AOC3 and αSMA are both positive in smooth muscle cells and basement membranes. X20 magnification

4.2.1.2 AOC3 in tumour tissues

We continued our analysis of AOC3 expression in a range of human tumours. In none of the analyzed tumours was AOC3 staining detectable in tumour cells. Expression was only observed in tumour associated stroma (**Figure 4.4**). In order to clearly distinguish epithelial structures from stromal areas, AUA1 mAb (in-house antibody against

EpCAM, red) was used for identifying epithelial cells and AOC3 for stromal myofibroblasts (green) in prostate and rectal tumour sections (**Figure 4.4A**). DAPI was used for nuclear staining (blue).

AOC3 expression in corresponding tumour tissues of GI tract is shown in **Figure 4.4B**. AOC3 is diffusely expressed in the tumour stroma, which reflects an increased number of myofibroblasts in colorectal and prostate adenocarcinomas. This observation is consistent with previous studies showing an increasing number of myofibroblasts around stroma in higher-grade tumours (Tsujino et al., 2007, Adegboyega et al., 2002).

A

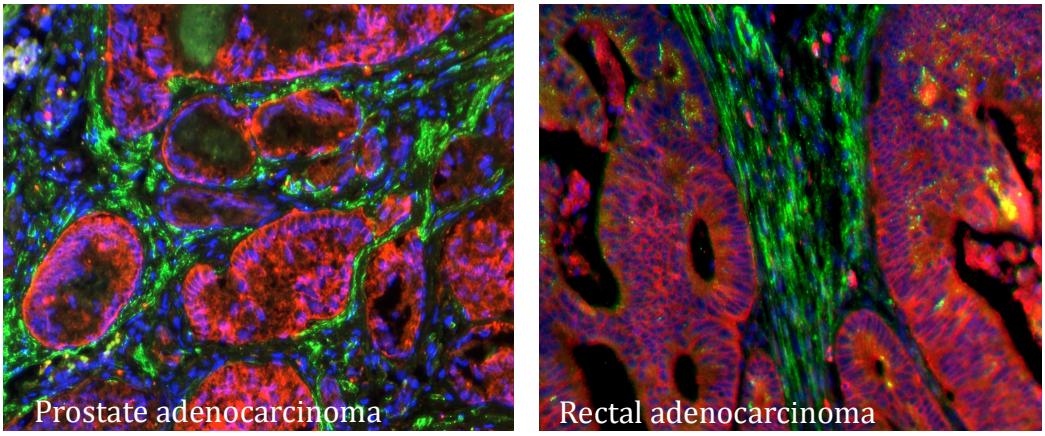

AOC3/AUA1 x20

B

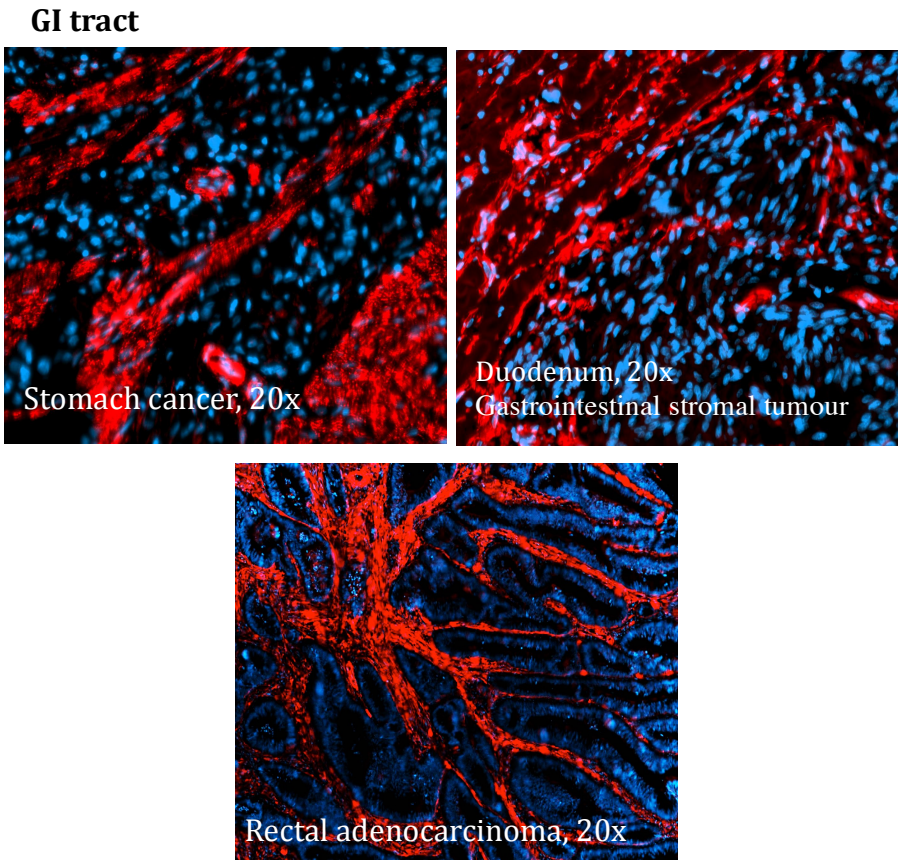

Figure 4.4
AOC3 expression in myofibroblasts of human tumour tissues
(A) Co-staining of human tumour tissues with AOC3 (green) for myofibroblasts and AUA1 (red) to identify epithelial cells. (B) AOC3 staining of myofibroblasts in GI tract tumour tissues. X20 magnification

Furthermore, myofibroblasts can also be detected by AOC3 mAb staining in lymphomas, ovary cystadenocarcinomas, endometrial adenocarcinomas and liver cancers (**Figure 4.5A)**. Surprisingly, myofibroblasts in the breast were AOC3-negtive, both in normal tissue and in ductal and lobular carcinomas. They were however, positive for αSMA expression. We have examined several additional tissue sections from both normal breast and breast cancers, including a breast cancer tissue array to

confirm this unexpected finding. The results are consistent and representative data are shown in **Figure 4.5B**.

Table 4.1 and **4.2** showed the summarized data obtained from tissue-array on the tissue distribution of AOC3. In some tissues, different expression profile for AOC3 compared to αSMA has been observed, such as in normal myometrium (AOC3+ve, αSMA-ve), normal salivary gland (AOC3-ve, αSMA+ve) and uterine cervix of squamous cell carcinoma (AOC3-ve, αSMA+ve) and breast tumour (AOC3-ve, αSMA+ve), which suggested the expression of AOC3 might be in a tissue specific manner or implied the further heterogeneity of myofibroblasts and fibroblasts in different tissues.

A

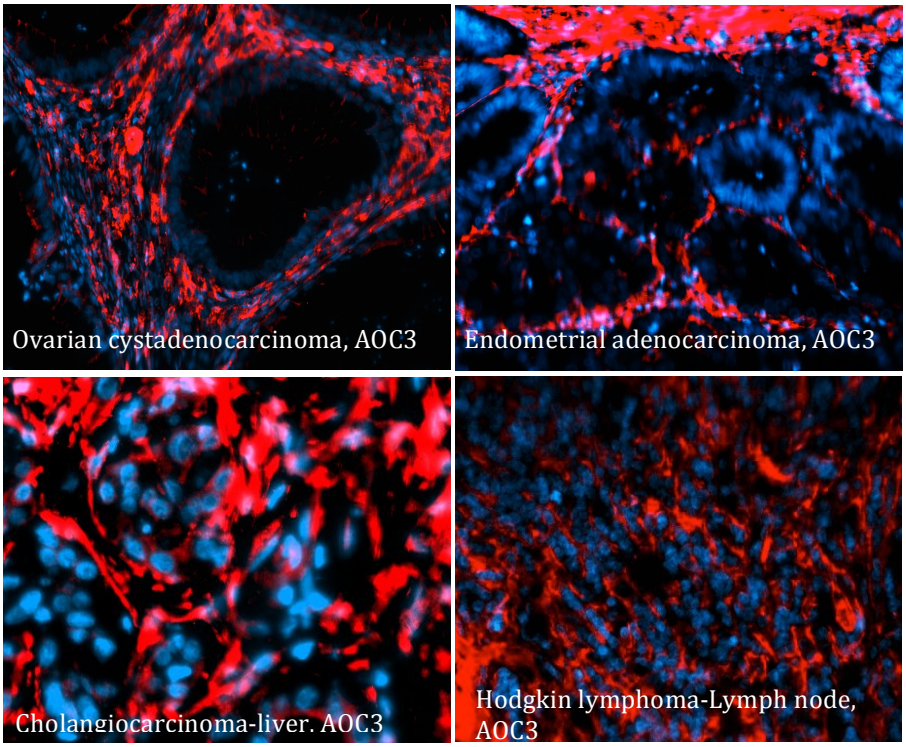

B

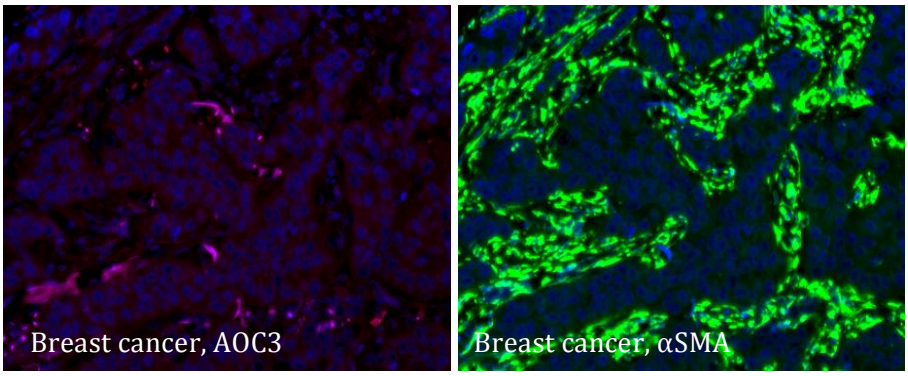

Figure 4.5
AOC3 expression in myofibroblasts is tissue-specific in other human tumour tissues
(A) AOC3 staining of myofibroblasts in other human tumour tissues (B) Myofibroblasts in breast cancer are AOC3-negative but αSMA-positive. Several different cases were tested and similar results were obtained. Representative result is shown here. X20 magnification

Organ	Diagnosis	AOC3 staining	αSMA staining	
Skin	Normal	-	-	
Breast	Normal	-	-	
Spleen	Normal	-	-	
Lymph node	Normal	-	-	
Skeletal muscle	Normal	-	-	
Lung	Normal	+	+	Positive cells are around alveolar walls
Salivary gland	Normal	-	+	
Liver	Normal	+	+	Hepatic stellate cells; positive cells in central vein and smooth muscle cells in the portal tract
Gallbladder	Normal	-	-	
Pancreas	Normal	+	+	Periacinar pancreatic stellate cells
Tonsil	Normal	-	-	
Stomach, antrum	Normal	+	+	myofibroblasts
Stomach, fundus	Normal	+	+	myofibroblasts
Small bowel	Normal	+	+	myofibroblasts
Colon	Normal	+	+	myofibroblasts
Rectum	Normal	+	+	myofibroblasts
Kidney	Normal	+	+	Interstitial cells and basement membrane
Urinary bladder	Normal	+	+	
Prostate	Normal	+	+	myofibroblasts
Testis	Normal	+	+	Peritubular myoid cells around seminiferous tubules
Uterine cervix	Normal	-	-	
Endometrium	Normal	+	+	myofibroblasts
Myometrium	Normal	-	+	Positive cells are smooth muscle cells
Placenta	Normal	-	-	
Adrenal gland	Normal	-	-	
Thyroid	Normal	-	-	
Cerebrum	Normal	-	-	
Cerebellum	Normal	-	-	

Table 4.1 Human normal tissue distribution of AOC3
Anomalies in the expression profile between AOC3 and αSMA staining are highlighted.

Organ	Diagnosis	AOC3 staining	αSMA staining	
Skin	Squamous cell carcinoma	-	+	
Subcutis	Liposarcoma	+	-	Adipocytes are positive
Breast	Ductal carcinoma in situ	-	+	
Breast	Infiltrating duct carcinoma	-	+	
Lymph node	Hodgkin lymphoma	+	+	
Bone	Osteocarcinoma	-	-	
Lung	Adenocarcinoma	-	-	
Lung	Squamous cell carcinoma	-	-	
Liver	Cholangiocarcinoma	+	+	Hepatic myofibroblasts
Esophagus	Squamous cell carcinoma	-	-	
Stomach	Adenocarcinoma	+	+	myofibroblasts
Stomach	Malignant lymphoma, diffuse large B cell	+	+	myofibroblasts
Stomach	Signet ring cell carcinoma	+	+	myofibroblasts
Duodenum	Gastrointestinal stromal tumor, malignant	+	+	myofibroblasts
Descending colon	Adenocarcinoma	+	+	myofibroblasts
Rectum	Adenocarcinoma	+	+	myofibroblasts
Kidney	Renal cell carcinoma	+	+	Interstitial cells and basement membrane
Urinary bladder	Transitional cell carcinoma	+	+	Smooth muscle cells are positive
Prostate	Adenocarcinoma	+	+	myofibroblasts
Testis	Seminoma	+	+	Peritubular myoid cells around seminiferous tubules
Uterine cervix	Squamous cell carcinoma	+	-	myofibroblasts
Endometrium	Adenocarcinoma	+	+	myofibroblasts
Ovary	Metastatic adenocarcinoma (from stomach)	+	+	myofibroblasts
Ovary	Mucinous cystadenocarcinoma	+	+	myofibroblasts
Thyroid	Papillary carcinoma	-	-	

Table 4.2 Tissue distribution of AOC3 in human cancers on a tissue microarray
Anomalies in the expression profile between AOC3 and αSMA staining are highlighted.

4.2.2 AOC3 expression in myofibroblast cultures

4.2.2.1 AOC3 is expressed in cultured colorectal derived myofibroblasts but not normal fibroblasts

Western blot and immunofluorescence experiments using monoclonal AOC3 antibody TK8-14 were performed on cultured cells to test for expression of AOC3. These experiments revealed the expression of AOC3 protein by colonic derived myofibroblast cultures but not by human foreskin or skin fibroblast cultures (**Figure 4.6**). All AOC3-positve myofibroblast cultures expressed AOC3 protein in 150 kDa under non-reduced conditions (**Figure 4.6A**) and immunofluorescent staining was performed on live cells without fixation. **Figure 4.6B** showed that the commercially available myofibroblast cell line, CCD 18CO clearly stained with both fluorescent labeled AOC3 and PR2D3, while the foreskin fibroblasts were completely unstained. This is in agreement with the mRNA expression data shown in Chapter 3 (see **Figure 3.7**).

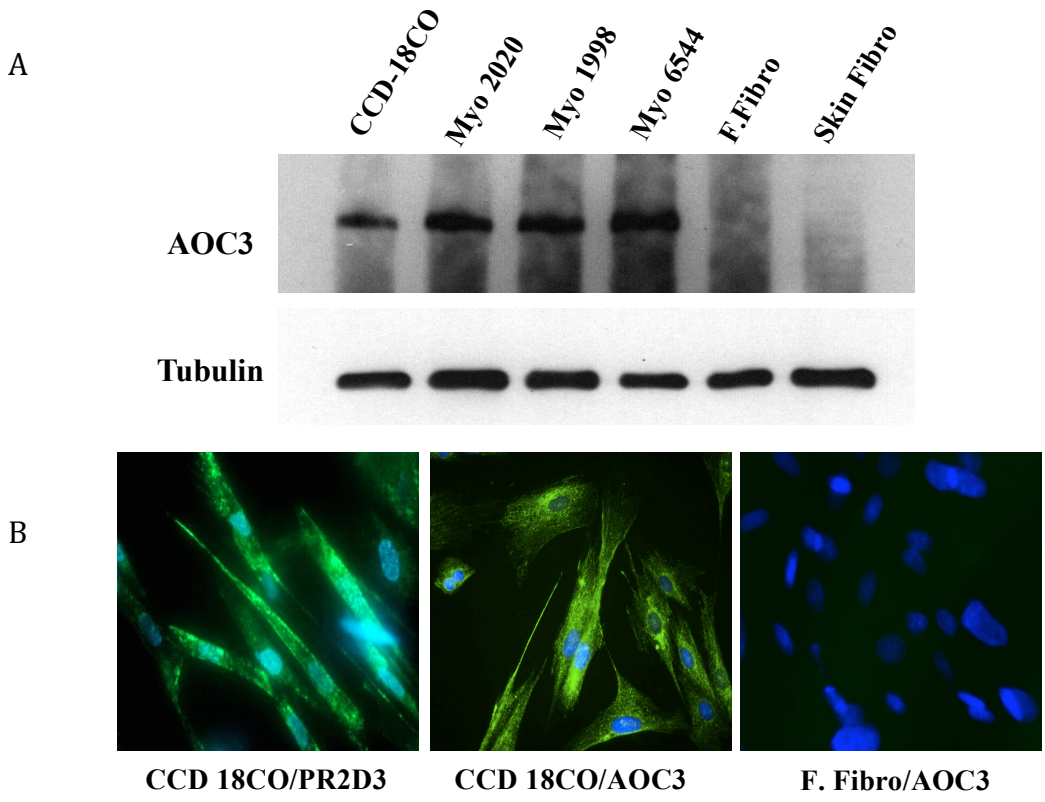

Figure 4.6
AOC3 protein expression in primary myofibroblast cultures but not fibroblast cells. (A) AOC3 protein was detected by western blot in commercially available CCD 18CO cell line, primary myofibroblasts myo2020, myo1998, myo6544, but not in foreskin fibroblasts or skin fibroblasts with anti AOC3 mAb (TK8-14). Tubulin was used as loading control. (B) Immunofluorescent staining of CCD 18CO and foreskin fibroblast cells with PR2D3 and AOC3 mAb. X20 magnification

4.2.2.2 Confirmation of the specificity of AOC3 via siRNA-mediated silencing of AOC3 in CCD 18CO

To confirm the specificity of the anti AOC3 staining in myofibroblasts, knockdown experiments were performed on CCD 18CO cells using transient transfection of siRNA sequences for AOC3 knockdown (siAOC3). Scrambled sequences were applied as control. *AOC3* mRNA expression of CCD 18CO was assessed by quantitative RT-PCR after 24 and 48 hours. Expression was calculated relative to the average normalized Ct for scrambled siRNA cells. The maximum mRNA knockdown of 98% reduction was achieved after 24 hours in 20nM of siAOC3 relative to scrambled control (**Figure 4.7A**). AOC3 protein expression level as determined by western blot was almost completely abolished up to 72 hours after introducing siRNA, (**Figure 4.7B**). The specificity of AOC3 knockdown was confirmed by the fact that there was no reduction of AOC3 message or protein level in scrambled siRNA control compared to untreated control in CCD 18CO.

A

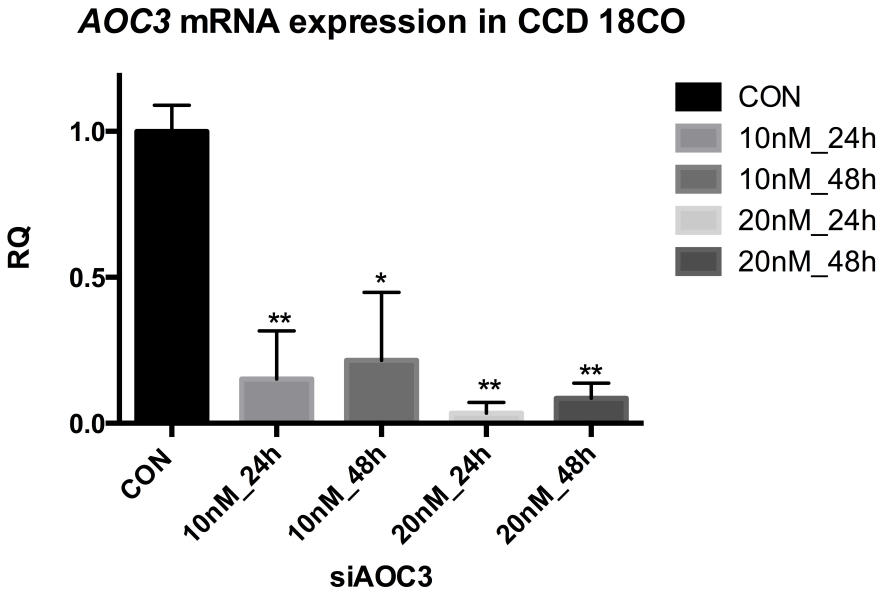

B

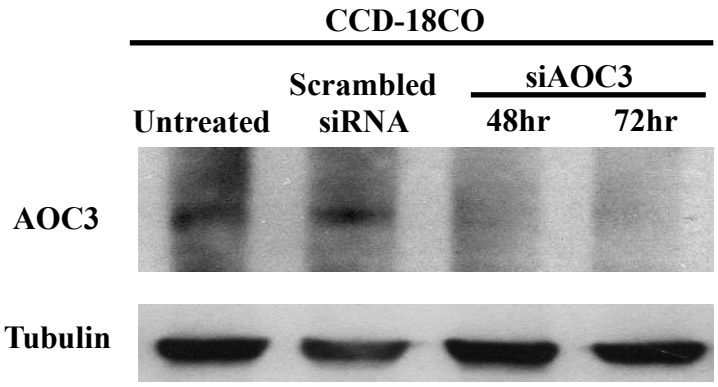

Figure 4.7
AOC3 mRNA and protein levels after siRNA mediated knockdown in CCD 18CO cells. Maximum knockdown was achieved at the (A) mRNA level of *AOC3* 24 hours, and at the (B) protein level after 48 hours, after transfection with AOC3 siRNA sequence and scrambled sequence as control. RQ= Relative quantity;
* $p<0.01$; ** $p<0.001$ versus scrambled siRNA control. Non-denaturing conditions used for western blot. n=3

4.2.2.3 Validation of *AOC3* mRNA expression in a range of human colonic primary myofibroblasts

AOC3 mRNA levels were assayed in a panel of 11 primary myofibroblast cultures derived from human colon (described in method **Chapter 2.2.2.2**), along with 2 fibroblast cultures, using TaqMan qRT-PCR primers and probe-sets. **Figure 4.8** showed that all myofibroblast cultures expressed AOC3 mRNA, but to varying extents. The majority of primary myofibroblast cultures showed high levels of *AOC3* mRNA expression; e.g. myo1998, myo6024, myo6544, CCD 18CO, myo6769, and myo6769C and myo6526. However, some myofibroblast cultures showed relatively lower expression of AOC3, e.g. myo6539, myo6550, myo6550C and myo7659. The AOC3 expression level is, however, nearly absent in foreskin and skin fibroblasts, which is consistent with our western blot and immunofluorescence results.

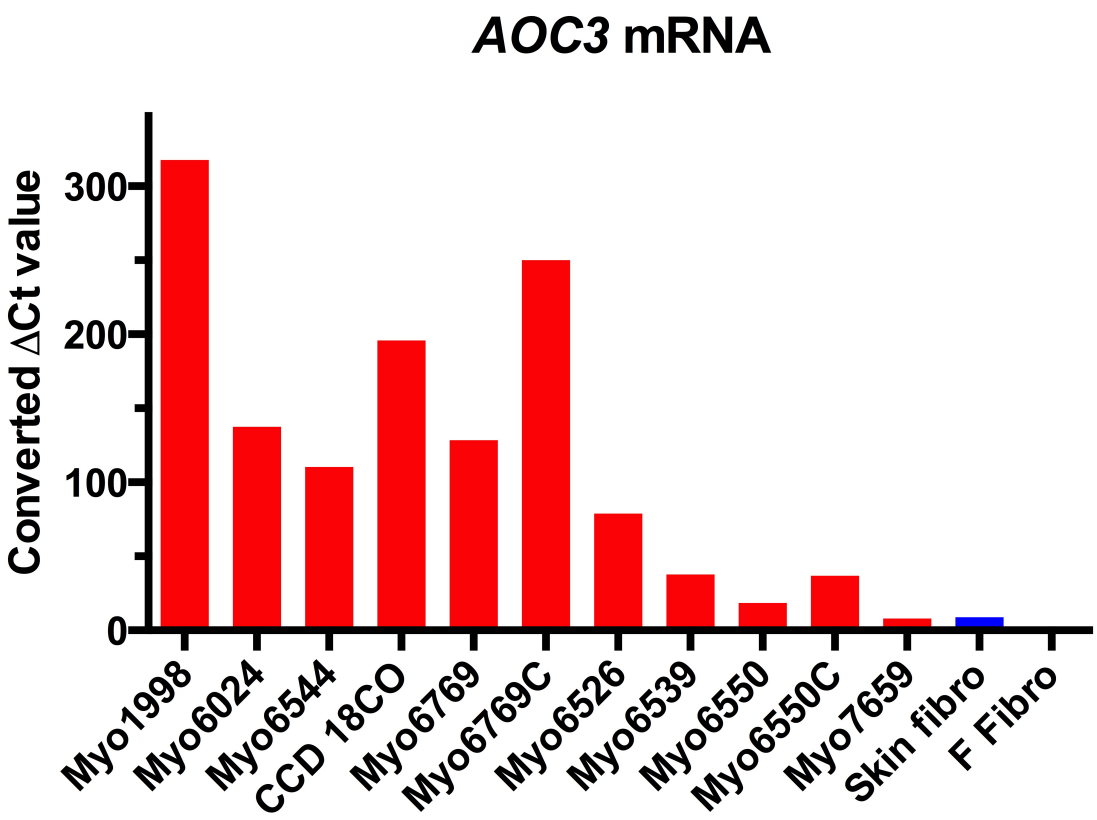

Figure 4.8
qRT-PCR validation of AOC3 mRNA expression in 11 myofibroblast and 2 fibroblast cultures. Expression levels for linearized, converted ΔCt values generated as described in materials and methods (**Chapter 2.3.3**) are shown. Briefly, ΔCt for each sample was subtracted from the highest ΔCt mean obtained (F. fibro: ΔCt mean 10.97 was used in this figure). Column in red: myofibroblast cultures; column in blue: fibroblast cultures.

4.2.2.4 Phenotypic characterization of primary myofibroblasts using AOC3 as a surface marker

As mentioned previously, AOC3 is a surface expressed protein. In order to assess the application of AOC3 as a surface marker, flow cytometric analysis was performed on a range of primary myofibroblasts with AOC3 mAb TK8-14, as well as with PR2D3 mAb. The antibody staining was performed on live cells, without any fixation. Among the myofibroblast cultures tested, 3 of these (myo6544, myo1998 and myo6526) were confirmed as reacting strongly with AOC3 and PR2D3 mAb (**Figure 4.9**). PR2D3 mAb showed a similar expression pattern to that obtained with AOC3 mAb, but with a little less intensity, Though myo6526 showed lower levels of expression, it was not negative for AOC3 or PR2D3 mAb, consistent with our qRT-PCR data shown in **Figure 4.8**. Anti AOC3 mAb again demonstrated specificity for myofibroblasts by showing completely negative expression in normal fibroblast cells (skin fibro, foreskin fibro) and CRC epithelial cells (SW1222, LS174T). Together, these data confirmed that anti AOC3 mAb is a specific surface-binding marker of myofibroblasts, which can be applied in flow cytometric analyses.

A

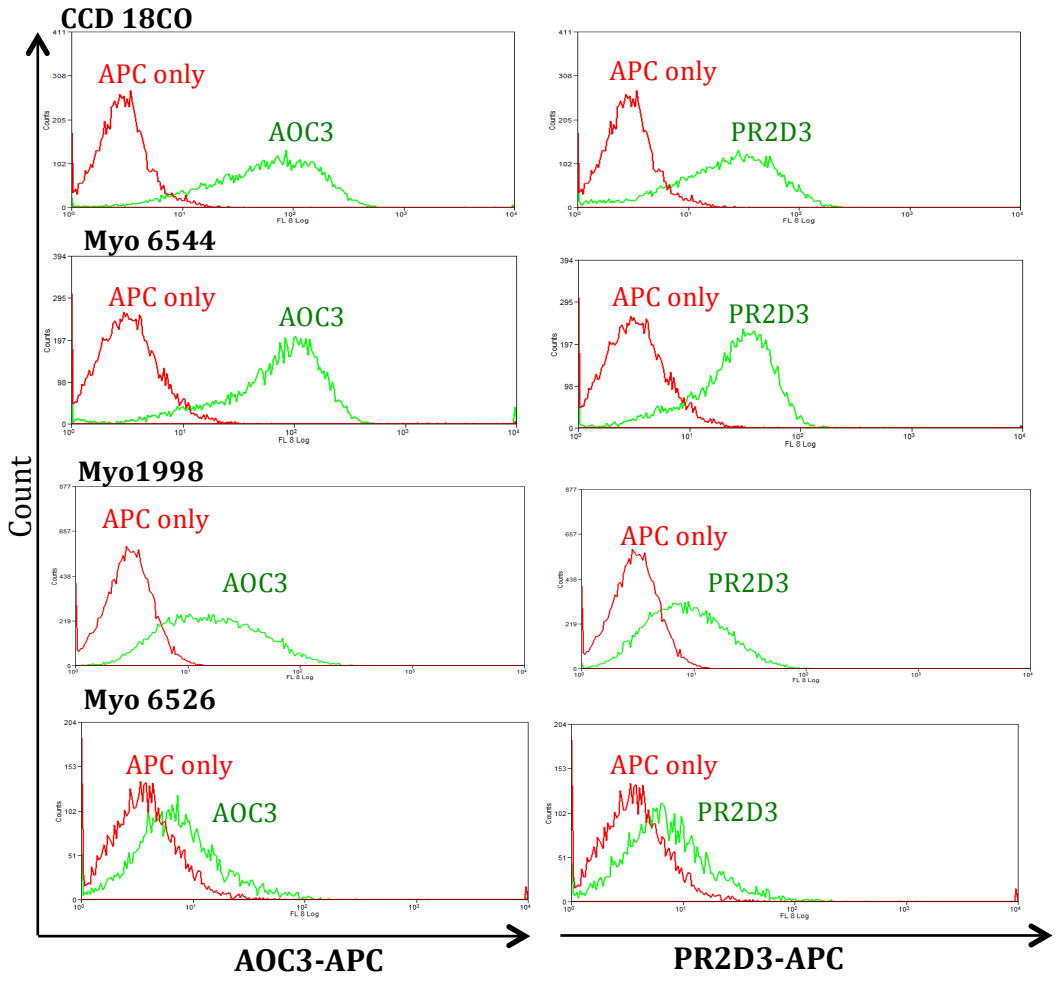

B

Fluorescence Intensity (mean value)			
	APC-only	AOC3-APC	PR2D3-APC
CCD 18CO	4.58	91.44	35.58
Myo6544	4.02	96.47	43.29
Myo1998	3.5	31.21	13.01
Myo6526	4.7	18.62	11.41

Figure 4 .9

Flow cytometry histograms of AOC3 and PR2D3 expression for three primary myofibroblast cell cultures (Myo6544, Myo1998, Myo6526) and CCD 18CO cells.

(A) The cells were subjected to a live staining with AOC3 or PR2D3 antibodies. Detection of the primary antibodies was via secondary antibody conjugated to allophycocyanin, APC (shown in green). Secondary antibody alone was used as a negative control (red). (B) The expression levels were quantified by taking the mean fluorescent intensity of the FACS histograms.

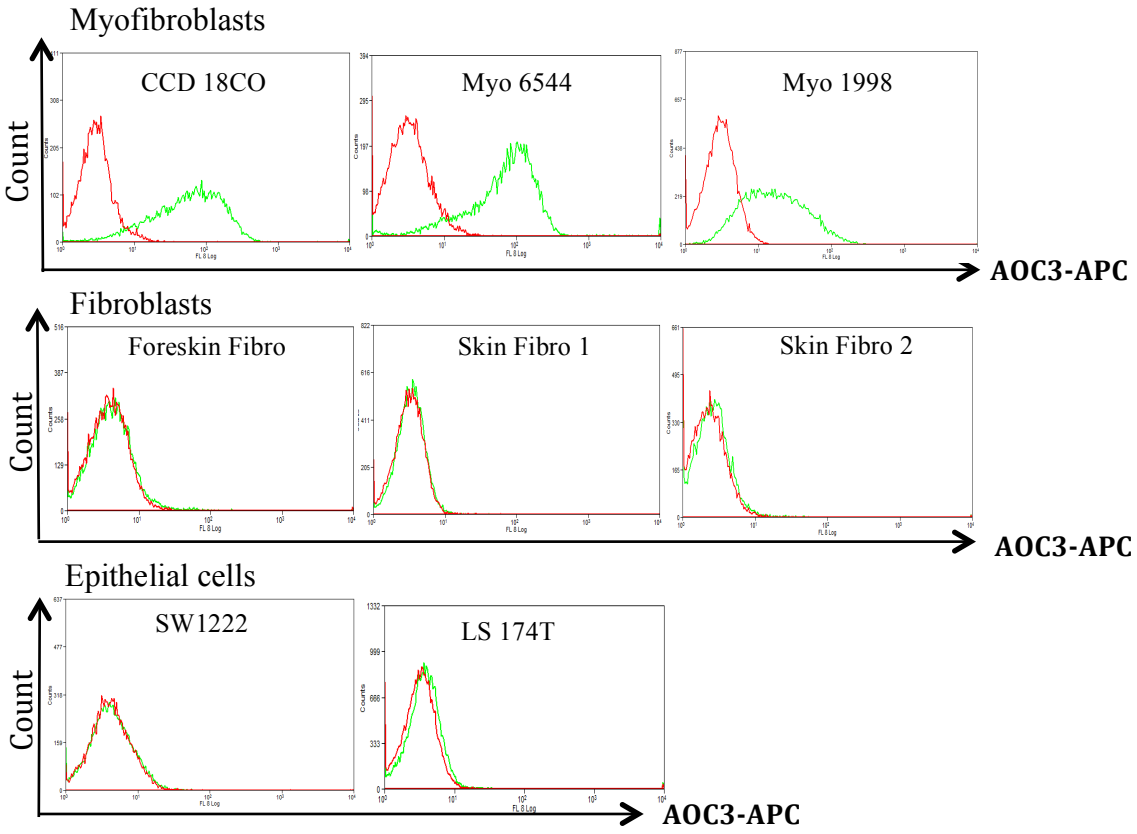

Figure 4 .10
AOC3 is a surface-expressed myofibroblast specific marker.
Flow cytometric analysis of primary myofibroblast cell cultures (Myo6544, Myo1998) and CCD 18CO cells. Fibroblast cells (foreskin fibro and two skin fibroblasts) and epithelial cells (SW1222, LS174T) show that myofibroblasts are positive for AOC3, whereas fibroblasts and epithelial cells do not express AOC3. Live cells were stained with AOC3 antibody, conjugated to APC (shown in green). APC secondary only was used as control (shown in red).

4.2.2.5 Surface expression of AOC3 enables FACS separation of myofibroblasts from epithelial cells (double staining)

Previous results have confirmed that AOC3 is specifically expressed by myofibroblasts and the anti AOC3 mAb can be used as a surface protein marker for identifying myofibroblasts. To assess the capacity of anti AOC3 mAb to separate cultured myofibroblasts from a mixed population of cells, we mixed primary myofibroblasts myo6544 with SW1222 cells (colorectal cancer derived cell line) in a ratio of 1: 1 before the analysis (**Figure 4.11**). The mixture of cells cannot be separated by cell size (FS/SS); however, double staining of AOC3-APC and AUA1-FITC showing the clear separation represented by the bimodal distributions.

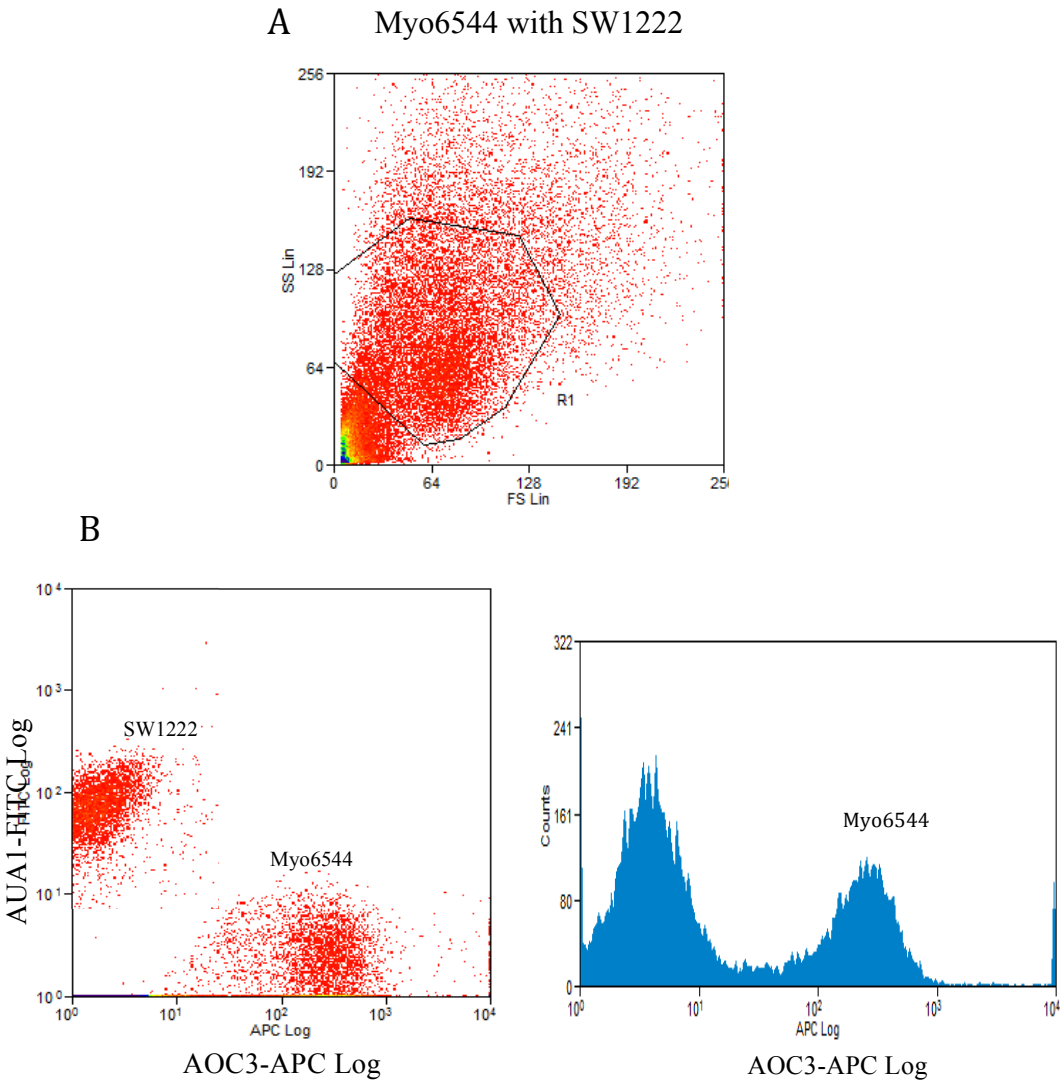

Figure 4.11
Separation of an artificial cell mixture of epithelial cells and myofibroblast cells by flow cytometry
Primary myo6544 were pre-mixed with SW1222 in a ratio 1:1 before the flow cytometry analysis. Cells were labeled with AOC3-APC for myofibroblasts, and AUA1-FITC for epithelial cells. (A) Cells size and granularity was demonstrated in FF/SS histogram and the main population of cells were gated to show the distribution of AOC3 versus AUA1 in 2D dot plot and 1D AOC3 histogram plot.

4.2.3 Regulation of AOC3 expression

4.2.3.1 Serum deprivation induces AOC3 expression in a time-dependent manner

TGFβ is a well-known key regulator of cell proliferation and differentiation, and has also been reported to upregulate expression of αSMA in myofibroblasts both *in vitro* and *in vivo* (Desmouliere et al., 1993, Ronnov-Jessen and Petersen, 1993). To understand whether AOC3 is involved in the TGFβ-depended response of myofibroblasts, TGFβ treatment was performed on CCD 18CO cells. In order to reduce the background level of any TGFβ contained in serum, TGFβ treatment was applied mostly using a serum free medium along with a 24hour-serum starvation beforehand. Unexpectedly, a dramatic increased level of AOC3 expression was found in the control group. To confirm the effect of serum on AOC3 expression, CCD 18CO cells were incubated with either normal serum (10% FBS) or serum free medium for various time periods. The protein expression levels of AOC3 under both conditions increased in a time dependent manner. However, at each respective time point, the AOC3 mRNA (**Figure 4.12B**) and protein levels as measured by western blot (**Figure 4.12A)** and by flow cytometry (**Figure 4.12C**), were significantly elevated in serum starved cells as compared to those maintained in 10% FBS after 48, 72 and 96 hours. For mRNA expression levels, qRT-PCR was more sensitive in detecting earlier increases in *AOC3* mRNA level from 24 hours (2.7-fold), to 48 hours (3.3-fold), 72 hours (3.6-fold) and 96 hours (4-fold) for cells under serum starvation relative to the cells grown in normal serum containing medium (**Figure 4.12B**). Our data suggested that the increased expression of AOC3 under serum starvation is due mainly to increased transcriptional levels in CCD 18CO cells.

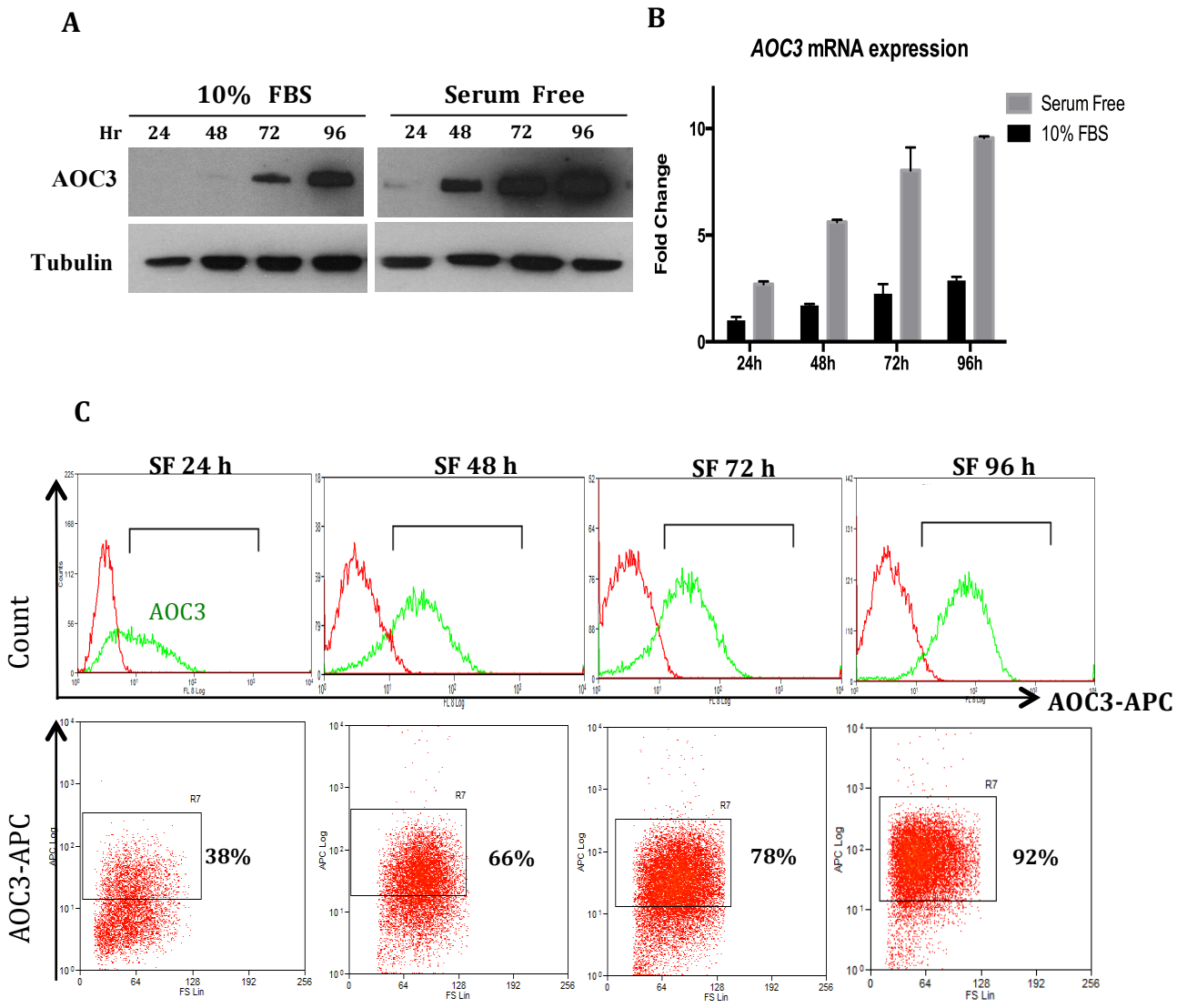

Figure 4.12
Serum starvation increased AOC3 expression in CCD 18CO cells
CCD 18CO cells were cultured with 10% FBS or without serum for 24, 48, 72 and 96 hours. AOC3 protein expression was measured using western blots (A) and flow cytometry (C). Tubulin is shown as loading control in western blots and APC labelled secondary antibody alone was used as control (shown in red) in flow cytometry. Gating in histogram plot is equal to the rectangle gating in dot plots, which represents the AOC3 positive population. (B) *AOC3* mRNA level was determined using qRT-PCR. Ct values were normalized to *UBC* and fold change was calculated relative to cells in 24hr with 10%FBS. All experiments were independently repeated at least three times, and similar results were obtained

4.2.3.2 TGFβ inhibition of AOC3 production

10% FBS-supplemented medium contains about 1,000-2,000pg/ml of latent TGFβ (Danielpour et al., 1989, Oida and Weiner, 2010), which might contribute to the delayed production of AOC3 in cells grown in 10% FBS serum containing medium, compared to in serum free medium. CCD 18CO cells were treated with or without 10ng/ml TGFβ and grown in either serum free or serum containing medium for various time periods. All cells were initially serum starved for 24 hours before treatment with TGFβ. Here, four separate conditions were tested: normal serum in medium (NS, 10%FBS), TGFβ/normal serum in medium, serum free medium (SF) and TGFβ/serum free medium (**Figure 4.13**).

Data showed the expression of AOC3 protein in CCD 18CO cells was significantly reduced by TGFβ in serum free medium in a time-dependent manner. In normal serum condition, AOC3 protein increased slowly with the time, however, the expression level was completely abolished when TGFβ was added into normal serum levels (**Figure 4.13C**). These observations are confirmed by flow cytometric analysis of CCD 18CO cells 96 hours after addition of TBFβ in both serum containing and serum free conditions. The inhibitory effects of TGFβ on AOC3 expression in CCD 18CO were also seen at the mRNA level in another repeat experiment (**Figure 4.13B**), suggesting transcriptional control.

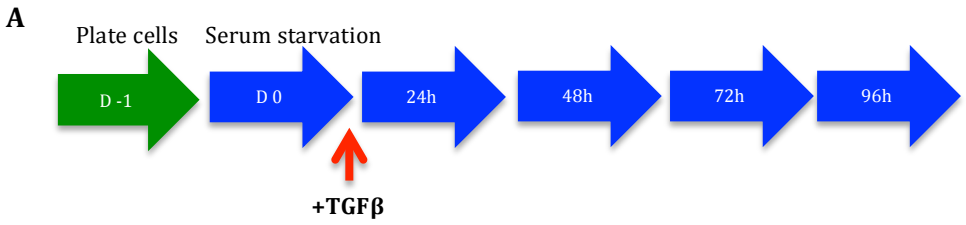
A
Plate cells
Serum starvation
D -1
D 0
24h
48h
72h
96h
+TGFβ

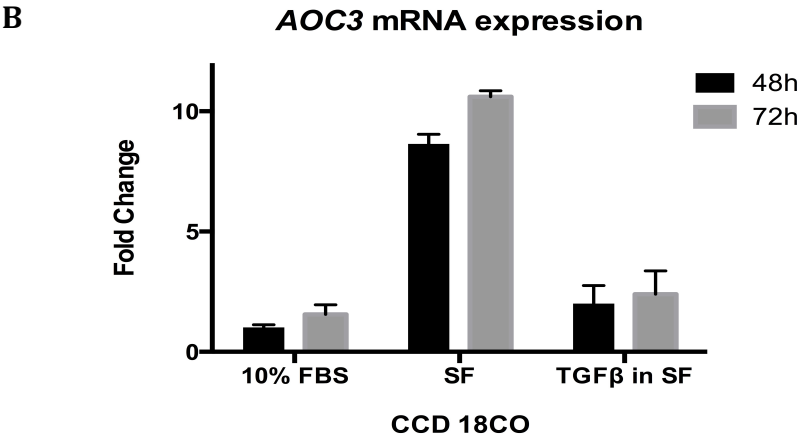
B
AOC3 mRNA expression
48h
72h
Fold Change
10
5
0
10% FBS
SF
TGFβ in SF
CCD 18CO

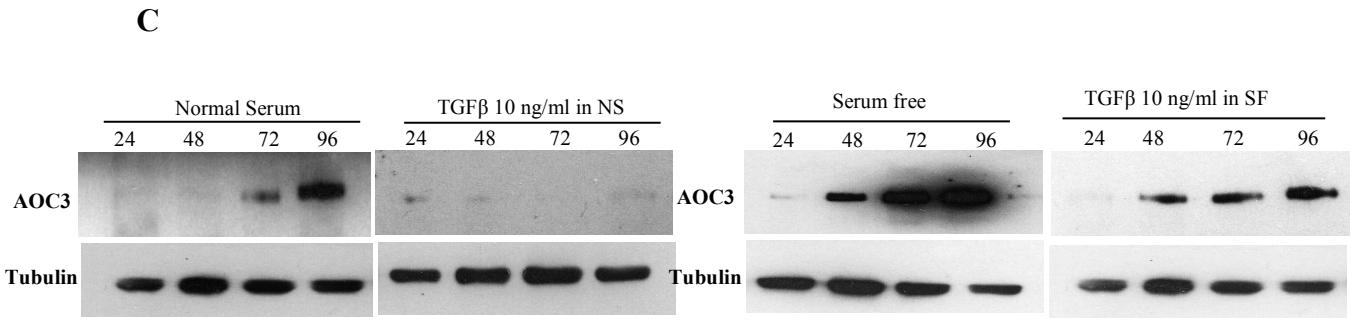
C
Normal Serum
TGFβ 10 ng/ml in NS
Serum free
TGFβ 10 ng/ml in SF
24 48 72 96
AOC3
Tubulin

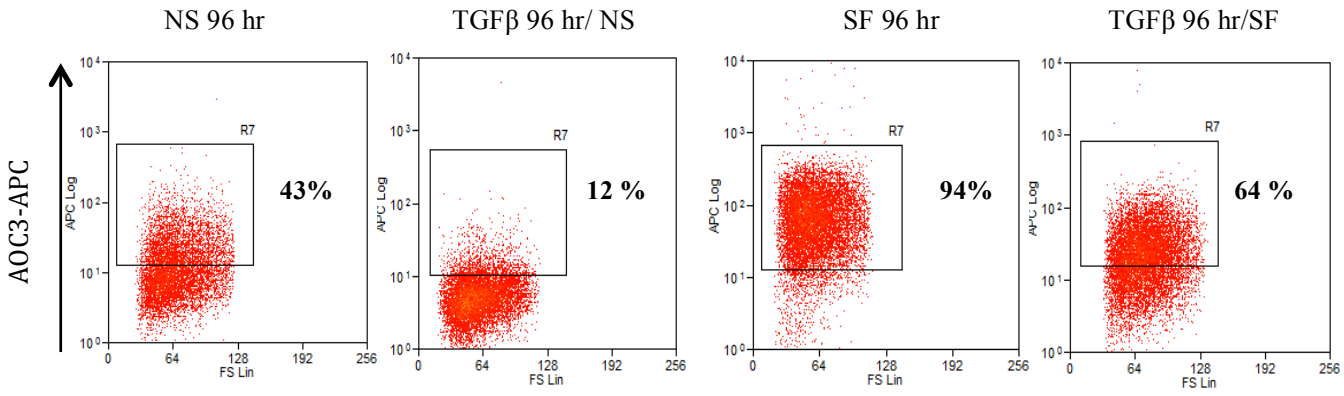
NS 96 hr
TGFβ 96 hr/ NS
SF 96 hr
TGFβ 96 hr/SF
AOC3-APC
APC Log
FS Lin
R7
43%
12 %
94%
64 %

Figure 4 .13
AOC3 expression is down regulated by TGFβ treatment
CCD 18CO cells were incubated with or without TGFβ 10ng/ml in serum free or normal serum containing medium for 24, 48, 72 and 96 hours. (A) Experimental design flow of TGFβ treatment. (B) *AOC3* mRNA level was determined using qRT-PCR. Ct values were normalized to *UBC* and fold change was calculated relative to cells in 48hr with 10%FBS. n=3 (C) AOC3 protein expression level was measured by western blot (24, 48, 72 and 96 hours) and flow cytometry (96 hours). Rectangle gating in dot plots represents the AOC3 positive population. NS: normal serum containing medium; SF: serum free medium. All experiments were independently repeated at least three times, and similar results were obtained

To further explore the apparent negative regulatory effect of TGFβ on AOC3 levels, we first induced high levels of AOC3 expression in CCD 18CO by growing cells under serum starvation for 96 hours, then followed by TGFβ addition in serum free medium for a further 96 hours (**Figure 4.14A**). **Figure 4.14B** shows that the *AOC3* mRNA level reached a 10-fold increase after 96 hours serum starvation, followed by a decrease after TGFβ treatment. Data indicated that TGFβ treatment not only inhibited the initial increase in AOC3 production after seeding cells, but also decreased the levels of mRNA from a relatively high starting point once the TGFβ was added. Together, these results suggested that TGFβ, either directly or indirectly, negatively regulates the transcription of AOC3. However, we did not see the same decrease of AOC3 expression on protein levels (**Figure 4.14C**). This suggested two possibilities: 1) that the inhibitory effect of TGFβ might just affect AOC3 expression at the transcriptional level or 2) AOC3 protein might have a long turnover time, during which the protein degrades slowly and all the accumulated protein is then detected by the western blot.

A

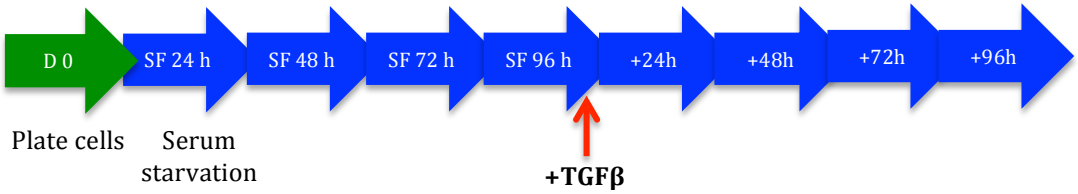
D 0
SF 24 h
SF 48 h
SF 72 h
SF 96 h
+24h
+48h
+72h
+96h
Plate cells
Serum starvation
+TGFβ

B

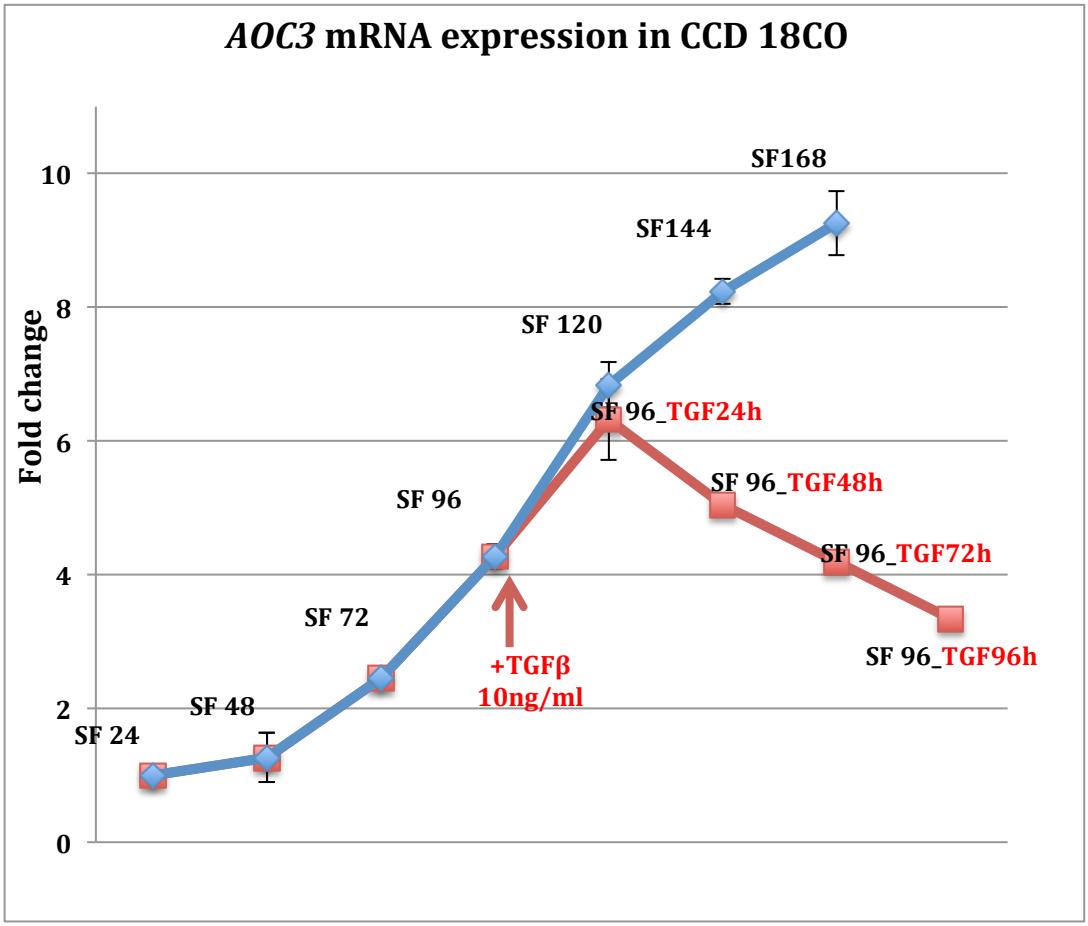
AOC3 mRNA expression in CCD 18CO
Fold change
0
2
4
6
8
10
SF 24
SF 48
SF 72
SF 96
SF 120
SF144
SF168
+TGFβ 10ng/ml
SF 96_TGF24h
SF 96_TGF48h
SF 96_TGF72h
SF 96_TGF96h

C

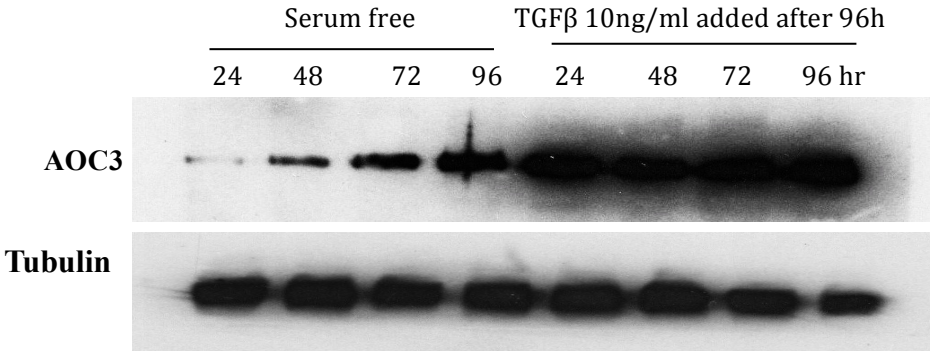
Serum free
TGFβ 10ng/ml added after 96h
24
48
72
96
24
48
72
96 hr
AOC3
Tubulin

Figure 4 .14
The inhibitory effect of TGFβ on AOC3 expression in CCD 18CO
(A) Experimental design for TGFβ treatment (B) *AOC3* mRNA level was determined using qRT-PCR. Cells were under serum starvation and followed by TGFβ 10ng/ml treatment. Ct values were normalized to *UBC* and fold change was calculated relative to cells in SF 24hr. (C) AOC3 protein expression level was measured by western blot and tubulin is shown as a loading control. All experiments were independently repeated at least three times, and similar results were obtained. Error bar of fold change represent the mean of triplicate technical repeats from one experiment.

In order to understand whether serum starvation can also induce the AOC3 expression in normal fibroblasts, foreskin fibroblast cells were incubated under serum free condition, as well as treated with TGFβ. In **Figure 4.15A,** neither serum starvation nor TGFβ addition have any effect on AOC3 expression in foreskin fibroblasts. However, TGFβ treatment dramatically increases the expression of αSMA protein in foreskin fibroblasts and CCD 18CO (**Figure 4.15B**). The increased levels of αSMA mRNA in fibroblast cells and myofibroblast cells are shown in **Figure 6. 12A** and **Figure 6.7**, respectively.)

A

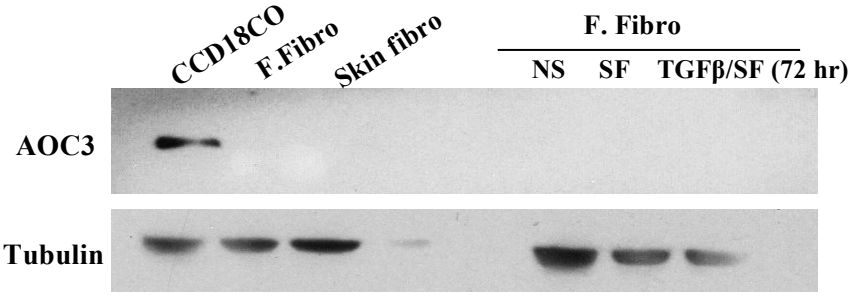

B αSMA expression

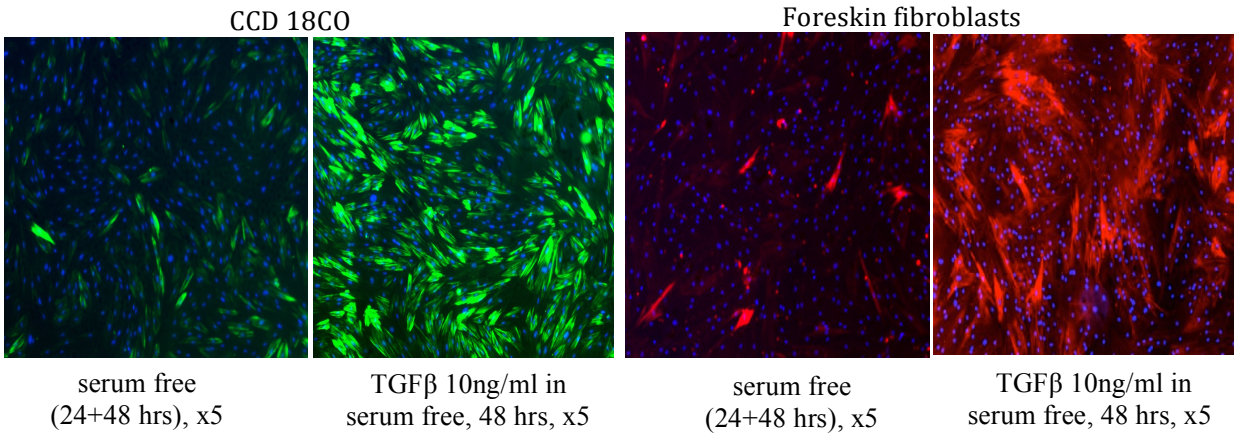

Figure 4 .15
AOC3 expression is not inducible in foreskin fibroblast cells
(A) Foreskin fibroblasts (F. fibro) were treated with serum starvation and TGFβ treatment for 72 hours. Protein expression was measured using western blots and tubulin is shown as loading control. NS: normal serum containing medium; SF: serum free medium. n=3 (B) Supporting data showing that TGFβ-induced αSMA expression in both CCD 18CO cells and foreskin fibroblast cells. Cells were stained with αSMA (shown in green in CCD 18CO and shown in red in foreskin fibroblasts, X5 magnification)

4.2.3.3 AOC3 functions as a SSAO enzyme in myofibroblasts

Semicarbazide-sensitive oxidase (SSAO) belongs to a family of copper-dependent enzymes that use topaquanine as cofactor and, as the name suggests, it is highly sensitive to inhibition by semicarbazide. The SSAO enzymes catalyze the general reaction $R\text{-}CH_2\text{-}NH_2+O_2+H_2O \rightarrow R\text{-}CHO+NH_3+H_2O_2$ and are found in adipocytes, endothelial cells and smooth muscle cells (Jaakkola et al., 1999). The previous results have demonstrated that AOC3 is expressed in myofibroblasts but have not indicated any functional relevance in the myofibroblasts. In order to evaluate the functional role of AOC3 in myofibroblasts, the Amplex® red monoamine oxidase assay was used to detect production of H_2O_2 in a fluorometric peroxidase-coupled reaction.

As shown in **Figure 4.16**, myofibroblast monoamine oxidase activity was assessed under serum free conditions 48 hours after addition of benzylamine as substrate. The enzyme activity was reduced by 80% after addition of the specific SSAO inhibitor semicarbazide (SEM), whereas about 80% of the enzyme activity remained insensitive to clorgyline, a general MAO inhibitor. By knocking down AOC3 in CCD 18CO cells, the enzyme activity was decreased by 85%, indicating that AOC3 is the major contributor to SSAO activity in myofibroblast cells.

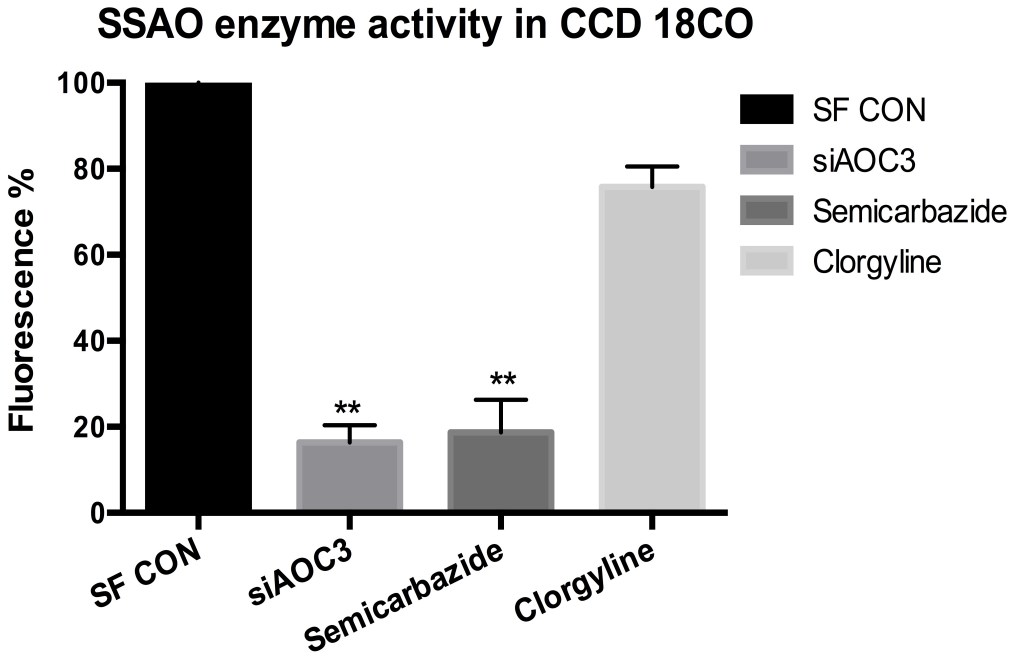

Figure 4 .16
Myofibroblast AOC3 is a SSAO enzyme
SSAO activity was determined by SSAO-mediated H_2O_2 production. siRNA of AOC3, semicarbazide (SEM 1mM, SSAO inhibitor) and Clorgyline (1mM, MAO-A inhibitor) were added under serum free conditions for 48 hours. The enzyme activity in untreated CCD 18CO control cells was set to 100% (control). # $p<0.05$; * $p<0.01$; ** $p<0.001$ versus serum free control. All experiments were independently repeated at least three times, and similar results were obtained.

4.3 Discussion

In this chapter we first demonstrated that AOC3 protein is expressed in myofibroblasts *in vitro* and *in vivo*. The tissue distribution of AOC3 was then assessed by extensive immunofluorescence analyses in both normal and tumour tissues. AOC3/VAP-1 was first identified as an endothelial, cell surface expressed oxidase that supports leukocyte emigration into inflammatory sites (Salmi and Jalkanen, 1992), and has been shown to be expressed in endothelial cells, in pericytes, smooth muscle cells and also in adipocytes (Smith et al., 1998, Jaakkola et al., 1999). Our results demonstrated the distribution of AOC3 in myofibroblasts in the gut, liver, prostate and pancreas, which substantially matched the profile determined by PR2D3 (Richman et al., 1987), as well as αSMA staining. **Table 4.1 & 4.2** summarises the data obtained for the tissue distribution of AOC3 compare to αSMA staining. In general, more intensive staining of AOC3 was observed in various tumours compared to the corresponding normal tissues, suggesting that AOC3 expression is often upregulated in some tumour tissues. Stronger staining might also result from myofibroblast activation and recruitment into tumour stroma (Tsujino et al., 2007, Yeung et al., 2013). However, the lack of staining in some tissues, especially in breast tissues, indicates heterogeneity of myofibroblasts and fibroblasts in different tissues, beyond that simply identified by the presence of AOC3.

The expression of AOC3 in a subset of colorectal derived myofibroblast cultures and its absence in fibroblast cultures is also shown by western blot and flow cytometric analysis. The AOC3 specificity in myofibroblasts has been confirmed by siRNA mediated AOC3 knockdown at both mRNA and protein levels. The specific surface expression of AOC3 in myofibroblast cells enables not only separation from normal

fibroblasts but also from epithelial cell mixtures by flow cytometric analysis. This application facilitates the use of AOC3 as a myofibroblast-specific surface marker in FACS sorting of fresh normal or tumour tissues, which will be discussed in **Chapter 5**.

AOC3 is a dual function protein in endothelial cells, as an adhesion molecule and SSAO enzyme, but it has only been reported to have enzymatic function in smooth muscle cells (Jaakkola et al., 1999). SSAO is known to be involved in amine-stimulated glucose transport in adipocytes (Zorzano et al., 2003), cell adhesion and lymphocyte trafficking in endothelial cells from lymphatic vessels (Jalkanen and Salmi, 2008). The SSAO enzyme activity is crucial for AOC3 activity, as the inhibition of the oxidase activity can block the AOC3/VAP-1 effect *in vivo* (Noonan et al., 2013). From our data, AOC3 in myofibroblasts demonstrated functional SSAO enzyme activity, which is sensitive to semicarbazide inhibition. A dramatic decrease in enzyme activity following siRNA mediated knock down of AOC3 in myofibroblast cells confirmed our results. SSAO catalyzes oxidative deamination of primary amines in a reaction that produces the corresponding aldehyde, hydrogen peroxide and ammonium. In various tissues, aldehydes and hydrogen peroxide generated by SSAO have been implicated in the pathogenesis in different diseases (Yu and Deng, 1998, Garpenstrand et al., 2004). However, there is emerging evidence of hydrogen peroxide acting as a signaling molecule that regulates the expression of other adhesion molecules, cell growth and apoptosis (Finkel, 1998, Stolen et al., 2004a, Veal and Day, 2011). The increased expression of AOC3 in myofibroblasts of cancer tissues may add significantly to these multiple biological functions and, in particular, may suggest AOC3's functional role is to do with H_2O_2 signaling.

Transforming growth factor β (TGFβ) has been suggested as being responsible for initiating and maintaining the activated state of myofibroblasts in fibrosis and cancers in many studies (De Wever et al., 2004, Kim et al., 2009, Hinz et al., 2012). Additionally, TGFβ has been shown to directly promote myofibroblast activation by inducing expression of αSMA (Ronnov-Jessen and Petersen, 1993, Desmouliere et al., 1993, Shi et al., 1996). Our data showed that AOC3 mRNA and protein level are down regulated in myofibroblasts following addition of TGFβ. We initially observed the increasing AOC3 expression in myofibroblasts under serum starvation, and that this increase in AOC3 expression was inhibited by TGFβ addition at both the transcriptional and translational level. Interestingly, neither serum starvation nor TGFβ addition have any effect on AOC3 expression in fibroblasts, suggesting that AOC3 expression cannot be induced in normal fibroblasts. The fact that αSMA expression is increased in fibroblasts after TGFβ has been used as an indicator of fibroblast activation. But it is important to note that even in activated fibroblasts, AOC3 is still able to distinguish between TGFβ activated fibroblasts and myofibroblasts.

CHAPTER FIVE

ISOLATION OF MYOFIBROBLASTS FROM FRESH TISSUES BY FACS USING AOC3 AS CELL SURFACE MARKER

CHAPTER 5: ISOLATION OF MYOFIBROBLASTS FROM FRESH TISSUES BY FACS USING AOC3 AS CELL SURFACE MARKER

5.1 Introduction

Cell separation is a powerful tool, widely used in many biological and clinical research areas. For research, the ability to sort cells into distinct populations facilitates the study of individual cell types from a heterogeneous population without contamination from other cell types. Stromal myofibroblasts have been proven as a heterogeneous c ell population based on immunohistological observation using various combinations of molecular markers (Sugimoto et al., 2006), as well as global gene expression profiling (Perou et al., 2000). Although investigators have been searching for a single biomarker that exclusively marks myofibroblast populations, no single gene has been demonstrated to process this characteristic as yet. Our results from previous chapters have demonstrated the specificity of AOC3 protein expression in myofibroblasts, and showed the application in flow cytometry for separation of myofibroblasts from other cells. Thus, the approach in this chapter relies on utilizing AOC3 as a surface marker to isolate myofibroblasts from fresh human tissues. Sorted myofibroblasts were then used for further characterization and comparative analysis of their gene expression profiles.

High yield purification of cells from fresh tissues often requires the combined use of mechanical dissection and enzymatic tissue disintegration. Enzymes typically used for tissue disintegration are collagenase and trypsin, often in combination with EDTA or DTT to minimize cell clumping and to support cell dissociation. Collagenases are endopeptidases that break the peptide bonds in collagen, which is a key component of the tissue extracellular matrix. Trypsin is a pancreatic serine protease, which cleaves

peptide chains on the C-terminal side of lysine and arginine amino acids, except when either is followed by proline. Thus, enzyme-mediated reduced surface molecules might contribute the variation of results obtained by immunostaining of intact tissues or FACS sorting of cells based enzymatic tissue digestion. Moreover, surface molecules mediate many immunological and other surfaced related functions such as cell adhesion and activation of signalling pathways. Some published evidence indicates that these enzymatic treatments may affect the expression of surface molecules and immune cell functions (Weigmann et al., 2007, Autengruber et al., 2012).

Working with primary cultures, enzymatic digestion protocols are routinely applied to the isolation of cells from gut tissues. We have observed that trypsin treatment has a considerable impact on the expression level of AOC3 protein on myofibroblast cultures. In this chapter, we also evaluated the impact of collagenase IV on surface expressed AOC3 that is used for isolation of myofibroblasts from fresh tissues. Together, we successfully isolated and profiled highly enriched populations of myofibroblasts from fresh human colonic tissues using AOC3 mAb, and demonstrated that surface expression of AOC3 is sensitive to proteolytic digestion.

5.2 Results

5.2.1 Myofibroblast isolation

In recent years, purification of myofibroblasts from stroma for culture and molecular profiling has gained more interest, and different techniques have been employed. As described in methods and materials, 10 primary myofibroblast cultures were established from human colonic tissues. Fresh tissues were disrupted into a cell suspension by mechanical and enzymatic digestion, after which cells were filtered out and seeded in adherent surface tissue flasks for a period of culture. Myofibroblasts were subsequently purified by keeping cells in normal DMEM with antibiotics, as other types of cells need extra growth factors in medium.

Our aim here was to use surface expressed AOC3 as a myofibroblast marker in FACS sorting. We noticed that preparations of myofibroblast single cell suspensions with trypsin decreased the expression level of AOC3 protein in flow cytometric analysis (**Figure 5.1**). To avoid the possibility that proteolysis digestion might compromise AOC3 protein expression during FACS of fresh tissues, we then explored two further digestion methods, collagenase IV (Worthington, USA) or a proprietary non-enzymatic EDTA based cell dissociating solution (Sigma, USA) (**Figure 5.2**). Collagenase digestion was followed by the standard procedure for establishing primary cultures, while non-enzymatic treatment was modified from the method of extraction colonic crypts from Ashley et al in Bodmer's laboratory (Ashley et al., 2014). Briefly, these mechanical disrupted tissues were incubated in non-enzymatic cell dissociation solution for 1 hour with agitation with glass beads (4 mm, undrilled; Fisher Scientific UK),

which help cell dissociation without excessive tissue disruption. Consequent steps are followed by standard procedures of FACS and flow cytometric analyses.

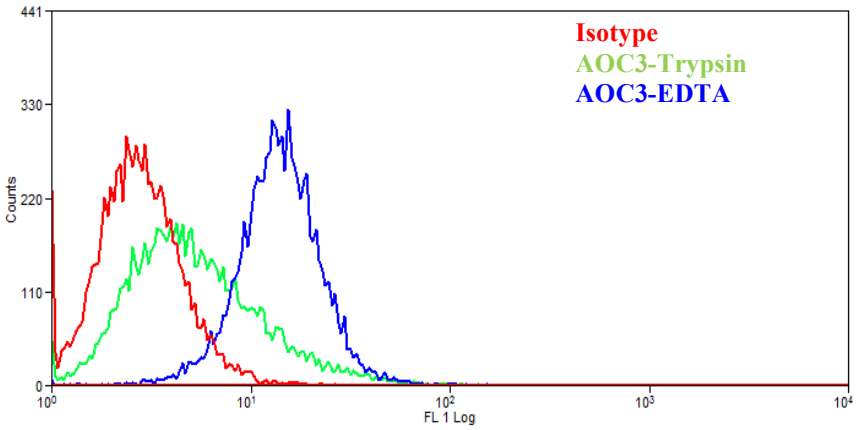

Figure 5.1
Trypsinization impaired AOC3 protein expression on CCD 18CO cells
Cell suspension was prepared by trypsin (shown in green) or EDTA solution (shown in blue), and then cells were labeled with AOC3-APC. Isotype-APC was labeled as control (shown in red).

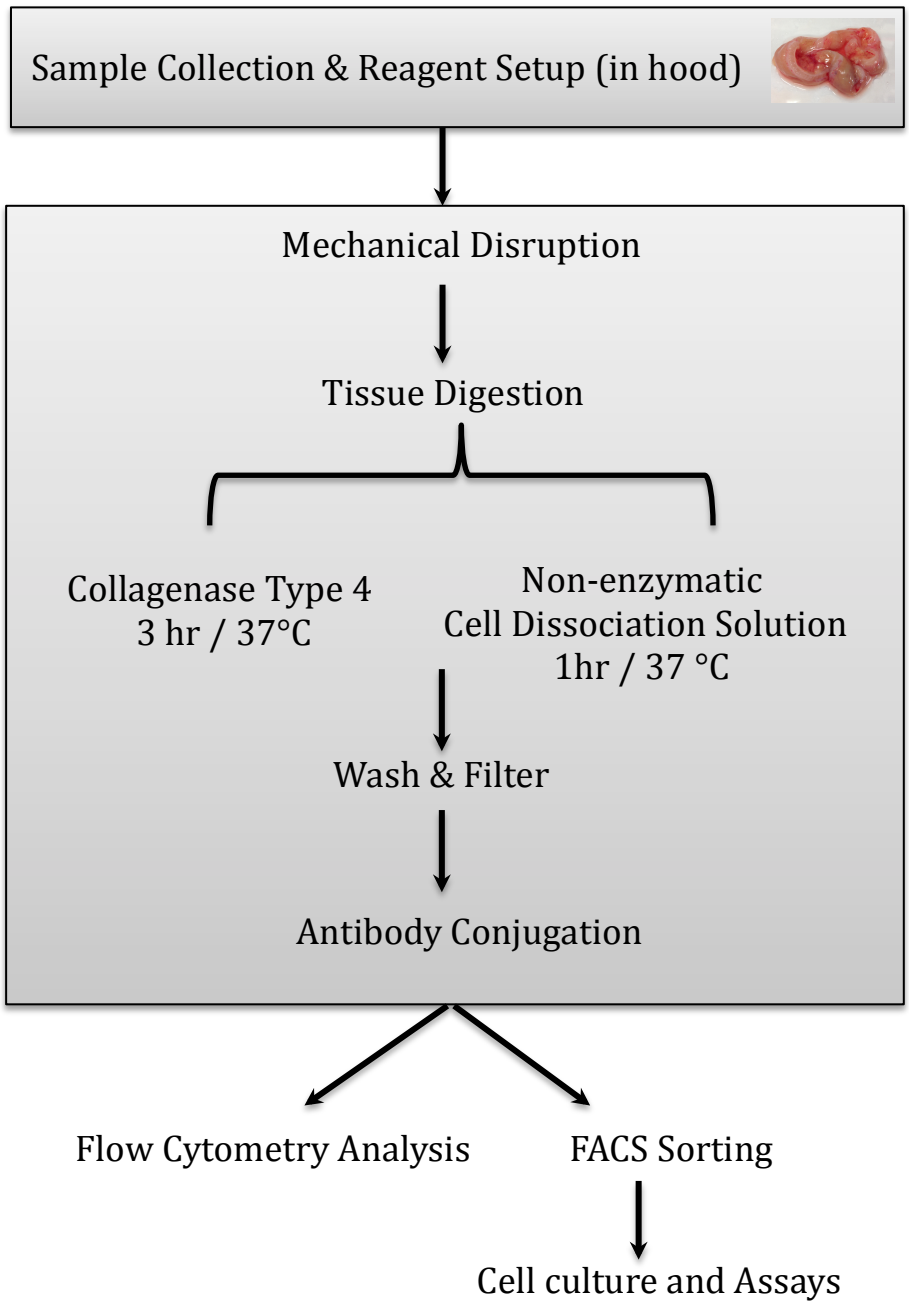

Figure 5.2
Experimental procedure for myofibroblast isolation

5.2.2 Flow cytometric analysis of fresh tissues

Fresh tissues from patients undergoing operations for colorectal tumour resections at the Oxford University Hospitals were used for flow cytometric analysis as well as FACS sorting in this study. Tissues were processed within 24 hours after operation.

5.2.2.1 Collagenase digestion affects expression level of surface expressed AOC3 on myofibroblasts (Patient 1)

Tissues from Patient 1 (P1) were prepared with two methods as mentioned previously. Single cell suspensions were labelled with AOC3-PE for myofibroblasts and EpCAM-FITC for epithelial cells. Firstly, we gated the same population of cells based on the forward and side scatter profiles (FF/SS, gate R1 and R2 in Figure 5.3) and then comparing the AOC3 and EpCAM staining profiles within these gated populations for either collagenase (**Figure 5.3A**) or non-enzymatic digestion (**Figure 5.3B**) methods. This procedure enabled the separation of the different major cell populations. For collagenase enzyme digested tissues, a considerable cell population can be seen, which is $EpCAM^{+ve}/AOC3^{-ve}$ (gate R2, Figure 5.3A), while there is only a marginal number of these cells found when using non-enzymatic digestion (gate R2, Figure 5.3B). From our previous experiments, we noticed that myofibroblasts are larger and more granular than other cells (gate R1). However, these cells were $AOC3^{-ve}$/ $EpCAM^{-ve}$ in collagenase-digested tissues, whereas the same population contained significant numbers of $AOC3^{+ve}$ /$EpCAM^{-ve}$ cells after non-enzymatic digestion. These results suggest that AOC3 surface expression is significantly disrupted by treatment with collagenase. In order to obtain reliable results for surface expression of AOC3, it is therefore necessary to use only non-enzymatic protocols for obtaining single cells suspensions.

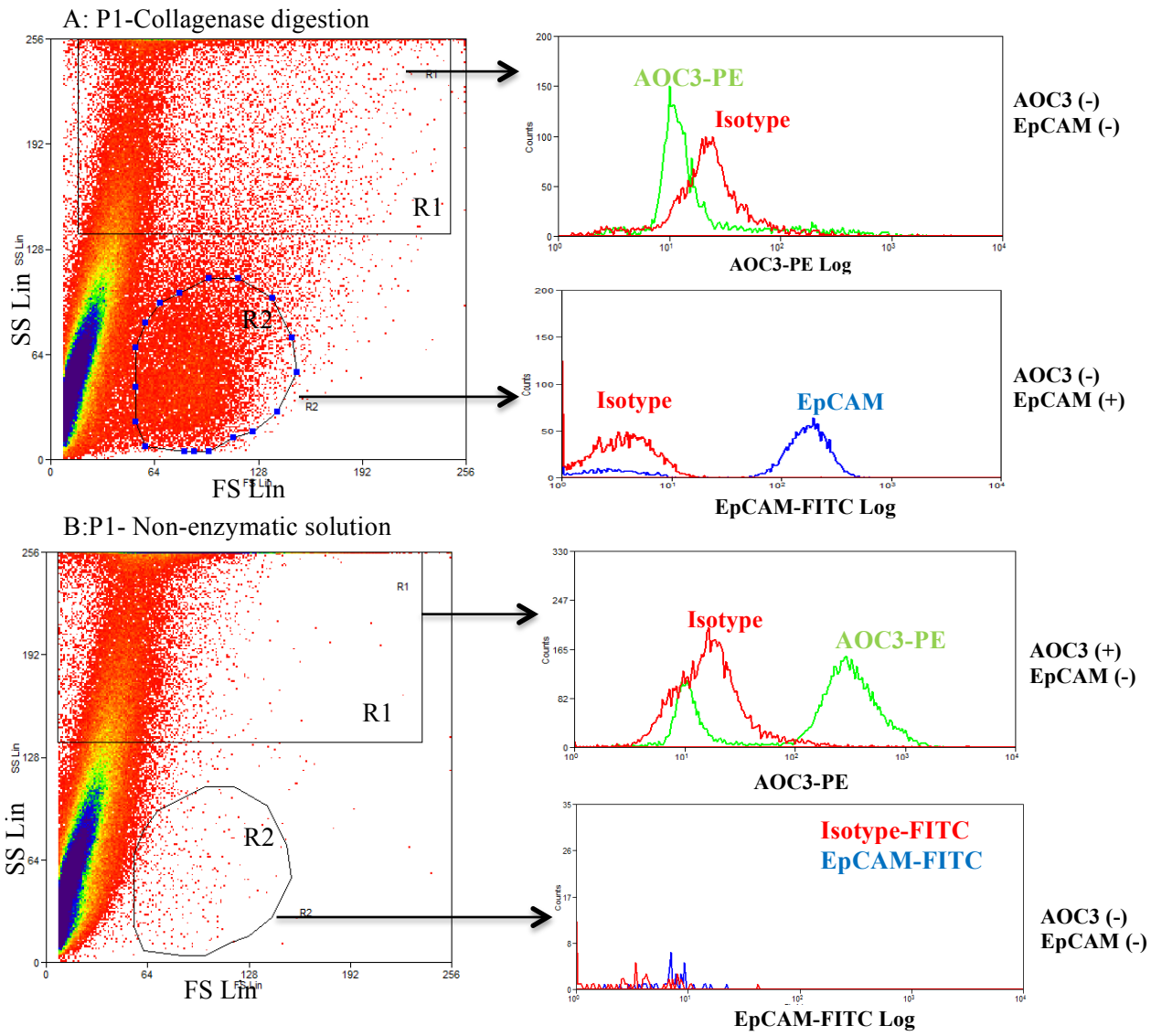

Figure 5.3

Patient 1. Comparison of Collagenase and non-enzymatic digestion on expression of AOC3 Collagenase digestion compromised the surface expression of AOC3 protein on myofibroblasts in fresh tissues but obtained a majority of epithelial cells. Cells were labelled with both AOC3-PE (shown in green) for myofibroblasts and EpCAM–FITC (shown in blue) for epithelial cells. Isotype was labelled as control (shown in red). PE: Phycoerythrin; FITC: Fluorescein isothiocyanate

5.2.2.2 Surface expression of AOC3 is sensitive to proteolytic digestion by trypsin. (Patient 2)

The second tissues from patient (P2) were processed under the same conditions with either collagenase or non-enzymatic solution. To confirm the proteolytic sensitivity of surface expression AOC3 protein, an additional step of 15 min trypsin-EDTA treatment was applied after the non-enzymatic digestion. In **Figure 5.4**, myofibroblast cells (R1 gated) were again $AOC3^{-ve}$ in collagenase treated tissues, while they were $AOC3^{+ve}$ in non-enzymatic digested tissues. However, after 15 minutes trypsin-EDTA treatment, R1 gated cells lost their AOC3 expression in flow cytometric analysis (**Figure 5.4B**). These findings confirmed that the surface expression AOC3 is sensitive to both collagenase digestion and trypsinization.

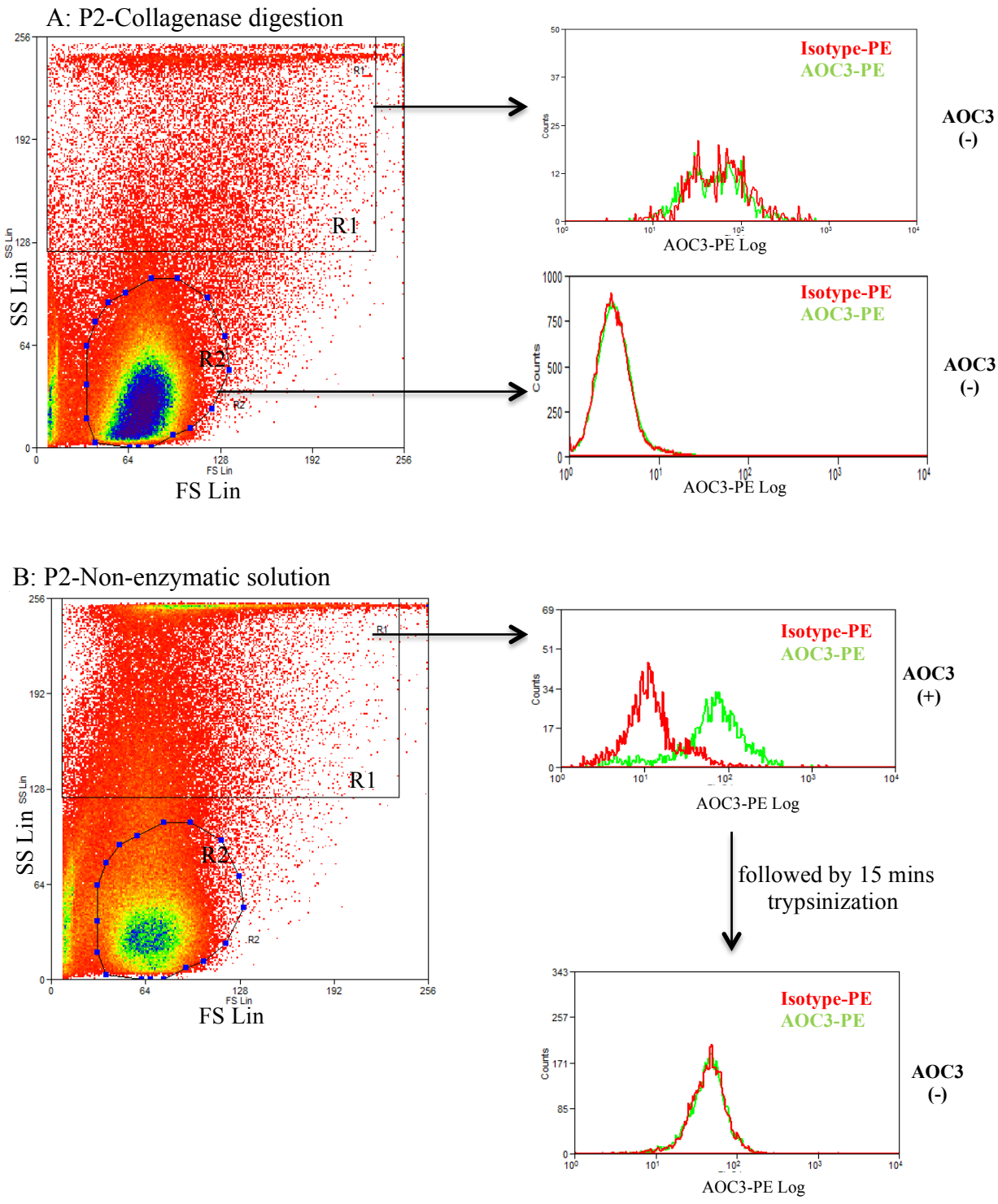

Figure 5.4
Patient 2: Comparison of collagenase and non-enzymatic digestion on expression of AOC3, with further confirmation of effect of trypsinization after non-enzymatic dissociation. Additional trypsinization confirms that surface expression of AOC3 is highly sensitive to proteolytic digestion.

5.2.2.3 Surface expression of PR2D3 is also sensitive to proteolytic digestion (Patient 3)

Final confirmation was performed on the third independent patient sample (P3). Since PR2D3 mAb recognizes the same protein with AOC3 mAb on myofibroblasts, we hypothesized that trypsinization would also affect PR2D3 expression. In **Figure 5.5**, the expression level of PR2D3 was clearly diminished by collagenase digestion, as well as by trypsin treatment. Together, the three independent samples and digestion experiments indicated clearly that both PR2D3 and AOC3 expression on myofibroblasts were sensitive to proteolytic digestion, which dramatically affected the result of flow cytometric analysis.

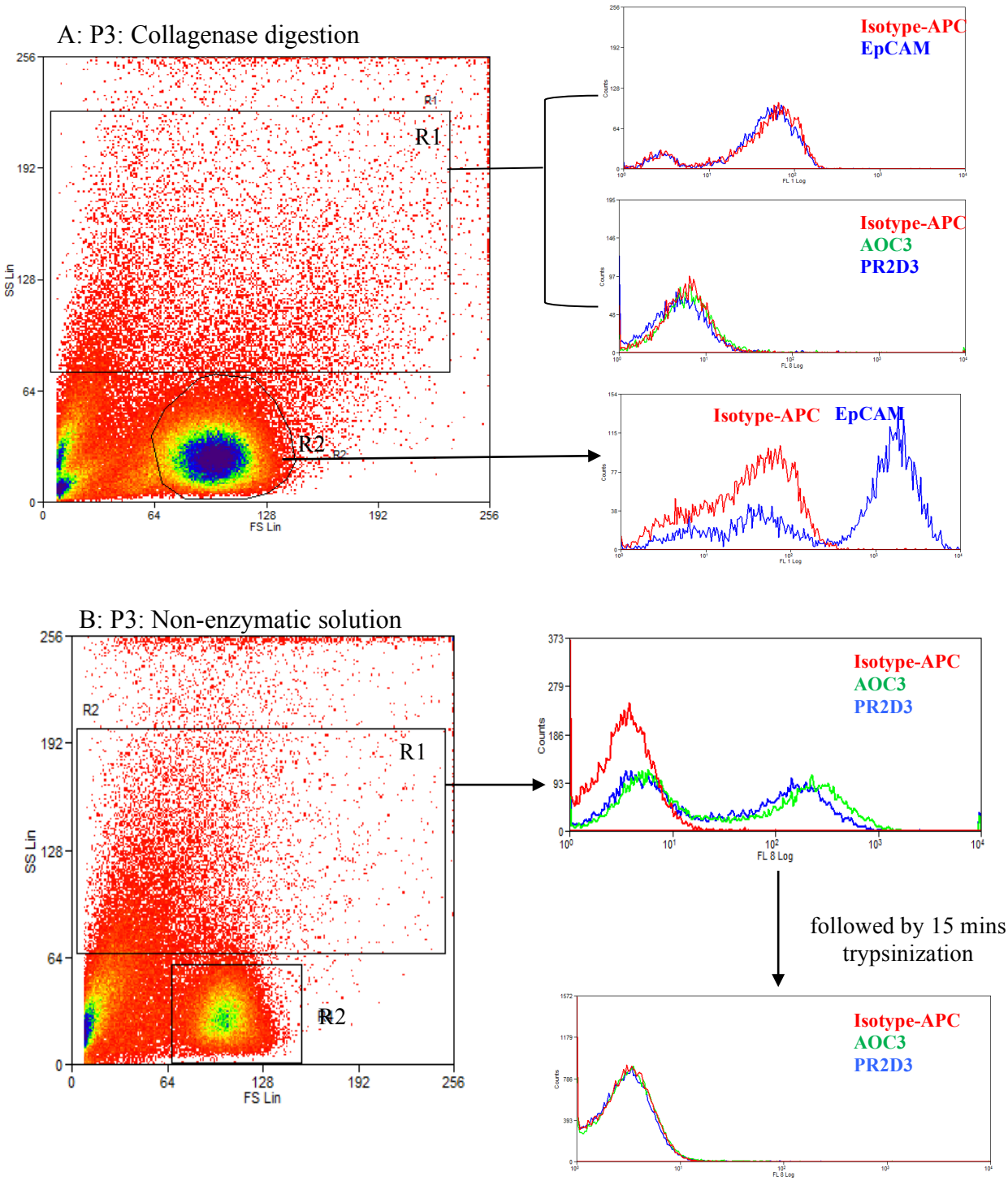

Figure 5.5
Patient 3. Comparison of collagenase and non-enzymatic digestion on expression of PR2D3 target protein and AOC3, with further confirmation of effect of trypsinization after non-enzymatic dissociation.
Trypsinization confirms that surface expression of AOC3 is highly sensitive to proteolytic digestion

5.2.2.4 AOC3 amino acid sequence reveals collagenase cleavage sites

Collagenase recognizes the peptide sequence: P-X-G-P, where X is most often a neutral amino acid (Ramshaw et al., 1998). Examination of the AOC3 amino acid sequence, which was obtained from Uniprot database (http://www.uniprot.org), identifies two collagenase cleavage sites. In **Figure 5.6**, the two collagenase cleavage sites between residues 306 and 317 in the AOC3 amino acid sequence are indicated; they are both positioned in extracellular portion of the protein, making them accessible to potential extracellular enzymatic cleavage. This finding is consistent with our results that during tissue digestion, collagenases result in cleavage of the extracellular part of AOC3 protein on myofibroblasts.

AOC3 amino acid sequence:
(NCBI Reference Sequence: NP_001264660.1)

Intracellular Transmembrane Extracellular

MNQKTILVLLILAVITIFALVCVLLVGRGGDGGEPSQLPHCPSVSPSAQP
WTHPGQSQLFADLSREELTAVMRFLTQRLGPGLVDAAQARPSDNCVF
SVELQLPPKAAALAHLDRGSPPPAREALAIVFFGRQPQPNVSELVVGP
LPHPSYMRDVTVERHGGPLPYHRRPVLFQEYLDIDQMIFNRELPQASG
LLHHCCFYKHRGRNLVTMTTAPRGLQSGDRATWFGLYYNISGAGFFLH
HVGLELLVNHKALDPARWTIQKVFYQGRYYDSLAQLEAQFEAGLVNVV
LIPDNGTGGSWSLKSPVPPGPAPPLQFYPQGPRFSVQGSRVASSLWT
FSFGLGAFSGPRIFDVRFQGERLVYEISLQEALAIYGGNSPAAMTTRYV
DGGFGMGKYTTPLTRGVDCPYLATYVDWHFLLESQAPKTIRDAFCVFE
QNQGLPLRRHHSDLYSHYFGGLAETVLVVRSMSTLLNYDYVWDTVFH
PSGAIEIRFYATGYISSAFLFGATGKYGNQVSEHTLGTVHTHSAHFKVD
LDVAGLENWVWAEDMVFVPMAVPWSPEHQLQRLQVTRKLLEMEEQA
AFLVGSATPRYLYLASNHSNKWGHPRGYRIQMLSFAGEPLPQNSSMA
RGFSWERIWWPG

P-X-G-P Collagenase type 4 cleave site (Pro-X-Glyc-Pro)

Figure 5.6
Amino sequence of AOC3 and potential cleavage sites of collagenase IV

5.2.3 Isolation of myofibroblasts from human fresh colon tissues by FACS

To isolate primary myofibroblast cells from fresh colonic tissues, tissues were finely minced and digested with non-enzymatic dissociation solution, followed by cell isolation using fluorescence-activated cell sorting (FACS) with anti-AOC3 mAb conjugated with FITC (**Figure 5.7**). Cell suspensions from colon tissues were labelled with AOC3- FITC. Cells are first gated by size and granularity based on forward and side scatter pulse area (FSC/SSC, gate R1) followed by further selection for single cells based on forward scatter pulse width and height (FSC-A/FSC-H, gate R2). Cell viability is measured by DAPI staining (FSC-A/405, gate R3). Cells expressing AOC3 are then gated FITC (488 nm) fluorescent signals as determined based on unstained samples (gate R3). The yield of sorting rate is about 2% for each tube. Sorted cells were seeded with 10% FBS DMEM and antibiotics in culture dishes for later analysis.

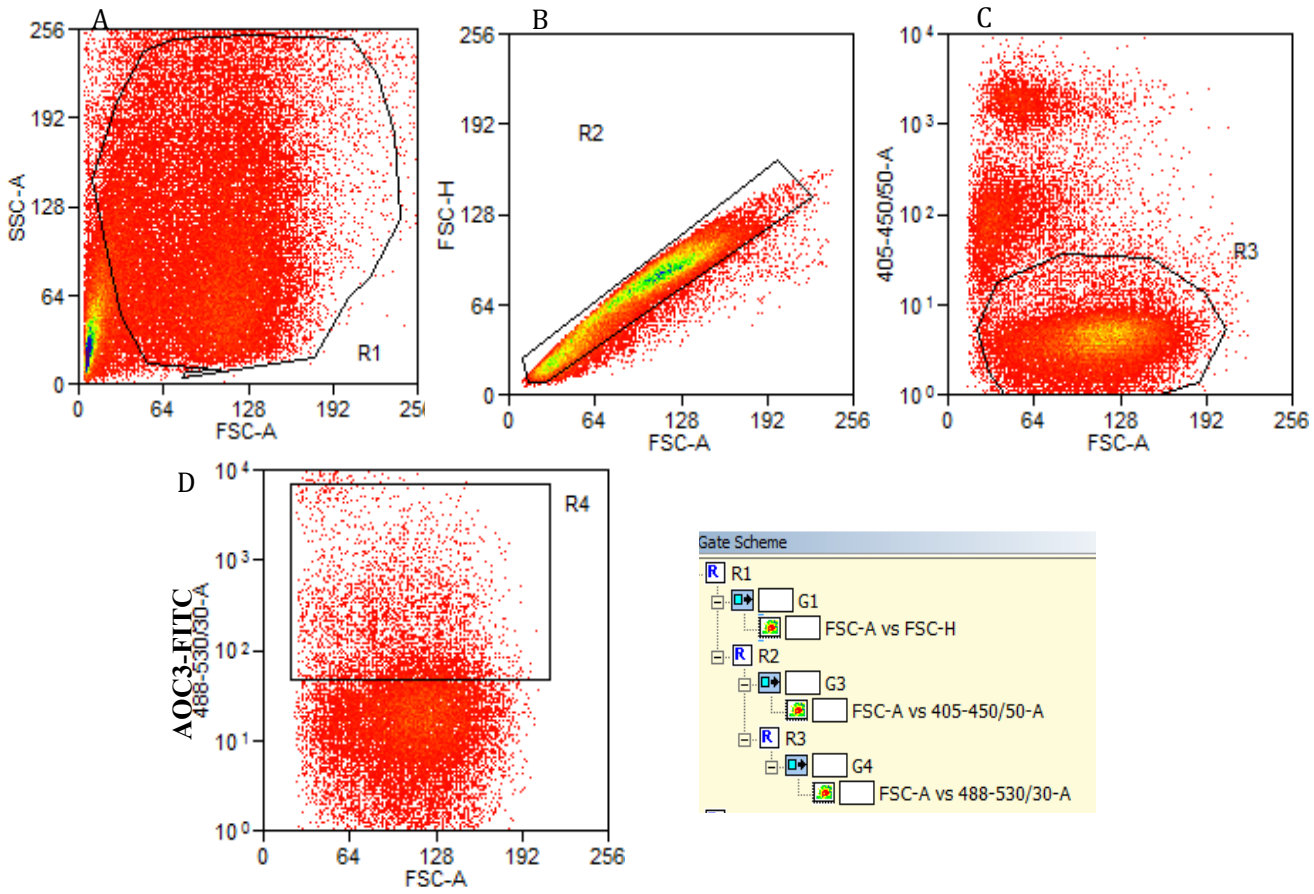

Figure 5.7
FACS isolation of myofibroblasts from fresh tissue
Diagram of FACS sorting of normal human colon tissues. Cell suspensions from colon tissues were labeled with AOC3-FITC. Cells were gated by size A) (FSC/SSC, gate R1), B) single cells (FSC-A/FSC-H, gate R2), C) viability (DAPI staining, R3), and D) fluorescent signals (AOC3-FITC, R4).

5.2.4 Characterization of AOC3-sorted myofibroblasts

After isolation of the desired cell population, AOC3+ve cells, it is very important to establish the purity of the selected population. Several fibroblast and myofibroblast markers were examined to confirm myofibroblast nature. In **Figure 5.8**, all of the AOC3-sorted cells expressed fibroblast markers: vimentin and anti-fibroblast surface protein; myofibroblast surface markers: AOC3 and PR2D3 uniformly. However, only a subset of sorted cells were positive for αSMA and MYH11, which are contractile protein markers (**Figure 5.8A**). Moreover, the expression level of *NKX2.3* and *SHOX2* (both intracellular proteins) were determined by qRT-PCR analysis, which indicated the significant enrichment for high expression of *NKX2.3* in *AOC3* in sorted cells. Expression of *SHOX2* was absent in the sorted cells (**Figure 5.8B**). Our data confirmed that we were successful in isolating a highly pure population of myofibroblast cells from fresh tissues by using AOC3 as a surface marker.

A

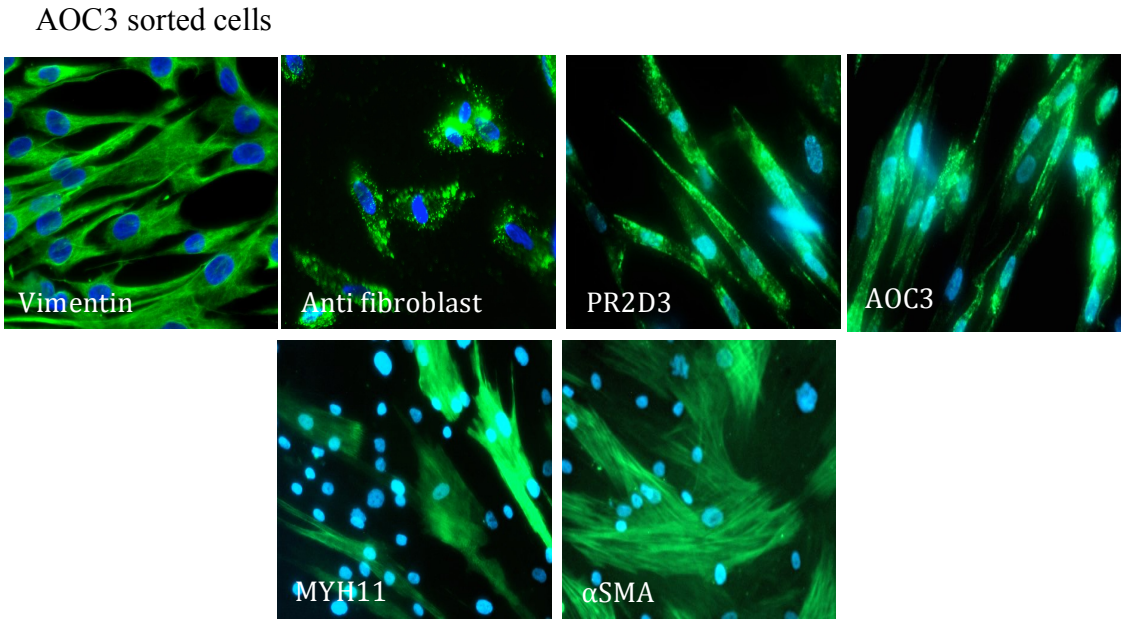

B

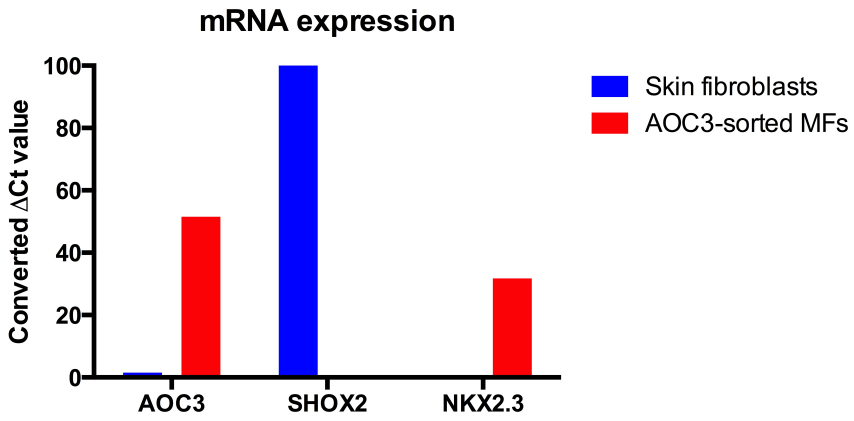

Figure 5.8
Characterization of AOC3-sorted myofibroblasts
(A) Immunofluorescent staining of AOC3-sorted myofibroblast cells with various markers (live cell staining of anti-fibroblast surface protein, PR2D3 and AOC3). X20 magnification (B) mRNA expression level of *AOC3* and *NKX2.3* on AOC3-sorted myofibroblasts; Expression levels for linearised, converted ΔCt values generated as described in materials and methods are shown. Briefly, ΔCt for each sample was subtracted from the highest ΔCt mean (AOC3 in F. fibro: ΔCt mean 9.33 was used in this figure). Column in red: myofibroblast cultures; column in blue: fibroblast cultures. *NKX2.3* mRNA level of skin fibro and *SHOX2* mRNA level of sorted cells were undetermined, as there was no measurable Ct for this sample, indicating very low or absent amount of starting mRNA.

5.3 Discussion

The observation that the use of enzymes to generate single cells suspensions in order to isolate cellular subsets from complex tissues has major effects on surface marker expression and cell function is not entirely new. Holt and colleagues showed that collagenase/DNAse digestion had a impact on expression of surface molecules such as HLA class II and interleukin-2 receptors on human peripheral blood leukocytes (Holt et al., 1986). Nonetheless, there have been no previous reports showing that proteolytic digestion comprised the expression level of surface-expressed AOC3. The specificity of AOC3 protein in myofibroblasts has been confirmed, but the sensitivity to enzyme treatment was not initially expected, especially given the routine use of trypsin or collagenase for flow cytometric analysis and FACS sorting of any surface expressed protein.

We were facing the problem that enzymatic digestion may have an effect on AOC3 protein expression when using trypsin on CCD 18CO cells for preparation of single cell suspensions (**Figure 5.1**). The expression level of AOC3 on cells was much lower than expected. We therefore modified the standard procedure of tissue dissociation to EDTA solution to overcome this problem and EDTA solution is used in all subsequent FACS-based characterization. In this study, three independent experiments of fresh tissue analysis demonstrated that collagenase-mediated tissue digestion released a considerable number of epithelial cells from tissues, compared to non-enzymatic dissociation solution. However, the extracellular domain of AOC3 protein on myofibroblasts was impaired by collagenase cleavage, as well as by trypsinization. Although the non-enzymatic dissociation solution has lower digestive capacity in tissues, it has only a marginal impact on surface expression of AOC3 protein. It would

therefore be highly recommended to set up optimized experimental conditions with respect to the enzyme used for generating single cell suspensions of either whole cells or cultured cells dependent on the cell type of interest to avoid difficulties in the detection of selected surface markers applying flow cytometric isolation or FACS analysis that are based on positive selection of antibody-stained target cells.

Together, these data indicated that AOC3 mAb could be applied to isolate and purify populations of myofibroblasts from fresh tissues using non-enzymatic treatment. Characterization of FACS sorted AOC3-positive myofibroblasts showed the uniform expression of AOC3, PR2D3, and vimentin. Also, the high mRNA expression level of *NKX2.3* and absence of *SHOX2* confirmed the purity of the myofibroblast population of sorted cells.

CHAPTER SIX

GENE REGULATION OF *NKX2.3 & SHOX2* IN MYOFIBROBLASTS AND FIBROBLASTS

CHPATER 6: GENE REGULATION OF *NKX2.3* & *SHOX2* IN MYOFIBROBLASTS AND FIBROBLASTS

6.1 Introduction

The important role of myofibroblasts in the tumour microenvironment is now quite widely accepted. However, the differences between myofibroblasts and fibroblasts from non-neoplastic tissue have not so far been well described. There still exists a significant ambiguity with respect to the definition and identification of myofibroblasts in the normal and tumour tissue. In preceding chapters, AOC3 was identified as a new marker that has enabled us to distinguish between myofibroblasts and fibroblasts more clearly than any other previously described marker. Other specific molecular markers are, however, needed to further validate our results for AOC3 in order to obtain a clear definition and recognition of myofibroblasts in stroma. In this chapter, we focus on myofibroblasts by studying recently established colorectal derived primary myofibroblast cultures from patients with colorectal cancer. In order to better understand the underlying mechanisms at the molecular level, whole genome mRNA expression profiles of primary myofibroblasts was generated and compared them to the profiles of skin derived skin fibroblasts. We then show that the microarray assessment of significantly differentially expressed genes between myofibroblast and fibroblast cultures identifies *NKX2.3* and *LRRC17* as potential myofibroblast markers, while the *SHOX2* and *TBX5* are identified as candidate markers for fibroblast cells. We then explore the differential control of these two sets of markers in myofibroblasts and fibroblasts.

6.2 Results

6.2.1 Establishment of primary colon myofibroblast cultures

Fresh material from primary tumours and normal tissue of 11 patients operated on for colorectal cancer at Oxford University Hospitals was used for the propagation of primary myofibroblast cultures as described in the Materials and Methods chapter (**Chapter 2.2.2.2** and **Table 2.1**). 4 cancer- and 9 non-cancer-associated myofibroblast cultures were established. Two sets of paired myofibroblasts, myo6550/myo6550C and myo6769/myo6769C, were isolated from cancer- and non-cancer-associated regions of whole colon tissues from the same patient. In addition, 4 primary fibroblast cultures (skin, foreskin) had previously been derived in the Cancer Immunogenetics Laboratory.

It would have been preferable to compare colon-derived myofibroblasts with colo-derived fibroblasts. However, there was no evidence of outgrowth of any other fibroblast like cell than the described isolated myofibroblast cultures. In order to have absolute negative control to compare to myofibroblasts, skin and foreskin fibroblasts were used in following experiments.

The first 4 successfully established primary myofibroblast cultures, two derived from tumour tissues (myo2020, myo2156) and two from normal tissues (myo1998, myo6024), together with the four fibroblast cell lines were used for microarray analysis.

6.2.2 Microarray analysis of gene expression between myofibroblasts and fibroblasts

Affymetrix U133 plus 2.0 micro-array mRNA expression profiles were obtained from 4 fibroblast cultures in addition to 4 myofibroblast cultures as described above (data of Myo2156 were omitted as this was later found to represent a mixed myofibroblast and epithelial cells based on the gene expression profile: high expression of *EPCAM* of myo2156). *Partek®Genomics Suite®* software was used to compare expression profiles between the myofibroblast cultures and fibroblast cultures. After correction for multiple testing (false discovery rate FDR cutoff of 0.05 set up), 4 unique genes remained significantly differentially expressed with high fold changes as shown by a 'volcano' plot (**Figure 6.1**). Genes expressed at significantly higher levels in myofibroblasts compared to fibroblasts represent potential markers of myofibroblasts; these are *NK2* transcription factor related, locus 3 (*NKX2.3*) and Leucine rich repeat containing 17 (*LRRC17*); while short stature homeobox 2 (*SHOX2*) and T-box 5 (*TBX5*) are highly expressed in fibroblast cells (**Figure 6.2A**). *OST4* and *C7orf44* have significant p-values but their fold changes are only 1.2 and 1.55 fold (myo down vs fibro), respectively, and so they were at this stage not further pursued.

Moreover, AOC3 (marked in red in the plot), the prime candidate gene from previous result, its significance of p ($p=0.064$) does not have to be corrected for multiple comparisons. Its fold change is 6.9 (myo up vs fibro).

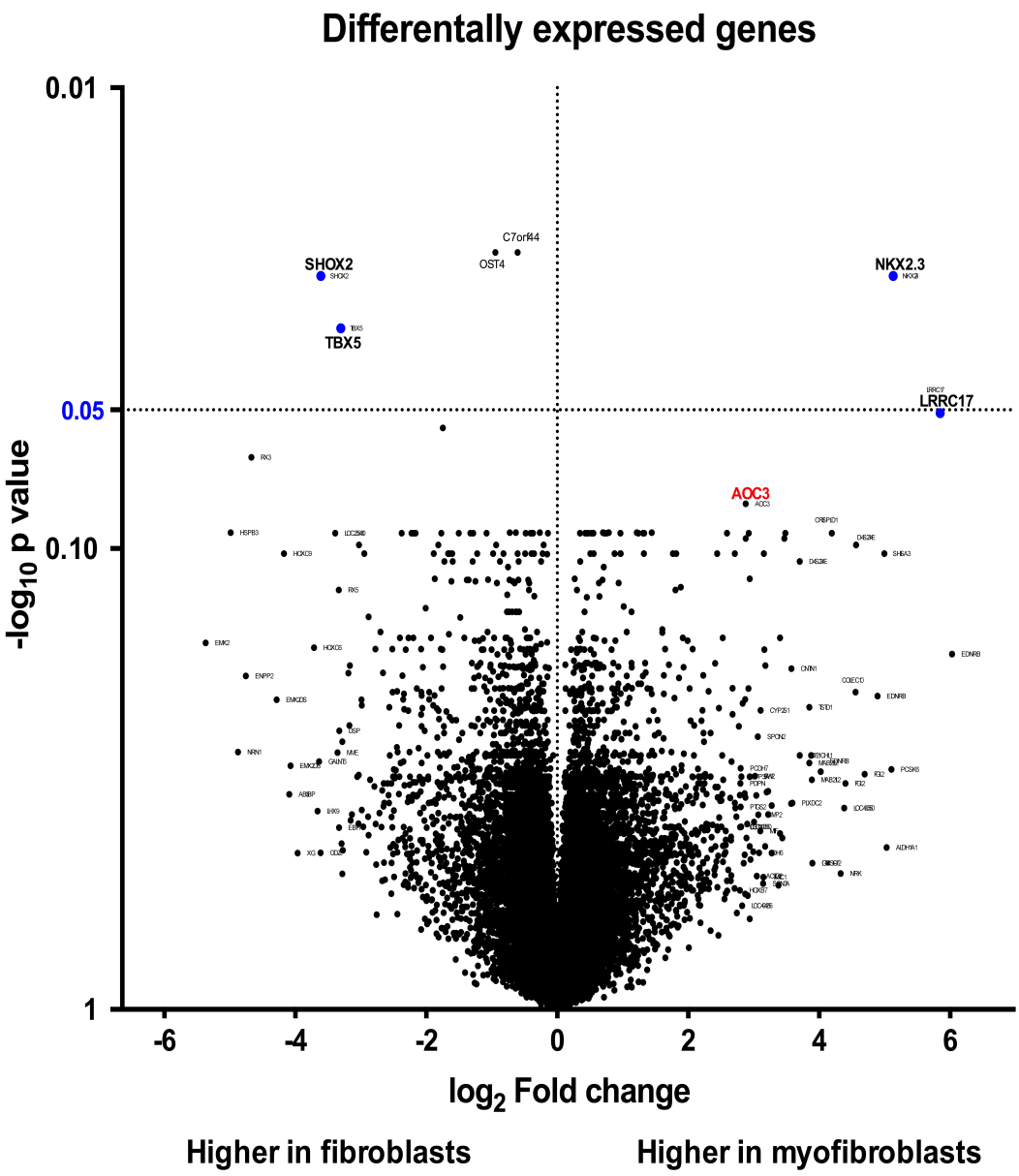

Figure 6.1
Volcano Plot representation of microarray data between myofibroblasts and fibroblasts
Microarray gene expression profiles of myofibroblast cultures group (positive fold-change) and fibroblast cultures group (negative fold-change) were plotted according to the $\log_2$ fold change (X axis) and $\log_{10}$ p-value (Y-axis). Genes were identified as having a significant change in expression if the corrected p-value was less than 0.05 and fold change is greater than 2 (blue dots).

The 4 selected significantly differentially expressed genes represent candidate markers for myofibroblasts or fibroblasts. mRNA expression levels from microarray data for both the myofibroblast-high (*NKX2.3, LRRC17*) and fibroblast-high (*SHOX2, TBX5*) candidate genes are shown for the entire panel of cell lines in **Figure 6.2B.**

A

Gene Symbol	Gene title	p-value	Step-up (p-value)	Fold change (myo vs. fibro)	Fold-Change (myo vs. fibro) (Description)
SHOX2	Short stature homeobox 2	5.97E-10	3.27E-05	-90.0583	myo down vs fibro
NKX2-3	NK2 transcription factor related, locus 3 (Drosophila)	2.34E-06	0.0256099	35.0344	myo up vs fibro
TBX5	T-box 5	3.65E-06	0.033282	-9.89776	myo down vs fibro
LRRC17	Leucine rich repeat containing 17	6.50E-06	0.050798	57.6304	myo up vs fibro

B

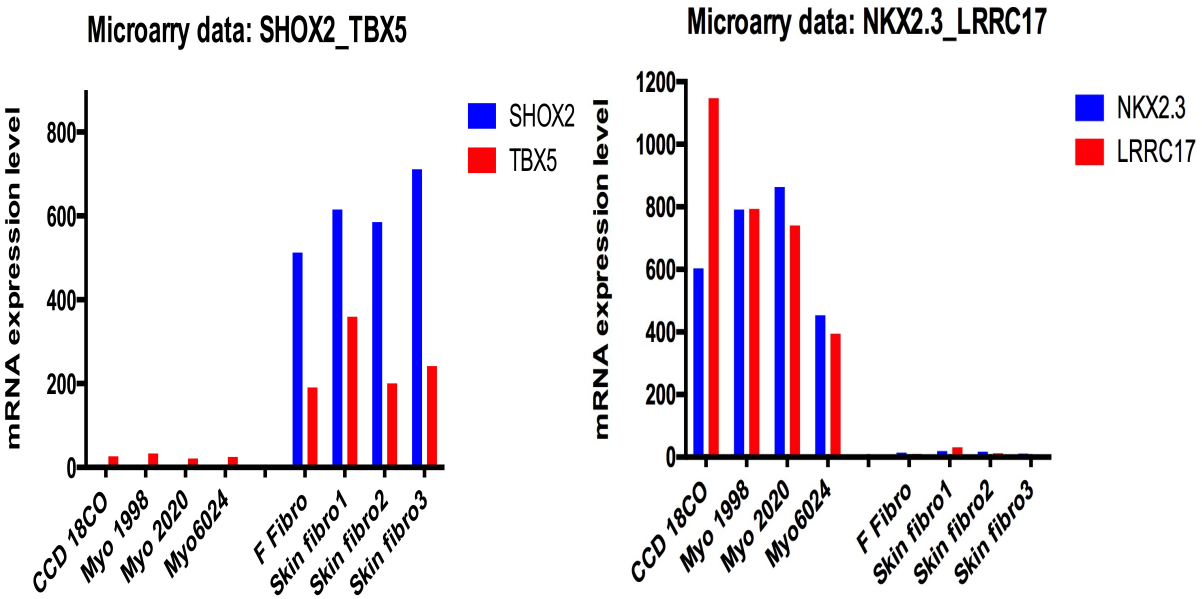

Figure 6.2
Detailed microarray mRNA expression of the top 4 differentially expressed candidate genes
(A) List of the top 4 genes that are most significantly differentially expressed between myofibroblasts and fibroblasts, ranking by p-value. Fold changes are given relative to myofibroblasts, such that negative fold changes reflect genes that are expressed at higher levels in fibroblasts compared to myofibroblasts. (B) *NKX2.3*, *SHOX2*, *LRRC17* and *TBX5* mRNA expression in myofibroblasts and fibroblasts measured by Affymetrix Human Genome U133 plus 2.0 microarray. *NKX2.3* and *LRRC17* are highly expressed in myofibroblasts, whereas *SHOX2* and *TBX5* are highly expressed in fibroblast cells.

6.2.3 *NKX2.3*

NKX2.3 has been identified as a gene associated with inflammatory bowel disease and been reported to be expressed in some colorectal cancers, however its exact role in the development and progression of colorectal cancer is still unclear. This is the first report describing *NKX2.3* expression in myofibroblasts and suggests that it might be a specific marker for distinguishing myofibroblasts from fibroblasts.

6.2.3.1 Validation of *NKX2.3* mRNA expression by qRT-PCR in primary myofibroblasts and fibroblasts

mRNA expression levels of the *NKX2.3* were verified by qRT-PCR in 11 primary myofibroblast cultures along with 2 fibroblast cultures. In **Figure 6.3**, mRNA expression of *NKX2.3* was detected in all 11 myofibroblast cultures to various extents, whereas it was completely absent in fibroblast cultures (no amplification), confirming the differences in gene expression we observed from the microarray data.

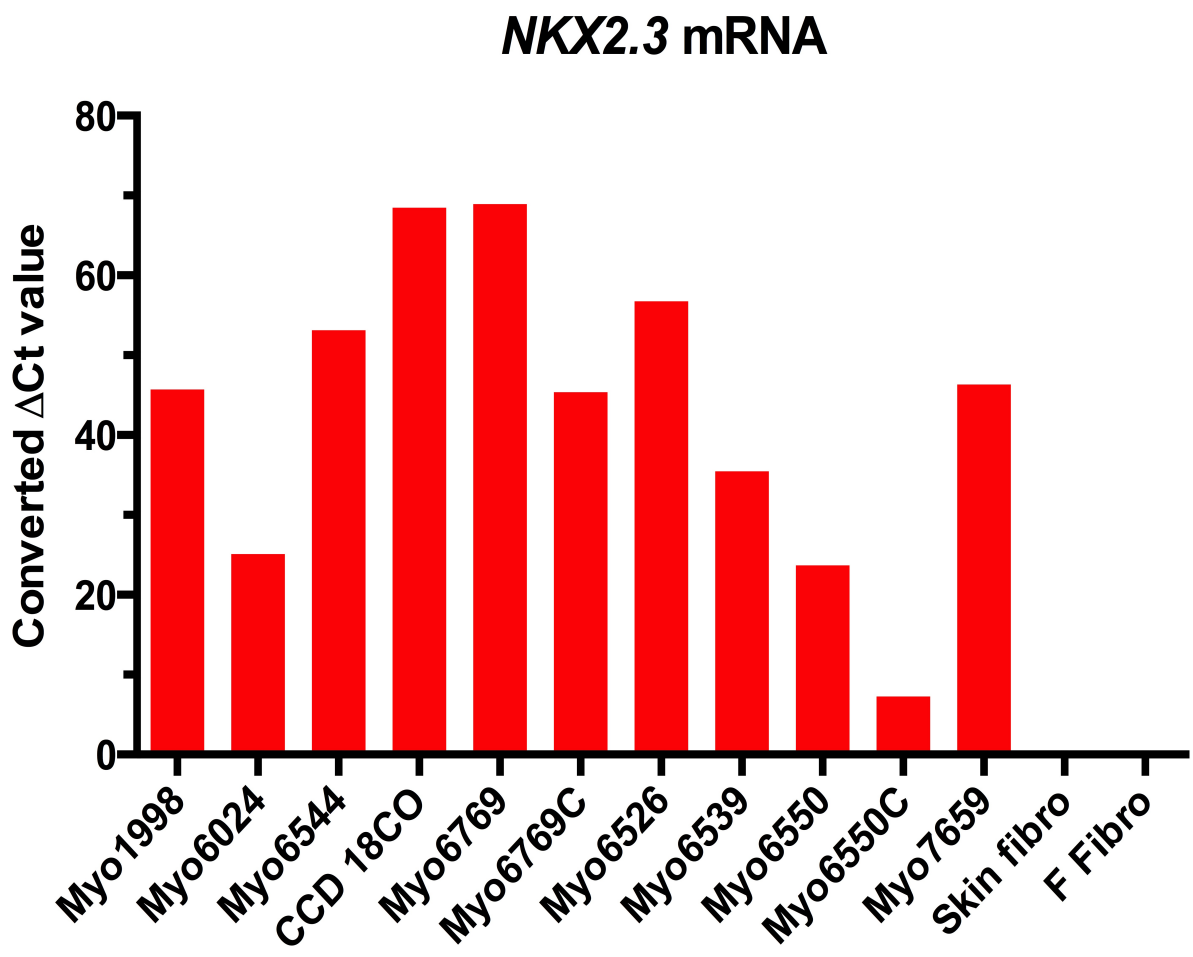

Figure 6.3
qRT-PCR validation of *NKX2.3* mRNA expression in myofibroblast cultures and fibroblast cultures
Expression levels for linearized, converted ΔCt values generated as described in materials and methods are shown. Briefly, ΔCt for each sample was subtracted from the highest ΔCt mean obtained (myo6550C: ΔCt mean 8.13 was used in this figure). The *NKX2.3* mRNA levels of skin fibroblasts and foreskin fibroblasts were undetectable. Column in red: myofibroblast cultures; column in blue: fibroblast cultures. All experiments were independently repeated at least three times, and similar results were obtained. Error bars are not shown for qPCR data, as the converted exponential value dose not preserve the variance in the primary data.

6.2.3.2 siRNA mediated knockdown of *NKX2.3* in CCD 18CO cells

CCD 18CO cells were selected to study the effect of *NKX2.3* knockdown because of the high level of *NKX2.3* mRNA expression in this line as well as its higher growth rate (**Figure 6.3**). Cells were transiently transfected with gene-specific siRNA sequences for *NKX2.3* knockdown (*siNKX2.3*) in 10nM and 20nM and a scrambled sequence used as a control (siCON). *NKX2.3* mRNA expression of CCD 18CO cells was assessed by qRT-PCR primer and probe-sets after 24 and 48 hours transfection. The level of expression was calculated relative to the average normalized Ct for untreated cells. The maximum mRNA knockdown was achieved using 20 nM of siRNA after 24 hours with an 80% reduction in *siNKX2.3* relative to scrambled control (**Figure 6.4**). The NKX2.3 protein level in CCD 18CO was still significantly decreased after 48 hours siRNA transfection, compared to siCON and untreated cells.

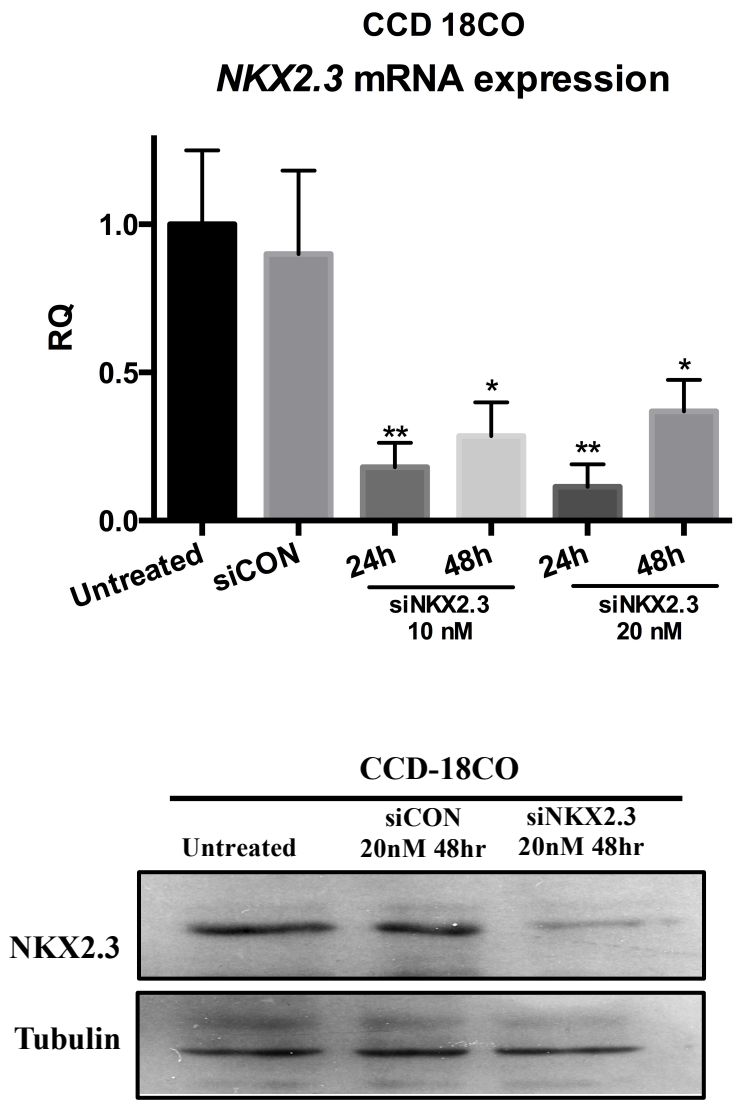

Figure 6.4
***NKX2.3* mRNA and protein expression levels after siRNA mediated knockdown in CCD 18CO cells.** Maximum knockdown was achieved at the mRNA levels of 20nM *NKX2.3* post 24 hours for mRNA (upper panel), protein level of NKX2.3 post 48 hours (lower panel). Transfection was with *NKX2.3* siRNA sequence and scrambled sequence as control. RQ= Relative quantity. All experiments were independently repeated at least three times, and similar results were obtained.

6.2.3.3 Identification of genes regulated by *NKX2.3*

To explore the role of *NKX2.3* in the control of gene expression in myofibroblasts, we first suppressed *NKX2.3* expression in two myofibroblast cultures, CCD 18CO and myo6526, which express high levels of NKX2.3 (**Figure 6.3**). In **Figure 6.5 top panel**, *siNKX2.3* and scrambled siRNA were transfected into both cell cultures. To analyze the possible regulatory effects of *NKX2.3* knockdown on gene expression of four genes of interest, *AOC3*, *ACTA2, MYH11* and *SHOX2*, qRT-PCR analysis was conducted with NKX2.3 knockdown and control cells from the two myofibroblasts **(Figure 6.5, bottom panel).**

Knocking down *NKX2.3* in myofibroblast cells led to a significant reduction of the expression of contractile genes, with a 70% and 88% reduction of *ACTA2* (αSMA) expression; 82% and 99% reduction of *MYH11* expression in Myo6526 and CCD 18CO, respectively ($p<0.001$, versus control for both of cultures). The expression of *AOC3* was also decreased by half in si*NKX2.3* myofibroblasts while the level of expression of *SHOX2* increased three fold. These results suggest a positive regulatory role for NKX2.3 in myofibroblasts on expression of ACTA2, MYH11 and AOC3 and a significant negative regulatory effect on the expression of SHOX2.

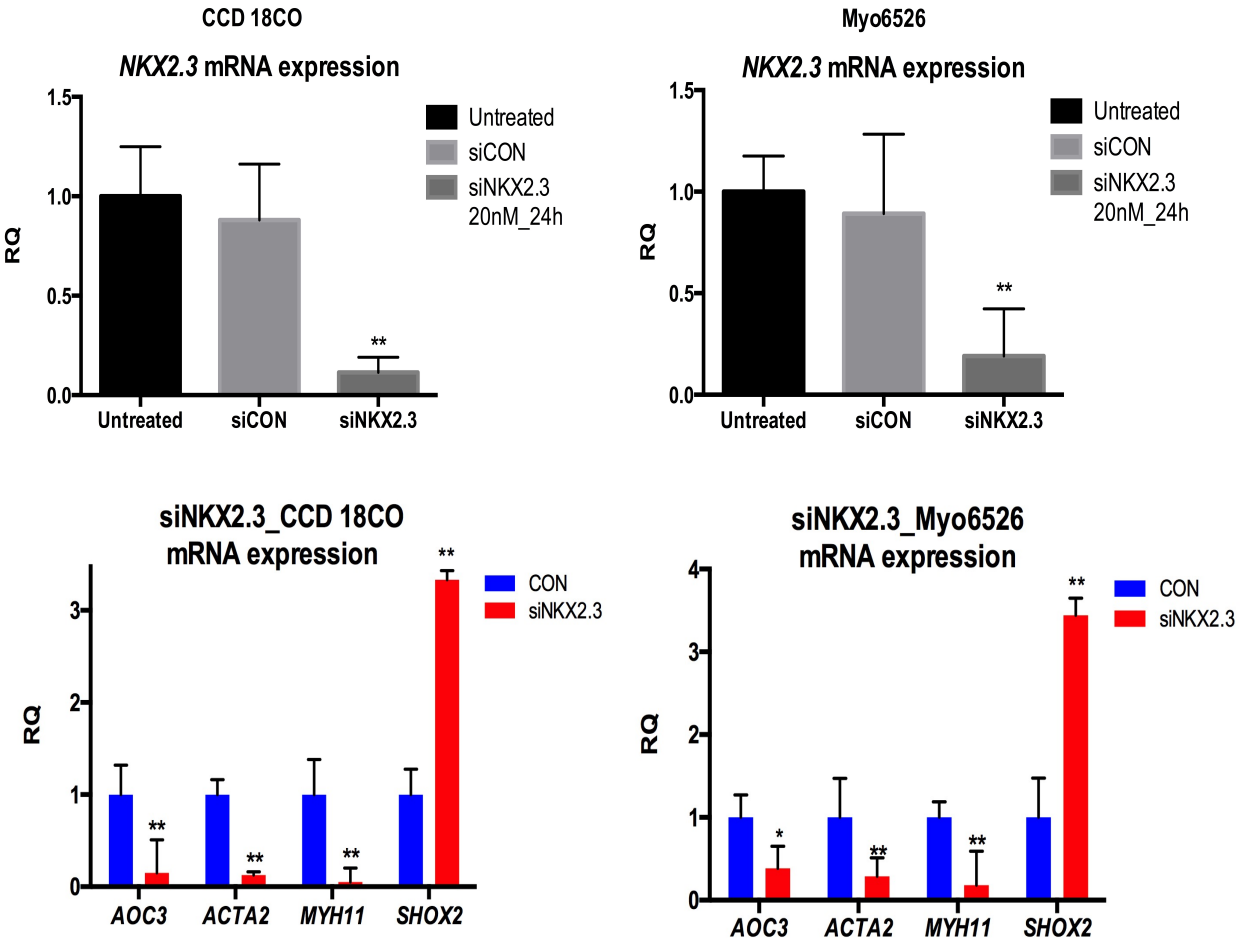

Figure 6.5
***ACTA2, MYH11* and *SHOX2* are regulated by *NKX2.3* in myofibroblasts.**
The relative expression of mRNA in CCD 18CO or Myo6526, transfected with *siNKX2.3* or scrambled sequence as control. Raw Ct values were normalized to UBC, and the fold changes were calculated via the ΔΔCt method relative to control. RQ= Relative quantity; Comparisons between blue and red bars. * P<0.01; ** P<0.001 . All experiments were independently repeated at least three times, and similar results were obtained. Error bars represent the mean of triplicate technical repeats from one experiment.

6.2.3.4 Putative *NKX2.3* binding sites on regulated gene promoters

The potential role of *NKX2.3* in regulating the expression of key myofibroblast related genes has been suggested by the siRNA experiments. In an attempt to find out how these functionally related genes are regulated in response to *NKX2.3*, the *NKX2.3* consensus sequence was used to search for putative binding sites in the promoters of these genes. The putative promoter region sequences (2kb upstream of the first exon of each gene) of *SHOX2, MYH11, ACTA2* and *AOC3* were downloaded from the UCSC Genome Bioinformatics site (https://genome.ucsc.edu/) and Ensembl Genome Browser (http://www.ensembl.org/index.html). The *NKX2.3* consensus sequence has not been characterized in detail, but others have used the published NKX2.5 consensus sequence: 5'-TNNAGTG-3' (Chen and Schwartz, 1995), as there is evidence that NKX2.3 and NKX2.5 bind to the same site *in vitro* (Pabst et al., 2000). The 2 Kb region for each gene contains at least one putative NKX2.3 consensus binding site further suggesting a direct regulatory role for NKX2.3 on the expression of all four genes. Further studies using promoter reporter constructs containing targeted deletion or mutation of these NKX2.3 binding sites would be necessary to confirm this.

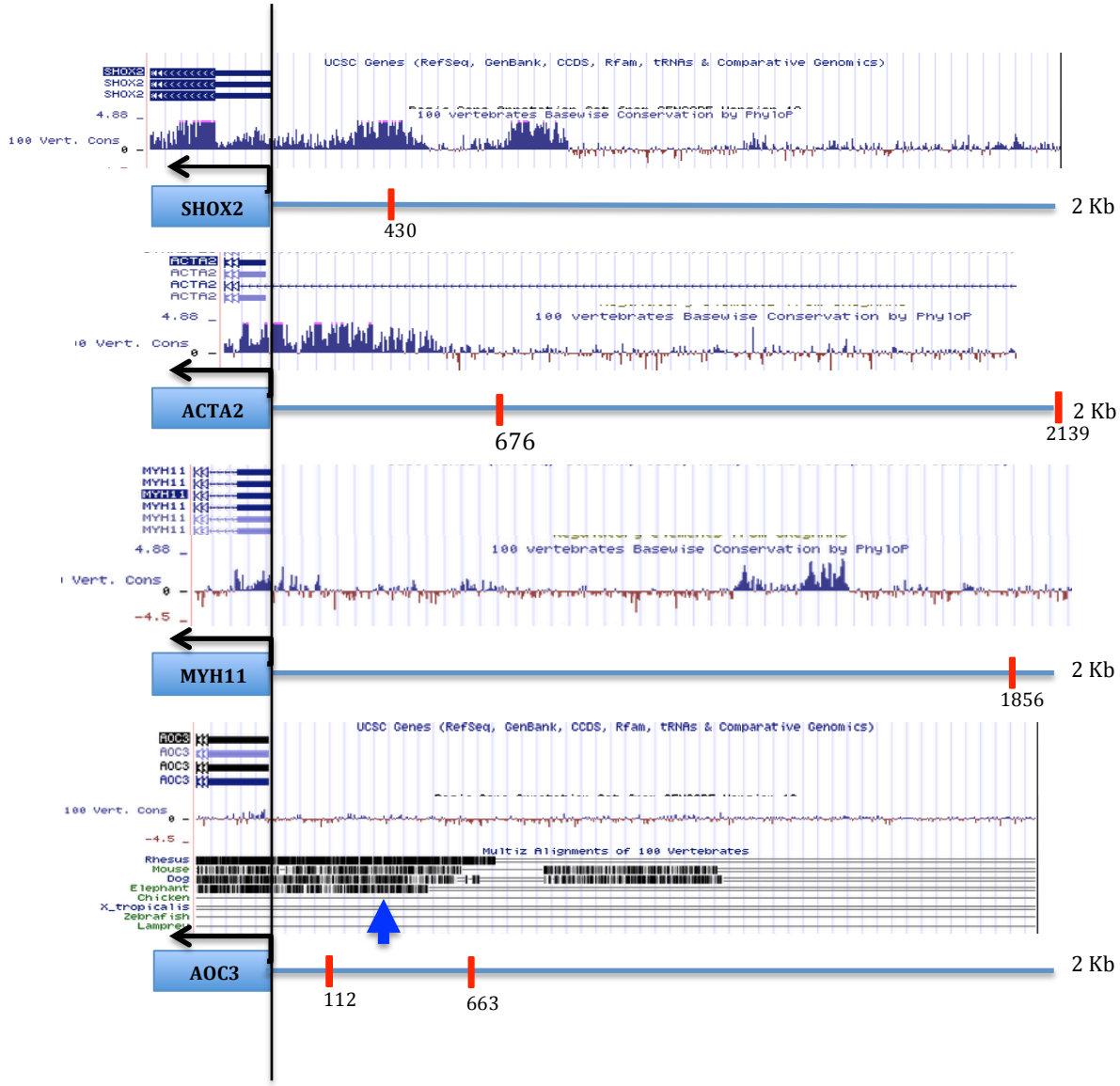

Figure 6.6
Prediction of putative NKX2.3 binding sites
Schematic diagram of the promoter regions of *SHOX2, ACTA2, MYH11* and *AOC3* with conservation across several species is plotted above. Red vertical bars represent the positions of putative *NKX2.3* binding sites. Note: AOC3 shows low conservatory in regulatory sequence but high conservation in coding sequence (indicated with blue thick arrow).

6.2.3.5 TGFβ induces *NKX2.3* and *ACTA* mRNA expression in myofibroblasts

Our previous data suggested tha*t ACTA2* is regulated by *NKX2.3* through the knockdown experiment. That TGFβ-induces αSMA expression in both myofibroblasts and normal fibroblasts has been well established in many studies, as well as in our data. Furthermore, NKX2.3 has been reported to regulate Bmp-2/4 signalling in mice (Pabst et al., 1999). To understand the potential effect of TGFβ on *NKX2.3* and *ACTA2,* mRNA expression levels of TGFβ-treated cells were assessed by qRT-PCR. Cells from Myo7395, a colonic derived primary myofibroblast culture that newly developed while this experiment was in process, were incubated in serum free medium for 24 hours before any treatment, and then TGFβ 10ng/ml was added for another 48 hours in serum free medium. In Figure 6.7, the mRNA expression levels of *NKX2.3* and *ACTA2* were significantly elevated in response to TGFβ ($p<0.01$ and $p<0.001$, respectively). Similar results have been observed in CCD 18CO cells (data not shown), suggesting that *ACTA2* and *NKX2.3* are upregulated in response to TGFβ treatment in myofibroblasts under serum free condition.

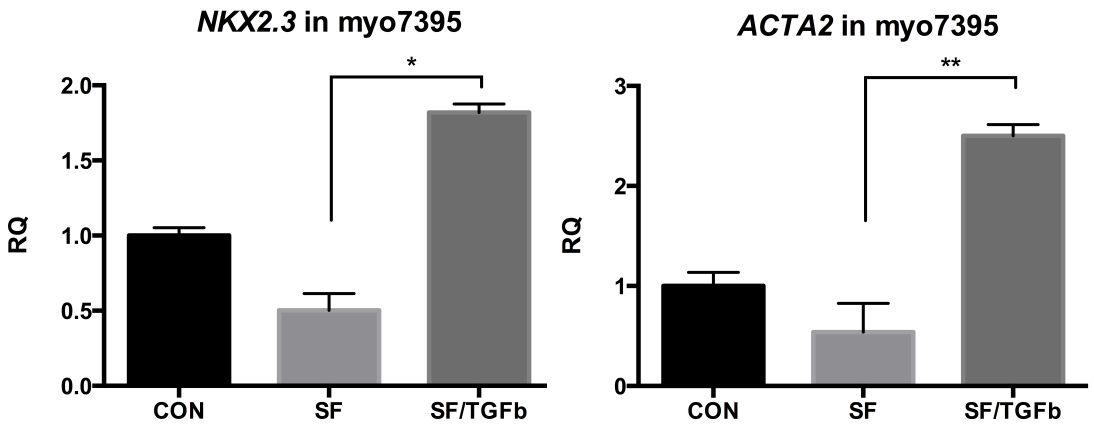

Figure 6.7
TGFβ treatment upregulates *NKX2.3* and *ACTA2* mRNA expression in primary myo7395
The relative expression of mRNA in normal serum (CON), serum free (SF) and TGFβ 10ng/ml under serum free condition (SF/TGFβ) for 48 hours. Raw Ct values were normalized to *UBC*, and the fold changes were calculated via the ΔΔCt method relative to control. RQ= Relative quantity; Comparisons between SF and SF/TGFβ
* P<0.01; ** P<0.001. All experiments were independently repeated at least three times, and similar results were obtained. Error bars represent the mean of triplicate technical repeats from one experiment.

6.2.3.6 *NKX2.3* is essential for myofibroblast contractility

One of the most studied features of myofibroblasts is their contraction ability, which is important during wound healing. The expression of αSMA in myofibroblasts is not only a marker for myofibroblast activation, but also may be important for myofibroblast contractility (Hinz et al., 2001). As *NKX2.3* downregulation significantly reduced the expression of αSMA (*ACTA2* mRNA) in myofibroblasts (**Figure 6.5**), the effect of *NKX2.3* downregulation on myofibroblast contractility was examined. Collagen contraction assays were conducted by transfecting CCD 18CO cells, foreskin fibroblasts and primary myo6526 cells with *siNKX2.3* and then treated with or without TGFβ (10 ng/ml) in serum free condition for a further 24 hours before measuring gel contraction. In **Figure 6.8**, the collagen gels were shrunken down to half of the original gel area in both myo6526 and CCD 18CO untreated controls, while foreskin fibroblasts showed no ability to contract collagen gels. Surprisingly, the size of collagen gels was not obviously changed relative to the original gel area in response to TGFβ. In contrast, *siNKX2.3*-CCD 18CO showed impaired ability to contract collagen gels, with only slightly contracted collagen gels ($p<0.001$, compared to CCD 18CO untreated cells) and similarly in the presence of TGFβ ($p<0.01$, compared to CCD 18CO with TGFβ). These data suggested that *NKX2.3* contributes towards myofibroblast contractility as well as is required for TGFβ-induced collagen gel contraction.

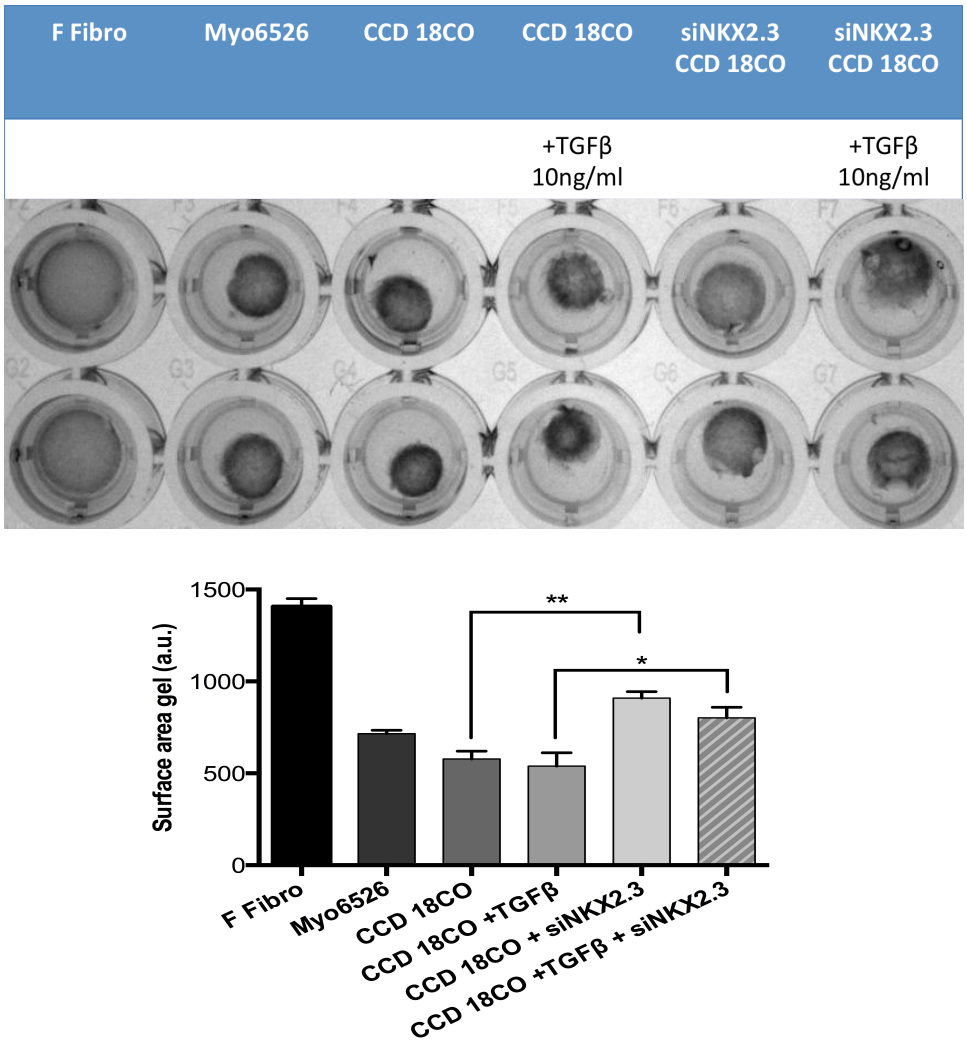

Figure 6.8
Knock down of *NKX2.3* attenuates the ability of myofibroblasts to contract the collagen gels. CCD 18CO cells were transfected with *siNKX2.3,* cultured in serum free medium and then treated with or without TGFβ (10ng/ml), and followed by the collagen gel contraction assay for 24 hours. a.u.=arbitrary unit; * P<0.01; ** P<0.001. Error bars represent the mean of triplicate technical repeats from one experiment.

6.2.3.7 *NKX2.3* mediates TGFβ-stimulated migration of myofibroblasts

To determine the possible role of *NKX2.3* in the migration of myofibroblasts, a Transwell® migration assay (modified Boyden chamber assay) was carried out. CCD 18CO cells were plated onto the upper surface of a Transwell® filter without any coating and allowed to migrate for 48 hours, after which the membranes were fixed and stained with crystal violet. Colorectal cancer cells, RKO were cultured at the bottom of the lower compartment as a source of chemoattractants for myofibroblasts. The migration of myofibroblasts can be observed in the presence of RKO cells (**Figure 6.9**). Addition of TGFβ (10ng/ml) to the upper compartment resulted in a further significant rise of the number of migrated cells. To confirm the role of *NKX2.3* in migration, we used the siRNA knockdown in CCD 18CO cells. As shown in **Figure 6.9,** silencing of *NKX2.3* expression reduced the number of migrated cells by 35% compared to CCD 18CO control (not significant), whereas *siNKX2.3* significantly inhibited the number of TGFβ-induced myofibroblast migrations by 60% compared to CCD 18CO with TGFβ, demonstrating that *NKX2.3* may play an important role in TGFβ-induced migration and contractile ability.

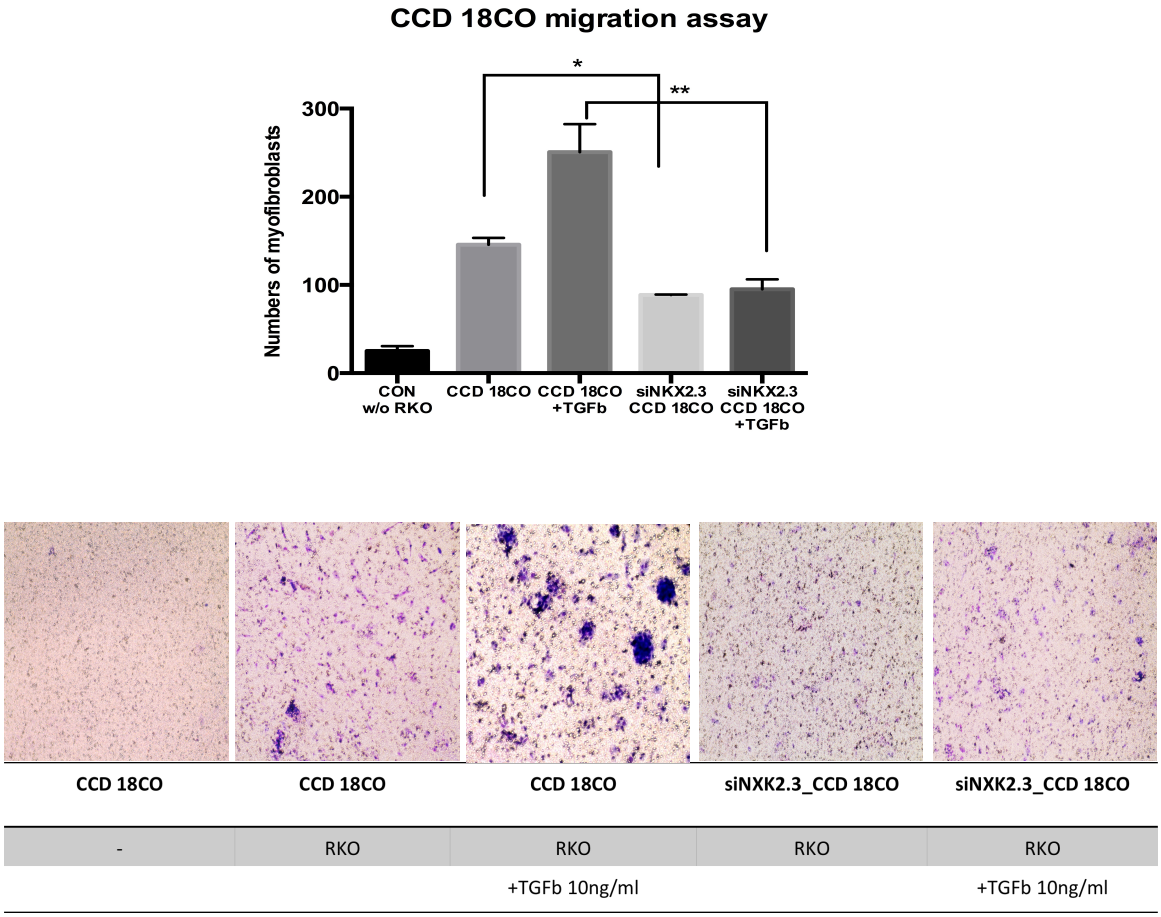

Figure 6.9
NKX2.3 knockdown decreased the migration ability of CCD 18CO cells
CCD 18CO were transfected with *siNKX2.3*. After 24 hours, cells were seeded on to the upper layer of a cell-permeable membrane in serum free medium, treated with or without TGFβ (10ng/ml). RKO colorectal cancer cells were seeded at the lower compartment as a stimulus for cell migration. After 48 hours, the membranes were fixed and stained with crystal violet. Data are means ± SE of triplicate determinations. Representative data are shown. * P<0.01; ** P<0.001. Error bars represent the mean of triplicate technical repeats from one experiment.

6.2.4 *SHOX2*

Short stature homeobox 2 (SHOX2) is a homeobox transcription factor, which has been shown from knockout mouse models to play an important role in the development of heart and limb. Our microarray data identified SHOX2 as being significantly differentially expressed in fibroblast cultures compared to myofibroblast cultures and we therefore further explored the possibility of this being a specific marker for fibroblasts.

6.2.4.1 qRT-PCR validation of *SHOX2* mRNA expression in cultured fibroblasts and colorectal derived myofibroblasts

The mRNA expression levels of the *SHOX2* were assayed from total RNA extracted from 11 primary myofibroblast cultures along with 2 fibroblast cultures using TaqMan qRT-PCR primer and probe-sets (**Figure 6.10**)**.** From our results, *SHOX2* mRNA level was absent in 5 out of 11 primary myofibroblast cultures (myo1998, myo6024, myo6550, CCD18CO, myo6769), and the remaining 6 myofibroblast cultures all had very low *SHOX2* expression levels. Conversely both fibroblast cultures showed much higher expression levels of *SHOX2,* much higher than any of those for the myofibroblasts. These results are consistent with our microarray data and confirm the specificity of SHOX2 in fibroblasts.

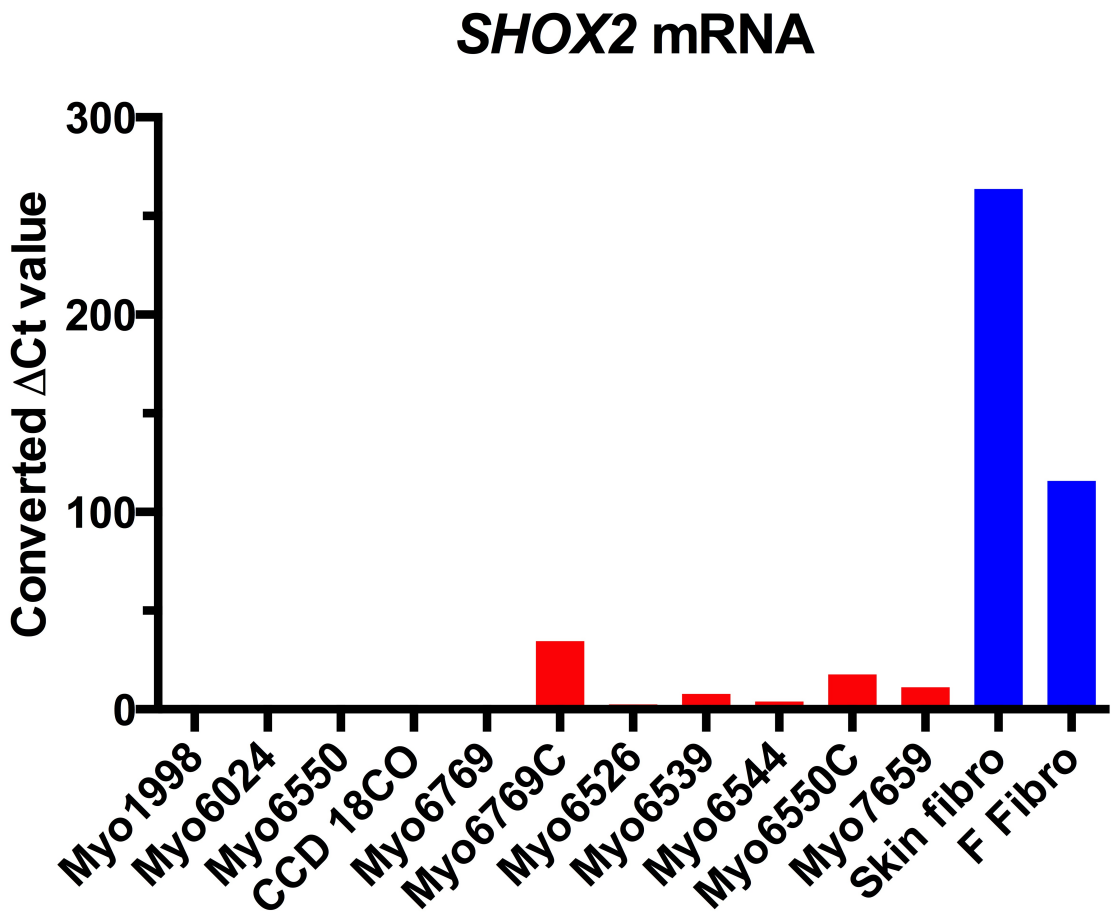

Figure 6.10
qRT-PCR validation of *SHOX2* mRNA expression in myofibroblasts
Expression levels for linearized, converted ΔCt values generated as described in materials and methods are shown (**Chapter 2.3.3**). Briefly, ΔCt for each sample was subtracted from the highest ΔCt mean obtained (myo6526: ΔCt mean 9.64 was used in this figure). The *SHOX2* mRNA levels of myo1998, myo6024, myo6550, CCD 18CO and myo6769 were undetermined (no recorded Ct). Columns in red: myofibroblast cultures; columns in blue: fibroblast cultures. Error bars are not shown for qPCR data, as the converted exponential value dose not preserve the variance in the primary data.

6.2.4.2 Effect of TGFβ on *ACTA2* and *SHOX2* expression of fibroblasts

TGFβ is known to directly promote fibroblast activation by inducing expression of αSMA. To understand the effect of TGFβ on skin fibroblasts, *ACTA2, SHOX2, NKX2.3* and *AOC3* mRNA expression was assessed by qRT-PCR after treatment with TGFβ. Skin fibroblasts were cultured in serum free medium for 24 hours before treatment, followed by addition of TGFβ 10ng/ml and incubation for another 48 hours in serum free medium. **Figure 6.11** showed that the mRNA expression level of *ACTA2* was significantly increased in response to TGFβ ($p<0.001$), as expected. *SHOX2* mRNA expression was reduced after TGFβ addition ($p<0.001$), whilst the mRNA level of *AOC3* remained unchanged either in serum free conditions or after TGFβ treatment, confirming the results obtained with western blots of protein levels as described in chapter 4 (**Figure 4. 15**). *NKX2.3* expression level in skin fibroblasts was not detectable even after TGFβ treatment. Our data confirmed a significant upregulation of ACTA2 in response to TGFβ and further demonstrated that SHOX2 is negatively regulated by TGFβ in fibroblast cells. These results also show that the lack of expression in fibroblasts of the two key genes of myofibroblasts, AOC3 and NKX2.3, is not directly due to transcriptional repression by SHOX2, as neither could be induced in fibroblasts after TGFβ mediated repression of SHOX2.

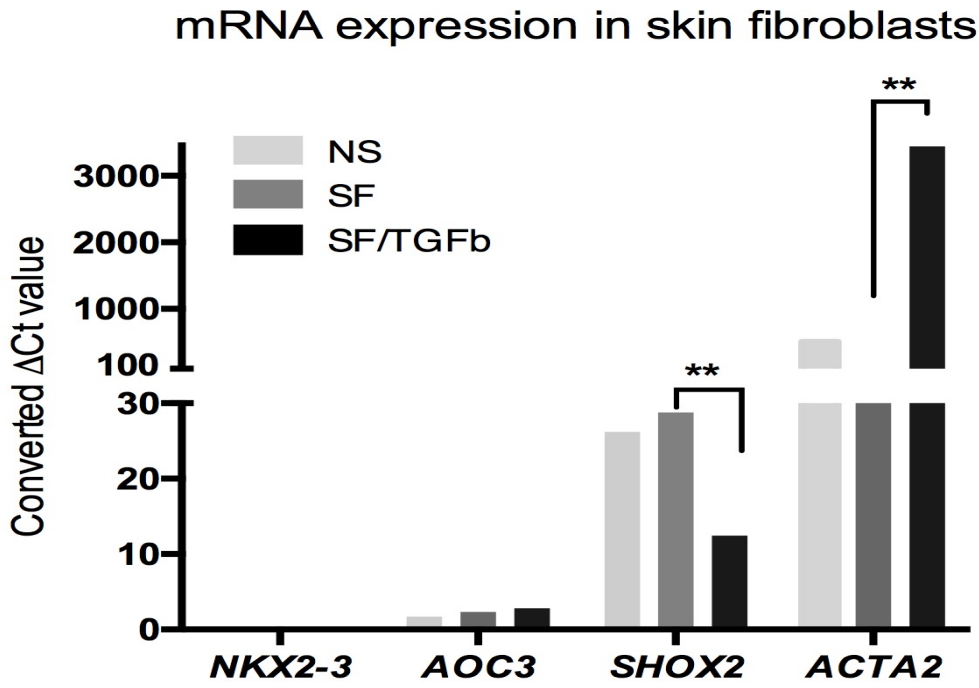

Figure 6.11
Gene expression of skin fibroblasts in response to TGFβ treatment
mRNA expression of *AOC3, ACTA2* and *SHOX2* was assessed in skin fibroblasts under normal serum (CON), serum free (SF) and TGFβ 10ng/ml under serum free condition (SF/TGFβ) for 48 hours. Expression levels for linearized, converted ΔCt values generated as described in materials and methods are shown (**Chapter 2.3.3**). Briefly, ΔCt for each sample was subtracted from the highest ΔCt mean obtained (AOC3 in NS: ΔCt mean 8.21 was used in this figure) *NKX2.3* mRNA level was undetectable (no CT measurement). NS: normal serum medium control; SF: serum free condition; SF/TGFβ: TGFβ treatment in serum free condition. ** P<0.001

To confirm our observation in different cell lines, foreskin fibroblasts and skin fibroblasts were treated with 10 ng/ml TGFβ for 48 hours in serum free medium. The mRNA levels of *ACTA2* and *SHOX2* were then assessed by qRT-PCR. In **Figure 6.12,** TGFβ induced *ACTA2* mRNA expression can be seen in both fibroblast cells ($p<0.001$), as well as the down regulation of SHOX2 expression level ($p<0.01$).

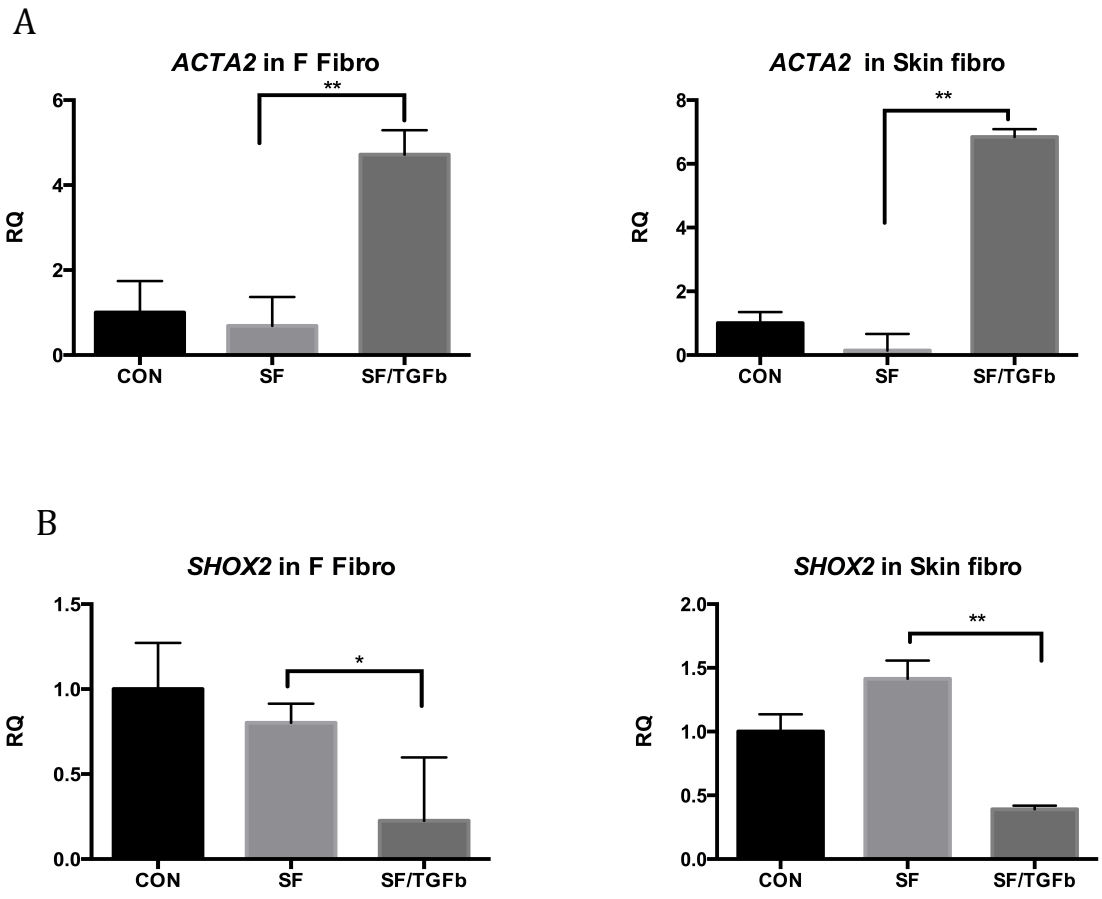

Figure 6.12
TGFβ modulates *ACTA2* and *SHOX2* mRNA expression in foreskin fibroblasts and skin fibroblasts
mRNA expression of *ACTA2* and *SHOX2* was assessed in foreskin fibroblasts and skin fibroblasts under normal serum (CON), serum free (SF) and TGFβ 10ng/ml under serum free condition (SF/TGFβ) for 48 hours. Raw Ct values were normalized to the *UBC*, and the fold changes were calculated via the ΔΔCt method relative to control. RQ= Relative quantity. Comparisons between SF and SF/TGFβ * P<0.01; ** P<0.001. n=3

6.2.5 NKX2.3 and AOC3 expression levels are positively correlated

Based on our results, *AOC3* and *NKX2.3* are the two key genes that define a myofibroblast expression signature. In **Figure 6.5**, we showed that *ACTA2*, *MYH11* and are positively regulated by *NKX2.3* and that *SHOX2 is* negatively regulated by *NKX2.3*. The results also demonstrate a modest decrease in *AOC3* mRNA expression in response to siRNA mediated silencing of *NKX2.3* in myofibroblasts (**Figure 6.5**). To understand the role of *AOC3* in the control of gene expression in myofibroblasts, CCD 18CO cells were transfected with siAOC3 and scrambled siRNA for 24 hours to achieve the maximum knockdown (**Figure 6.13A**). The gene effects of *AOC3* knockdown were assessed by qRT-PCR with siAOC3_CCD 18CO compared to siCON_CCD 18CO cells. **Figure 6.13B** showed that only *NKX2.3* expression was affected by knocking down *AOC3*, with a significant decrease (p<0.01), while *MYH11, ACTA2* and *SHOX2* mRNA expression remained unchanged. Together, these results suggest a possible positive feedback loop between expression of NKX2.3 and AOC3 in myofibroblasts.

A

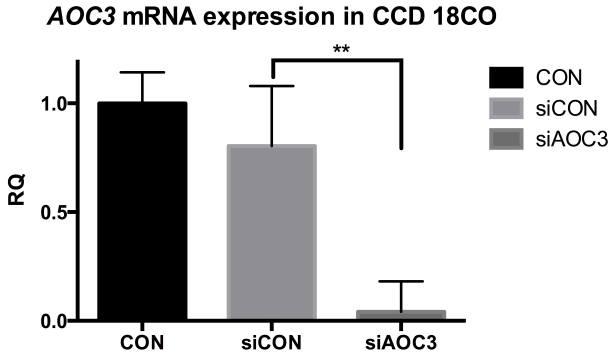

B

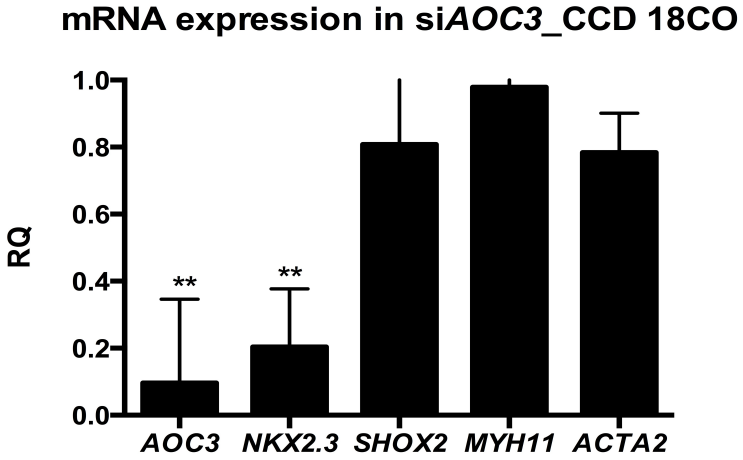

Figure 6.13
***AOC3* silencing decreases *NKX2.3* expression in CCD 18CO cells.**
Relative mRNA expression in CCD 18CO cells, transfected with siAOC3 or scrambled sequence as control. (A) Cells were harvested after 24 hours transfection with 20 nM siAOC3. (B) siAOC3_CCD 18CO cells were examined for the expression of candidate genes (*NKX2.3, SHOX2, MYH11* and *ACTA2*) relative to siCON. Raw Ct values were normalized to the UBC, and the fold changes were calculated via the ΔΔCt method relative to CON in (A) or siCON in (B). RQ= Relative quantity; Comparisons between black and grey bars * P<0.01; ** P<0.001. n=3

6.3 Discussion

Through a genome-wide analysis of microarray based mRNA expression profile differences between myofibroblast and fibroblast cell lines, we identified four additional markers that distinguish between myofibroblasts and fibroblasts. These include the homeobox transcription factor *NKX2.3* in myofibroblasts and *SHOX2*, another transcription factor, in fibroblasts. qRT-PCR was used to validate the mRNA expression level of these two candidate genes across all colorectal derived myofibroblasts and normal fibroblasts. *NKX2.3* is significantly expressed in myofibroblasts and completely absent in fibroblasts at mRNA and protein level, whereas the *SHOX2* is highly expressed only in fibroblasts.

NKX2.3 is a homeodomain transcription factor, which has been associated with inflammatory bowel disease by genome-wide associated studies with increased levels of mRNA in Crohn's disease patients (Franke et al., 2008, Yamazaki et al., 2009). Within the gastrointestinal tract, NKX2.3 has been reported to be expressed mesenchymally in the mouse gastrointestinal tract and spleen (Pabst et al., 1997, Fu et al., 1998) and a negative regulator of crypt cell proliferation by regulating downstream targets, Bmp-2 and Bmp-4 (Pabst et al., 1999, Roberts, 2000). Targeted deletion of *Nkx2.3* in mice leads to profound abnormalities in small intestine and spleen as it functions as a negative regulator of crypt cell proliferation (Pabst et al., 1999). It has been reported that *Nkx2.5* repressed αSMA expression in rat myofibroblasts (Hu et al., 2010), but there are so far no reports linking NKX2.3 expression to myofibroblasts.

In this chapter, we first demonstrated the expression of *NKX2.3* in primary myofibroblasts and confirmed the specificity by knocking down *NKX2.3*. Silencing *NKX2.3* resulted in an increase of *SHOX2* expression and a decrease of *MYH11* and *ACTA2* expression in myofibroblasts, suggesting that these genes might be directly regulated by *NKX2.3*. This observation was strengthened by showing *NKX2.3* putative binding sites in the 2kb region of the promoter region of these genes. Luciferase reporter assays using promoter constructs containing inactivating mutations of the putative NKX2.3 binding sites would provide conclusive evidence of direct transcriptional control of these genes by NKX2.3. The functional significance of NKX2.3 expression was assessed by measuring myofibroblast contractility and migration ability. αSMA expression is known to be essential for myofibroblast contraction during wound healing. Knock down of *NKX2.3* reduced the contractile ability of myofibroblasts, and also abolished TGFβ-induced collagen gel contraction and myofibroblast migration, suggesting that *NKX2.3* is crucial for mediating the function of myofibroblasts by regulating αSMA expression. Our results also suggested a potential inter-relationship between the regulation of expression of *NKX2.3* and *AOC3*, two key genes of myofibroblasts.

SHOX2, is a homologue of the short stature homeobox gene *SHOX* in humans. Mutation of *Shox2* in mice has demonstrated a crucial role for this gene in the development of heart and limb (Cobb et al., 2006, Yu et al., 2007, Espinoza-Lewis et al., 2009). High levels of *SHOX2* mRNA expression in fibroblasts, as compared to primary myofibroblasts, were confirmed by qRT-PCR. In fibroblasts, SHOX2 expression is decreased in response to addition of TGFβ, while the expression of αSMA is increased, as expected. Interestingly, TGFβ addition cannot induce *NKX2.3* expression in

fibroblasts, which makes the NKX2.3 expression exclusively in myofibroblasts. Our results clearly suggest that TGFβ activated fibroblasts, with increased expression of αSMA can still be clearly distinguished from myofibroblasts by use of the additional markers NKX2.3 and AOC3.

Together, results in this chapter demonstrate that NKX2.3 is crucial for maintenance of myofibroblast characteristics and probably is a key switch for determining the difference between fibroblasts and myofibroblasts. The result is a novel and clear definition of myofibroblasts using the expression signatures of AOC3 and NKX2.3.

CHAPTER SEVEN

GENERAL DISCUSSION

CHAPTER 7: GENERAL DISCUSSION

7.1 AOC3 is a novel myofibroblasts marker *in vivo* and *in vitro*

AOC3/VAP-1 protein was first identified by Salmi and Jalkanen in the mouse endothelial venules (Salmi and Jalkanen, 1992). Since then, they have performed extensive functional studies of AOC3/VAP-1 in endothelial cells and characterised its roles in inflammation and leukocyte trafficking. In addition to endothelial cells, AOC3/VAP-1 expression has also been reported in pericytes, adipocytes and smooth muscle cells (Salmi and Jalkanen, 1992, Salmi et al., 1993). Literature reviews of earlier studies did reveal reports of the tissue distribution of AOC3/VAP-1 on pericryptal cells in mouse and human gut, but we now believe that authors incorrectly interpreted these as endothelial cells (Stolen et al., 2005, Salmi and Jalkanen, 2006). Pericryptal cells in the human colon are myofibroblasts, as originally identified by PR2D3 mAb staining (Richman et al., 1987), followed by the αSMA staining (Sappino et al., 1989) as well as supported by results in this thesis using co-staining with multiple markers to confirm these pericryptal cells are $PR2D3^{+ve}$, αSMA^{+ve}, VIM^{+ve} and $CD31^{-ve}$ (**Figure 3.5**).

We identified AOC3 as the target protein of the PR2D3 mAb and characterised the tissue specific expression profile of this surface-expressed oxidase in myofibroblasts in a range of normal and tumour tissues and cell cultures. Plenty of immune-based and molecular biology techniques were used to interrogate the expression and regulation of AOC3 in myofibroblasts. Commercial anti-AOC3 (Clone 393112 from R&D systems) was used for immunofluorescence analysis to show the tissue distribution of AOC3

substantially matched that determined by PR2D3 (Richman et al., 1987). **Tables 4.1 & 4.2** summarise the data obtained so far on the tissue distribution of AOC3.

However, some differences in staining patterns between AOC3 and αSMA, such as in breast tumours, suggest further heterogeneity of myofibroblasts and fibroblasts in different tissues. The specificity of AOC3 in tissue myofibroblasts has been further validated by the absence of staining of pericryptal cells in guts of AOC3 knock out mice (Stolen et al., 2005). We also confirmed the AOC3 staining specificity in cultured myofibroblast cells by using siRNA mediated gene knock down experiment on CCD 18CO cells.

To date, there are only limited choices available so far for selecting a surface marker to identify myofibroblasts; one that has most often been used in human studies is the cell-surface glycoprotein THY1 (thymocyte differentiation antigen-1, also known as CD90). Our own data from mRNA microarrays suggest that this protein is uniformly, highly expressed in both myofibroblast and fibroblast cultures. THY1 has been used by others to separate a subset of fibroblasts from liver, lung and ovary (Sempowski et al., 1996, Koumas et al., 2001, Koumas et al., 2003). This subset of $THY1^{+ve}$ fibroblasts are claimed to be myofibroblasts due to either baseline expression of αSMA, or the capacity to express αSMA in response to TGFβ. According to the results put forward in this thesis, we would suggest that these cells represented activated fibroblasts. By using anti-AOC3 sorted myofibroblasts from fresh tissues, on the other hand, we can demonstrate the high purity of myofibroblasts not only based on expression of PR2D3, NKX2.3 and enrichment of AOC3, but also on the absence of fibroblast marker, SHOX2. It must be noted that the heterogeneous staining of αSMA and MYH11 on

AOC3 sorted myofibroblasts (**Figure 5.8A**) highlights the inadequacy of these two markers on their own to identify myofibroblasts.

7.2 Regulation of AOC3 and NKX2.3 in myofibroblasts

siRNA-mediated gene knock down experiments of either AOC3, or NKX2.3 on myofibroblast cells provides evidence of a potential positive feedback loop between AOC3 and NKX2.3 expression.

In endothelial cells, increased expression levels of AOC3 and NKX2.3 have been reported in inflammatory bowel disease (IBD)(Yamazaki et al., 2009, Yu et al., 2010b, Koutroubakis et al., 2002). Mucosal Vascular Addressin Cell Adhesion Molecule 1 (MADCAM1) is a lymphocyte homing receptor selectively expressed on gut-associated endothelial cells, which facilitates lymphocytes binding through interaction with α4β7 integrin during inflammation (Ogawa et al., 2005). It has been shown that NKX2.3 up-regulates MADCAM1 expression directly through transcriptional regulation (Pabst et al., 2000, Wang et al., 2000, Yamazaki et al., 2009, Yu et al., 2010a), whilst elevated levels of AOC3 enzyme activity have been shown to facilitate the expression of MADCAM1 in IBD (Liaskou et al., 2011). Thus, both AOC3 and NKX2.3 are essential for lymphocyte trafficking and regulation in endothelial cells. The authors of these studies do not, however, suggest a direct mechanism involving NKX2.3 mediated upregulation of AOC3, both of which then positively affect MADCAM1 expression levels. We hypothesize that increased AOC3 expression in endothelial cells, mediated by NKX2.3, might reflect a positive feedback loop between NKX2.3 and AOC3, and

perhaps even involving MADCAM1, similar to the positive feedback loop we observed between AOC3 and NKX2.3 in myofibroblasts.

Although AOC3 is not a transcription factor, siRNA knockdown of AOC3 had a more profound negative effect on NKX2.3 expression than the effect of NKX2.3 knockdown on AOC3 levels (**Figure 6.5 & 6.13**), suggesting that AOC3 is able to mediate this transcriptional regulation of NKX2.3 expression in myofibroblasts through an intermediate or indirect signalling mechanism. Securing specific inhibitors of the copper amine oxidase enzyme activity of AOC3 will facilitate experiments to determine whether the AOC3 mediated effect on NKX2.3 levels involves a potential signalling role of the enzyme activity of AOC3, perhaps through H_2O_2.

7.3 NKX2.3 is a key regulator of myofibroblast phenotype and an antagonistic mechanism between NKX2.3 and SHOX2 expression defines the balance between fibroblast and myofibroblast phenotypes

We identified NKX2.3 as part of a myofibroblast signature and SHOX2 as a fibroblast signature through a global gene expression analysis by comparing microarray mRNA expression profiles of myofibroblasts and fibroblasts. Subsequent to our identification of NKX2.3 and SHOX2 as a specific markers of myofibroblasts and fibroblasts respectively, Higuchi et al. (June 2015) reported NKX2.3 expression in a subset of human gastrointestinal myofibroblasts, while *SHOX2* and *TBX5* genes were found to be upregulated in non-gastrointestinal fibroblasts, in agreement with our results for the colon. By clustering the expression profiles obtained from fibroblasts from different organs, they report that *NKX2.3* gene expression is organ-specific and restricted to duodenum, ileum and colon (Higuchi et al., 2015).

In this thesis, for the first time, we explored the regulation of NKX2.3 target genes in colonic derived myofibroblasts. siRNA mediated knockdown of NKX2.3 in myofibroblasts resulted in a decrease in expression of contractile genes, αSMA and MYH11 as well as an increase in SHOX2 expression. This suggests that NKX2.3 is important in maintaining the distinction between myofibroblasts and fibroblasts, and thereby potentially controlling the balance of epithelial-mesenchymal interactions in the gut. This is supported by the evidence of abnormal gut development and function in NKX2.3 knock out mice (Pabst et al., 1999).

The fact that NKX2.3 and NKX2.5, another member of the NKX family, share the same

consensus sequence in vertebrates (Fu et al., 1998, Pabst et al., 1999) suggests that NKX2.5 is the most important homologue of NKX2.3. *Nkx2.5* regulates heart development by regulating expression of various genes (Kasahara et al., 1998), while *Nkx2.3* may significantly influence gene expression within the intestine (Pabst et al., 1999). Thus, it is worth noting some studies of NKX2.5 which might related to NKX2.3.

Hu and colleagues demonstrated that the αSMA gene promoter contains the NKX2.5 consensus sequence motif and reported a negative correlation between αSMA and NKX2.5 expression in rat lung fibroblasts (Hu et al., 2010). This identification of a negative regulatory role of NKX2.5 on αSMA provides additional support for our evidence for a regulatory role of the *NKX* genes on αSMA, but suggests that while NKX2.5 negatively controls transcription in lung fibroblasts, NKX2.3 positively controls αSMA expression in the human colonic myofibroblasts.

Espinoza et al described an apparent antagonistic mechanism between expressions of SHOX2 and NKX2.5. Overexpression of SHOX2 in rat cardiomyocytes resulted in extensive repression of NKX2.5 (Espinoza-Lewis et al., 2009). Moreover, SHOX2 and NKX2.5 have been shown to physically interact and a genome wide co-occupancy of NKX2.5, SHOX2 and TBX5 on gene promoters has also been described (Ye et al., 2015). Together with our results demonstrating NKX2.3 mediated repression of SHOX2 in myofibroblasts, there is, therefore, good evidence of a negative feedback mechanism between SHOX2 and NKX2.3. We suggest that NKX2.3 is the key regulator of expression of genes that define the distinction between fibroblasts and myofibroblasts.

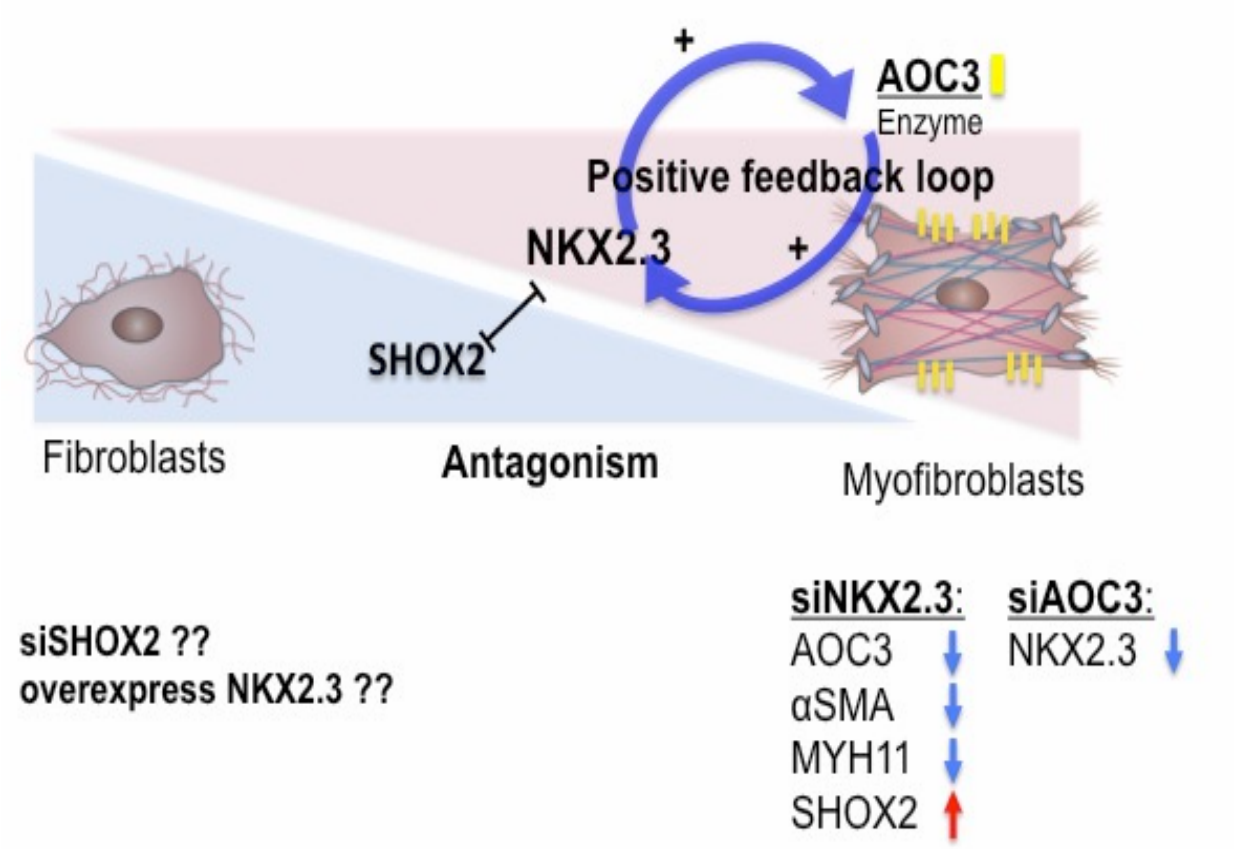

Figure 7.1
Schematic model of gene regulation between myofibroblasts and fibroblasts
NKX2.3 and AOC3 are two key genes in myofibroblasts from our results. Based on the work of this thesis, we show a positive feedback loop between AOC3 and NKX2.3 in myofibroblasts, and SHOX2-NKX2.3 negative regulation between myofibroblasts and fibroblasts. Pictures of fibroblasts and myofibroblasts are adapted from (Falke et al., 2015)

7.4 Control of NKX2.3, AOC3, αSMA, and SHOX2 expression in myofibroblasts and fibroblasts by TGFβ (Figure 7.2)

The current definition of myofibroblast differentiation and activation involves a number of growth factors including PDGF, angiotensin and TGFβ (Hinz, 2007). Cells identified through positive expression for αSMA and referred to as myofibroblasts, are frequently associated with liver, lung and kidney disease, and can be directly activated by TGFβ (Milani et al., 1991, Zhang et al., 1996, Abbate et al., 2002). During early experiments on the regulatory role of TGFβ on fibroblasts and myofibroblasts, it became clear that in order to control for the TGFβ present in fetal calf serum, it is necessary to perform experiments in the absence of serum, with or without addition of TGFβ. Our results revealed a surprising but significant up-regulation of ACO3 expression simply by culturing myofibroblast cells in serum free conditions, raising the possibility of a serum containing factor that negatively regulates the expression of AOC3 at both the protein and mRNA level (**Figure 4.12**). This increase in AOC3 expression in the absence of serum was significantly inhibited by TGFβ addition. Furthermore, TGFβ treatment in cells already grown in serum results in a further decrease in the levels of AOC3, implying that the concentration of TGFβ in serum is sufficient to depress, but not fully inhibit, expression of AOC3. The initial increase in AOC3 mRNA and protein levels following up to 96 hours serum starvation, is followed by a significant decrease in mRNA levels within 48 hours after TGFβ is added, but this does not appear to translate into a decrease in the levels of protein as measured by western blot. It will be necessary to repeat these experiments with longer incubation periods in TGFβ and also to determine the half-life of AOC3 protein in myofibroblasts, in order to establish whether this simply reflects residual levels of AOC3, or a direct

effect of TGFβ on protein turnover. The ability of TGFβ to decrease AOC3 levels whilst increasing NKX2.3 was initially surprising given earlier results implying a positive feedback loop between AOC3 and NKX2.3, such that we might have expected that any increase in NKX2.3 would result in an increase in AOC3. In order to reconcile our observations, we suggest a model where the negative affect of TGFβ on AOC3 levels dominates the positive transcriptional control of AOC3 by NKX2.3 (**Figure 7.2**). An important observation from the results of TGFβ treatment of fibroblasts was that neither serum starvation nor TGFβ addition had any effect on either NKX2.3 or AOC3 expression level in skin fibroblasts. However, as expected from many previous studies, TGFβ dramatically increases the expression of αSMA in both fibroblasts and myofibroblasts.

Bmp-2 and Bmp-4 have been identified as downstream targets of NKX2.3 in regulating gut morphogenesis (Roberts, 2000). This suggests that NKX2.3 might be involved in the TGFβ/Smad signalling pathway. We have shown that NKX2.3 expression is up regulated in response to TGFβ treatment in both primary myofibroblasts and CCD 18CO cells, as well as that NKX2.3 is required for TGFβ-induced αSMA-mediated myofibroblast contractility and migration. Conversely, SHOX2 is down regulated in response to TGFβ in fibroblasts, whilst αSMA expression is increased, but NKX2.3 expression is not induced by TGFβ treatment in fibroblasts. Together, these experiments show that myofibroblasts and fibroblasts have significantly different expression profiles with respect to these few key genes, and that they differ dramatically in their response to TGFβ. Thus TGFβ inhibits AOC3 and SHOX2 expression while increasing NKX2.3 and αSMA expression in myofibroblasts, but only increases αSMA expression in fibroblasts. The results clearly imply that TGFβ activated fibroblasts and

myofibroblasts are significantly different cell types, and provides clear evidence disputing the notion that myofibroblasts represent activated fibroblasts.

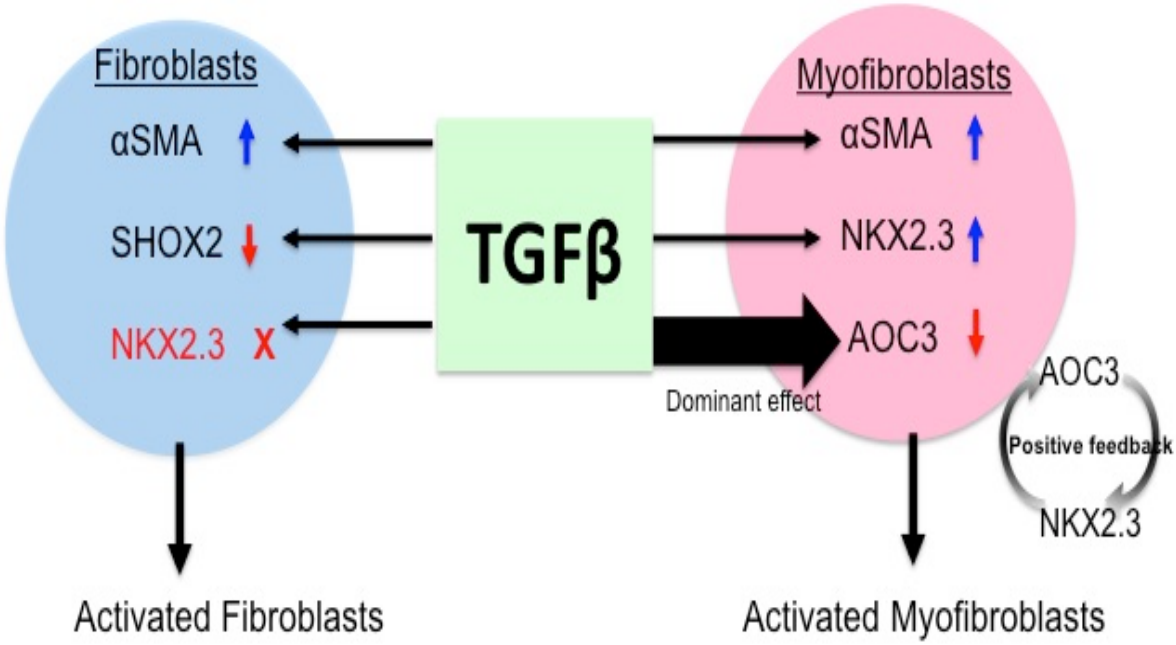

Figure 7.2 TGFβ effect on myofibroblasts and fibroblasts
A schema integrating the work of this thesis based on the control of gene expression by TGFβ regulation. In myofibroblasts, TGFβ regulates AOC3 independently from NKX2.3, and this regulation is dominant over the positive feedback interaction between AOC3 and NKX2.3.

7.5 Myofibroblasts, activated fibroblasts and fibroblasts in tissues

As discussed in the general introduction (**Chapter 1**), the earliest description of myofibroblasts by Gabbiani after injury or during would healing, suggested that myofibroblasts were modified fibroblasts that had acquired smooth muscle features, including expression of α smooth muscle actin (αSMA)(Gabbiani et al., 1971, Majno et al., 1971). Following the demonstration by Desmouliere et al that TGFβ stimulated αSMA in connective tissue fibroblasts (Desmouliere et al., 1993), it became widely accepted that myofibroblasts could be defined as TGFβ activated fibroblasts. However, through careful study of the gene expression signatures of fibroblasts and colon derived myofibroblasts, the results in this thesis begin to give a finer classification of different types of fibroblasts and myofibroblasts, and how they relate to each other.

The effect of serum starvation and TGFβ treatment of the myofibroblasts and fibroblasts has shown that TGFβ activated myofibroblast and TGFβ activated fibroblast are two quite distinct cell types, although they do share some common features, such as the elevated level of αSMA expression in response to TGFβ. Therefore, while TGFβ indeed activates fibroblasts to increase αSMA expression, which to date has been the main way to define a myofibroblast (Webber et al., 2010), our data reveals a clear distinction between TGFβ activated fibroblasts and TGFβ activated myofibroblasts as demonstrated by their AOC3, NKX2.3 and SHOX2 expression profiles.

The fibroblast activation protein (FAP) has been shown to be specific for activated fibroblasts in wounds and many epithelial cancers, including colorectal cancers (Garin-Chesa et al., 1990). It is not expressed in normal tissue fibroblasts but does show some

staining with fibroblasts in culture (Rettig et al., 1986, Rettig et al., 1988, Henry et al., 2007), which might be due to activation by the FBS commonly used in tissue culture media, possibly because of the small amounts of TGFβ contained in FBS. FAP has been reported to be negative in myofibroblasts defined as pericryptal cells in colon, which is supported by our microarray data showing low to moderate FAP mRNA expression levels among all primary myofibroblasts and fibroblast cultures. It is intriguing that tissue microarrays of breast cancer demonstrated a complete absence of AOC3 expression in stromal cells (**Figure 7.3**) whereas high levels of FAP staining have been reported in breast cancer associated stromal cells (Tchou et al., 2013), suggesting that the stromal cells in breast cancer might be activated fibroblasts rather than myofibroblasts.

The Bodmer laboratory (Yeung et al., 2013) has demonstrated a very substantial presence of myofibroblasts in lymph node metastases of colorectal cancer, with a correlation between the extent of apparent myofibroblast activation and the aggressiveness of the cancer. The staining with antibody to AOC3 of a metastasis involved lymph node shown in **Figure7.4** clearly shows that the activated cells are indeed myofibroblasts and not just activated fibroblasts. Myofibroblasts may be expected to secrete a quite different profile of growth factors when stimulated by aggressive cancers in distant metastases than activated fibroblasts. It is therefore essential for evaluating the clinical importance of the interaction between myofibroblasts and cancer epithelial cells to be able to distinguish activated fibroblasts from myofibroblasts in cancer tissues.

A growing body of evidence has demonstrated that the stromal environment in cancer is very heterogeneous, containing a mixture of cell types including myofibroblasts, fibroblasts and very likely activated fibroblasts (Sugimoto et al., 2006). The new combination of markers described in this thesis now enables a finer distinction between cell types and includes AOC3, FAP, NKX2.3 and SHOX2 (and potentially LRRC17 and TBX5), along with smoothelin for identifying smooth muscle cells (van der Loop et al., 1996). As showed in **Table 7.1**, these can now clearly distinguish between myofibroblasts, fibroblasts, activated fibroblasts and smooth muscle cells using currently available mAbs, and can be combined with other epithelial markers and endothelial markers, if desired.

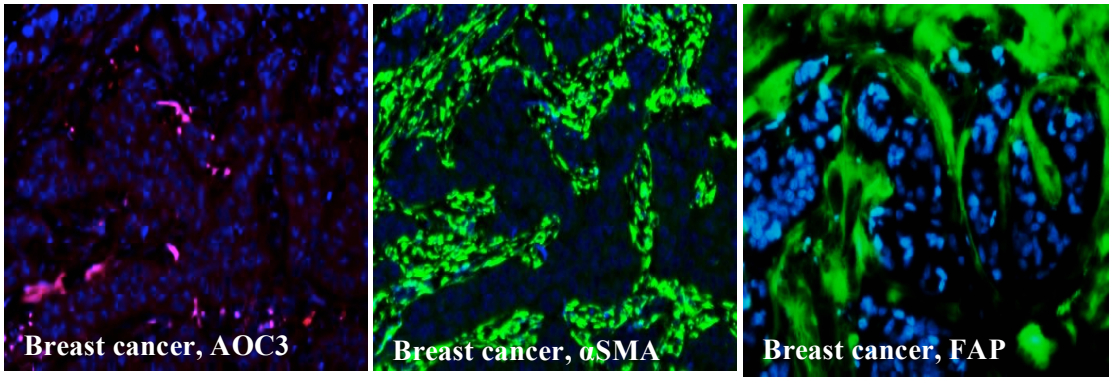

Figure 7.3
AOC3, αSMA and FAP expression within breast cancer stroma indicate the presence of activated fibroblasts (IF, FFPE)
Immunofluorescence staining of paraffin-embedded sections of human breast cancer with AOC3, αSMA and FAP antibodies. Note, AOC3 and αSMA are co-stained in one slice, while FAP staining is on a different slice. X20 magnification

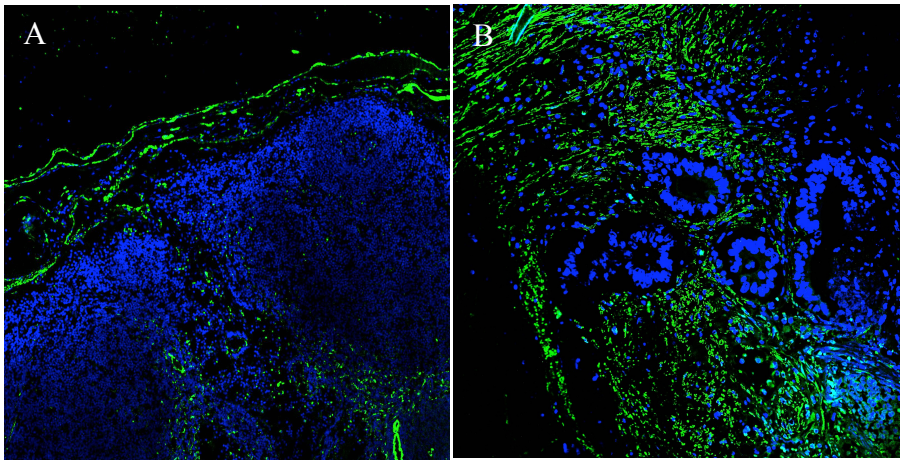

Figure 7.4
AOC3 staining on myofibroblasts in a macro-metastasis involved lymph node (IF, FFPE)
Confocal immunofluorescence of paraffin-embedded section of lymph nodes with AOC3 (green) for myofibroblasts and DAPI (blue). (A) Micrometastasis x5 magnification. (B) Macrometastasis x5 magnification. (Tissue sections courtesy Dr TM Yeung)

	AOC3	NKX2.3	SHOX2	αSMA	FAPs	Vimentin (VIM)	Smoothelin	THY-1 CD90
MFs	+	+		++/-	-	+	-	+
Fs			++	--/+	-	+	-	+
aFs			+	++	+	+	-	+
Smooth muscle	+	+	+	+	-	-	+	-

Table 7.1
Molecular markers for myofibroblasts, fibroblasts and activated fibroblasts identification in stroma
Due to the fact of the heterogeneous staining of αSMA on myofibroblasts and fibroblasts, we used double marks to indicate the staining pattern. ++/- means the majority MFs are stained by αSMA; --/+ means only subset of Fs are positive to αSMA. Fs: fibroblasts; aFs: activated fibroblasts; MFs: myofibroblasts; αSMA: α smooth muscle actin.

7.6 Summary

In this thesis, we have shown the solid evidence of the specificity of AOC3 expression in myofibroblasts and characterised the expression of AOC3 in a wide range of normal and cancerous tissues. However, myofibroblasts derived from different tissues may have subtle differences in gene expression profiles such that their unambiguous identification is beyond a simple staining of one marker, as emphasised by the lack of staining of AOC3 in some tissues. By studying the potential transcriptional targets of NKX2.3 in myofibroblasts and through future similar work to identify the transcriptional targets of SHOX2 in fibroblasts, we may further characterise the functional differences between these cells. The clearly defined simple expression signature for distinguishing these cell type will benefit the future studies of the stromal and tumour microenvironment.

REFERENCES

REFERENCES

2007. Genome-wide association study of 14,000 cases of seven common diseases and 3,000 shared controls. *Nature,* 447**,** 661-78.

ABBATE, M., ZOJA, C., ROTTOLI, D., CORNA, D., TOMASONI, S. & REMUZZI, G. 2002. Proximal tubular cells promote fibrogenesis by TGF-beta1-mediated induction of peritubular myofibroblasts. *Kidney Int,* 61**,** 2066-77.

ABELLA, A., GARCIA-VICENTE, S., VIGUERIE, N., ROS-BARO, A., CAMPS, M., PALACIN, M., ZORZANO, A. & MARTI, L. 2004. Adipocytes release a soluble form of VAP-1/SSAO by a metalloprotease-dependent process and in a regulated manner. *Diabetologia,* 47**,** 429-38.

ABELLA, A., MARTI, L., CAMPS, M., CLARET, M., FERNANDEZ-ALVAREZ, J., GOMIS, R., GUMA, A., VIGUERIE, N., CARPENE, C., PALACIN, M., TESTAR, X. & ZORZANO, A. 2003. Semicarbazide-sensitive amine oxidase/vascular adhesion protein-1 activity exerts an antidiabetic action in Goto-Kakizaki rats. *Diabetes,* 52**,** 1004-13.

ADEGBOYEGA, P. A., MIFFLIN, R. C., DIMARI, J. F., SAADA, J. I. & POWELL, D. W. 2002. Immunohistochemical study of myofibroblasts in normal colonic mucosa, hyperplastic polyps, and adenomatous colorectal polyps. *Arch Pathol Lab Med,* 126**,** 829-36.

AIRENNE, T. T., NYMALM, Y., KIDRON, H., SMITH, D. J., PIHLAVISTO, M., SALMI, M., JALKANEN, S., JOHNSON, M. S. & SALMINEN, T. A. 2005. Crystal structure of the human vascular adhesion protein-1: unique structural features with functional implications. *Protein Sci,* 14**,** 1964-74.

ANDOH, A., TAKAYA, H., SAOTOME, T., SHIMADA, M., HATA, K., ARAKI, Y., NAKAMURA, F., SHINTANI, Y., FUJIYAMA, Y. & BAMBA, T. 2000. Cytokine regulation of chemokine (IL-8, MCP-1, and RANTES) gene expression in human pancreatic periacinar myofibroblasts. *Gastroenterology,* 119**,** 211-9.

ARIMURA, Y., ISSHIKI, H., ONODERA, K., NAGAISHI, K., YAMASHITA, K., SONODA, T., MATSUMOTO, T., TAKAHASHI, A., TAKAZOE, M., YAMAZAKI, K., KUBO, M., FUJIMIYA, M., IMAI, K. & SHINOMURA, Y. 2014. Characteristics of Japanese inflammatory bowel disease susceptibility loci. *J Gastroenterol,* 49**,** 1217-30.

ARORA, P. D., NARANI, N. & MCCULLOCH, C. A. 1999. The compliance of collagen gels regulates transforming growth factor-beta induction of alpha-smooth muscle actin in fibroblasts. *Am J Pathol,* 154**,** 871-82.

ARVILOMMI, A. M., SALMI, M. & JALKANEN, S. 1997. Organ-selective regulation of vascular adhesion protein-1 expression in man. *Eur J Immunol,* 27**,** 1794-800.

ASHLEY, N., JONES, M., OUARET, D., WILDING, J. & BODMER, W. F. 2014. Rapidly derived colorectal cancer cultures recapitulate parental cancer characteristics and enable personalized therapeutic assays. *J Pathol,* 234**,** 34-45.

AUTENGRUBER, A., GEREKE, M., HANSEN, G., HENNIG, C. & BRUDER, D. 2012. Impact of enzymatic tissue disintegration on the level of surface molecule expression and immune cell function. *Eur J Microbiol Immunol (Bp),* 2**,** 112-20.

BARCELLOS-HOFF, M. H. & AKHURST, R. J. 2009. Transforming growth factor-beta in breast cancer: too much, too late. *Breast Cancer Res,* 11**,** 202.

BENYON, R. C. & ARTHUR, M. J. 2001. Extracellular matrix degradation and the role of hepatic stellate cells. *Semin Liver Dis,* 21**,** 373-84.
BIBEN, C., WANG, C. C. & HARVEY, R. P. 2002. NK-2 class homeobox genes and pharyngeal/oral patterning: Nkx2-3 is required for salivary gland and tooth morphogenesis. *Int J Dev Biol,* 46**,** 415-22.
BLASCHKE, R. J., MONAGHAN, A. P., SCHILLER, S., SCHECHINGER, B., RAO, E., PADILLA-NASH, H., RIED, T. & RAPPOLD, G. A. 1998. SHOT, a SHOX-related homeobox gene, is implicated in craniofacial, brain, heart, and limb development. *Proc Natl Acad Sci U S A,* 95**,** 2406-11.
BOBICK, B. E. & COBB, J. 2012. Shox2 regulates progression through chondrogenesis in the mouse proximal limb. *J Cell Sci,* 125**,** 6071-83.
BONAIUTO, E., LUNELLI, M., SCARPA, M., VETTOR, R., MILAN, G. & DI PAOLO, M. L. 2010. A structure-activity study to identify novel and efficient substrates of the human semicarbazide-sensitive amine oxidase/VAP-1 enzyme. *Biochimie,* 92**,** 858-68.
BONO, P., SALMI, M., SMITH, D. J. & JALKANEN, S. 1998. Cloning and characterization of mouse vascular adhesion protein-1 reveals a novel molecule with enzymatic activity. *J Immunol,* 160**,** 5563-71.
BRAND, T., ANDREE, B., SCHNEIDER, A., BUCHBERGER, A. & ARNOLD, H. H. 1997. Chicken NKx2-8, a novel homeobox gene expressed during early heart and foregut development. *Mech Dev,* 64**,** 53-9.
BRITTAN, M., HUNT, T., JEFFERY, R., POULSOM, R., FORBES, S. J., HODIVALA-DILKE, K., GOLDMAN, J., ALISON, M. R. & WRIGHT, N. A. 2002. Bone marrow derivation of pericryptal myofibroblasts in the mouse and human small intestine and colon. *Gut,* 50**,** 752-7.
BROEKEMA, M., HARMSEN, M. C., VAN LUYN, M. J., KOERTS, J. A., PETERSEN, A. H., VAN KOOTEN, T. G., VAN GOOR, H., NAVIS, G. & POPA, E. R. 2007. Bone marrow-derived myofibroblasts contribute to the renal interstitial myofibroblast population and produce procollagen I after ischemia/reperfusion in rats. *J Am Soc Nephrol,* 18**,** 165-75.
CALON, A., LONARDO, E., BERENGUER-LLERGO, A., ESPINET, E., HERNANDO-MOMBLONA, X., IGLESIAS, M., SEVILLANO, M., PALOMO-PONCE, S., TAURIELLO, D. V., BYROM, D., CORTINA, C., MORRAL, C., BARCELO, C., TOSI, S., RIERA, A., ATTOLINI, C. S., ROSSELL, D., SANCHO, E. & BATLLE, E. 2015. Stromal gene expression defines poor-prognosis subtypes in colorectal cancer. *Nat Genet,* 47**,** 320-9.
CHAMBERS, R. C., LEONI, P., KAMINSKI, N., LAURENT, G. J. & HELLER, R. A. 2003. Global expression profiling of fibroblast responses to transforming growth factor-beta1 reveals the induction of inhibitor of differentiation-1 and provides evidence of smooth muscle cell phenotypic switching. *Am J Pathol,* 162**,** 533-46.
CHEN, C. Y. & SCHWARTZ, R. J. 1995. Identification of novel DNA binding targets and regulatory domains of a murine tinman homeodomain factor, nkx-2.5. *J Biol Chem,* 270**,** 15628-33.
CHO, J. H. 2008. The genetics and immunopathogenesis of inflammatory bowel disease. *Nat Rev Immunol,* 8**,** 458-66.
CHRISTIAN, S., WINKLER, R., HELFRICH, I., BOOS, A. M., BESEMFELDER, E., SCHADENDORF, D. & AUGUSTIN, H. G. 2008. Endosialin (Tem1) is a marker

of tumor-associated myofibroblasts and tumor vessel-associated mural cells. *Am J Pathol,* 172**,** 486-94.
CLEMENT-JONES, M., SCHILLER, S., RAO, E., BLASCHKE, R. J., ZUNIGA, A., ZELLER, R., ROBSON, S. C., BINDER, G., GLASS, I., STRACHAN, T., LINDSAY, S. & RAPPOLD, G. A. 2000. The short stature homeobox gene SHOX is involved in skeletal abnormalities in Turner syndrome. *Hum Mol Genet,* 9**,** 695-702.
COBB, J., DIERICH, A., HUSS-GARCIA, Y. & DUBOULE, D. 2006. A mouse model for human short-stature syndromes identifies Shox2 as an upstream regulator of Runx2 during long-bone development. *Proc Natl Acad Sci U S A,* 103**,** 4511-5.
CUI, W. J., LIU, Y., ZHOU, X. L., WANG, F. Z., ZHANG, X. D. & YE, L. H. 2010. Myosin light chain kinase is responsible for high proliferative ability of breast cancer cells via anti-apoptosis involving p38 pathway. *Acta Pharmacol Sin,* 31**,** 725-32.
CZOMPOLY, T., LABADI, A., KELLERMAYER, Z., OLASZ, K., ARNOLD, H. H. & BALOGH, P. 2011. Transcription factor Nkx2-3 controls the vascular identity and lymphocyte homing in the spleen. *J Immunol,* 186**,** 6981-9.
DANIELPOUR, D., KIM, K. Y., DART, L. L., WATANABE, S., ROBERTS, A. B. & SPORN, M. B. 1989. Sandwich enzyme-linked immunosorbent assays (SELISAs) quantitate and distinguish two forms of transforming growth factor-beta (TGF-beta 1 and TGF-beta 2) in complex biological fluids. *Growth Factors,* 2**,** 61-71.
DE WEVER, O., DEMETTER, P., MAREEL, M. & BRACKE, M. 2008. Stromal myofibroblasts are drivers of invasive cancer growth. *Int J Cancer,* 123**,** 2229-38.
DE WEVER, O., NGUYEN, Q. D., VAN HOORDE, L., BRACKE, M., BRUYNEEL, E., GESPACH, C. & MAREEL, M. 2004. Tenascin-C and SF/HGF produced by myofibroblasts in vitro provide convergent pro-invasive signals to human colon cancer cells through RhoA and Rac. *Faseb j,* 18**,** 1016-8.
DENG, Z., LIU, P., MARLTON, P., CLAXTON, D. F., LANE, S., CALLEN, D. F., COLLINS, F. S. & SICILIANO, M. J. 1993. Smooth muscle myosin heavy chain locus (MYH11) maps to 16p13.13-p13.12 and establishes a new region of conserved synteny between human 16p and mouse 16. *Genomics,* 18**,** 156-9.
DESMOULIERE, A., GEINOZ, A., GABBIANI, F. & GABBIANI, G. 1993. Transforming growth factor-beta 1 induces alpha-smooth muscle actin expression in granulation tissue myofibroblasts and in quiescent and growing cultured fibroblasts. *J Cell Biol,* 122**,** 103-11.
DIETRICH, D., HASINGER, O., LIEBENBERG, V., FIELD, J. K., KRISTIANSEN, G. & SOLTERMANN, A. 2012. DNA methylation of the homeobox genes PITX2 and SHOX2 predicts outcome in non-small-cell lung cancer patients. *Diagn Mol Pathol,* 21**,** 93-104.
DIMANCHE-BOITREL, M. T., VAKAET, L., JR., PUJUGUET, P., CHAUFFERT, B., MARTIN, M. S., HAMMANN, A., VAN ROY, F., MAREEL, M. & MARTIN, F. 1994. In vivo and in vitro invasiveness of a rat colon-cancer cell line maintaining E-cadherin expression: an enhancing role of tumor-associated myofibroblasts. *Int J Cancer,* 56**,** 512-21.
DIREKZE, N. C., JEFFERY, R., HODIVALA-DILKE, K., HUNT, T., PLAYFORD, R. J., ELIA, G., POULSOM, R., WRIGHT, N. A. & ALISON, M. R. 2006. Bone marrow-

derived stromal cells express lineage-related messenger RNA species. *Cancer Res,* 66**,** 1265-9.
DONNELLAN, W. L. 1965. The structure of the colonic mucosa. The epithelium and subepithelial reticulohistiocytic complex. *Gastroenterology,* 49**,** 496-514.
DOUCET, C., BROUTY-BOYE, D., POTTIN-CLEMENCEAU, C., JASMIN, C., CANONICA, G. W. & AZZARONE, B. 1998. IL-4 and IL-13 specifically increase adhesion molecule and inflammatory cytokine expression in human lung fibroblasts. *Int Immunol,* 10**,** 1421-33.
DRISKELL, R. R. & WATT, F. M. 2015. Understanding fibroblast heterogeneity in the skin. *Trends Cell Biol,* 25**,** 92-9.
DUGINA, V., FONTAO, L., CHAPONNIER, C., VASILIEV, J. & GABBIANI, G. 2001. Focal adhesion features during myofibroblastic differentiation are controlled by intracellular and extracellular factors. *J Cell Sci,* 114**,** 3285-96.
ENRIQUE-TARANCON, G., CASTAN, I., MORIN, N., MARTI, L., ABELLA, A., CAMPS, M., CASAMITJANA, R., PALACIN, M., TESTAR, X., DEGERMAN, E., CARPENE, C. & ZORZANO, A. 2000. Substrates of semicarbazide-sensitive amine oxidase co-operate with vanadate to stimulate tyrosine phosphorylation of insulin-receptor-substrate proteins, phosphoinositide 3-kinase activity and GLUT4 translocation in adipose cells. *Biochem J,* 350 Pt 1**,** 171-80.
ESPINOZA-LEWIS, R. A., YU, L., HE, F., LIU, H., TANG, R., SHI, J., SUN, X., MARTIN, J. F., WANG, D., YANG, J. & CHEN, Y. 2009. Shox2 is essential for the differentiation of cardiac pacemaker cells by repressing Nkx2-5. *Dev Biol,* 327**,** 376-85.
EYDEN, B. 2001. The fibronexus in reactive and tumoral myofibroblasts: further characterisation by electron microscopy. *Histol Histopathol,* 16**,** 57-70.
FALKE, L. L., GHOLIZADEH, S., GOLDSCHMEDING, R., KOK, R. J. & NGUYEN, T. Q. 2015. Diverse origins of the myofibroblast-implications for kidney fibrosis. *Nat Rev Nephrol,* 11**,** 233-44.
FARIN, H. F., VAN ES, J. H. & CLEVERS, H. 2012. Redundant sources of Wnt regulate intestinal stem cells and promote formation of Paneth cells. *Gastroenterology,* 143**,** 1518-1529 e7.
FARROW, B., ALBO, D. & BERGER, D. H. 2008. The role of the tumor microenvironment in the progression of pancreatic cancer. *J Surg Res,* 149**,** 319-28.
FINKEL, T. 1998. Oxygen radicals and signaling. *Curr Opin Cell Biol,* 10**,** 248-53.
FRANKE, A., FISCHER, A., NOTHNAGEL, M., BECKER, C., GRABE, N., TILL, A., LU, T., MULLER-QUERNHEIM, J., WITTIG, M., HERMANN, A., BALSCHUN, T., HOFMANN, S., NIEMIEC, R., SCHULZ, S., HAMPE, J., NIKOLAUS, S., NURNBERG, P., KRAWCZAK, M., SCHURMANN, M., ROSENSTIEL, P., NEBEL, A. & SCHREIBER, S. 2008. Genome-wide association analysis in sarcoidosis and Crohn's disease unravels a common susceptibility locus on 10p12.2. *Gastroenterology,* 135**,** 1207-15.
FU, Y., YAN, W., MOHUN, T. J. & EVANS, S. M. 1998. Vertebrate tinman homologues XNkx2-3 and XNkx2-5 are required for heart formation in a functionally redundant manner. *Development,* 125**,** 4439-49.
FUYUHIRO, Y., YASHIRO, M., NODA, S., KASHIWAGI, S., MATSUOKA, J., DOI, Y., KATO, Y., HASEGAWA, T., SAWADA, T. & HIRAKAWA, K. 2011. Upregulation of cancer-associated myofibroblasts by TGF-beta from scirrhous gastric carcinoma cells. *Br J Cancer,* 105**,** 996-1001.

GABBIANI, G., RYAN, G. B., LAMELIN, J. P., VASSALLI, P., MAJNO, G., BOUVIER, C. A., CRUCHAUD, A. & LUSCHER, E. F. 1973. Human smooth muscle autoantibody. Its identification as antiactin antibody and a study of its binding to "nonmuscular" cells. *Am J Pathol,* 72**,** 473-88.

GABBIANI, G., RYAN, G. B. & MAJNE, G. 1971. Presence of modified fibroblasts in granulation tissue and their possible role in wound contraction. *Experientia,* 27**,** 549-50.

GARIN-CHESA, P., OLD, L. J. & RETTIG, W. J. 1990. Cell surface glycoprotein of reactive stromal fibroblasts as a potential antibody target in human epithelial cancers. *Proc Natl Acad Sci U S A,* 87**,** 7235-9.

GARPENSTRAND, H., BERGQVIST, M., BRATTSTROM, D., LARSSON, A., ORELAND, L., HESSELIUS, P. & WAGENIUS, G. 2004. Serum semicarbazide-sensitive amine oxidase (SSAO) activity correlates with VEGF in non-small-cell lung cancer patients. *Med Oncol,* 21**,** 241-50.

GARPENSTRAND, H., EKBLOM, J., BACKLUND, L. B., ORELAND, L. & ROSENQVIST, U. 1999. Elevated plasma semicarbazide-sensitive amine oxidase (SSAO) activity in Type 2 diabetes mellitus complicated by retinopathy. *Diabet Med,* 16**,** 514-21.

GOKTURK, C., NILSSON, J., NORDQUIST, J., KRISTENSSON, M., SVENSSON, K., SODERBERG, C., ISRAELSON, M., GARPENSTRAND, H., SJOQUIST, M., ORELAND, L. & FORSBERG-NILSSON, K. 2003. Overexpression of semicarbazide-sensitive amine oxidase in smooth muscle cells leads to an abnormal structure of the aortic elastic laminas. *Am J Pathol,* 163**,** 1921-8.

GREGORIEFF, A. & CLEVERS, H. 2005. Wnt signaling in the intestinal epithelium: from endoderm to cancer. *Genes Dev,* 19**,** 877-90.

GUAZZI, S., PRICE, M., DE FELICE, M., DAMANTE, G., MATTEI, M. G. & DI LAURO, R. 1990. Thyroid nuclear factor 1 (TTF-1) contains a homeodomain and displays a novel DNA binding specificity. *EMBO J,* 9**,** 3631-9.

GUDJONSSON, T., ADRIANCE, M. C., STERNLICHT, M. D., PETERSEN, O. W. & BISSELL, M. J. 2005. Myoepithelial cells: their origin and function in breast morphogenesis and neoplasia. *J Mammary Gland Biol Neoplasia,* 10**,** 261-72.

HE, X. C., ZHANG, J., TONG, W. G., TAWFIK, O., ROSS, J., SCOVILLE, D. H., TIAN, Q., ZENG, X., HE, X., WIEDEMANN, L. M., MISHINA, Y. & LI, L. 2004. BMP signaling inhibits intestinal stem cell self-renewal through suppression of Wnt-beta-catenin signaling. *Nat Genet,* 36**,** 1117-21.

HEATH, J. P. 1996. Epithelial cell migration in the intestine. *Cell Biol Int,* 20**,** 139-46.

HENRY, L. R., LEE, H. O., LEE, J. S., KLEIN-SZANTO, A., WATTS, P., ROSS, E. A., CHEN, W. T. & CHENG, J. D. 2007. Clinical implications of fibroblast activation protein in patients with colon cancer. *Clin Cancer Res,* 13**,** 1736-41.

HIGUCHI, Y., KOJIMA, M., ISHII, G., AOYAGI, K., SASAKI, H. & OCHIAI, A. 2015. Gastrointestinal Fibroblasts Have Specialized, Diverse Transcriptional Phenotypes: A Comprehensive Gene Expression Analysis of Human Fibroblasts. *PLoS One,* 10**,** e0129241.

HINZ, B. 2007. Formation and function of the myofibroblast during tissue repair. *J Invest Dermatol,* 127**,** 526-37.

HINZ, B., CELETTA, G., TOMASEK, J. J., GABBIANI, G. & CHAPONNIER, C. 2001. Alpha-smooth muscle actin expression upregulates fibroblast contractile activity. *Mol Biol Cell,* 12**,** 2730-41.

HINZ, B., PHAN, S. H., THANNICKAL, V. J., PRUNOTTO, M., DESMOULIERE, A., VARGA, J., DE WEVER, O., MAREEL, M. & GABBIANI, G. 2012. Recent developments in myofibroblast biology: paradigms for connective tissue remodeling. *Am J Pathol,* 180**,** 1340-55.

HIRSCHFELDOVA, K., SOLC, R., BAXOVA, A., ZAPLETALOVA, J., KEBRDLOVA, V., GAILLYOVA, R., PRASILOVA, S., SOUKALOVA, J., MIHALOVA, R., LNENICKA, P., FLORIANOVA, M. & STEKROVA, J. 2012. SHOX gene defects and selected dysmorphic signs in patients of idiopathic short stature and Leri-Weill dyschondrosteosis. *Gene,* 491**,** 123-7.

HOLT, P. G., ROBINSON, B. W., REID, M., KEES, U. R., WARTON, A., DAWSON, V. H., ROSE, A., SCHON-HEGRAD, M. & PAPADIMITRIOU, J. M. 1986. Extraction of immune and inflammatory cells from human lung parenchyma: evaluation of an enzymatic digestion procedure. *Clin Exp Immunol,* 66**,** 188-200.

HONG, S., NOH, H., TENG, Y., SHAO, J., REHMANI, H., DING, H. F., DONG, Z., SU, S. B., SHI, H., KIM, J. & HUANG, S. 2014. SHOX2 is a direct miR-375 target and a novel epithelial-to-mesenchymal transition inducer in breast cancer cells. *Neoplasia,* 16**,** 279-90 e1-5.

HU, B., WU, Y. M., WU, Z. & PHAN, S. H. 2010. Nkx2.5/Csx represses myofibroblast differentiation. *Am J Respir Cell Mol Biol,* 42**,** 218-26.

HU, B., WU, Z. & PHAN, S. H. 2003. Smad3 mediates transforming growth factor-beta-induced alpha-smooth muscle actin expression. *Am J Respir Cell Mol Biol,* 29**,** 397-404.

HUMPHREYS, B. D., LIN, S. L., KOBAYASHI, A., HUDSON, T. E., NOWLIN, B. T., BONVENTRE, J. V., VALERIUS, M. T., MCMAHON, A. P. & DUFFIELD, J. S. 2010. Fate tracing reveals the pericyte and not epithelial origin of myofibroblasts in kidney fibrosis. *Am J Pathol,* 176**,** 85-97.

HUMPHRIES, A. & WRIGHT, N. A. 2008. Colonic crypt organization and tumorigenesis. *Nat Rev Cancer,* 8**,** 415-24.

INFANTE, J. R., MATSUBAYASHI, H., SATO, N., TONASCIA, J., KLEIN, A. P., RIALL, T. A., YEO, C., IACOBUZIO-DONAHUE, C. & GOGGINS, M. 2007. Peritumoral fibroblast SPARC expression and patient outcome with resectable pancreatic adenocarcinoma. *J Clin Oncol,* 25**,** 319-25.

IRJALA, H., SALMI, M., ALANEN, K., GRENMAN, R. & JALKANEN, S. 2001. Vascular adhesion protein 1 mediates binding of immunotherapeutic effector cells to tumor endothelium. *J Immunol,* 166**,** 6937-43.

IWAISAKO, K., BRENNER, D. A. & KISSELEVA, T. 2012. What's new in liver fibrosis? The origin of myofibroblasts in liver fibrosis. *J Gastroenterol Hepatol,* 27 Suppl 2**,** 65-8.

JAAKKOLA, K., KAUNISMAKI, K., TOHKA, S., YEGUTKIN, G., VANTTINEN, E., HAVIA, T., PELLINIEMI, L. J., VIROLAINEN, M., JALKANEN, S. & SALMI, M. 1999. Human vascular adhesion protein-1 in smooth muscle cells. *Am J Pathol,* 155**,** 1953-65.

JAAKKOLA, K., NIKULA, T., HOLOPAINEN, R., VAHASILTA, T., MATIKAINEN, M. T., LAUKKANEN, M. L., HUUPPONEN, R., HALKOLA, L., NIEMINEN, L., HILTUNEN, J., PARVIAINEN, S., CLARK, M. R., KNUUTI, J., SAVUNEN, T., KAAPA, P., VOIPIO-PULKKI, L. M. & JALKANEN, S. 2000. In vivo detection of vascular adhesion protein-1 in experimental inflammation. *Am J Pathol,* 157**,** 463-71.

JALKANEN, S. & SALMI, M. 1993. Vascular adhesion protein-1 (VAP-1)--a new adhesion molecule recruiting lymphocytes to sites of inflammation. *Res Immunol,* 144**,** 746-9; discussion 754-62.
JALKANEN, S. & SALMI, M. 2001. Cell surface monoamine oxidases: enzymes in search of a function. *EMBO J,* 20**,** 3893-901.
JALKANEN, S. & SALMI, M. 2008. VAP-1 and CD73, endothelial cell surface enzymes in leukocyte extravasation. *Arterioscler Thromb Vasc Biol,* 28**,** 18-26.
JONES, C. & EHRLICH, H. P. 2011. Fibroblast expression of alpha-smooth muscle actin, alpha2beta1 integrin and alphavbeta3 integrin: influence of surface rigidity. *Exp Mol Pathol,* 91**,** 394-9.
KALLURI, R. & NEILSON, E. G. 2003. Epithelial-mesenchymal transition and its implications for fibrosis. *J Clin Invest,* 112**,** 1776-84.
KALLURI, R. & WEINBERG, R. A. 2009. The basics of epithelial-mesenchymal transition. *J Clin Invest,* 119**,** 1420-8.
KASAHARA, H., BARTUNKOVA, S., SCHINKE, M., TANAKA, M. & IZUMO, S. 1998. Cardiac and extracardiac expression of Csx/Nkx2.5 homeodomain protein. *Circ Res,* 82**,** 936-46.
KAYE, G. I., LANE, N. & PASCAL, R. R. 1968. Colonic pericryptal fibroblast sheath: replication, migration, and cytodifferentiation of a mesenchymal cell system in adult tissue. II. Fine structural aspects of normal rabbit and human colon. *Gastroenterology,* 54**,** 852-65.
KEMIK, O., SUMER, A., KEMIK, A. S., ITIK, V., DULGER, A. C., PURISA, S. & TUZUN, S. 2010. Human vascular adhesion protein-1 (VAP-1): serum levels for hepatocellular carcinoma in non-alcoholic and alcoholic fatty liver disease. *World J Surg Oncol,* 8**,** 83.
KIM, K. K., WEI, Y., SZEKERES, C., KUGLER, M. C., WOLTERS, P. J., HILL, M. L., FRANK, J. A., BRUMWELL, A. N., WHEELER, S. E., KREIDBERG, J. A. & CHAPMAN, H. A. 2009. Epithelial cell alpha3beta1 integrin links beta-catenin and Smad signaling to promote myofibroblast formation and pulmonary fibrosis. *J Clin Invest,* 119**,** 213-24.
KINNMAN, N., FRANCOZ, C., BARBU, V., WENDUM, D., REY, C., HULTCRANTZ, R., POUPON, R. & HOUSSET, C. 2003. The myofibroblastic conversion of peribiliary fibrogenic cells distinct from hepatic stellate cells is stimulated by platelet-derived growth factor during liver fibrogenesis. *Lab Invest,* 83**,** 163-73.
KNEIP, C., SCHMIDT, B., SEEGEBARTH, A., WEICKMANN, S., FLEISCHHACKER, M., LIEBENBERG, V., FIELD, J. K. & DIETRICH, D. 2011. SHOX2 DNA methylation is a biomarker for the diagnosis of lung cancer in plasma. *J Thorac Oncol,* 6**,** 1632-8.
KOSINSKI, C., LI, V. S., CHAN, A. S., ZHANG, J., HO, C., TSUI, W. Y., CHAN, T. L., MIFFLIN, R. C., POWELL, D. W., YUEN, S. T., LEUNG, S. Y. & CHEN, X. 2007. Gene expression patterns of human colon tops and basal crypts and BMP antagonists as intestinal stem cell niche factors. *Proc Natl Acad Sci U S A,* 104**,** 15418-23.
KOSKINEN, K., VAINIO, P. J., SMITH, D. J., PIHLAVISTO, M., YLA-HERTTUALA, S., JALKANEN, S. & SALMI, M. 2004. Granulocyte transmigration through the endothelium is regulated by the oxidase activity of vascular adhesion protein-1 (VAP-1). *Blood,* 103**,** 3388-95.

KOUMAS, L., KING, A. E., CRITCHLEY, H. O., KELLY, R. W. & PHIPPS, R. P. 2001. Fibroblast heterogeneity: existence of functionally distinct Thy 1(+) and Thy 1(-) human female reproductive tract fibroblasts. *Am J Pathol,* 159**,** 925-35.

KOUMAS, L., SMITH, T. J., FELDON, S., BLUMBERG, N. & PHIPPS, R. P. 2003. Thy-1 expression in human fibroblast subsets defines myofibroblastic or lipofibroblastic phenotypes. *Am J Pathol,* 163**,** 1291-300.

KOUTROUBAKIS, I. E., PETINAKI, E., VARDAS, E., DIMOULIOS, P., ROUSSOMOUSTAKAKI, M., MANIATIS, A. N. & KOUROUMALIS, E. A. 2002. Circulating soluble vascular adhesion protein 1 in patients with inflammatory bowel disease. *Eur J Gastroenterol Hepatol,* 14**,** 405-8.

KURKIJARVI, R., ADAMS, D. H., LEINO, R., MOTTONEN, T., JALKANEN, S. & SALMI, M. 1998. Circulating form of human vascular adhesion protein-1 (VAP-1): increased serum levels in inflammatory liver diseases. *J Immunol,* 161**,** 1549-57.

KURKIJARVI, R., YEGUTKIN, G. G., GUNSON, B. K., JALKANEN, S., SALMI, M. & ADAMS, D. H. 2000. Circulating soluble vascular adhesion protein 1 accounts for the increased serum monoamine oxidase activity in chronic liver disease. *Gastroenterology,* 119**,** 1096-103.

LATIANO, A., PALMIERI, O., LATIANO, T., CORRITORE, G., BOSSA, F., MARTINO, G., BISCAGLIA, G., SCIMECA, D., VALVANO, M. R., PASTORE, M., MARSEGLIA, A., D'INCA, R., ANDRIULLI, A. & ANNESE, V. 2011. Investigation of multiple susceptibility loci for inflammatory bowel disease in an Italian cohort of patients. *PLoS One,* 6**,** e22688.

LEADER, M., COLLINS, M., PATEL, J. & HENRY, K. 1987. Vimentin: an evaluation of its role as a tumour marker. *Histopathology,* 11**,** 63-72.

LEBLEU, V. S., TADURI, G., O'CONNELL, J., TENG, Y., COOKE, V. G., WODA, C., SUGIMOTO, H. & KALLURI, R. 2013. Origin and function of myofibroblasts in kidney fibrosis. *Nat Med,* 19**,** 1047-53.

LEE, K. H., XU, Q. & BREITBART, R. E. 1996. A new tinman-related gene, nkx2.7, anticipates the expression of nkx2.5 and nkx2.3 in zebrafish heart and pharyngeal endoderm. *Dev Biol,* 180**,** 722-31.

LEJA, J., ESSAGHIR, A., ESSAND, M., WESTER, K., OBERG, K., TOTTERMAN, T. H., LLOYD, R., VASMATZIS, G., DEMOULIN, J. B. & GIANDOMENICO, V. 2009. Novel markers for enterochromaffin cells and gastrointestinal neuroendocrine carcinomas. *Mod Pathol,* 22**,** 261-72.

LI, J., QU, X. & BERTRAM, J. F. 2009. Endothelial-myofibroblast transition contributes to the early development of diabetic renal interstitial fibrosis in streptozotocin-induced diabetic mice. *Am J Pathol,* 175**,** 1380-8.

LI, R., LI, H., LUO, H. J., LIN, Z. X., JIANG, Z. W. & LUO, W. H. 2013. SSAO inhibitors suppress hepatocellular tumor growth in mice. *Cell Immunol,* 283**,** 61-9.

LI, S., LU, X., CHI, P. & PAN, J. 2012. Identification of Nkx2-3 and TGFB1I1 expression levels as potential biomarkers to predict the effects of FOLFOX4 chemotherapy. *Cancer Biol Ther,* 13**,** 443-9.

LIASKOU, E., KARIKOSKI, M., REYNOLDS, G. M., LALOR, P. F., WESTON, C. J., PULLEN, N., SALMI, M., JALKANEN, S. & ADAMS, D. H. 2011. Regulation of mucosal addressin cell adhesion molecule 1 expression in human and mice by vascular adhesion protein 1 amine oxidase activity. *Hepatology,* 53**,** 661-72.

LIJNEN, P., PETROV, V. & FAGARD, R. 2003. Transforming growth factor-beta 1-mediated collagen gel contraction by cardiac fibroblasts. *J Renin Angiotensin Aldosterone Syst,* 4**,** 113-8.
LIU, X., HU, H. & YIN, J. Q. 2006. Therapeutic strategies against TGF-beta signaling pathway in hepatic fibrosis. *Liver Int,* 26**,** 8-22.
LOIKKANEN, I., TOLJAMO, K., HIRVIKOSKI, P., VAISANEN, T., PAAVONEN, T. K. & VAARALA, M. H. 2009. Myosin VI is a modulator of androgen-dependent gene expression. *Oncol Rep,* 22**,** 991-5.
LUO, D., WILSON, J. M., HARVEL, N., LIU, J., PEI, L., HUANG, S., HAWTHORN, L. & SHI, H. 2013. A systematic evaluation of miRNA:mRNA interactions involved in the migration and invasion of breast cancer cells. *J Transl Med,* 11**,** 57.
LYONS, I., PARSONS, L. M., HARTLEY, L., LI, R., ANDREWS, J. E., ROBB, L. & HARVEY, R. P. 1995. Myogenic and morphogenetic defects in the heart tubes of murine embryos lacking the homeo box gene Nkx2-5. *Genes Dev,* 9**,** 1654-66.
MADISON, B. B., BRAUNSTEIN, K., KUIZON, E., PORTMAN, K., QIAO, X. T. & GUMUCIO, D. L. 2005. Epithelial hedgehog signals pattern the intestinal crypt-villus axis. *Development,* 132**,** 279-89.
MAJNO, G., GABBIANI, G., HIRSCHEL, B. J., RYAN, G. B. & STATKOV, P. R. 1971. Contraction of granulation tissue in vitro: similarity to smooth muscle. *Science,* 173**,** 548-50.
MARTELIUS, T., SALMI, M., KROGERUS, L., LOGINOV, R., SCHOULTZ, M., KARIKOSKI, M., MIILUNIEMI, M., SOOTS, A., HOCKERSTEDT, K., JALKANEN, S. & LAUTENSCHLAGER, I. 2008. Inhibition of semicarbazide-sensitive amine oxidases decreases lymphocyte infiltration in the early phases of rat liver allograft rejection. *Int J Immunopathol Pharmacol,* 21**,** 911-20.
MARTTILA-ICHIHARA, F., CASTERMANS, K., AUVINEN, K., OUDE EGBRINK, M. G., JALKANEN, S., GRIFFIOEN, A. W. & SALMI, M. 2010. Small-molecule inhibitors of vascular adhesion protein-1 reduce the accumulation of myeloid cells into tumors and attenuate tumor growth in mice. *J Immunol,* 184**,** 3164-73.
MASAMUNE, A., WATANABE, T., KIKUTA, K. & SHIMOSEGAWA, T. 2009. Roles of pancreatic stellate cells in pancreatic inflammation and fibrosis. *Clin Gastroenterol Hepatol,* 7**,** S48-54.
MATHYS, K. C., PONNAMPALAM, S. N., PADIVAL, S. & NAGARAJ, R. H. 2002. Semicarbazide-sensitive amine oxidase in aortic smooth muscle cells mediates synthesis of a methylglyoxal-AGE: implications for vascular complications in diabetes. *Biochem Biophys Res Commun,* 297**,** 863-9.
MAULA, S. M., SALMINEN, T., KAITANIEMI, S., NYMALM, Y., SMITH, D. J. & JALKANEN, S. 2005. Carbohydrates located on the top of the "cap" contribute to the adhesive and enzymatic functions of vascular adhesion protein-1. *Eur J Immunol,* 35**,** 2718-27.
MCANULTY, R. J. 2007. Fibroblasts and myofibroblasts: their source, function and role in disease. *Int J Biochem Cell Biol,* 39**,** 666-71.
MEDEMA, J. P. & VERMEULEN, L. 2011. Microenvironmental regulation of stem cells in intestinal homeostasis and cancer. *Nature,* 474**,** 318-26.
MEGGYESI, N., KISS, L. S., KOSZARSKA, M., BORTLIK, M., DURICOVA, D., LAKATOS, L., MOLNAR, T., LENICEK, M., VITEK, L., ALTORJAY, I., PAPP, M., TULASSAY, Z., MIHELLER, P., PAPP, J., TORDAI, A., ANDRIKOVICS, H., LUKAS, M. & LAKATOS, P. L. 2010. NKX2-3 and IRGM variants are associated with

disease susceptibility to IBD in Eastern European patients. *World J Gastroenterol,* 16**,** 5233-40.
MESZAROS, Z., KARADI, I., CSANYI, A., SZOMBATHY, T., ROMICS, L. & MAGYAR, K. 1999. Determination of human serum semicarbazide-sensitive amine oxidase activity: a possible clinical marker of atherosclerosis. *Eur J Drug Metab Pharmacokinet,* 24**,** 299-302.
MIFFLIN, R. C., SAADA, J. I., DI MARI, J. F., ADEGBOYEGA, P. A., VALENTICH, J. D. & POWELL, D. W. 2002. Regulation of COX-2 expression in human intestinal myofibroblasts: mechanisms of IL-1-mediated induction. *Am J Physiol Cell Physiol,* 282**,** C824-34.
MILANI, S., HERBST, H., SCHUPPAN, D., STEIN, H. & SURRENTI, C. 1991. Transforming growth factors beta 1 and beta 2 are differentially expressed in fibrotic liver disease. *Am J Pathol,* 139**,** 1221-9.
MORIN, N., LIZCANO, J. M., FONTANA, E., MARTI, L., SMIH, F., ROUET, P., PREVOT, D., ZORZANO, A., UNZETA, M. & CARPENE, C. 2001. Semicarbazide-sensitive amine oxidase substrates stimulate glucose transport and inhibit lipolysis in human adipocytes. *J Pharmacol Exp Ther,* 297**,** 563-72.
MUZYKANTOV, V. R. 2001. Targeting of superoxide dismutase and catalase to vascular endothelium. *J Control Release,* 71**,** 1-21.
NOLTE, S. V., XU, W., RENNEKAMPFF, H. O. & RODEMANN, H. P. 2008. Diversity of fibroblasts--a review on implications for skin tissue engineering. *Cells Tissues Organs,* 187**,** 165-76.
NOONAN, T., LUKAS, S., PEET, G. W., PELLETIER, J., PANZENBECK, M., HANIDU, A., MAZUREK, S., WASTI, R., RYBINA, I., ROMA, T., KRONKAITIS, A., SHOULTZ, A., SOUZA, D., JIANG, H., NABOZNY, G. & MODIS, L. K. 2013. The oxidase activity of vascular adhesion protein-1 (VAP-1) is essential for function. *Am J Clin Exp Immunol,* 2**,** 172-85.
OGAWA, H., BINION, D. G., HEIDEMANN, J., THERIOT, M., FISHER, P. J., JOHNSON, N. A., OTTERSON, M. F. & RAFIEE, P. 2005. Mechanisms of MAdCAM-1 gene expression in human intestinal microvascular endothelial cells. *Am J Physiol Cell Physiol,* 288**,** C272-81.
OIDA, T. & WEINER, H. L. 2010. Depletion of TGF-beta from fetal bovine serum. *J Immunol Methods,* 362**,** 195-8.
OOTANI, A., LI, X., SANGIORGI, E., HO, Q. T., UENO, H., TODA, S., SUGIHARA, H., FUJIMOTO, K., WEISSMAN, I. L., CAPECCHI, M. R. & KUO, C. J. 2009. Sustained in vitro intestinal epithelial culture within a Wnt-dependent stem cell niche. *Nat Med,* 15**,** 701-6.
ORIMO, A., GUPTA, P. B., SGROI, D. C., ARENZANA-SEISDEDOS, F., DELAUNAY, T., NAEEM, R., CAREY, V. J., RICHARDSON, A. L. & WEINBERG, R. A. 2005. Stromal fibroblasts present in invasive human breast carcinomas promote tumor growth and angiogenesis through elevated SDF-1/CXCL12 secretion. *Cell,* 121**,** 335-48.
ORIMO, A. & WEINBERG, R. A. 2007. Heterogeneity of stromal fibroblasts in tumors. *Cancer Biol Ther,* 6**,** 618-9.
OWENS, B. M. & SIMMONS, A. 2013. Intestinal stromal cells in mucosal immunity and homeostasis. *Mucosal Immunol,* 6**,** 224-34.
PABST, O., FORSTER, R., LIPP, M., ENGEL, H. & ARNOLD, H. H. 2000. NKX2.3 is required for MAdCAM-1 expression and homing of lymphocytes in spleen and mucosa-associated lymphoid tissue. *EMBO J,* 19**,** 2015-23.

PABST, O., HERBRAND, H. & ARNOLD, H. H. 1998. Nkx2-9 is a novel homeobox transcription factor which demarcates ventral domains in the developing mouse CNS. *Mech Dev,* 73**,** 85-93.

PABST, O., SCHNEIDER, A., BRAND, T. & ARNOLD, H. H. 1997. The mouse Nkx2-3 homeodomain gene is expressed in gut mesenchyme during pre- and postnatal mouse development. *Dev Dyn,* 209**,** 29-35.

PABST, O., ZWEIGERDT, R. & ARNOLD, H. H. 1999. Targeted disruption of the homeobox transcription factor Nkx2-3 in mice results in postnatal lethality and abnormal development of small intestine and spleen. *Development,* 126**,** 2215-25.

PEROU, C. M., SORLIE, T., EISEN, M. B., VAN DE RIJN, M., JEFFREY, S. S., REES, C. A., POLLACK, J. R., ROSS, D. T., JOHNSEN, H., AKSLEN, L. A., FLUGE, O., PERGAMENSCHIKOV, A., WILLIAMS, C., ZHU, S. X., LONNING, P. E., BORRESEN-DALE, A. L., BROWN, P. O. & BOTSTEIN, D. 2000. Molecular portraits of human breast tumours. *Nature,* 406**,** 747-52.

PESSINA, P., CONTI, V., PACELLI, F., ROSA, F., DOGLIETTO, G. B., BRUNELLI, S. & BOSSOLA, M. 2010. Skeletal muscle of gastric cancer patients expresses genes involved in muscle regeneration. *Oncol Rep,* 24**,** 741-5.

PHAN, S. H. 2008. Biology of fibroblasts and myofibroblasts. *Proc Am Thorac Soc,* 5**,** 334-7.

POPOVA, A. P., BOZYK, P. D., GOLDSMITH, A. M., LINN, M. J., LEI, J., BENTLEY, J. K. & HERSHENSON, M. B. 2010. Autocrine production of TGF-beta1 promotes myofibroblastic differentiation of neonatal lung mesenchymal stem cells. *Am J Physiol Lung Cell Mol Physiol,* 298**,** L735-43.

POWELL, D. W., ADEGBOYEGA, P. A., DI MARI, J. F. & MIFFLIN, R. C. 2005. Epithelial cells and their neighbors I. Role of intestinal myofibroblasts in development, repair, and cancer. *Am J Physiol Gastrointest Liver Physiol,* 289**,** G2-7.

POWELL, D. W., MIFFLIN, R. C., VALENTICH, J. D., CROWE, S. E., SAADA, J. I. & WEST, A. B. 1999. Myofibroblasts. I. Paracrine cells important in health and disease. *Am J Physiol,* 277**,** C1-9.

POWELL, D. W., PINCHUK, I. V., SAADA, J. I., CHEN, X. & MIFFLIN, R. C. 2011. Mesenchymal cells of the intestinal lamina propria. *Annu Rev Physiol,* 73**,** 213-37.

PRICE, M. 1993. Members of the Dlx- and Nkx2-gene families are regionally expressed in the developing forebrain. *J Neurobiol,* 24**,** 1385-99.

PRICE, M., LAZZARO, D., POHL, T., MATTEI, M. G., RUTHER, U., OLIVO, J. C., DUBOULE, D. & DI LAURO, R. 1992. Regional expression of the homeobox gene Nkx-2.2 in the developing mammalian forebrain. *Neuron,* 8**,** 241-55.

PUSKARIC, S., SCHMITTECKERT, S., MORI, A. D., GLASER, A., SCHNEIDER, K. U., BRUNEAU, B. G., BLASCHKE, R. J., STEINBEISSER, H. & RAPPOLD, G. 2010. Shox2 mediates Tbx5 activity by regulating Bmp4 in the pacemaker region of the developing heart. *Hum Mol Genet,* 19**,** 4625-33.

RAMSHAW, J. A., SHAH, N. K. & BRODSKY, B. 1998. Gly-X-Y tripeptide frequencies in collagen: a context for host-guest triple-helical peptides. *J Struct Biol,* 122**,** 86-91.

REEVES, H. L. & FRIEDMAN, S. L. 2002. Activation of hepatic stellate cells--a key issue in liver fibrosis. *Front Biosci,* 7**,** d808-26.

RETTIG, W. J., CHESA, P. G., BERESFORD, H. R., FEICKERT, H. J., JENNINGS, M. T., COHEN, J., OETTGEN, H. F. & OLD, L. J. 1986. Differential expression of cell surface antigens and glial fibrillary acidic protein in human astrocytoma subsets. *Cancer Res,* 46**,** 6406-12.

RETTIG, W. J., GARIN-CHESA, P., BERESFORD, H. R., OETTGEN, H. F., MELAMED, M. R. & OLD, L. J. 1988. Cell-surface glycoproteins of human sarcomas: differential expression in normal and malignant tissues and cultured cells. *Proc Natl Acad Sci U S A,* 85**,** 3110-4.

RICHMAN, P. I. & BODMER, W. F. 1988. Control of differentiation in human colorectal carcinoma cell lines: epithelial-mesenchymal interactions. *J Pathol,* 156**,** 197-211.

RICHMAN, P. I., TILLY, R., JASS, J. R. & BODMER, W. F. 1987. Colonic pericrypt sheath cells: characterisation of cell type with new monoclonal antibody. *J Clin Pathol,* 40**,** 593-600.

ROBERTS, D. J. 2000. Molecular mechanisms of development of the gastrointestinal tract. *Dev Dyn,* 219**,** 109-20.

ROCK, J. R. & HOGAN, B. L. 2011. Epithelial progenitor cells in lung development, maintenance, repair, and disease. *Annu Rev Cell Dev Biol,* 27**,** 493-512.

RONNOV-JESSEN, L. & PETERSEN, O. W. 1993. Induction of alpha-smooth muscle actin by transforming growth factor-beta 1 in quiescent human breast gland fibroblasts. Implications for myofibroblast generation in breast neoplasia. *Lab Invest,* 68**,** 696-707.

RONTY, M. J., LEIVONEN, S. K., HINZ, B., RACHLIN, A., OTEY, C. A., KAHARI, V. M. & CARPEN, O. M. 2006. Isoform-specific regulation of the actin-organizing protein palladin during TGF-beta1-induced myofibroblast differentiation. *J Invest Dermatol,* 126**,** 2387-96.

SALMI, M. & JALKANEN, S. 1992. A 90-kilodalton endothelial cell molecule mediating lymphocyte binding in humans. *Science,* 257**,** 1407-9.

SALMI, M. & JALKANEN, S. 1996. Human vascular adhesion protein 1 (VAP-1) is a unique sialoglycoprotein that mediates carbohydrate-dependent binding of lymphocytes to endothelial cells. *J Exp Med,* 183**,** 569-79.

SALMI, M. & JALKANEN, S. 2001. VAP-1: an adhesin and an enzyme. *Trends Immunol,* 22**,** 211-6.

SALMI, M. & JALKANEN, S. 2006. Developmental regulation of the adhesive and enzymatic activity of vascular adhesion protein-1 (VAP-1) in humans. *Blood,* 108**,** 1555-61.

SALMI, M., KALIMO, K. & JALKANEN, S. 1993. Induction and function of vascular adhesion protein-1 at sites of inflammation. *J Exp Med,* 178**,** 2255-60.

SAPPINO, A. P., DIETRICH, P. Y., SKALLI, O., WIDGREN, S. & GABBIANI, G. 1989. Colonic pericryptal fibroblasts. Differentiation pattern in embryogenesis and phenotypic modulation in epithelial proliferative lesions. *Virchows Arch A Pathol Anat Histopathol,* 415**,** 551-7.

SAPPINO, A. P., SCHURCH, W. & GABBIANI, G. 1990. Differentiation repertoire of fibroblastic cells: expression of cytoskeletal proteins as marker of phenotypic modulations. *Lab Invest,* 63**,** 144-61.

SCHMITT-GRAFF, A., DESMOULIERE, A. & GABBIANI, G. 1994. Heterogeneity of myofibroblast phenotypic features: an example of fibroblastic cell plasticity. *Virchows Arch,* 425**,** 3-24.

SCHNEIDER, K. U., DIETRICH, D., FLEISCHHACKER, M., LESCHBER, G., MERK, J., SCHAPER, F., STAPERT, H. R., VOSSENAAR, E. R., WEICKMANN, S., LIEBENBERG, V., KNEIP, C., SEEGEBARTH, A., ERDOGAN, F., RAPPOLD, G. & SCHMIDT, B. 2011. Correlation of SHOX2 gene amplification and DNA methylation in lung cancer tumors. *BMC Cancer,* 11**,** 102.

SCHWELBERGER, H. G. 2010. Structural organization of mammalian copper-containing amine oxidase genes. *Inflamm Res,* 59 Suppl 2**,** S223-5.

SEILER, N. 2002. Ammonia and Alzheimer's disease. *Neurochem Int,* 41**,** 189-207.

SEMBA, S., KODAMA, Y., OHNUMA, K., MIZUUCHI, E., MASUDA, R., YASHIRO, M., HIRAKAWA, K. & YOKOZAKI, H. 2009. Direct cancer-stromal interaction increases fibroblast proliferation and enhances invasive properties of scirrhous-type gastric carcinoma cells. *Br J Cancer,* 101**,** 1365-73.

SEMPOWSKI, G. D., DERDAK, S. & PHIPPS, R. P. 1996. Interleukin-4 and interferon-gamma discordantly regulate collagen biosynthesis by functionally distinct lung fibroblast subsets. *J Cell Physiol,* 167**,** 290-6.

SHATTUCK-BRANDT, R. L., VARILEK, G. W., RADHIKA, A., YANG, F., WASHINGTON, M. K. & DUBOIS, R. N. 2000. Cyclooxygenase 2 expression is increased in the stroma of colon carcinomas from IL-10(-/-) mice. *Gastroenterology,* 118**,** 337-45.

SHEPPARD, D. 2006. Transforming growth factor beta: a central modulator of pulmonary and airway inflammation and fibrosis. *Proc Am Thorac Soc,* 3**,** 413-7.

SHI, Y., O'BRIEN, J. E., JR., FARD, A. & ZALEWSKI, A. 1996. Transforming growth factor-beta 1 expression and myofibroblast formation during arterial repair. *Arterioscler Thromb Vasc Biol,* 16**,** 1298-305.

SHIMADA, M., ANDOH, A., HATA, K., TASAKI, K., ARAKI, Y., FUJIYAMA, Y. & BAMBA, T. 2002. IL-6 secretion by human pancreatic periacinar myofibroblasts in response to inflammatory mediators. *J Immunol,* 168**,** 861-8.

SINGER, II, KAWKA, D. W., KAZAZIS, D. M. & CLARK, R. A. 1984. In vivo co-distribution of fibronectin and actin fibers in granulation tissue: immunofluorescence and electron microscope studies of the fibronexus at the myofibroblast surface. *J Cell Biol,* 98**,** 2091-106.

SMITH, D. J., SALMI, M., BONO, P., HELLMAN, J., LEU, T. & JALKANEN, S. 1998. Cloning of vascular adhesion protein 1 reveals a novel multifunctional adhesion molecule. *J Exp Med,* 188**,** 17-27.

SOLE, M., HERNANDEZ-GUILLAMON, M., BOADA, M. & UNZETA, M. 2008. p53 phosphorylation is involved in vascular cell death induced by the catalytic activity of membrane-bound SSAO/VAP-1. *Biochim Biophys Acta,* 1783**,** 1085-94.

STANLEY, E. G., BIBEN, C., ELEFANTY, A., BARNETT, L., KOENTGEN, F., ROBB, L. & HARVEY, R. P. 2002. Efficient Cre-mediated deletion in cardiac progenitor cells conferred by a 3'UTR-ires-Cre allele of the homeobox gene Nkx2-5. *Int J Dev Biol,* 46**,** 431-9.

STOLEN, C. M., MADANAT, R., MARTI, L., KARI, S., YEGUTKIN, G. G., SARIOLA, H., ZORZANO, A. & JALKANEN, S. 2004a. Semicarbazide sensitive amine oxidase overexpression has dual consequences: insulin mimicry and diabetes-like complications. *Faseb j,* 18**,** 702-4.

STOLEN, C. M., MARTTILA-ICHIHARA, F., KOSKINEN, K., YEGUTKIN, G. G., TURJA, R., BONO, P., SKURNIK, M., HANNINEN, A., JALKANEN, S. & SALMI, M. 2005.

Absence of the endothelial oxidase AOC3 leads to abnormal leukocyte traffic in vivo. *Immunity,* 22**,** 105-15.
STOLEN, C. M., YEGUTKIN, G. G., KURKIJARVI, R., BONO, P., ALITALO, K. & JALKANEN, S. 2004b. Origins of serum semicarbazide-sensitive amine oxidase. *Circ Res,* 95**,** 50-7.
STRONG, L. H., BERTHIAUME, F. & YARMUSH, M. L. 1997. Control of fibroblast populated collagen lattice contraction by antibody targeted photolysis of fibroblasts. *Lasers Surg Med,* 21**,** 235-47.
STRUTZ, F. & NEILSON, E. G. 2003. New insights into mechanisms of fibrosis in immune renal injury. *Springer Semin Immunopathol,* 24**,** 459-76.
STRUTZ, F., OKADA, H., LO, C. W., DANOFF, T., CARONE, R. L., TOMASZEWSKI, J. E. & NEILSON, E. G. 1995. Identification and characterization of a fibroblast marker: FSP1. *J Cell Biol,* 130**,** 393-405.
SUGIMOTO, H., MUNDEL, T. M., KIERAN, M. W. & KALLURI, R. 2006. Identification of fibroblast heterogeneity in the tumor microenvironment. *Cancer Biol Ther,* 5**,** 1640-6.
TARLINTON, D., LIGHT, A., METCALF, D., HARVEY, R. P. & ROBB, L. 2003. Architectural defects in the spleens of Nkx2-3-deficient mice are intrinsic and associated with defects in both B cell maturation and T cell-dependent immune responses. *J Immunol,* 170**,** 4002-10.
TCHOU, J., ZHANG, P. J., BI, Y., SATIJA, C., MARJUMDAR, R., STEPHEN, T. L., LO, A., CHEN, H., MIES, C., JUNE, C. H., CONEJO-GARCIA, J. & PURE, E. 2013. Fibroblast activation protein expression by stromal cells and tumor-associated macrophages in human breast cancer. *Hum Pathol,* 44**,** 2549-57.
THEISS, A. L., SIMMONS, J. G., JOBIN, C. & LUND, P. K. 2005. Tumor necrosis factor (TNF) alpha increases collagen accumulation and proliferation in intestinal myofibroblasts via TNF receptor 2. *J Biol Chem,* 280**,** 36099-109.
TOKUNOU, M., NIKI, T., EGUCHI, K., IBA, S., TSUDA, H., YAMADA, T., MATSUNO, Y., KONDO, H., SAITOH, Y., IMAMURA, H. & HIROHASHI, S. 2001. c-MET expression in myofibroblasts: role in autocrine activation and prognostic significance in lung adenocarcinoma. *Am J Pathol,* 158**,** 1451-63.
TSUJINO, T., SESHIMO, I., YAMAMOTO, H., NGAN, C. Y., EZUMI, K., TAKEMASA, I., IKEDA, M., SEKIMOTO, M., MATSUURA, N. & MONDEN, M. 2007. Stromal myofibroblasts predict disease recurrence for colorectal cancer. *Clin Cancer Res,* 13**,** 2082-90.
TUXHORN, J. A., AYALA, G. E., SMITH, M. J., SMITH, V. C., DANG, T. D. & ROWLEY, D. R. 2002. Reactive stroma in human prostate cancer: induction of myofibroblast phenotype and extracellular matrix remodeling. *Clin Cancer Res,* 8**,** 2912-23.
VAN DER LOOP, F. T., SCHAART, G., TIMMER, E. D., RAMAEKERS, F. C. & VAN EYS, G. J. 1996. Smoothelin, a novel cytoskeletal protein specific for smooth muscle cells. *J Cell Biol,* 134**,** 401-11.
VAN DOP, W. A., UHMANN, A., WIJGERDE, M., SLEDDENS-LINKELS, E., HEIJMANS, J., OFFERHAUS, G. J., VAN DEN BERGH WEERMAN, M. A., BOECKXSTAENS, G. E., HOMMES, D. W., HARDWICK, J. C., HAHN, H. & VAN DEN BRINK, G. R. 2009. Depletion of the colonic epithelial precursor cell compartment upon conditional activation of the hedgehog pathway. *Gastroenterology,* 136**,** 2195-2203 e1-7.

VARIS, A., WOLF, M., MONNI, O., VAKKARI, M. L., KOKKOLA, A., MOSKALUK, C., FRIERSON, H., JR., POWELL, S. M., KNUUTILA, S., KALLIONIEMI, A. & EL-RIFAI, W. 2002. Targets of gene amplification and overexpression at 17q in gastric cancer. *Cancer Res,* 62**,** 2625-9.

VEAL, E. & DAY, A. 2011. Hydrogen peroxide as a signaling molecule. *Antioxid Redox Signal,* 15**,** 147-51.

VERMEULEN, L., DE SOUSA, E. M. F., VAN DER HEIJDEN, M., CAMERON, K., DE JONG, J. H., BOROVSKI, T., TUYNMAN, J. B., TODARO, M., MERZ, C., RODERMOND, H., SPRICK, M. R., KEMPER, K., RICHEL, D. J., STASSI, G. & MEDEMA, J. P. 2010. Wnt activity defines colon cancer stem cells and is regulated by the microenvironment. *Nat Cell Biol,* 12**,** 468-76.

WADA, T., SAKAI, N., MATSUSHIMA, K. & KANEKO, S. 2007. Fibrocytes: a new insight into kidney fibrosis. *Kidney Int,* 72**,** 269-73.

WANG, C. C., BIBEN, C., ROBB, L., NASSIR, F., BARNETT, L., DAVIDSON, N. O., KOENTGEN, F., TARLINTON, D. & HARVEY, R. P. 2000. Homeodomain factor Nkx2-3 controls regional expression of leukocyte homing coreceptor MAdCAM-1 in specialized endothelial cells of the viscera. *Dev Biol,* 224**,** 152-67.

WANG, R. J., WU, P., CAI, G. X., WANG, Z. M., XU, Y., PENG, J. J., SHENG, W. Q., LU, H. F. & CAI, S. J. 2014. Down-regulated MYH11 expression correlates with poor prognosis in stage II and III colorectal cancer. *Asian Pac J Cancer Prev,* 15**,** 7223-8.

WANG, X., ZBOU, C., QIU, G., FAN, J., TANG, H. & PENG, Z. 2008. Screening of new tumor suppressor genes in sporadic colorectal cancer patients. *Hepatogastroenterology,* 55**,** 2039-44.

WEBBER, J., STEADMAN, R., MASON, M. D., TABI, Z. & CLAYTON, A. 2010. Cancer exosomes trigger fibroblast to myofibroblast differentiation. *Cancer Res,* 70**,** 9621-30.

WEERSMA, R. K., STOKKERS, P. C., CLEYNEN, I., WOLFKAMP, S. C., HENCKAERTS, L., SCHREIBER, S., DIJKSTRA, G., FRANKE, A., NOLTE, I. M., RUTGEERTS, P., WIJMENGA, C. & VERMEIRE, S. 2009. Confirmation of multiple Crohn's disease susceptibility loci in a large Dutch-Belgian cohort. *Am J Gastroenterol,* 104**,** 630-8.

WEIGMANN, B., TUBBE, I., SEIDEL, D., NICOLAEV, A., BECKER, C. & NEURATH, M. F. 2007. Isolation and subsequent analysis of murine lamina propria mononuclear cells from colonic tissue. *Nat Protoc,* 2**,** 2307-11.

WOLFORT, S. F., REIKEN, S. R., BERTHIAUME, F., TOMPKINS, R. G. & YARMUSH, M. L. 1996. Control of hypertrophic scar growth using antibody-targeted photolysis. *J Surg Res,* 62**,** 17-22.

YAMANASHI, T., NAKANISHI, Y., FUJII, G., AKISHIMA-FUKASAWA, Y., MORIYA, Y., KANAI, Y., WATANABE, M. & HIROHASHI, S. 2009. Podoplanin expression identified in stromal fibroblasts as a favorable prognostic marker in patients with colorectal carcinoma. *Oncology,* 77**,** 53-62.

YAMAZAKI, K., TAKAHASHI, A., TAKAZOE, M., KUBO, M., ONOUCHI, Y., FUJINO, A., KAMATANI, N., NAKAMURA, Y. & HATA, A. 2009. Positive association of genetic variants in the upstream region of NKX2-3 with Crohn's disease in Japanese patients. *Gut,* 58**,** 228-32.

YANG, T., ZHANG, H., CAI, S. Y., SHEN, Y. N., YUAN, S. X., YANG, G. S., WU, M. C., LU, J. H. & SHEN, F. 2013. Elevated SHOX2 expression is associated with tumor recurrence of hepatocellular carcinoma. *Ann Surg Oncol,* 20 Suppl 3**,** S644-9.
YE, W., WANG, J., SONG, Y., YU, D., SUN, C., LIU, C., CHEN, F., ZHANG, Y., WANG, F., HARVEY, R. P., SCHRADER, L., MARTIN, J. F. & CHEN, Y. 2015. A common Shox2-Nkx2-5 antagonistic mechanism primes the pacemaker cell fate in the pulmonary vein myocardium and sinoatrial node. *Development,* 142**,** 2521-32.
YEN, T. H. & WRIGHT, N. A. 2006. The gastrointestinal tract stem cell niche. *Stem Cell Rev,* 2**,** 203-12.
YEUNG, T. M., BUSKENS, C., WANG, L. M., MORTENSEN, N. J. & BODMER, W. F. 2013. Myofibroblast activation in colorectal cancer lymph node metastases. *Br J Cancer,* 108**,** 2106-15.
YEUNG, T. M., CHIA, L. A., KOSINSKI, C. M. & KUO, C. J. 2011. Regulation of self-renewal and differentiation by the intestinal stem cell niche. *Cell Mol Life Sci,* 68**,** 2513-23.
YU, L., GU, S., ALAPPAT, S., SONG, Y., YAN, M., ZHANG, X., ZHANG, G., JIANG, Y., ZHANG, Z., ZHANG, Y. & CHEN, Y. 2005. Shox2-deficient mice exhibit a rare type of incomplete clefting of the secondary palate. *Development,* 132**,** 4397-406.
YU, L., LIU, H., YAN, M., YANG, J., LONG, F., MUNEOKA, K. & CHEN, Y. 2007. Shox2 is required for chondrocyte proliferation and maturation in proximal limb skeleton. *Dev Biol,* 306**,** 549-59.
YU, P. H. 1998. Deamination of methylamine and angiopathy; toxicity of formaldehyde, oxidative stress and relevance to protein glycoxidation in diabetes. *J Neural Transm Suppl,* 52**,** 201-16.
YU, P. H. & DENG, Y. L. 1998. Endogenous formaldehyde as a potential factor of vulnerability of atherosclerosis: involvement of semicarbazide-sensitive amine oxidase-mediated methylamine turnover. *Atherosclerosis,* 140**,** 357-63.
YU, P. H., LAI, C. T. & ZUO, D. M. 1997. Formation of formaldehyde from adrenaline in vivo; a potential risk factor for stress-related angiopathy. *Neurochem Res,* 22**,** 615-20.
YU, W., HEGARTY, J. P., BERG, A., CHEN, X., WEST, G., KELLY, A. A., WANG, Y., PORITZ, L. S., KOLTUN, W. A. & LIN, Z. 2011. NKX2-3 transcriptional regulation of endothelin-1 and VEGF signaling in human intestinal microvascular endothelial cells. *PLoS One,* 6**,** e20454.
YU, W., LIN, Z., HEGARTY, J. P., JOHN, G., CHEN, X., FABER, P. W., KELLY, A. A., WANG, Y., PORITZ, L. S., SCHREIBER, S. & KOLTUN, W. A. 2010a. Genes regulated by Nkx2-3 in siRNA-mediated knockdown B cells: implication of endothelin-1 in inflammatory bowel disease. *Mol Genet Metab,* 100**,** 88-95.
YU, W., LIN, Z., KELLY, A. A., HEGARTY, J. P., PORITZ, L. S., WANG, Y., LI, T., SCHREIBER, S. & KOLTUN, W. A. 2009. Association of a Nkx2-3 polymorphism with Crohn's disease and expression of Nkx2-3 is up-regulated in B cell lines and intestinal tissues with Crohn's disease. *J Crohns Colitis,* 3**,** 189-95.
YU, W., LIN, Z., PASTOR, D. M., HEGARTY, J. P., CHEN, X., KELLY, A. A., WANG, Y., PORITZ, L. S. & KOLTUN, W. A. 2010b. Genes regulated by Nkx2-3 in

sporadic and inflammatory bowel disease-associated colorectal cancer cell lines. *Dig Dis Sci,* 55**,** 3171-80.
ZEISBERG, E. M., POTENTA, S. E., SUGIMOTO, H., ZEISBERG, M. & KALLURI, R. 2008. Fibroblasts in kidney fibrosis emerge via endothelial-to-mesenchymal transition. *J Am Soc Nephrol,* 19**,** 2282-7.
ZEISBERG, M. & KALLURI, R. 2008. Fibroblasts emerge via epithelial-mesenchymal transition in chronic kidney fibrosis. *Front Biosci,* 13**,** 6991-8.
ZHANG, H. Y., GHARAEE-KERMANI, M., ZHANG, K., KARMIOL, S. & PHAN, S. H. 1996. Lung fibroblast alpha-smooth muscle actin expression and contractile phenotype in bleomycin-induced pulmonary fibrosis. *Am J Pathol,* 148**,** 527-37.
ZHANG, J. & LI, L. 2005. BMP signaling and stem cell regulation. *Dev Biol,* 284**,** 1-11.
ZHU, L., VRANCKX, R., KHAU VAN KIEN, P., LALANDE, A., BOISSET, N., MATHIEU, F., WEGMAN, M., GLANCY, L., GASC, J. M., BRUNOTTE, F., BRUNEVAL, P., WOLF, J. E., MICHEL, J. B. & JEUNEMAITRE, X. 2006. Mutations in myosin heavy chain 11 cause a syndrome associating thoracic aortic aneurysm/aortic dissection and patent ductus arteriosus. *Nat Genet,* 38**,** 343-9.
ZORZANO, A., ABELLA, A., MARTI, L., CARPENE, C., PALACIN, M. & TESTAR, X. 2003. Semicarbazide-sensitive amine oxidase activity exerts insulin-like effects on glucose metabolism and insulin-signaling pathways in adipose cells. *Biochim Biophys Acta,* 1647**,** 3-9.

APPENDIX

RESULTS OF MICROARRAY COMPARISONS

Table A1

List of 500 most significantly up regulated genes in myofibroblasts, sorted by fold change. Fold change given as myofibroblast versus fibroblasts. P value adjusted for multiple testing using false discovery rate FDR step up.

Gene Symbol	Step-up p-value	Fold change
EDNRB	0.169318	65.2769
LRRC17	0.050798	57.6304
NKX2-3	0.0256099	35.0344
PCSK6	0.301318	34.415
ALDH1A1	0.445149	32.7034
SHISA3	0.102606	31.9163
EDNRB	0.208829	29.6918
FGL2	0.308633	25.9082
D4S234E	0.0982316	23.6494
COLEC10	0.204974	23.5322
FGL2	0.323323	21.156
LOC400550	0.365841	20.8742
NRK	0.507432	20.0882
CRISPLD1	0.0925492	18.3129
EDNRB	0.30469	16.2823
IGF2 /// INS-IGF2	0.481589	14.8878
MAB21L2	0.317493	14.8217
CHL1	0.281029	14.7099
TSTD1	0.221097	14.4333
MAB21L2	0.291955	14.4182
D4S234E	0.106667	13.0252
TCF21	0.281029	13.0249
PLXDC2	0.356595	12.0454
CNTN1	0.182253	11.9353
TCF21	0.357631	11.9019
CNTNAP3	0.0925492	11.1853
PNMAL1	0.0950708	11.0641
NRXN3	0.424387	10.832
GPRC5B	0.415241	10.589
CARD16	0.156187	10.585
TMTC1	0.53802	10.412
PNMA2	0.457836	9.68185
CD200	0.361215	9.68164
GPR37	0.37779	9.33204
F11R	0.337733	9.18782
CDH6	0.44266	9.02377
SCN9A	0.16571	8.95961
STAMBPL1	0.102606	8.92042
TMTC1	0.516339	8.87152
SCN3A	0.533629	8.84323
CYP2S1	0.224466	8.61855
MITF	0.410284	8.59737
CDH6	0.457357	8.46816
BMP2	0.378216	8.40472
SPON2	0.255927	8.3687
ACTG2	0.513748	8.2797
RAI2	0.311858	8.10732
PARM1	0.454874	7.97557
ADAMTS19	0.472592	7.73992

PCDH9	0.116364	7.68392
TMEM176B	0.636141	7.68212
PCDH7	0.312634	7.67172
LEPREL1	0.44287	7.67166
PLAT	0.0925492	7.59914
SCN9A	0.201218	7.57863
TMTC1	0.566405	7.5033
FOXF1	0.396173	7.46345
PCDH7	0.424347	7.41381
ERAP2	0.34683	7.34096
SFRP1	0.561449	7.32185
OR51E2	0.212579	7.30449
CDH6	0.461709	7.28346
BMP2	0.339902	7.26609
CARD16 /// CASP1	0.216704	7.12564
LOC404266	0.595644	7.08495
CYP39A1	0.312634	7.02795
LOC400550	0.401499	7.01255
PCDH7	0.299598	6.9759
PTGS2	0.363458	6.96931
PDPN	0.323323	6.94546
CST1	0.401944	6.93197
HOXB7	0.551268	6.92194
AOC3	0.062939	6.92087
PDE10A	0.243099	6.84152
MGP	0.617438	6.6897
GPR63	0.381552	6.6542
STOX2	0.365572	6.59392
KIAA1211	0.102606	6.56198
CD200	0.356595	6.55923
TRPA1	0.546533	6.53953
CNTNAP3B	0.228915	6.39892
SOX5	0.200874	6.39525
RGS2	0.289738	6.32637
LPAR3	0.512011	6.30983
LXN	0.422289	6.29778
NRXN3	0.42962	6.29524
GPX3	0.525776	6.27371
ERAP2	0.347481	6.24081
PTGER3	0.498024	6.11658
IGF2 /// INS-IGF2	0.552923	6.05122
STAMBPL1	0.0925492	6.03244
SMOC2	0.439466	5.95693
CLDN1	0.409852	5.95437
HHEX	0.42876	5.95366
HOXB7	0.559841	5.94492
TNFSF4	0.456113	5.93668
SFRP1	0.575625	5.86899
NRXN3	0.461367	5.85149
BMP6	0.317493	5.79498
ENPP4	0.441287	5.78582
EYA4	0.478334	5.77383
CCL11	0.156187	5.7722
LIF	0.281029	5.73933
PCDH7	0.341121	5.73603
PARM1	0.401796	5.69045
GPR37	0.352211	5.68088
WISP1	0.352536	5.61576
CDCP1	0.221893	5.53912
TMEM176A	0.690977	5.51374

ANO1	0.464413	5.49538
ERAP2	0.34683	5.46776
UCP2	0.329381	5.46193
ATRNL1	0.401796	5.45295
SEMA6D	0.408403	5.44994
NRK	0.543336	5.44883
HSD17B2	0.477238	5.38878
RASSF2	0.44266	5.33197
PTGER3	0.491048	5.33065
PRKAR2B	0.329175	5.32778
INMT	0.177512	5.32507
A2M	0.511046	5.29125
CDH6	0.497964	5.27218
TMEM178	0.397866	5.18578
IGFBP5	0.422948	5.12643
CNTN4	0.449726	5.11763
CHI3L1	0.675047	5.0768
CDCP1	0.251415	5.0761
SLC16A14	0.312634	5.07478
HGF	0.531221	4.99774
ZNF804A	0.547849	4.98099
LIPG	0.204122	4.95953
LOC100509635	0.397357	4.95615
EPHX4	0.407792	4.91111
PITX1	0.504834	4.90275
SNCA	0.4696	4.88085
BAMBI	0.341014	4.85455
SEMA6A	0.52228	4.84958
CNTN1	0.395974	4.84703
DDIT4L	0.308633	4.79781
CNTN1	0.312634	4.7949
KRT7	0.546533	4.77572
ITPR1	0.323323	4.76105
CACNB2	0.309855	4.75578
TEK	0.408228	4.75407
SOBP	0.26257	4.73228
PNMA2	0.523127	4.72112
PDE5A	0.429254	4.71436
OLR1	0.251197	4.70913
LYPD1	0.526065	4.70649
SVEP1	0.533953	4.70587
FAT3	0.481701	4.69005
BMP6	0.188413	4.68874
HHEX	0.333575	4.68345
FAT3	0.479884	4.68212
RERG	0.360244	4.66918
PTGS2	0.402948	4.61218
CNTNAP3	0.236437	4.60146
SVEP1	0.540954	4.59453
ARAP2	0.507367	4.59406
GPX3	0.552115	4.59232
FAM49A	0.312634	4.58872
KRT7	0.506987	4.58617
CD24	0.648408	4.5615
RASGRF2	0.323323	4.54665
TMTC1	0.594533	4.54168
C18orf1	0.493326	4.50545
PROM1	0.538654	4.49667
KRT18	0.593005	4.48822
PLAU	0.312634	4.46813

RARRES2	0.575625	4.45977
LOC100131199	0.461367	4.45871
IQCA1	0.514785	4.45705
SVEP1	0.518676	4.45375
SEMA6D	0.412875	4.4492
CACNB2	0.323323	4.44317
TFPI2	0.300633	4.43647
PDE5A	0.456113	4.43221
PLAU	0.417012	4.39362
STOX2	0.341851	4.37021
MITF	0.41304	4.35253
KIAA1107	0.331439	4.34472
PCDH7	0.34683	4.34434
KIAA1107	0.408228	4.32139
TPD52	0.444825	4.31697
SPRY1	0.242013	4.26017
ISL2	0.281029	4.24847
RDH10	0.551819	4.2107
STAU2	0.356469	4.20655
IGFBP5	0.463767	4.20612
PDPN	0.31293	4.20566
IVNS1ABP	0.165137	4.19069
MCTP2	0.465056	4.18251
HOXA3	0.312634	4.18243
KRT7	0.481589	4.16204
GPR39	0.551883	4.16171
STOX2	0.415579	4.1611
CDH6	0.450217	4.16104
PLCXD3	0.518578	4.12699
PEG3	0.236262	4.10611
GPRC5B	0.516339	4.09131
PTGER3	0.543124	4.07828
PCSK6	0.455724	4.07784
CHI3L1	0.634361	4.07215
PTGER3	0.516391	4.06673
GPC4	0.439317	4.062
ENC1	0.460182	4.05038
ANO1	0.456113	4.04087
MST4	0.449615	4.0326
MYH2	0.734569	4.03126
PDE5A	0.452193	4.02335
ARMC9	0.158327	3.97916
LOC645513	0.352536	3.96123
BCHE	0.615483	3.95535
RTN1	0.507439	3.9378
DHRS3	0.547339	3.93567
CD1D	0.439047	3.93047
PDE5A	0.425292	3.92606
ELOVL2	0.545744	3.92382
IGFBP5	0.441287	3.91671
ABCC4	0.328139	3.90234
LUZP2	0.435236	3.87601
EPHA5	0.533625	3.87579
UCP2	0.49833	3.87116
AGPAT9	0.46688	3.85982
WISP1	0.391235	3.85941
HGF	0.638598	3.85384
HOXB2	0.587385	3.84628
GALNT13	0.523709	3.84623
PLEKHH2	0.414771	3.84386

GPRC5B	0.474081	3.83516
WLS	0.278827	3.8205
BMP4	0.59439	3.81791
GCNT2	0.51787	3.80826
CLDN1	0.490829	3.80756
DSC3	0.474501	3.80724
IGFBP5	0.442314	3.78916
SEL1L3	0.156187	3.77825
PRO2964	0.40872	3.73814
CCDC68	0.52228	3.73346
PDE9A	0.295701	3.7303
ABCC4	0.303225	3.72785
IL33	0.514423	3.72138
PDE5A	0.359114	3.72016
SYPL2	0.559801	3.71481
PTGER3	0.538654	3.71109
IVNS1ABP	0.121366	3.6947
ITPR1	0.336319	3.69448
GPRC5A	0.44266	3.69096
PCSK6	0.437007	3.67402
RDH10	0.596412	3.6699
IGF2 /// INS-IGF2	0.592903	3.65641
PLEKHH2	0.365604	3.64173
LOC100506542	0.513189	3.63878
SYT15	0.190858	3.63464
TMEM56	0.401944	3.63058
C12orf59	0.531439	3.62637
NRXN3	0.400641	3.62418
RSPO3	0.658916	3.61351
FAM65C	0.56685	3.5888
CD24	0.663648	3.57863
VCAM1	0.628266	3.56705
EYA4	0.558779	3.55342
ENC1	0.480297	3.54051
PLA2G4A	0.505549	3.53831
NRTN	0.461709	3.53236
DSG2	0.612765	3.52797
SEL1L3	0.102606	3.52699
FIBIN	0.352211	3.52321
ABCC4	0.308633	3.51988
FAM198B	0.609077	3.51663
CFH /// CFHR1	0.558779	3.50491
VAT1L	0.418798	3.50313
ENPP4	0.402948	3.49853
IVNS1ABP	0.123038	3.49435
ITPR1	0.343336	3.49397
IVNS1ABP	0.366992	3.48841
EPHA5	0.653858	3.4851
CHST15	0.425168	3.47866
GPC4	0.458443	3.47283
ERAP2	0.425273	3.46113
MAMDC2	0.210938	3.45515
CASP1	0.506913	3.44443
D4S234E	0.300414	3.4367
PKIB	0.499872	3.43166
PEG10	0.415579	3.42743
EPHA5	0.569061	3.42602
FAM46C	0.573438	3.41925
FAM198B	0.65266	3.41539
SEL1L3	0.102606	3.40582

HBD	0.529679	3.4053
ADAMTS19	0.549389	3.39707
P2RX5	0.439345	3.39431
PLEKHH2	0.402335	3.38981
LOC100192378	0.527982	3.38846
WLS	0.349152	3.37626
IGFBP5	0.463336	3.3649
TSPAN7	0.41632	3.36117
RDH10	0.589906	3.35755
RASGRF2	0.276497	3.34571
CD24	0.656758	3.33232
ZFPM2	0.316578	3.32849
MCTP2	0.515324	3.32467
FNDC1	0.401796	3.32436
NOG	0.459679	3.31637
CLSTN2	0.448407	3.2928
SLC27A6	0.693576	3.29011
MUSK	0.42962	3.28473
RHOBTB3	0.341121	3.27283
FIBIN	0.402621	3.26512
CD24	0.689311	3.26454
SVIP	0.178627	3.26302
TNIK	0.42617	3.2558
EDIL3	0.60457	3.24979
FLJ39632	0.538093	3.24799
LIMCH1	0.562903	3.24736
SLC39A8	0.463332	3.24712
LEF1	0.57204	3.24655
SLC38A11	0.742132	3.23406
KAL1	0.465674	3.22194
EXOC6	0.342939	3.21772
PRKAA2	0.308633	3.21359
MST4	0.362579	3.19968
SEMA6A	0.639526	3.19446
CD24	0.599296	3.19061
EPHA3	0.676597	3.18751
SLC39A8	0.454963	3.18155
SFRP1	0.666547	3.17875
STXBP6	0.519176	3.17642
MMP10	0.638396	3.17498
PKP2	0.333229	3.16996
TPD52L1	0.478859	3.15096
RHOBTB3	0.341014	3.14975
ARHGAP20	0.444825	3.14908
TFPI2	0.4642	3.14726
CLIC6	0.773024	3.14577
FLJ43390	0.401796	3.13486
SOX5	0.165137	3.13451
ELOVL2	0.533512	3.13135
LOC100192378	0.437007	3.11991
TSPAN12	0.373604	3.11097
NKX3-2	0.384095	3.10864
PDE10A	0.206544	3.0897
PEG3	0.188402	3.08836
KCND3	0.507665	3.08433
SVIP	0.257948	3.08096
TPD52L1	0.437007	3.07271
DACT1	0.462615	3.07153
PTPRO	0.467244	3.0696
WLS	0.384579	3.05954

RHOBTB3	0.312634	3.05914
CCDC69	0.312634	3.04602
LOC100506725	0.152078	3.04446
ARMC9	0.149799	3.04207
PTGER3	0.57017	3.03365
EDNRA	0.628266	3.03086
CNTN4	0.543433	3.0308
PPME1	0.274709	3.02979
EDIL3	0.679725	3.02845
SUSD2	0.312634	3.02073
MBP	0.425273	3.01982
BDKRB1	0.466256	3.01573
PDPN	0.320417	3.00763
P4HA3	0.314008	3.00714
CHRM3	0.590716	3.00104
AR	0.567259	2.99991
DACH1	0.557338	2.99823
DSG2	0.582549	2.99706
SH2D5	0.312634	2.98512
EDIL3	0.57958	2.97066
LPAR3	0.61097	2.96128
CHRM2	0.444825	2.95629
GNG4	0.432873	2.95374
KCNJ8	0.656663	2.95053
ATRNL1	0.475727	2.94929
HOXB3	0.572587	2.93092
PPME1	0.251415	2.92704
CCDC3	0.352536	2.92162
ABCB1	0.438382	2.92108
PARP8	0.339529	2.91908
FBXL13	0.251197	2.91767
CADPS2	0.437007	2.9105
STXBP6	0.467467	2.90441
SORBS1	0.561587	2.8986
TMEM158	0.235516	2.89516
GCH1	0.436845	2.89466
PTGER3	0.582549	2.89408
STXBP6	0.57838	2.88802
CD24	0.724667	2.8868
KCNJ2	0.57868	2.88653
TNIK	0.458443	2.88396
ADAMTS8	0.479338	2.88101
KCND3	0.478832	2.87321
LIMCH1	0.608886	2.87248
NEURL1B	0.436229	2.87212
GNG4	0.497716	2.8628
ISOC1	0.485139	2.8617
REN	0.452473	2.86112
C10orf58	0.438382	2.85373
NALCN	0.435236	2.84606
CD274	0.519181	2.84355
RHOBTB3	0.373822	2.83088
MYOCD	0.719306	2.82971
LIMCH1	0.581962	2.82553
TAP2	0.352558	2.8223
PPP1R9A	0.46688	2.81903
CNNM2	0.429791	2.81272
GFRA1	0.740297	2.81198
MYO5A	0.50358	2.81161
OR51E2	0.254219	2.80871

AR	0.601452	2.80793
KLHL13	0.666527	2.80775
CXCR7	0.679007	2.80693
LYN	0.382924	2.80152
CRISPLD2	0.481589	2.8012
LGALS3BP	0.41304	2.79978
SLC4A4	0.333229	2.79648
ITGA2	0.339902	2.7936
LOC572558	0.374962	2.79231
CASP1	0.51539	2.78919
APOL1	0.444825	2.77417
MYO10	0.224884	2.77412
CASP1	0.390608	2.77223
MGAT5	0.500177	2.77095
MAPK10	0.444825	2.76573
PLN	0.448407	2.76148
RARRES1	0.504834	2.76128
CDH1	0.719819	2.76095
LOC645513	0.356305	2.75978
SSX2IP	0.438158	2.75972
ITGB3	0.375363	2.75897
PCSK6	0.309855	2.75885
TNIK	0.444825	2.75872
KCTD16	0.533996	2.75582
KCNJ8	0.650828	2.75472
KBTBD8	0.415579	2.75336
GFRA1	0.708045	2.7515
GUCY1B3	0.524923	2.74794
CAMK1D /// LOC283070	0.531439	2.73811
LRRC1	0.345491	2.73609
ICAM1	0.461709	2.73406
C16orf87	0.274709	2.72603
CHRDL1	0.6304	2.72441
STAMBPL1	0.206526	2.72286
SEMA4D	0.456113	2.71412
IL11	0.484289	2.71014
LOC285943	0.317493	2.70444
CHN2	0.561449	2.69427
FRY	0.431506	2.69317
SVEP1	0.409852	2.68358
CTSH	0.527745	2.68197
OGFRL1	0.201852	2.68081
IMPA2	0.532803	2.67781
SLC4A4	0.310917	2.66933
RARRES3	0.57838	2.66776
CD9	0.440639	2.66436
HGF	0.703693	2.66276
BST2	0.561671	2.65998
GRIA1	0.558779	2.65222
HGF	0.639115	2.65016
NHSL1	0.281029	2.64968
ST8SIA1	0.5616	2.64889
HGF	0.565672	2.64318
SLC4A4	0.408403	2.64259
OGFRL1	0.236262	2.64087
PDE10A	0.349455	2.64058
SFRP1	0.679014	2.63531
LOC151162 /// MGAT5	0.564238	2.63492
MMP3	0.78355	2.63209
HOXA5	0.342939	2.62442

RARRES1	0.570618	2.61899
TNIK	0.456744	2.61836
TSPAN8	0.688555	2.61662
NPPB	0.545763	2.61172
ICAM1	0.500398	2.61011
PPP4R4	0.631252	2.60971
JUP	0.362938	2.60769
ETS2	0.487691	2.60564
FRMPD4	0.435428	2.59806
RAVER2	0.374962	2.59322
WFDC1	0.820933	2.59216
KCND3	0.551883	2.59059
FGF7 /// KGFLP1 /// KGFLP2	0.741989	2.58975
SLC4A4	0.312634	2.5878
IL32	0.497001	2.58752
PEG10	0.486157	2.58462
TMTC2	0.595926	2.58284
TYRP1	0.507506	2.57969
STRBP	0.32398	2.57899
FAM83D	0.519444	2.57563
SLC25A27	0.540411	2.56794
USP44	0.345489	2.5675
ARMC9	0.306612	2.55424
LOC100507063	0.680715	2.55396
USP2	0.317493	2.55385
KIAA1211	0.185823	2.55304
PLN	0.389794	2.54646
LOC643792	0.317493	2.54538
CASP1	0.508818	2.54238
ICAM1	0.459679	2.53996
SH3BGRL2	0.177082	2.53659
FKBP5	0.407996	2.53373
KISS1	0.401477	2.53071
GPR126	0.489998	2.52908
SCN4B	0.331439	2.52765
MGAT4A	0.449845	2.52753
LIMS3	0.443226	2.52569
LYN	0.407996	2.51968
RBP7	0.414412	2.51737
DIRC3	0.42962	2.51694
CHRM3	0.574941	2.51272
PVR	0.0925492	2.51269
LOC100131199	0.513189	2.5092
SLC40A1	0.75321	2.50806
PVR	0.102606	2.50646
LRRN3	0.569513	2.50329
SSX2IP	0.431936	2.49807
NALCN	0.505214	2.49465
CASP1	0.460627	2.4921
SORBS1	0.620567	2.4902
ITGB3	0.429164	2.48941
AR	0.612388	2.48819
ANKRD6	0.588408	2.48631
MBP	0.443226	2.48589
XIST	0.873844	2.48474
MYH1	0.645237	2.48316
PVR	0.0925492	2.48271
SVEP1	0.48899	2.47976
DENND2A	0.701511	2.47917
SCARB1	0.189034	2.47875

PCDH10	0.745403	2.47704
LOC100506979	0.503161	2.4754
PRPS1	0.375495	2.47486
GBP3	0.512356	2.4724
RAB11FIP1	0.438382	2.46635
FRY	0.460182	2.46584
GCA	0.582549	2.46448
CD44	0.52228	2.45623
EXOC6	0.415579	2.4551
RASSF5	0.386465	2.45501
OSBPL10	0.358312	2.4548
FAM155A	0.609727	2.45354
QSOX1	0.351467	2.45258
PITX1	0.501408	2.45195
GLRX	0.464789	2.45121
MTUS1	0.537388	2.44657
SSX2IP	0.456744	2.44225
GRIA1	0.593005	2.43952
RTN1	0.52154	2.43527
FRY	0.196357	2.42863
OGFRL1	0.281029	2.42407
SSX2IP	0.356595	2.42261
SSFA2	0.312634	2.42038
SEMA6D	0.540728	2.41876
CACNB2	0.388858	2.41847
SERPINB9	0.470491	2.41826
MYO10	0.286946	2.41824
HOXB5	0.590637	2.40674
NR3C2	0.592054	2.40648
FAM124A	0.599192	2.40279
ARSK	0.325761	2.3983
HOXB3	0.532025	2.39744
RAB11FIP1	0.458144	2.39556
ADAM19	0.581539	2.39521
RPS6KA6	0.464459	2.3845
DCLK2	0.557338	2.38103
PIK3AP1	0.538654	2.37921
STIM2	0.435572	2.37808
BEX2	0.665999	2.37803
VIPR2	0.545744	2.37464
ABCC4	0.444825	2.37288
PRKCH	0.546268	2.36981
XIST	0.871457	2.36832
FAM186A	0.455908	2.36639
ANKH	0.386664	2.36268
SLC4A4	0.196357	2.36197
MCAM	0.747468	2.36181
ARHGAP28	0.485139	2.36127
C1orf118	0.408276	2.3601
PVR	0.0925492	2.35792
FABP1	0.803733	2.35294
GPX2	0.76308	2.35275
HBG1 /// HBG2	0.515449	2.34994
MYH11	0.707092	2.34689
MITF	0.456113	2.34545
AKR1B10	0.600764	2.34349
NSUN6	0.384579	2.34208
HIST1H3B	0.677011	2.33827
PLBD1	0.46688	2.33697
EEPD1	0.543718	2.33103

PLA2G16	0.438382	2.32957
IGFBP5	0.402948	2.32474
PVR	0.0923591	2.32472
STOM	0.257365	2.32427
FAM132B	0.513525	2.32238
FLJ36031	0.455724	2.32063
FABP1	0.77992	2.31953
SYNGR2	0.362938	2.31776
DUXAP10	0.484377	2.3176
RERG	0.516339	2.31697
SVEP1	0.480448	2.31489
C2CD3	0.312634	2.31476
CYP24A1	0.579815	2.31451
CHN2	0.514707	2.31078
PADI2	0.68883	2.31038
SLITRK5	0.685489	2.30956
TLR3	0.640901	2.30473
SDK1	0.280731	2.30399
MYO10	0.312634	2.30348
TNFSF18	0.513468	2.30334
RGNEF	0.333646	2.30046
EDNRA	0.643609	2.30007
RAB27B	0.618335	2.29943
ISL1	0.484351	2.29743
DCN	0.630604	2.29711
SEMA3A	0.656663	2.29532
KCNE1	0.512787	2.29457
CLIC6	0.794827	2.29173
DIO2	0.520513	2.29099
NHSL1	0.243099	2.28994
C2CD2	0.342939	2.28919
LOC401097	0.688555	2.28665
CYP2B6	0.655758	2.28634
MAGEA3	0.734883	2.28596
SIK1	0.43944	2.28576
DTX4	0.513385	2.28529
FLJ39632	0.598819	2.28345
KRTAP4-12	0.51857	2.28258
MBP	0.429151	2.27986
CCDC69	0.441786	2.27713
MYH10	0.533027	2.27662
TSPAN12	0.42962	2.27533
ANKH	0.44266	2.2748
MCAM	0.762705	2.27422
SLC1A1	0.506987	2.27371
CD274	0.538063	2.26694
LOC100291393 /// SHC2	0.368585	2.26555
PMAIP1	0.624634	2.26356
CABLES1	0.467622	2.26277
RHOBTB3	0.32398	2.26179
SCN5A	0.464413	2.25983
GJD3	0.640644	2.25673
FKBP1A	0.352211	2.25231
PM20D2	0.278827	2.25186
LYN	0.357139	2.25021
FCGR2A	0.281029	2.24735
GUCY1B3	0.538967	2.24521
RRM2	0.59443	2.2415
CABLES1	0.525405	2.24057
TGFB2	0.7831	2.23932

CCL2	0.482233	2.23518
FGF7	0.765746	2.23306
FAM49A	0.425273	2.23242
RSPO2	0.605038	2.22705
RGNEF	0.383429	2.22522
GULP1	0.663648	2.22323
FZD4	0.476083	2.21992
ABCG1	0.462196	2.21976
GYG2	0.592624	2.21973
TGFB2	0.805866	2.21868
PRICKLE1	0.523314	2.21679
MYO10	0.276011	2.21618
RGNEF	0.384619	2.21561
RASL11B	0.481526	2.21532
TUBA4A	0.381552	2.21509
DCBLD1	0.308633	2.21049
CGA	0.409612	2.21009
SLC19A1	0.200874	2.20892
ANXA3	0.784453	2.20358
LOC100507197	0.514707	2.20342
XIST	0.894582	2.20025
RCAN1	0.312634	2.19982
GKAP1	0.180877	2.19953
TTC9	0.177082	2.19753
NT5C2	0.352536	2.19593
NAV3	0.13716	2.19583
MYH11	0.692802	2.19516
ERG	0.57958	2.19408
KLK10	0.78696	2.19368
VWA5A	0.533953	2.19346
PLCXD3	0.616332	2.19228
LOC645513	0.424777	2.19038
LOC643650	0.611673	2.19034
MPZL3	0.551268	2.18867
ITGB3	0.478859	2.18825
ITGA2	0.332578	2.18516
TPD52	0.536534	2.18509
STC1	0.728695	2.18381
TMEM56	0.460182	2.18073
TGFB2	0.798786	2.17998
COL14A1	0.862228	2.17931
FLJ23867 /// QSOX1	0.281029	2.1792
ZNF238	0.590032	2.17754
PID1	0.772557	2.17753
LOC285043	0.46688	2.17526
TSIX	0.887485	2.1719
SSX2IP	0.464413	2.17121
ZNF280B	0.523314	2.17112
TNNT2	0.308611	2.16917
MCOLN3	0.512356	2.16062
HSPA12A	0.530866	2.15999
HBB	0.555164	2.15976
DIO2	0.426166	2.15775
MAP3K9	0.360227	2.15665
MRVI1	0.536696	2.15552
KIF13B	0.527745	2.15284
SYT15	0.210938	2.14927
GMPR	0.394708	2.14921
TAP2	0.418798	2.14909
SGMS2	0.251415	2.14735

CLEC2B	0.821271	2.1462
METTL7A	0.688792	2.14588
MYEF2	0.42617	2.14541
SLC39A8	0.549891	2.14525
ACSL5	0.511048	2.14482
C2CD3	0.321497	2.1433
RBP1	0.591799	2.14113
NFE2L3	0.436845	2.14073
STC1	0.652341	2.1404
CORIN	0.657747	2.1401
MYH10	0.524129	2.13773
DSC3	0.538726	2.13691
STIM2	0.504834	2.13686
IGFBP7	0.640382	2.13508
BHMT	0.717359	2.13354
ASPN	0.640335	2.13322
HLX	0.312634	2.1326
CARD6	0.737423	2.13033
SOBP	0.479771	2.13021
CACNB4	0.44266	2.12499
GFRA1	0.797071	2.12309
NFASC	0.740488	2.12168
GABBR1 /// UBD	0.674396	2.11772
SCARB1	0.198899	2.11715
NRP2	0.401796	2.11607
STC1	0.695663	2.1152
DACH1	0.289738	2.11491
SOX4	0.539963	2.11231
MCAM	0.784489	2.11183
LINGO2	0.674828	2.10973
FILIP1L	0.312634	2.10841
CACNB2	0.516339	2.10672
EDN1	0.656924	2.10457
LOC346887	0.42962	2.10419
CDCP1	0.216704	2.10136
SYNGR3	0.561747	2.10134
MCTP2	0.512356	2.10115
TRPV2	0.410168	2.09916
TGM2	0.531439	2.09846
XIST	0.894031	2.09809
ETS2	0.617896	2.09789
FAM155A	0.726493	2.09719
DENND2A	0.680083	2.09388
GLI2	0.479338	2.09255
COL4A1	0.693884	2.09177
PPARG	0.653343	2.09121
MARCKSL1	0.606839	2.09007
PEAR1	0.642886	2.08979
DNAJC22	0.189034	2.08848
SVIP	0.151716	2.08731
TSLP	0.325761	2.0858
AGR2	0.7831	2.08368
MLXIP	0.312634	2.08344
SVIP	0.358312	2.08078
HBB	0.522389	2.08016
MAP3K5	0.590032	2.0786
HIST1H2BC	0.450915	2.07751
NPC1	0.356595	2.07329
CSF1	0.703685	2.07301
MAP3K4	0.462615	2.073

MYEF2	0.352211	2.07087
RNF207	0.456426	2.07002
MLLT11	0.580928	2.0677
PPP1R9A	0.554572	2.06737
ROR2	0.599468	2.06735
FAM46C	0.657621	2.06685
ANKH	0.374882	2.06517
C18orf1	0.44287	2.06372
CLMN	0.336064	2.06362
PLEKHA6	0.542102	2.06232
CDK1	0.673391	2.06079
SOX4	0.535086	2.06059
SLCO3A1	0.491434	2.06015
ARMC9	0.251415	2.05935
SLC39A8	0.561587	2.05749
CACNB2	0.457182	2.05682
RAB27B	0.620106	2.05675

Table A2

List of 500 most significantly down regulated genes in myofibroblasts (up regulated in fibroblasts), sorted by fold change. Fold change given as myofibroblast versus fibroblasts. P value adjusted for multiple testing using false discovery rate FDR step up

Gene Symbol	Step-up p-value	Fold change
SHOX2	3.27E-05	-90.0583
EMX2	0.16011	-41.3154
HSPB3	0.0923591	-31.7363
NRN1	0.276497	-29.3723
ENPP2	0.189034	-27.0332
IRX3	0.0633998	-25.4563
EMX2OS	0.212688	-19.4846
HOXC9	0.102606	-18.0624
ABI3BP	0.341351	-17.0706
EMX2OS	0.295898	-16.8398
XG	0.457836	-15.6047
HOXC6	0.163968	-13.1176
LHX9	0.371414	-12.648
GALNT6	0.289738	-12.4271
ODZ2	0.457182	-12.2478
SHOX2	0.0256099	-12.2001
LOC255480	0.0925492	-10.4749
MME	0.277062	-10.2391
IRX5	0.123038	-10.1077
EBF1	0.402948	-10.0766
DSP	0.248627	-10.0405
TBX5	0.0332817	-9.89776
PCOLCE2	0.436845	-9.79488
C8orf4	0.262515	-9.72471
DPT	0.507665	-9.71594
KCNK2	0.451856	-9.67696
CPXM2	0.186288	-9.1272
CXCL12	0.242013	-9.02177
LOC255480	0.179521	-8.98478
C4orf31	0.389007	-8.9121
TMEM119	0.37779	-8.78868
ADAMTSL1	0.312634	-8.30959
ZNF385D	0.395277	-8.19194
RNF182	0.309855	-8.17029
CA12	0.212688	-7.93759
GRIA3	0.369188	-7.92727
CRABP2	0.21889	-7.9178
SIM1	0.401796	-7.78903
OSR2	0.456113	-7.54653
MAB21L1	0.38174	-7.40066
CRNDE	0.140615	-7.37438
HAPLN1	0.418768	-7.3635
COL5A3	0.317493	-7.25658
TBX15	0.328244	-6.92077
PRRX1	0.165137	-6.8539
XG	0.396	-6.83833
HAPLN1	0.485139	-6.78931
TFAP2A	0.623209	-6.75581
AGTR1	0.374962	-6.57164
CRNDE	0.151716	-6.49175

HOXC8	0.401944	-6.42922
ENPP2	0.334975	-6.38094
DPT	0.525649	-6.37959
FBLN2	0.362561	-6.28975
WNT16	0.323323	-6.27383
LRRC15	0.480448	-6.25156
EN1	0.356469	-6.23758
DPT	0.523314	-6.1893
COL5A3	0.323323	-6.02269
TRPC4	0.342662	-5.96567
AGTR1	0.356469	-5.9374
ANPEP	0.221097	-5.90844
ENPP1	0.281029	-5.87957
MXRA5	0.445149	-5.84659
ADAMTSL1	0.323323	-5.79746
CCDC85A	0.560492	-5.79283
APOD	0.382567	-5.7759
GABBR2	0.481187	-5.77533
CXCL12	0.402621	-5.73196
KRTAP1-1	0.165137	-5.72326
CA12	0.204974	-5.71901
ADAMTSL1	0.312634	-5.68792
FOXD1	0.459679	-5.67583
SLIT3	0.438158	-5.67531
PODXL	0.370052	-5.64091
MME	0.301318	-5.6307
ADRA2A	0.515449	-5.62117
PRELP	0.314578	-5.57423
SCIN	0.44266	-5.51624
CA12	0.203986	-5.44362
WISP2	0.455724	-5.42964
TFAP2A	0.621471	-5.4283
ENPP1	0.276497	-5.42045
EBF1	0.42876	-5.37205
TNFRSF19	0.340692	-5.34076
C11orf41	0.242013	-5.33102
DNAJC6	0.312634	-5.31572
TBX5	0.156187	-5.28356
NLGN1	0.291955	-5.24826
LOC152742	0.0925492	-5.18281
GRIA3	0.188732	-5.15273
EBF1	0.425273	-5.14788
PRRX1	0.212579	-5.10926
HECW2	0.289738	-5.08738
TRPC4	0.401944	-5.07594
IL20RB	0.536534	-5.07404
PCOLCE	0.206544	-5.07227
ADAMTSL1	0.223148	-5.04909
ELFN1	0.326497	-5.03923
HAPLN1	0.432739	-5.0156
HEPH	0.528826	-4.99707
TGFA	0.444192	-4.99674
FAM19A5	0.507432	-4.98807
RUNX3	0.414957	-4.98694
C11orf41	0.16571	-4.97528
SIX1	0.530866	-4.93482
KBTBD11	0.354471	-4.86815
ADD2	0.533953	-4.86583
GREM2	0.543055	-4.85921
ENPP1	0.224884	-4.83497

EBF1	0.34683	-4.80912
TOX2	0.459679	-4.80267
KRT19	0.276497	-4.77993
PAPPA	0.325761	-4.77871
BEX1	0.40672	-4.76644
SIM1	0.425273	-4.75604
KRTAP1-5	0.470878	-4.74528
KLF4	0.49171	-4.74508
GREM2	0.517881	-4.71333
SEMA5A	0.0925492	-4.67818
FOXC1	0.352211	-4.66582
ZIC1	0.512011	-4.64959
LOC643401	0.458036	-4.64923
FAM19A5	0.480315	-4.63385
CLEC3B	0.342544	-4.5959
INPP4B	0.321497	-4.58815
TBX5	0.156187	-4.58719
C11orf87	0.545763	-4.5524
LOC339535	0.0925492	-4.47776
FBLN1	0.321497	-4.46987
BAALC	0.343335	-4.45979
LOC100292909	0.344667	-4.43796
DLX1	0.479771	-4.43307
HLA-DPA1	0.516339	-4.4248
EMILIN2	0.201218	-4.41587
ZNF385D	0.452473	-4.40976
NLGN1	0.342662	-4.3794
GREM2	0.530909	-4.3473
PAPPA	0.27113	-4.33375
NTNG1	0.31293	-4.29021
FOXL2	0.374962	-4.2729
SERPINB2	0.519575	-4.26736
PRELP	0.336641	-4.24449
RUNX1T1	0.317493	-4.24331
PAPPA	0.229194	-4.22418
LHX2	0.670715	-4.22319
RUNX1T1	0.165137	-4.21876
PRRX2	0.204974	-4.21785
TNFRSF19	0.291873	-4.20328
GRIA3	0.243099	-4.2017
JAG1	0.548079	-4.19982
KRT19	0.208395	-4.19702
PLXNC1	0.31835	-4.17235
BAALC	0.221879	-4.17067
GABBR2	0.42962	-4.15849
LOC100506697	0.323323	-4.15331
THRB	0.570618	-4.14879
SEMA5A	0.180877	-4.14057
IRX1	0.436859	-4.14034
CYP27C1	0.317493	-4.12445
PLAC9	0.364882	-4.10889
LDB2	0.389426	-4.08079
MSX1	0.248627	-4.0728
SLC7A14	0.635972	-4.06157
NES	0.471111	-4.05656
ADAMTSL4	0.537374	-4.01841
HOXC10	0.581188	-3.99653
LOC644246	0.402948	-3.98078
SLC7A14	0.56849	-3.97416
HOTAIR	0.65266	-3.96438

GRIA3	0.281029	-3.94565
GALNT6	0.316578	-3.92354
GABBR2	0.455589	-3.92343
FBLN1	0.312634	-3.91826
TBX3	0.442135	-3.90393
LOC400043	0.645488	-3.89408
CRIP1	0.468393	-3.89188
RUNX1T1	0.212579	-3.88206
ENPP1	0.204974	-3.87446
MARVELD2	0.156187	-3.80975
SHOX	0.50428	-3.80105
DLX2	0.57958	-3.78829
TWIST2	0.355561	-3.78206
STAC	0.481701	-3.77948
DKK1	0.382262	-3.7612
C11orf87	0.577527	-3.76014
CYP1B1	0.616376	-3.74782
LPXN	0.551555	-3.73017
PAPPA	0.218814	-3.71873
KIAA1217	0.396173	-3.71862
SASH1	0.102606	-3.69938
C13orf18	0.208526	-3.66193
IRX2	0.116364	-3.65257
ADCY4	0.351643	-3.64295
JAG1	0.516339	-3.64049
TFAP2C	0.61022	-3.6404
RUNX3	0.415579	-3.6217
MLPH	0.357631	-3.61716
BGN	0.429728	-3.61527
LOC644246	0.453827	-3.60093
FLT1	0.685473	-3.5929
MFAP2	0.389426	-3.58821
LPPR4	0.639953	-3.58654
LDB3	0.593355	-3.58105
FOXC1	0.222212	-3.58021
PAPPA	0.256986	-3.55752
GABBR2	0.419505	-3.55477
GUCY1A2	0.321497	-3.54848
MARVELD2	0.276497	-3.5433
FOLR3	0.347481	-3.53319
TWIST2	0.437726	-3.52868
LOC100505880	0.0982316	-3.52537
PLXNC1	0.374967	-3.52398
FLT1	0.696602	-3.51398
DNM1	0.224884	-3.5136
DOCK10	0.341644	-3.50782
CACNA1A	0.234231	-3.49571
XGPY2	0.448696	-3.48119
TGFBR3	0.533996	-3.47476
GAS1	0.326497	-3.47426
OLFML2B	0.490661	-3.46858
VIM	0.298813	-3.46221
TBX18	0.42962	-3.45663
C11orf41	0.281029	-3.44977
MEGF6	0.475936	-3.44169
APCDD1	0.450217	-3.43893
ALDH3A2	0.328981	-3.4299
CA12	0.165292	-3.42942
TWIST1	0.0925492	-3.41308
TRHDE	0.665999	-3.40453

HDAC9	0.201218	-3.39851
SSTR1	0.421441	-3.39701
CADPS	0.450806	-3.39296
PAPPA	0.323323	-3.38854
KIAA1217	0.437007	-3.38198
FSTL1	0.16571	-3.37264
PRLR	0.558779	-3.36807
SHOX2	0.0547385	-3.35892
HOMER2	0.180339	-3.34646
FAM19A5	0.531439	-3.3464
LOC100287387	0.403893	-3.34533
EPB41L3	0.667125	-3.33707
LY6K	0.617142	-3.32878
EMILIN2	0.243099	-3.32184
JAG1	0.533996	-3.32122
CSMD2	0.251197	-3.30962
TRPC4	0.346751	-3.3088
RAGE	0.278827	-3.30858
MIR214	0.384095	-3.30703
PLCE1	0.106667	-3.29877
FN1	0.323323	-3.28735
RIPK4	0.534034	-3.27448
THRB	0.590735	-3.27318
DCLK1	0.678308	-3.26257
IGDCC4	0.539163	-3.25682
MSX1	0.281029	-3.23321
LOC730101	0.308633	-3.23112
AKAP6	0.225734	-3.22956
BGN	0.332578	-3.22151
INPP4B	0.44848	-3.21986
LOC100510557 /// MUC6	0.317493	-3.21066
CYP1B1	0.660196	-3.19766
LOC100134259	0.499872	-3.17717
GALNTL2	0.529679	-3.17515
RNF150	0.102606	-3.1744
CCDC102B	0.702443	-3.16369
HOXC4	0.394706	-3.1601
SASH1	0.153448	-3.1494
BGN	0.341863	-3.14764
FN1	0.276816	-3.14053
ABI3BP	0.498762	-3.13714
HOXC11	0.595375	-3.13174
NGF	0.102606	-3.12829
ADAMTS6	0.545495	-3.1261
CXXC5	0.232047	-3.12397
ALDH3A2	0.312634	-3.11823
BEND6	0.381427	-3.1044
C11orf87	0.604	-3.06542
PLCE1	0.117775	-3.06307
AKAP6	0.318789	-3.06277
CDON	0.463867	-3.04804
SEMA5A	0.102606	-3.04003
MYPN	0.235749	-3.03651
LDOC1	0.562117	-3.03592
JAG1	0.638598	-3.02919
NRG1	0.452392	-3.0286
C13orf15	0.507665	-3.01426
SRY	0.519444	-3.00241
STEAP1	0.545495	-2.99914
LNX1	0.545763	-2.99601

ANK1	0.348379	-2.99063
MYO1D	0.68282	-2.98962
NRG1	0.495039	-2.97376
MGC87042	0.2985	-2.97308
EFNB2	0.691301	-2.97125
APBB1IP	0.536733	-2.96512
CDH8	0.518676	-2.96171
RGN	0.52598	-2.94998
FRMD3	0.484289	-2.94647
LOC100288092	0.383429	-2.94646
VIT	0.589271	-2.94191
GLIS1	0.48465	-2.93239
USP9Y	0.778859	-2.92759
TNFRSF19	0.312634	-2.9248
CNTN3	0.512763	-2.9208
CH25H	0.701511	-2.91979
TRPC4	0.235749	-2.91557
GRP	0.683572	-2.90964
CST6	0.382567	-2.90601
EGFL6	0.617242	-2.90061
HAPLN1	0.437007	-2.89645
TBX3	0.441287	-2.89606
LGR4	0.562314	-2.88383
PAPPA	0.312089	-2.88059
TBX3	0.406474	-2.87991
ADAMTSL1	0.297717	-2.8765
CADPS	0.47112	-2.86981
CCRL1	0.631809	-2.86555
HDAC9	0.495147	-2.86112
ANK1	0.448407	-2.85931
SCIN	0.489738	-2.8473
CXXC5	0.308633	-2.84625
EFCAB2	0.259893	-2.82833
MEGF6	0.314008	-2.82829
SOX11	0.686804	-2.8224
LGR4	0.53068	-2.81231
LRRC15	0.579816	-2.79814
ALDH3A2	0.318191	-2.79644
FCRLA	0.141013	-2.78894
OXTR	0.41632	-2.78482
SLIT2	0.635501	-2.76994
CYP1B1	0.680322	-2.76956
FAM101A	0.392319	-2.75099
TGFBR3	0.559055	-2.74911
C1orf53	0.286903	-2.7488
SOX9	0.612081	-2.74579
CAPG	0.3579	-2.73986
EFNB2	0.599192	-2.73945
JAG1	0.601438	-2.73346
SASH1	0.251415	-2.73181
TNC	0.611704	-2.73005
GLT8D2	0.402948	-2.71348
ALDH3B1	0.457836	-2.70991
MATN2	0.342939	-2.70553
PITX2	0.429628	-2.69845
KRTAP1-3	0.430186	-2.69609
TBX18	0.476083	-2.68826
WNT5A	0.485139	-2.68547
TBX3	0.422948	-2.68394
ZNF521	0.511305	-2.67888

TBX3	0.414771	-2.67708
SIX2	0.702296	-2.67685
MOCOS	0.312634	-2.67475
CD248	0.314398	-2.65597
ABCA6	0.452473	-2.65361
QPCT	0.486182	-2.653
PTGFR	0.365257	-2.65243
POSTN	0.831829	-2.6494
NIPAL2	0.407996	-2.64735
NES	0.494295	-2.64251
ADAM12	0.700659	-2.63994
NRP1	0.438407	-2.63709
GPNMB	0.436845	-2.63535
PTGFR	0.453547	-2.62726
NRG1	0.516981	-2.62657
IGF2BP3	0.635753	-2.62447
HOXD10	0.561844	-2.62355
FMN2	0.507417	-2.62213
ZEB2	0.427131	-2.61908
FMN2	0.488207	-2.61898
NTF3	0.411617	-2.61464
CACNA1C	0.497964	-2.61145
PRLR	0.598819	-2.59881
C10orf114	0.289738	-2.59835
CPXM2	0.382616	-2.5933
FLT1	0.686854	-2.59309
C8orf79	0.456113	-2.58649
TGFA	0.44266	-2.57654
PDE1C	0.74839	-2.57251
TBX3	0.390368	-2.55558
CYP7B1	0.529572	-2.55387
NAP1L3	0.28333	-2.54609
TRNP1	0.402948	-2.5394
VEPH1	0.416211	-2.5383
FBLN1	0.312634	-2.53352
PITPNM3	0.523374	-2.53348
KCNC4	0.444825	-2.53319
SIPA1L1	0.457182	-2.53131
APCDD1L	0.459679	-2.52951
FST	0.352536	-2.52919
GRIA3	0.289738	-2.52676
TFAP2C	0.642647	-2.52602
SYTL2	0.489806	-2.52257
HOXD11	0.525449	-2.52016
KLF4	0.508341	-2.51944
SYNPO2	0.520513	-2.51671
MAFB	0.525124	-2.51611
FAM119A	0.360244	-2.51489
CXXC5	0.312634	-2.51399
SHISA2	0.665097	-2.50828
CDC42EP5	0.0925492	-2.5057
PDZRN3	0.447738	-2.50133
SGK223	0.521985	-2.49553
STAT4	0.295837	-2.48674
LYPD6B	0.755296	-2.48541
KCNJ6	0.618335	-2.48279
LOC79015	0.491887	-2.48193
S100A4	0.462959	-2.47968
TCEA3	0.201218	-2.47688
SYNPO2	0.505701	-2.47687

LOC730091	0.309855	-2.47452
KIAA1958	0.552305	-2.4741
OPCML	0.523919	-2.47384
AEBP1	0.177082	-2.46519
SIPA1L2	0.412875	-2.46111
GLYATL2	0.295898	-2.46007
SYTL2	0.558779	-2.45259
SEMA3F	0.412875	-2.45232
UBL3	0.303456	-2.45176
FRMD3	0.510229	-2.45138
MOCOS	0.286896	-2.4503
CCNYL1	0.592239	-2.44373
TRIM16	0.396173	-2.44215
PLCL1	0.346014	-2.44187
PPP1R14C	0.520919	-2.43827
POSTN	0.840191	-2.43794
ARHGEF40	0.0925492	-2.43654
WIPF1	0.280731	-2.43533
IRX2	0.320961	-2.43316
C6orf132	0.383429	-2.43158
LPCAT2	0.491706	-2.43097
SLC43A3	0.493163	-2.42971
ACTC1	0.753429	-2.42332
FBLN7	0.432818	-2.42232
GPNMB	0.36167	-2.41973
KIAA1549	0.396634	-2.41724
GATA2	0.560077	-2.41662
COL8A1	0.711097	-2.41587
FILIP1	0.401796	-2.41516
KITLG	0.312634	-2.41213
GAS1	0.201218	-2.40974
VEPH1	0.190858	-2.40956
C8orf84	0.734446	-2.40709
PARD6G	0.493181	-2.40657
SLC44A1	0.303225	-2.40436
RPS4Y1	0.876331	-2.39831
VEPH1	0.243099	-2.39252
TMEM132D	0.618335	-2.38819
BVES	0.39549	-2.38645
ADAMTSL1	0.410284	-2.38639
ADAM12	0.734569	-2.38032
ABI3BP	0.550471	-2.37412
DUSP4	0.522171	-2.37398
KDM5D	0.745944	-2.3739
SOX11	0.728046	-2.37
ZNF521	0.566405	-2.36481
LIPC	0.573113	-2.36218
TNIP3	0.365678	-2.36208
RUNX1T1	0.276011	-2.35408
BEND6	0.412875	-2.35371
IRAK3	0.437007	-2.35204
EIF1AY	0.881279	-2.35102
RIPK3	0.479884	-2.34894
FAM110B	0.533625	-2.34842
METRNL	0.445149	-2.34815
SETBP1	0.443295	-2.34649
FLT1	0.703475	-2.34641
FAM162B	0.655284	-2.34222
GALNTL1	0.52299	-2.34151
LOC100128252	0.441248	-2.34074

SYNPO2	0.56361	-2.33864
PRLR	0.558779	-2.33517
PSG2	0.702443	-2.33449
EHD3	0.102606	-2.33348
CYorf15B	0.640473	-2.32902
PRR16	0.478859	-2.32764
SOCS5	0.300633	-2.324
SSTR1	0.389426	-2.31512
ISLR	0.804844	-2.31351
CECR1	0.730378	-2.30862
ADAM33	0.462377	-2.30843
EPB41L3	0.691815	-2.30783
NFATC4	0.234231	-2.3069
SLC7A8	0.52228	-2.30544
PDGFA	0.56662	-2.30416
SOX11	0.71851	-2.30338